

INFORMATION TO USERS

This reproduction was made from a copy of a document sent to us for microfilming. While the most advanced technology has been used to photograph and reproduce this document, the quality of the reproduction is heavily dependent upon the quality of the material submitted.

The following explanation of techniques is provided to help clarify markings or notations which may appear on this reproduction.

1. The sign or "target" for pages apparently lacking from the document photographed is "Missing Page(s)". If it was possible to obtain the missing page(s) or section, they are spliced into the film along with adjacent pages. This may have necessitated cutting through an image and duplicating adjacent pages to assure complete continuity.
2. When an image on the film is obliterated with a round black mark, it is an indication of either blurred copy because of movement during exposure, duplicate copy, or copyrighted materials that should not have been filmed. For blurred pages, a good image of the page can be found in the adjacent frame. If copyrighted materials were deleted, a target note will appear listing the pages in the adjacent frame.
3. When a map, drawing or chart, etc., is part of the material being photographed, a definite method of "sectioning" the material has been followed. It is customary to begin filming at the upper left hand corner of a large sheet and to continue from left to right in equal sections with small overlaps. If necessary, sectioning is continued again--beginning below the first row and continuing on until complete.
4. For illustrations that cannot be satisfactorily reproduced by xerographic means, photographic prints can be purchased at additional cost and inserted into your xerographic copy. These prints are available upon request from the Dissertations Customer Services Department.
5. Some pages in any document may have indistinct print. In all cases the best available copy has been filmed.

**University
Microfilms
International**

300 N. Zeeb Road
Ann Arbor, MI 48106

8324895

Tapp, James Bryan

RELATIONSHIPS OF ROCK CLEAVAGE FABRICS TO INCREMENTAL AND
ACCUMULATED STRAIN IN A PORTION OF THE BLUE RIDGE, VIRGINIA

The University of Oklahoma

PH.D. 1983

**University
Microfilms
International** 300 N. Zeeb Road, Ann Arbor, MI 48106

PLEASE NOTE:

In all cases this material has been filmed in the best possible way from the available copy. Problems encountered with this document have been identified here with a check mark .

1. Glossy photographs or pages
2. Colored illustrations, paper or print
3. Photographs with dark background
4. Illustrations are poor copy
5. Pages with black marks, not original copy
6. Print shows through as there is text on both sides of page
7. Indistinct, broken or small print on several pages
8. Print exceeds margin requirements
9. Tightly bound copy with print lost in spine
10. Computer printout pages with indistinct print
11. Page(s) _____ lacking when material received, and not available from school or author.
12. Page(s) _____ seem to be missing in numbering only as text follows.
13. Two pages numbered _____. Text follows.
14. Curling and wrinkled pages _____
15. Other _____

University
Microfilms
International

THE UNIVERSITY OF OKLAHOMA

GRADUATE COLLEGE

RELATIONSHIPS OF ROCK CLEAVAGE FABRICS TO
INCREMENTAL AND ACCUMULATED STRAIN IN A
PORTION OF THE BLUE RIDGE, VIRGINIA

A DISSERTATION

SUBMITTED TO THE GRADUATE FACULTY

in partial fulfillment of the requirements for the

degree of

DOCTOR OF PHILOSOPHY OF SCIENCE

By

JAMES BRYAN TAPP

1983

RELATIONSHIPS OF ROCK CLEAVAGE FABRICS TO
INCREMENTAL AND ACCUMULATED STRAIN IN A
PORTION OF THE BLUE RIDGE, VIRGINIA
A DISSERTATION

APPROVED FOR THE SCHOOL OF GEOLOGY AND GEOPHYSICS

By

Richard A. Walsh

James L. Allen

Walter R. King

Richard A. Bushong Jr.

ABSTRACT

The deformation history of a small portion of the Virginia Great Valley is described. Pressure solution acted to form two geometrically distinct cleavages in the Conococheague Formation. Pressure solution is an important deformation mechanism in the formation of rock fabrics in fine grained carbonate rocks deformed under low temperature, low confining pressure and low strain rate conditions.

Limestone layers contain a penetrative cleavage (here termed Sp) formed by the dimensional orientation of calcite microspar and are thickened in the hinge zones of folds and thinned on the limbs of folds. Dolomite layers contain a spaced solution cleavage (here termed Ss) and maintain constant thickness around folds. Cleavage does not transect the fold axes in the fold hinge zones.

One hundred oriented samples of the Conococheague Formation were collected. Incremental strain and accumulated strain were measured using syntectonic fibrous calcite and deformed ooids respectively. Layering was initially inclined as much as 30° to compression. The deformation was locally non-coaxial as viewed by the deforming material on the fold limbs but was irrotational as viewed from a global reference frame (preserved in fold axis). Penetrative cleavage(Sp) parallels the elongation axis of accumulated strain. Spaced cleavage zones are curved. The initial and final orientation of Ss are nearly identical with the initial and final orientations of incremental elongation.

Cleavage was formed by pervasive pressure solution and some twinning (in crystals larger than 120 microns in diameter) in limestone layers and pressure solution along discrete zones in dolomite layers. Crystal size, strain rate and composition controlled deformation mechanism. The presence of impurities such as phyllosilicates aid in

the formation of discrete solution zones. Pervasive pressure solution forms cleavage in micritic limestones containing less than 1% phyllosilicates by volume. Spaced solution zones form in sucrosic dolomites that contain more than 1% phyllosilicates by volume.

Volume loss due to pressure solution is estimated by comparing the abundances of metallic elements between matrix and pressure solution zones using electron dot maps prepared on an EDX system. Hinge zones and steeply dipping limbs of folds have closer spacing and greater volume loss than shallowly dipping limbs of folds. The hinge zones of folds experienced the greatest strain rate and volume loss. Strain rates in limestones are greater than in dolomites.

ACKNOWLEDGMENTS

It is difficult to completely acknowledge all of the help received in any endeavor. It is perhaps impossible to acknowledge all of the help received during the course of study involved in the Ph.D. degree. For this reason I gratefully acknowledge all of the teachers who have attempted to teach me. Direct thanks are due those who were involved in this thesis. I give my greatest thanks to Dr. John Wickham who first showed me the wonder of structural geology and introduced me to the present subject. Dr. Wickham has shown me what it is to teach and do research. I also thank Dr. Jud Ahern who served as mentor and critic during this study. I thank Drs. Robert Du Bois, Richard Groshong, Charles Harper and Ralph Rogers who critically read the manuscript and whose comments served to improve both the style and scientific merit of this report. I give special thanks to my wife, Gayle, who assisted me in the field work and greatly clarified my thinking in times of confusion. Without her continual support and timely input, I would have not survived this thesis. Marjorie Starr and Jeanette Standridge typed large portions of this manuscript and provided moral support during its preparation. Although this thesis is directly or indirectly the result of interactions with several people, I alone am responsible for the information and presentation contained herein. Any errors of omission or logic are strictly my own. Funding for this study was provided by the Geological Society of America in the form of a Penrose Field Grant and by the National Science Foundation who are gratefully acknowledged. Time on the microprobe was provided by Phillips Petroleum Company. The dot maps were prepared by Dr. Ben Powell at Phillips Petroleum Research and Dr. Robert Ogilvie at The Oral Roberts University Department of Anatomy.

TABLE OF CONTENTS

	Page
ABSTRACT.....	iii
ACKNOWLEDGMENTS.....	v
TABLES.....	viii
ILLUSTRATIONS.....	ix
INTRODUCTION.....	1
Purpose and Scope of Study.....	1
Statement of Problem.....	1
Mechanisms Which Form Cleavage (Review).....	3
Physical Mechanisms.....	3
Chemical Mechanisms.....	4
Pressure Solution.....	4
Recrystallization.....	5
Crystallization.....	6
Summary.....	6
METHODOLOGY.....	9
Location of Study Area.....	9
Field Description.....	12
Procedure.....	13
Estimation of Accumulated Strain.....	30
Preparation of Oriented Thin Sections.....	31
Measurement of Axial Ratios and Orientations.....	31
Estimation of Incremental Strain.....	32
Derivation of Equations.....	50
Basic Concepts of Infinitesimal Strain.....	50
Incremental Nature of Progressive Strain.....	53
Estimating Orientation and magnitude of Incremental Strain.....	53
Discussion of Procedure.....	58
RESULTS.....	66
Folds.....	66
General Observations.....	66
Discussion.....	84
Cleavage.....	85
General Observations.....	85
Penetrative Cleavage (Sp).....	89
General Observations.....	89
Discussion.....	94
Spaced Cleavage (Ss).....	109
General Observations.....	109
Discussion.....	114

Estimation of Volume Loss by Pressure Solution.....	125
Introduction.....	125
General Observations.....	134
Discussion.....	136
Estimation of Strain Rate from Solution Zone Spacing....	138
CONCLUSIONS.....	142
REFERENCES.....	146
APPENDIX A: Computer Programs.....	152
APPENDIX B: Strain Paths with Area Strain < 2.0.....	183
APPENDIX C: Strain Paths with Area Strain > 2.0.....	228

TABLES

Table		Page
1.	Interlimb angle from 10 folds in the field area. The folds measured represent a range of fold sizes from outcrop scale to thin section scale.....	71
2.	Mean and standard deviation of ooid long axis orientation, mean standard deviation and range of Sp orientation, range of ss orientation and location on fold for 9 samples containing well developed Sp. All measurements are in degrees. Orientations are in degrees relative to bedding.....	98
3.	Initial, final and ranges of orientations of incremental and accumulated strain and Ss. All measurements are relative to bedding and are in degrees.....	119
4.	Spacing of solution zones in 8 samples from various portions of folds. Spacing was measured perpendicular to the solution zone trace. Measurements are in centimeters.....	122
5.	Data from microprobe analysis listed as weight percent of 7 elements. The percentages are based on a ZAF correction program. The microprobe was standardized on a 20 micron beam diameter. All beam diameters are in microns. The ZAF correction incorporates adsorption coefficient, takeoff angle and backscatter fluorescence. The program does not correct for CO ₂ or H ₂ O.....	133
6.	Estimates of volume loss due to pressure solution using $A_2/A_1 = (1-(V'/V))$. Fractional numbers represent samples that show volume loss for that element. The procedure used is described in the text.....	137
7.	Calculated strain rates using equation 4 (from Fletcher and Pollard, 1981). The strain rates are for solution cleavage spacing measured in samples from different parts of folds.....	139

ILLUSTRATIONS

Figure	Page
1. Generalized geologic map of thesis area. The study is limited to the Conococheague Formation on the eastern limb of the Massanutten Synclinorium.	10
2. Photograph of folding in outcrop. Hammer is 16 inches long. This is the largest scale folding that is observed directly in the field. View is to the southwest and up-plunge. This photograph was taken near sample 905 on the Stone Bridge -Federal Hill traverse in the hinge zone of the Federal Hill anticline..	14
3. Photograph of thin section of sample 805. The thin section is a 1"x2" section. View is downplunge to the northeast. This sections shows a variable fold shape and a fanned cleavage.....	14
4. Contoured density plot for poles to bedding for the total Conococheague Formation. Diagram prepared from Kalsbeek plot computer program. 223 observations.....	16
5. Contoured density plot for poles to cleavage for total Conococheague formation. 184 observations. Plots for individual traverses can be seen in figures 14 and 19.....	18
6. Schematic drawing of the cleavage - bedding relationships an asymmetric fold with an inclined hinge surface.	20
7. Cross-sections of traverses. The sections show location of samples and local folds. The sections were prepared by projecting data onto the plane of section. Fold shapes are modeled after folds seen on individual traverses. Bedding and cleavage orientations have been corrected to apparent dips on the plane of section.....	22
8. Plots of ooid axial ratios, accumulated strain ellipse and statistical values for samples containing deformed ooids. These plots are not oriented in space but are presented as they were digitized.....	33
9. Possible displacement paths drawn for a pair of quartz grains. The paths show the path for each grain centroid relative to the suture. The paths represent the two possible interpretations of displacement path based on the assumptions that A) fiber growth occurs at the grain boundary and B) fiber growth occurs at the suture.....	44
10. Incremental strain path for shallow and steep limbs of a fold. This figure illustrates the sense of range of orientation for incremental shortening that an observer standing on the bedding plane would see through time during folding. This figure is drawn assuming that fiber growth is at the grain boundary.....	46

11. Composite strain paths for samples 816, 850, 937 and 950. These paths were prepared using the techniques described in this section. Horizontal axis is orientation of maximum shortening relative to bedding. Vertical axis is time.....48
12. Photomicrograph of fiber singlet from sample 816. The field of view is approximately 1.5 mm. The technique used to determine the incremental strain history from singlet fiber sets is described in this section.....60
13. Photomicrograph of double fiber set from sample 850. The field of view is approximately 1.5mm. The technique used to determine incremental strain history from these fibers is discussed in this section.....60
14. Density contour plots for poles to bedding on traverses in the field area. Lower hemisphere projection. The plots show the local fold axis.....67
15. Lower hemisphere plots of fold axes. Axes marked by a dot are calculated using Fisher and Watson statistical techniques. Axes marked with a + are field measurements. Circles are the radius of cones of confidence. The triangle is the total data pole from the statistical analysis.....69
16. Cleavage - isogon plots for five samples using the techniques described by Treagus (1982).72
17. Traverse cross-sections with superimposed accumulated strain measures from deformed ooids. The ellipses are oriented in space. Dashed line represents cleavage orientation at that location. Sample number and axial ratios are shown.....76
18. Traverse cross-sections with superimposed incremental strain paths. Plots show orientation of incremental and accumulated shortening axis through time relative to bedding. The horizontal axis represents angle to bedding of the elongation axis. The vertical axis represents time. The incremental strain path is labeled i. The accumulated strain path is labeled a.....80
19. Density plots of poles to cleavage on traverses. Lower hemisphere projection. Plots show local fold axis.....86
20. Scanning Electron Photomicrograph of dimensional fabric (Sp) in sample 817. Scale bar is 10 microns long.....90
21. SEM image of refraction of Sp around detrital dolomite grain in sample 815. Magnification is 250X.....90
22. SEM image of cleavage refraction at a lithologic boundary where Sp and Ss connect in sample 809. The upper portion of the photograph is sucrosic dolomite with 1% phyllosilicates by volume. The lower portion is calcite microspar. Magnification is 500X.....92
23. Photomicrograph of truncation of quartz grain and calcite pressure shadow as well as truncation of Sp (left) by Ss in sample 807.....92
24. SEM photomicrograph of sample 809 showing non-alignment of platy rock constituents on Sp. The platy material is muscovite. Large crystals are dolomite. Magnification is 500X.....95

25.	SEM photomicrograph of solution pitting of quartz grain on Sp. Cleavage is poorly developed. Sample 831. Magnification is 500X.....	95
26.	Sketches of cleavage orientation across two folds showing that cleavage does not transect the folds. The folds have a central dolomite layer that has Ss cleavage. The upper and lower units are limestones with Sp cleavage. Neither Ss or Sp transect the fold axis. Note cleavage refraction. Scale bar represents 2 millimeters on sample.....	99
27.	SEM photomicrograph of deformation by twinning and wedging of dolomite core of ooid in sample 831. Magnification is 200X.....	102
28.	SEM image of twinned dolomite grains in sample 831. Magnification is 1000X.....	102
29.	Photomicrograph of ooids that have been deformed by pressure solution in sample 936. The ooids are mantled ooids with dolomitic cores. The cores have been deformed by twinning and pressure solution.....	105
30.	SEM photomicrograph of sample 936 showing truncation of deformed ooid by pressure solution zone. Magnification is 100X.....	105
31.	Photomicrograph of sample 928 showing non-mantled ooids that have the same dimensional fabric as Sp and have been cut by solution zones.....	107
32.	Photograph of thin section of sample 808 in plane polarized light. The thin section is 2"x3". This figure shows how solution zones curve and how they are formed by coalescing microsurfaces. The solution zones tend to terminate at boundaries between dolomite (dark) and limestone (light).....	110
33.	Photomicrograph of undulating Ss zone in sample 937.....	110
34.	SEM photograph of sample 809 showing truncation of dolomite in Ss. Note phyllosilicates accumulated in the zone are wrapped around the dolomite crystal. Magnification is 1500X.....	112
35.	Photograph of 2"x3" thin section of sample 814 showing variation of apparent offset direction and amount on Ss.....	112
36.	Photograph of 1"x2" thin section of sample 937 showing the curvature of Ss within the dolomites. Ss becomes nearly parallel with bedding in the limestone layer indicating that slip along limestone layers has occurred.....	115
37.	SEM photomicrograph of sample 809 showing the relationship between Ss and tension gashes. Magnification is 100X.....	115
38.	Photomicrograph of sample 816 showing truncation of pressure shadow by pressure solution zone.....	117
39.	Plot of elemental composition of sample 809 using EDS. This sample is representative of the samples analyzed....	127

40. Representative electron dot map images of sample 937 showing
- a) Secondary electron image of surface.
 - b) K alpha for magnesium.
 - c) K alpha for aluminum.
 - d) K alpha for silicon.
 - e) K alpha for potassium.
 - f) K alpha for calcium.....129

INTRODUCTION

Purpose and Scope of Study

This research was undertaken to understand the nature and origin of rock cleavage in the Conococheague Formation in the northwestern portion of Virginia and the West Virginia Panhandle.

The purpose of the research is to 1) describe the strain history and geometry of cleavage in a naturally deformed carbonate rock sequence, 2) determine which mechanism(s) acted to form the cleavage fabrics and textures observed and 3) determine the relative timing of the mechanisms involved in cleavage formation. The procedure entails 1) field description and measurement of cleavage occurrence and orientation, 2) description and measurement of cleavage in hand specimen and thin-section and 3) calculation of incremental strain paths and measurement of accumulated strain orientation.

Statement of Problem

In this paper cleavage is defined as a deformation-induced fabric which consists of planar discontinuities in rocks defined by preferred orientation of inequant minerals, laminar mineral aggregates or some combination of these (Hobbs, Means and Williams, 1976). Cleavage is a shortening fabric (Siddans, 1972; Wood, 1974; Hobbs, Means and Williams, 1976). The orientation of cleavage is generally accepted as being statistically perpendicular to the principal axis of shortening (Siddans, 1972; Wood, 1974; Groshong, 1975a). Cleavage differs from fracture in that it is a shortening fabric which produces a rock fabric by the physical rotation or internal deformation of rock constituents or the chemical mass transfer or reorganization of rock constituents (Siddans, 1972; Geiser, 1974, 1975; Wood, 1974; Groshong,

1975a, 1975b, 1976; Gray, 1978; Bell, 1981).

Rock cleavage has been studied for over a century. The nature and origin of rock cleavage is still poorly understood. There is not a standard classification scheme for rock cleavage (Hobbs, Means and Williams, 1976; Powell, 1979). Present cleavage terminology is ambiguous and is often misunderstood and misused. The lack of a descriptive classification scheme is a major problem in the understanding of rock cleavage formation (Hobbs, Means and Williams, 1976; Powell, 1979). A good descriptive classification system should be devoid of explicit genetic implications. Rock cleavage terms currently in use are coupled with genetic interpretations (Powell, 1979).

Two morphologically distinct cleavages found in the Conococheague Formation in northwestern Virginia and the West Virginia Panhandle are studied in this paper. The first cleavage type, a penetrative cleavage(Sp), is defined by the dimensional orientation of microspar calcite, such that the long axis of the microspar parallels the cleavage. The second cleavage type, a spaced cleavage, consists of discrete planar zones defined by the presence of coalesced, anastomosing zones of phyllosilicates. There has been truncation of rock constituents along these surfaces. The material along these surfaces is predominantly phyllosilicates which, in some cases, appear to be chloritized.

The literature contains descriptions of these two cleavage types from this locality (Wickham, 1969, 1972; Cloos, 1971, Edmundson and Nunan, 1973). The penetrative cleavage form has been described as a slaty cleavage (Wickham 1969, 1972; Edmundson and Nunan, 1973) or simply as cleavage (Cloos, 1971). The term slaty cleavage should be reserved for cleavage in rocks composed predominantly of phyllosilicates (Hobbs, Means and Williams, 1976). The spaced cleavage present has been described as a fracture cleavage (Edmundson and Nunan, 1973) following the convention of de Sitter (1964), or as a solution cleavage (Wickham, 1969, 1972; Cloos, 1971). The term spaced cleavage(Ss) will be used for this cleavage morphology. The surface terminology Ss and Sp does not carry any connotation of relative age of

formation of that surface.

Rock cleavage is a fabric which is found in a wide variety of rock types and may form in response to many deformation processes and environments. More than one mechanism may act to form rock cleavage in a single progressive deformation event.

Mechanisms Which Form Cleavage (Review)

There are two general categories of mechanisms which have been proposed to form cleavage. The first, physical mechanisms, consists of mechanical rotation and/or flattening of minerals within the deforming rock mass. The second, chemical mechanisms, consists of recrystallization, neocrystallization and pressure solution.

Physical Mechanisms

During deformation, particles will change orientation or shape. The rotation of particles in a system may occur early during the initial dewatering of a sediment or during post-lithification deformation. Maxwell (1962) suggested that cleavage forms during tectonic dewatering of the sediment prior to lithification. He based his model on the similarity in orientation of cleavage surfaces and clastic dikes in an outcrop of the Martinsburg Slate in New Jersey. This hypothesis has been accepted and used by many authors (Powell, 1969, 1972a, 1972b, 1973, 1974; Clark, 1970, 1974; Alterman, 1973; Boulter, 1974; Roy, 1978).

Detailed studies at the localities used by Maxwell and others have shown that the near parallelism of cleavage and clastic dikes is coincidental only on some exposures, and that tectonic dewatering does not explain the formation of cleavage (Epstein and Epstein, 1969; Wood, 1974; Geiser, 1974, 1975; Holeywell and Tullis, 1975; Groshong, 1976, Beutner, 1978, 1980; Gregg, 1979). Further evidence against the theory of tectonic dewatering is the presence of deformed fossils with the direction of principal elongation parallel with the cleavage trace, and the occurrence of cleavage in igneous rocks (Wood, 1974).

Tullis (1976) derived expressions for the perpendicular of the final orientation of a population of inequant, deformable, rod-like

grains undergoing axial strain in a homogeneous matrix using the principles outlined by March (1932), and for a population of rigid spheroids of revolution in an axially deformed viscous fluid using the principles of Jeffery (1923). In both the March and Jeffery models, the final orientation of inequant particles is dependent on the deviatoric strain orientation and the shape of the suspended particles. Willis (1977) derived kinematic linear and displacement models to describe the final orientation of inequant grains in response to deformation, assuming that 1) there is no interference between particles, 2) the deformation is slow and viscous, 3) the particles behave as rigid bodies, and 4) angular momentum is preserved. The Willis model predicts the same orientations as the March and Jeffery models given the same initial and boundary conditions. Both Tullis (1976) and Willis (1977) conclude that rock fabrics formed by physical rotation will be perpendicular to the axis of maximum principal shortening.

In limestones and dolomites, Wenk et al., (1973), Wenk and Shore (1975), Rutter and Rusbridge (1977), and Wagner et al., (1982), found that strong preferred orientation fabrics will develop in cold work deformation by intracrystalline deformation.

Many workers agree that penetrative rock fabrics formed by physical mechanisms should have an orientation statistically perpendicular to the orientation axis of maximum principal finite shortening (Groshong, 1975a; Ramsay, 1976; Tullis, 1976; Willis, 1977; Bell, 1981).

Chemical Mechanisms

The chemical processes which can act to form cleavage are pressure solution, recrystallization and neocrystallization. Chemical formation of cleavage may involve the reorientation of crystal lattices, the formation of discrete planar discontinuities, or the formation of new crystal lattices within a deforming system.

Pressure Solution. Pressure solution is the solutional mass transfer of material from a region of high stress to one of lower stress. Pressure solution initiates at points of grain to grain

contact in a non-hydrostatic stress field in the presence of a fluid (de Boer, 1977). Pressure solution surfaces form normal to the direction of maximum principal stress (Weyl, 1959; Durney, 1972, 1976, 1978; Elliott, 1973; Rutter, 1976; de Boer, 1977).

The models of pressure solution use the principle [developed by Gibbs (1878)] of equilibrium of a non-hydrostatically stressed solid in a hydrostatic fluid. The mechanisms of pressure solution have been studied quantitatively and experimentally by Durney (1976) and Rutter (1976), who concluded that all are equally possible in nature. Kinetically, all are rapid enough to produce realistic strain rates at low temperatures and low values of deviatoric stress.

Material removed by solution in an area of relatively high stress will precipitate locally in an area of relatively lower stress (Groshong, 1975a; Durney, 1976; Sprunt and Nur, 1977; Fletcher and Pollard, 1981; Fletcher, 1982).

Pressure solution is important in the formation of cleavage in slates, carbonates, and sandstones (Durney, 1972; Geiser, 1974, 1975; Groshong, 1975a, 1975b, 1976; Gray, 1978; Alvarez, Engelder, and Geiser, 1978; Gill, 1980), and as a pervasive phenomenon (Elliott, 1973). The formation of discrete planar discontinuities is important in the interpretation of curved solution surfaces in folds (Groshong, 1975b; Fletcher and Pollard, 1981). Fletcher and Pollard (1981) show that pressure solution surfaces initiate at a point and propagate outward. As the surface forms, its orientation will change as the fold limb rotates, resulting in an S-shaped solution surface.

Solution surfaces have been recognized as discrete cleavage surfaces (Plessman, 1964, 1966) by the truncation of fossils and rock particles at cleavage surfaces and by the presence of accumulated insoluble material on the solution cleavage surfaces.

Recrystallization. Recrystallization is the reorganization of a crystal lattice. Recrystallization lowers the free energy of a deformed crystal by eliminating dislocations (recovery), forming high angle crystal boundaries (primary recrystallization), forming nearly equant crystals (normal grain growth) or forming a few large crystals

(secondary recrystallization). Recrystallization is thermally activated and will produce unstrained crystals which may have high angle boundaries or a preferred orientation (Rutter, 1974; Tullis, 1973, 1976; Wenk, Venkitesubramanian and Baker, 1973; Wenk and Shore, 1975; Rutter and Rusbridge, 1977). Recrystallization may occur after deformation or as a syntectonic process.

During recrystallization the preferred orientations which form will reflect the orientation of maximum compressive stress as opposed to the the orientation of maximum principal elongation (Hobbs, 1968). Rutter (1974) estimates that at geologic strain rates limestone below a temperature of 400° C will deform by twinning, slip and pressure solution. Limestone above 400° C will deform by intracrystalline flow. In rocks deformed above 400° C rock cleavage fabrics will form by recrystallization. Rutter and Rusbridge (1977) found that during hot working in non-coaxial deformations the morphologic dimensional fabric of calcite will be statistically perpendicular to the axis of maximum finite shortening and the optic axis will be statistically perpendicular to axis of maximum shortening of the last increment of deformation.

Crystallization. Crystallization is the formation of new mineral phases during metamorphism or diagenesis (Spry, 1968). Crystallization in a deforming system results from the destruction of unstable material with diffusion and precipitation of new stable mineral constituents. The new lattice system will form with an orientation which is thermodynamically favorable with the stress field in which it forms (Kamb, 1959).

Rock cleavage fabrics formed by crystallization will preserve an expression of the deformation history of the system in which it forms (Hobbs, 1966).

Summary

Rock cleavage is formed by a wide variety of rock textures in various rock lithologies and deformation environments. The mechanism(s) which form rock cleavage are dependent on deviatoric stress, strain rate, temperature, crystal size and composition of the rock. Rock

cleavage may be formed by:

- 1) Alignment of platy particles during tectonic dewatering before lithification of the sediment. In many slates there is an apparent similarity of orientation of cleavage surfaces and clastic dikes (Maxwell, 1962; Powell, 1969, 1972a, 1972b, 1973, 1974; Clark, 1970, 1974; Alterman, 1973; Boulter, 1974; Roy, 1978).
- 2) Alignment of inequant particles by mechanical rotation, or flattening, during deformation, to an orientation perpendicular to bulk finite shortening (Cloos, 1947, 1971; Dieterich, 1969; Siddans, 1972; Wood, 1974; Tullis and Wood, 1975; Beutner, 1978, 1980; Bell, 1981). This alignment would occur after lithification.
- 3) Formation of discrete solution zones (Plessman, 1964, 1966; Durney, 1972, 1976; Geiser, 1974, 1975; Groshong, 1975a, 1975b, 1976; Alvarez, Engelder, and Geiser, 1978, Gray, 1978).
- 4) Neo-crystallization or recrystallization (Etheridge, 1973; Etheridge and Hobbs, 1974; Holeywell and Tullis, 1975; Tullis, 1976; White and Knipe, 1978).

The controversy surrounding the origin of cleavage may be due to several factors:

- 1) Rock cleavage is found in a wide range of lithologies and deformation environments, suggesting that one single mechanism may not explain its origin.
- 2) Rock cleavage is formed by a wide variety of textural elements (Williams, 1972) suggesting that there may be an interdependence of cleavage-forming mechanisms.

In order to distinguish whether a particular cleavage was formed by physical or chemical mechanisms, it is necessary that a fundamental difference exists between the geometry and morphology of cleavage formed by physical mechanisms and those cleavages formed by chemical mechanisms.

In a smoothly continuous rock material that has experienced a homogeneous, coaxial deformation, the principal axes of accumulated

strain will parallel the principal axes of stress. If a rock volume has experienced a deformation in which the principal axes of accumulated strain deviate from the principal axes of incremental strain, the deformation is non-coaxial.

A cleavage trace formed by a purely physical mechanism, such as rotation or flattening of minerals, should be statistically normal to the accumulated principal shortening axis (Groshong, 1975). A cleavage formed progressively by a chemical mechanism will be generally perpendicular to the axis of maximum principal compressive stress during cleavage formation. If it is assumed that for any instant in time the deformation is coaxial for that instant in time a cleavage fabric formed in that time frame by a chemical mechanism should be parallel with the orientation of maximum extensional stress and therefore parallel with the elongation axis of maximum principal elongation for that increment of time. If the deformation is non-coaxial over the event as a whole, the geometry of a cleavage formed by a chemical mechanism formed either progressively or instantaneously will differ from the geometry of a cleavage formed by a physical mechanism, provided that the difference in the orientation of incremental strain and accumulated strain are measurable.

To determine which mechanisms have formed individual cleavage surfaces data should be collected in an area that possesses 1) a variety of cleavage textures with measurable geometry in more than one lithology, 2) a fold hinge surface parallel cleavage that can be attributed to a single deformation event, 3) accumulated strain markers, 4) incremental strain markers and was deformed in a non-coaxial environment.

METHODOLOGY

In a study of rock cleavage it is necessary to first describe and classify the cleavage in such a way that there are no explicit genetic implications inherent in the terminology. Second, the displacements which are related to that cleavage must be determined. Third, the history of those displacements must be determined either through direct observation of displacement path or through the careful application of experimental techniques. Displacement history can be used to infer the mechanism of cleavage formation in a natural deformation environment.

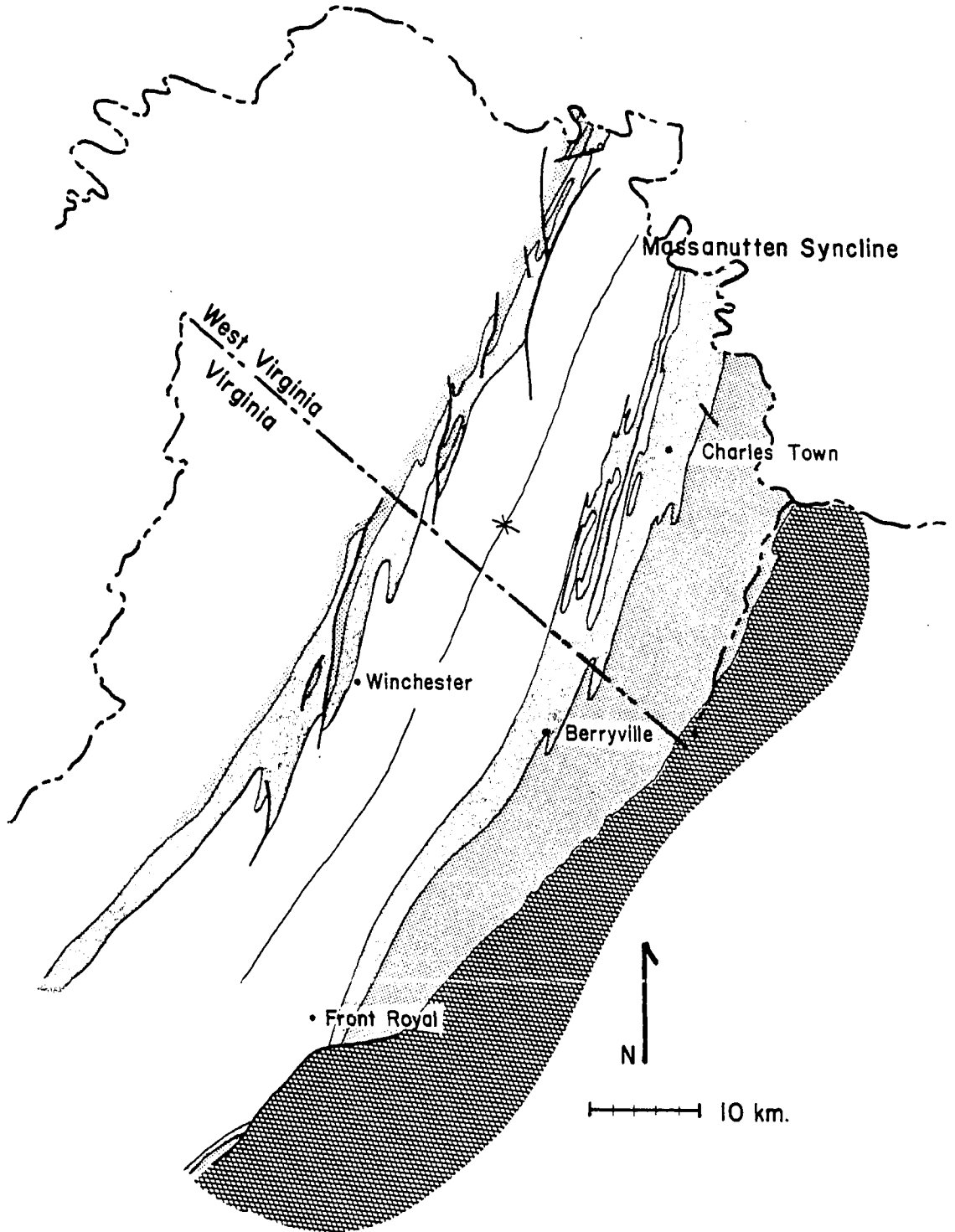
Rock cleavage has been described in a wide variety of tectonic settings and rock types. In order to determine whether a cleavage was formed by a physical or chemical mechanism, comparisons must be made in an area possessing the attributes previously discussed. The following sections describe the formation and region selected for this study and describe the procedures used.

Location of Study Area

The selected study area is in northwestern Virginia and the West Virginia Panhandle (see Figure 1). This study is limited to the Cambrian Conococheague Formation. This region and formation satisfy the necessary conditions for the study of the mechanisms of cleavage formation discussed in the previous section. The Conococheague possesses at least two distinct cleavage types (Wickham, 1969, 1972; Cloos, 1971). The cleavage is statistically axial planar (Wickham 1969, 1972). The region has experienced a deformation of approximately plane strain on surfaces normal to the fold axes (Cloos, 1971). The Conococheague contains at least one ooid horizon which has been used to measure finite strain (Cloos, 1971), and incremental strain markers (Wickham, 1973). The folding in the region is asymmetric (Wickham

Figure 1: Generalized geologic map of thesis area. The study is limited to the Conococheague Formation on the eastern limb of the Massanutten Synclinorium. Scale is 1:500,000. Map symbols mean:

Ordovician units	
Conococheague Formation	
Cambrian units	
Precambrian units	
Formation contact	
Fault	
State Boundary	



1969, 1972, 1978), implying that the deformation environment was non-coaxial (Elliott, 1972).

Field Description

The Conococheague Formation is an upper Cambrian or lower Ordovician shallow stable shelf carbonate sequence. The Conococheague Formation is overlain by the Ordovician Stonehenge Formation and underlain by the Cambrian Elbrook Formation. The Conococheague Formation can be divided into three members based on lithology. The lowermost unit is a sandy limestone with intercalated dolomite stringers, containing ooids, rip-up clasts and algal mats. It is slightly more resistant than the underlying and overlying units, producing hills 10-15 meters above the surrounding units. The middle member of the formation consists of regularly interbedded limestone and dolomite layers with thicknesses varying from 1 cm. to 2 meters. This unit, on the average, is less resistant than the lower unit and forms a shallow valley in which the dolomitic units stand in minor relief. The upper member consists of distinctive thinly interbedded algal dolomites and limestones (which has been loosely termed ribbon-rock) and sandy bioclastic limestones. The fossil debris found in the bioclastic layers are crinoid and trilobite fragments. The upper member is slightly more resistant, forming a low hill of 5-10 meters relief.

Poor outcrop quality and density made it impossible to construct a continuous outcrop map of the study area. The members described above were not recognized in all of the areas mapped. The formation boundaries of the Conococheague Formation are assigned in the literature as the first appearance of sand at the base of the Conococheague and as the first appearance of trilobite fragments at the top of the Conococheague. These criteria were not useful in determining the contacts in this study. The criterion used for recognition of the Elbrook contact is the presence of a moderately indurated ochre marlstone at the top of the Elbrook. The criterion used for the recognition of the Stonehenge Formation is the last occurrence of bioclastics and the appearance of a steel gray, massive

weathering, finely laminated limestone. The contacts identified, using these criteria, closely match the contacts mapped by Edmundson and Nunan (1973) using the criteria reported in the literature.

The map area is crossed by a series of asymmetric and sometimes overturned folds (see Plate 1). Folding is evident on all scales of observation (see Figures 2 and 3). Poles to bedding fall on a narrow tectonic girdle (see Figure 4) supporting the conclusion that the deformation may be considered to be a single, uniform event of plane strain. Poles to cleavage fall along a slightly broader but coaxial girdle (see Figure 5), showing that the cleavage is axial planar and syntectonic, fanning around the fold axis.

Procedure

Mapping was done on aerial photographs at scales of 1 in.=660 ft. and 1 in.=1320 ft., and on topographic maps during the summers of 1978 and 1979. During that time 7 traverses were mapped across the Conococheague Formation. These traverses and the samples collected on them serve as the basis for this study. One hundred oriented samples were collected during the field seasons. These samples were collected on both the shallowly dipping upper limbs of folds and the steep to overturned lower limbs of folds. Hinge traces were marked on the maps as accurately as possible. The actual location of the hinge traces is approximate because fold hinges are narrow and usually not well exposed. Location relative to fold hinges was determined by the angular relation of bedding and cleavage. (Refer to Figure 6 for a description of the geometric relation of bedding to an axial planar cleavage on an asymmetric fold.) Samples collected on the traverses were located in terms of their structural position on the fold and in present day geographic space. The samples were oriented by marking a planar surface so that this surface could be reoriented in the lab. The samples collected represented a wide variety of cleavage type and occurrence, possessed deformed ooids, or displayed good probability of containing incremental strain markers.

Cross-sections (Figures 7a-g.) were constructed from the data

Figure 2: Photograph of folding in outcrop. Hammer is 16 inches long, this is the largest scale folding that is observed directly in the field. View is to the southwest and up-plunge. This photograph was taken near sample 905 on the Stone Bridge - Federal Hill traverse in the hinge zone of the Federal Hill anticline.

Figure 3: Photograph of thin section of sample 805. The thin section is a 1"x2" section. View is downplunge to the northeast. This sections shows a variable fold shape and a fanned cleavage.

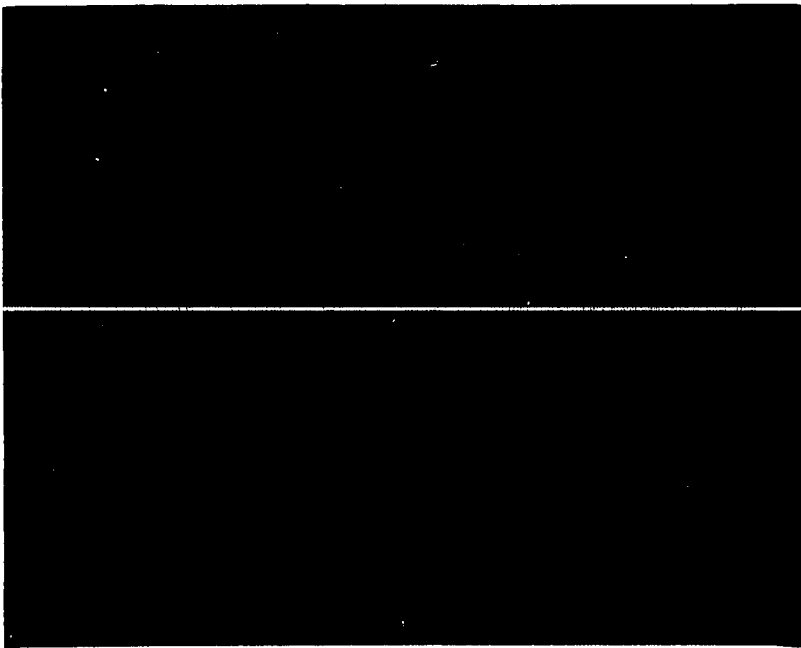
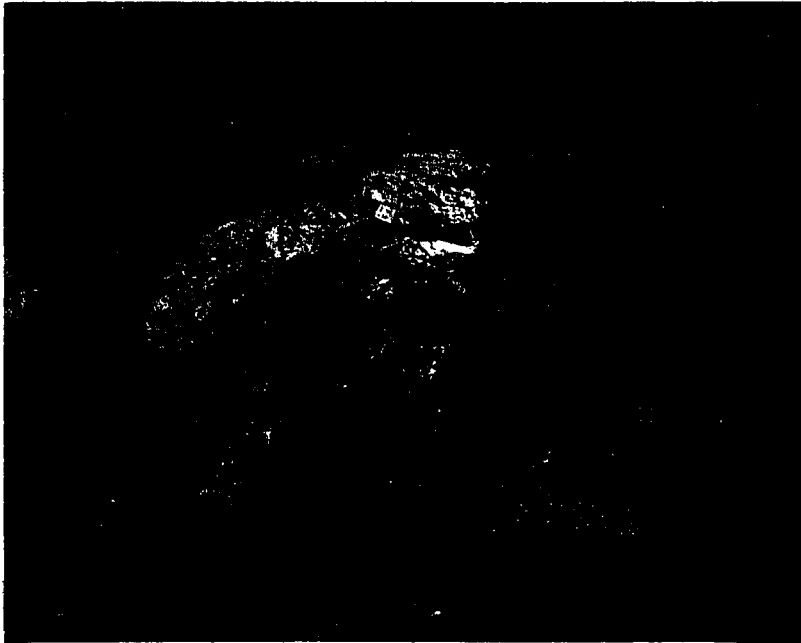
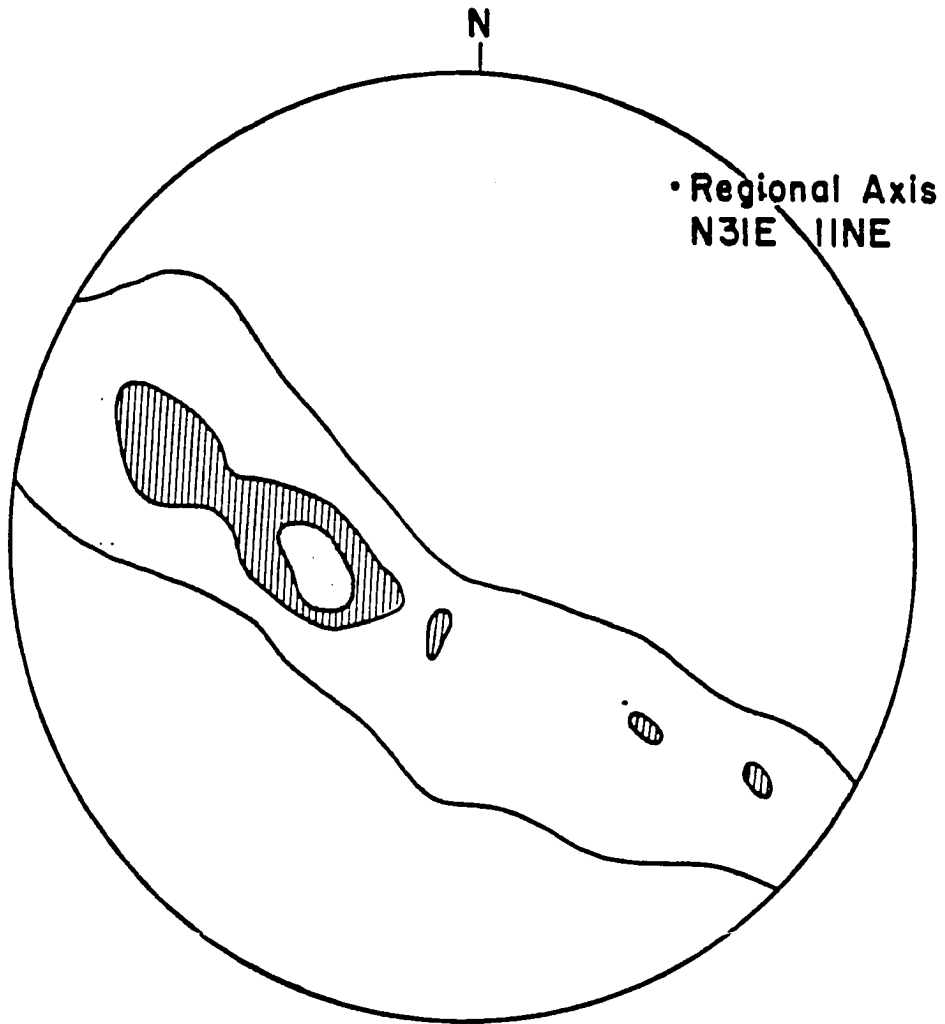


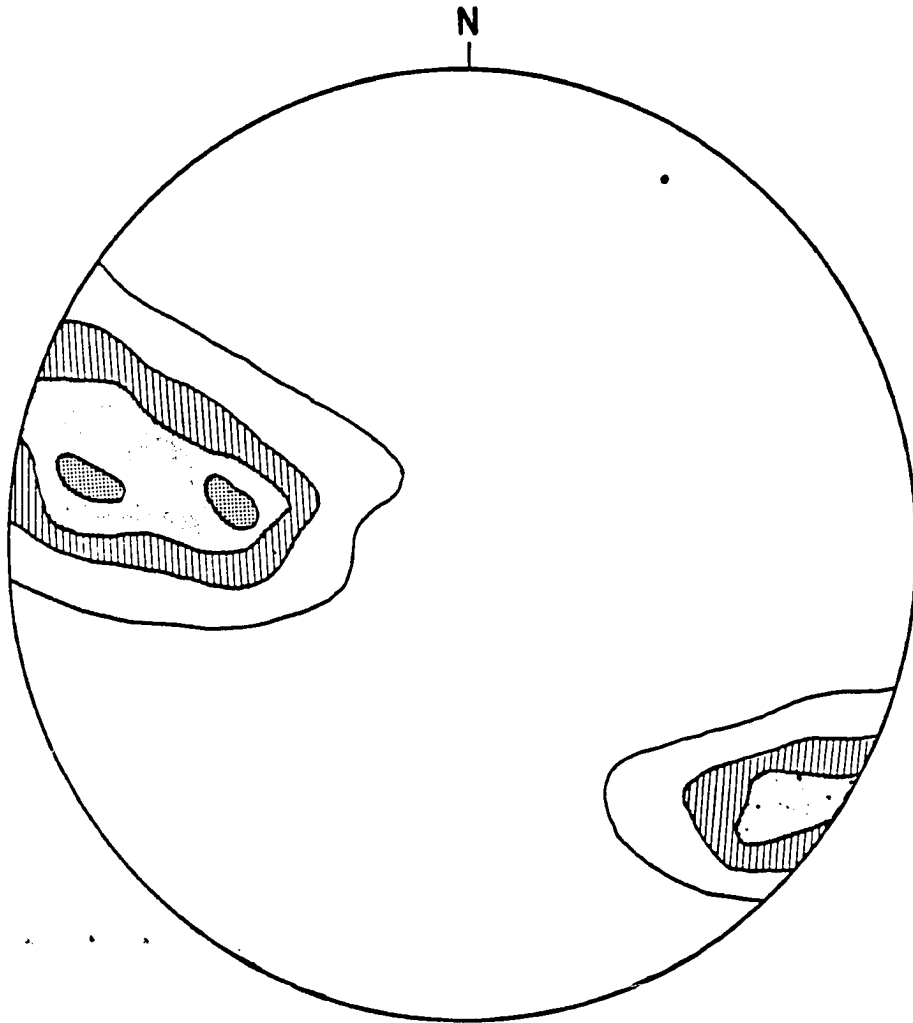
Figure 4: Contoured density plot for poles to bedding for the total Conococheague Formation. Diagram prepared from Kalsbeek plot computer program. 223 observations.



□ 10-15 %
▨ 5-10 %

□ 0-5 %

Figure 5: Contoured density plot for poles to cleavage for total Conococheague formation. 184 observations. Plots for individual traverses can be seen in figures 14 and 19.



15-20 %

0-5 %

10-15 %

5-10%

Figure 6: Schematic drawing of the cleavage - bedding relationships in an asymmetric fold with an inclined hinge surface. The fold shown has a slightly convergent cleavage fan. Steep limb attenuation is 33% (this is the mean attenuation in the field area). The acute angle formed by the cleavage bedding intersection points toward the fold hinge. If up can be determined in the field it can be used to locate local folds and determine whether they are anticlines or synclines.

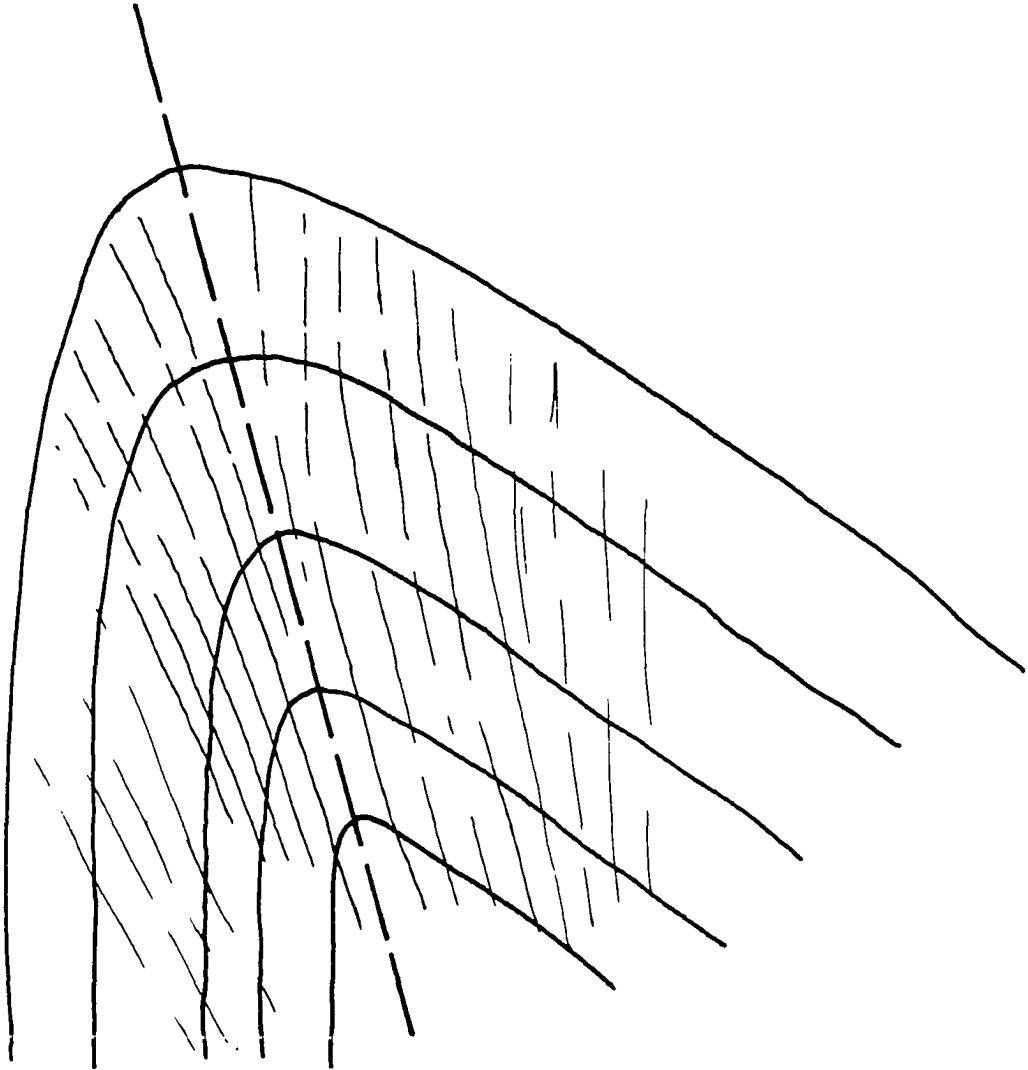


Figure 7(a-g): Cross-sections of traverses. The sections show location of samples and local folds. The sections were prepared by projecting data onto the plane of section. Fold shapes are modeled after folds seen on individual traverses. Bedding and cleavage orientations have been corrected to apparent dips on the plane of section.

23

Eco
ce
A'

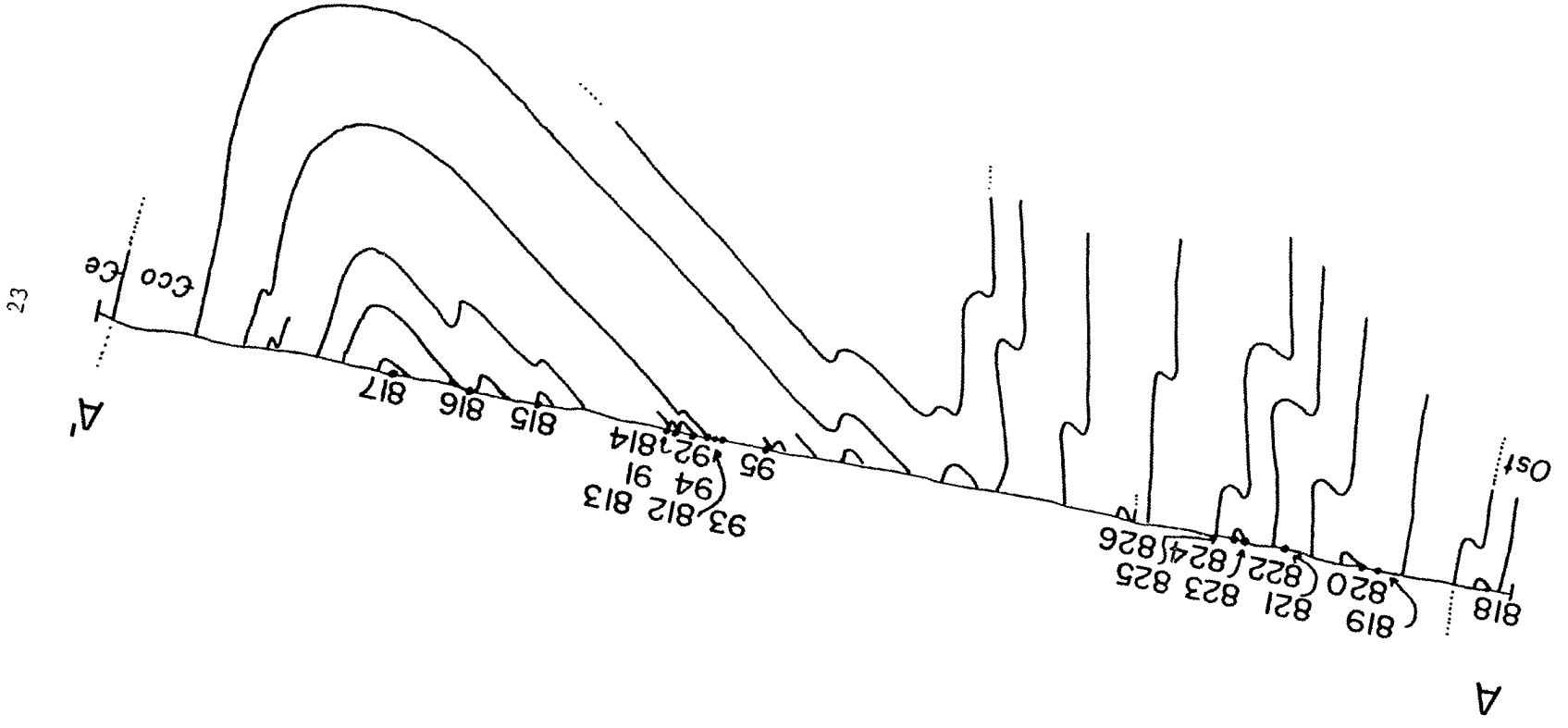
93, 812, 813
(94, 91
95, 192, 1814

818
(819, 821, 823, 825
820, 822, 824, 826

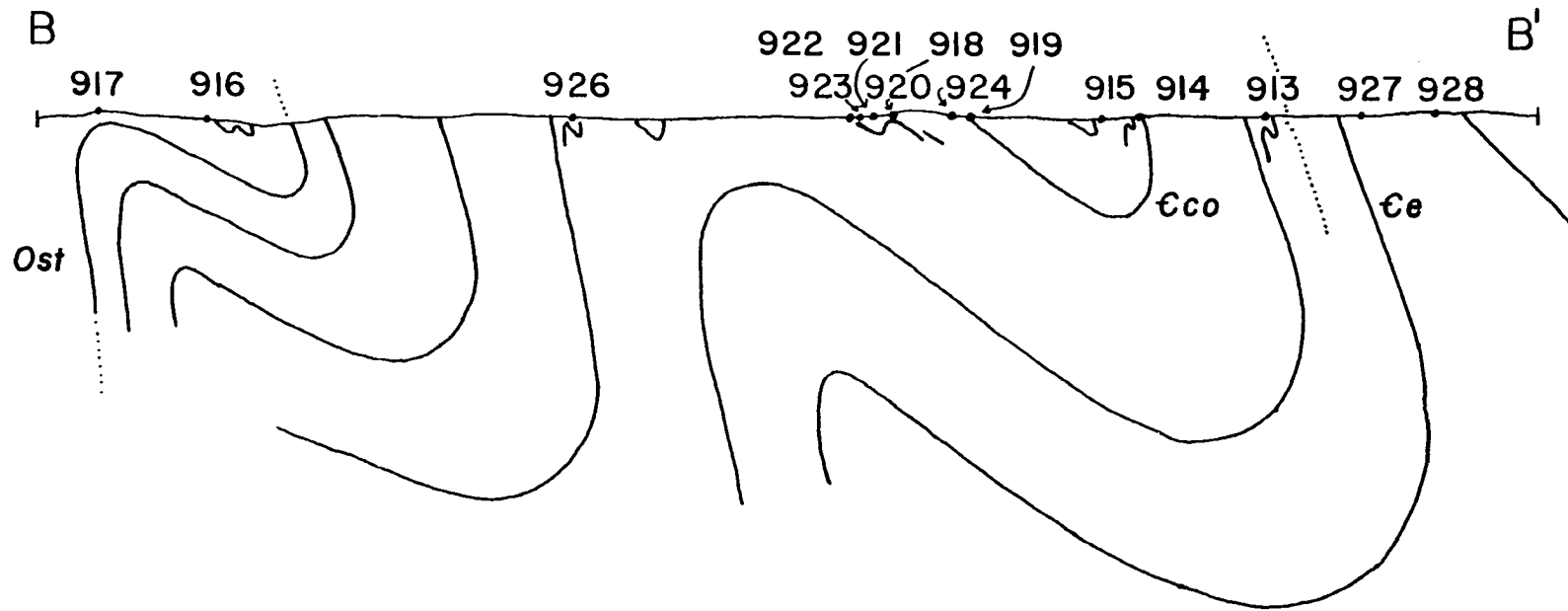
A

Ost

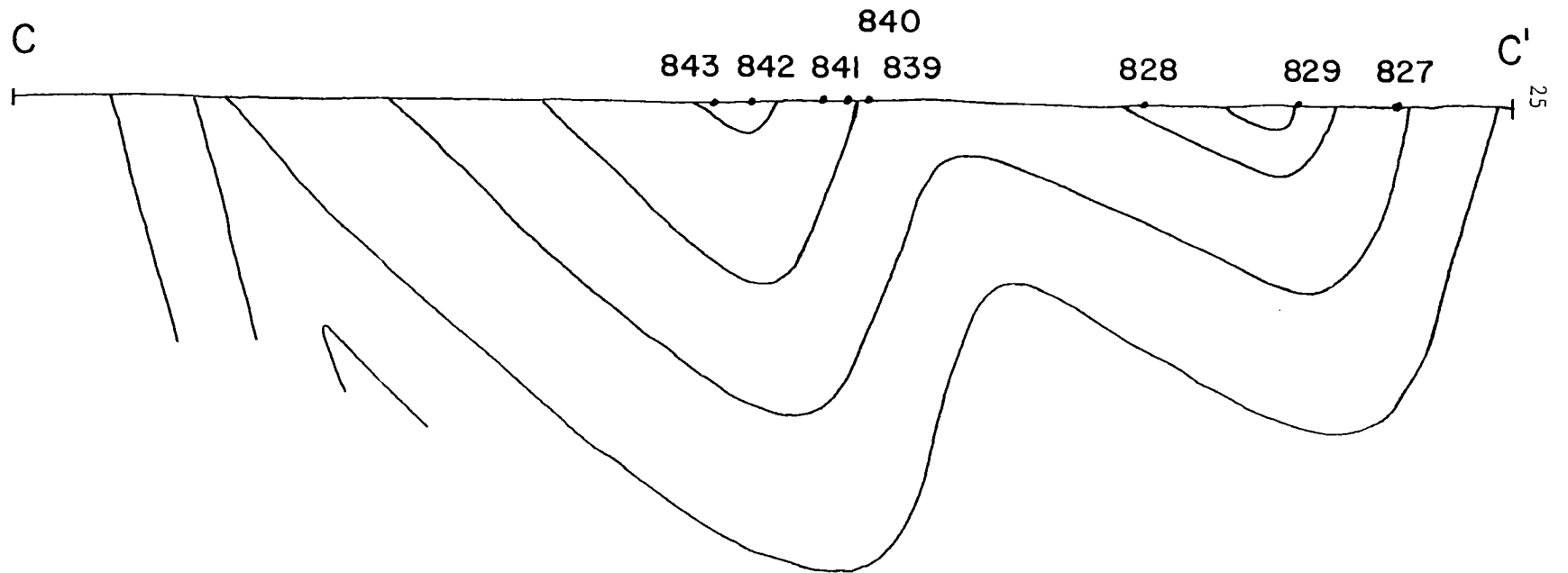
Stone Bridge - Federal Hill



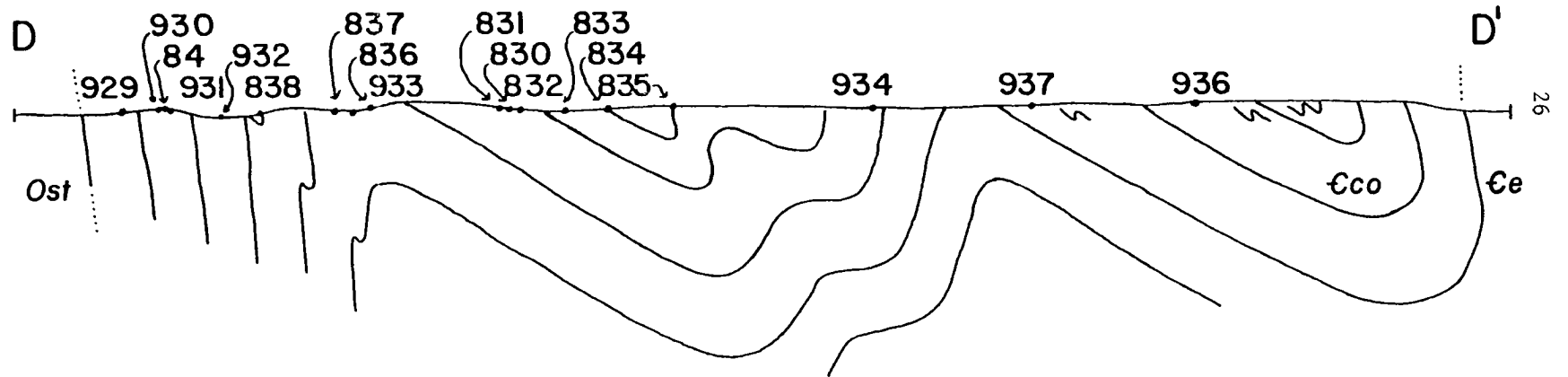
Millwood - Blandy



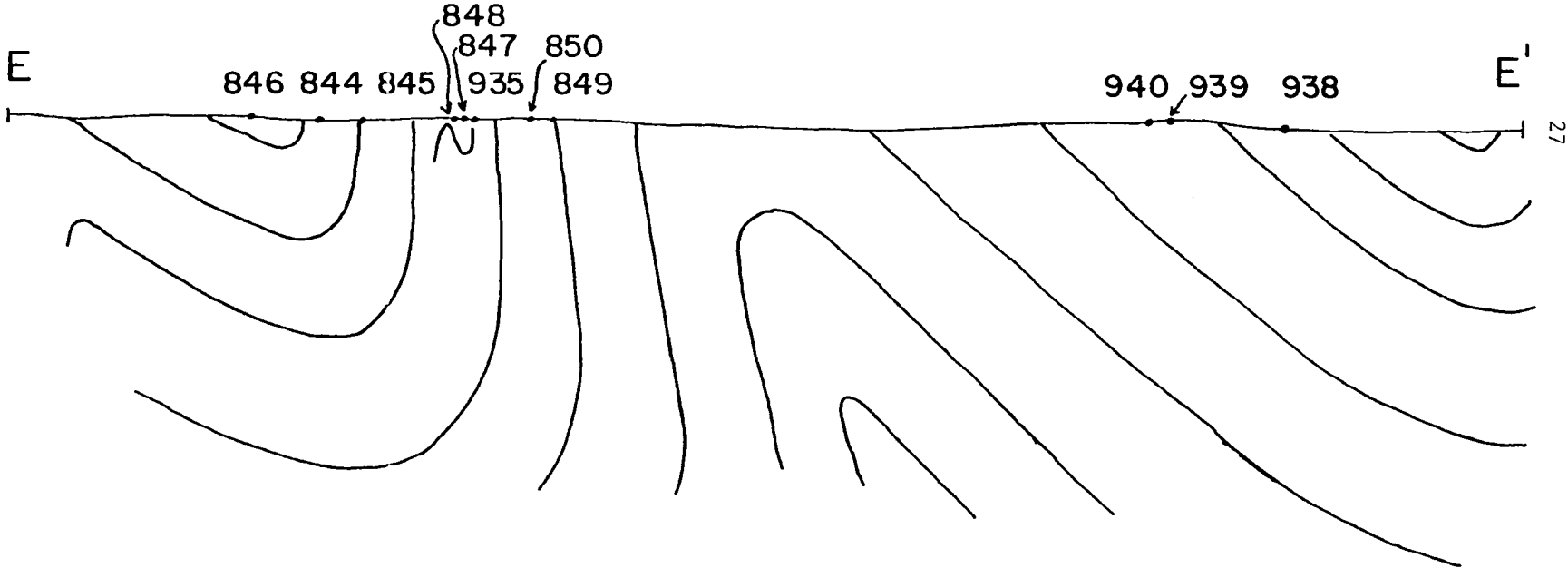
Longwood - 651



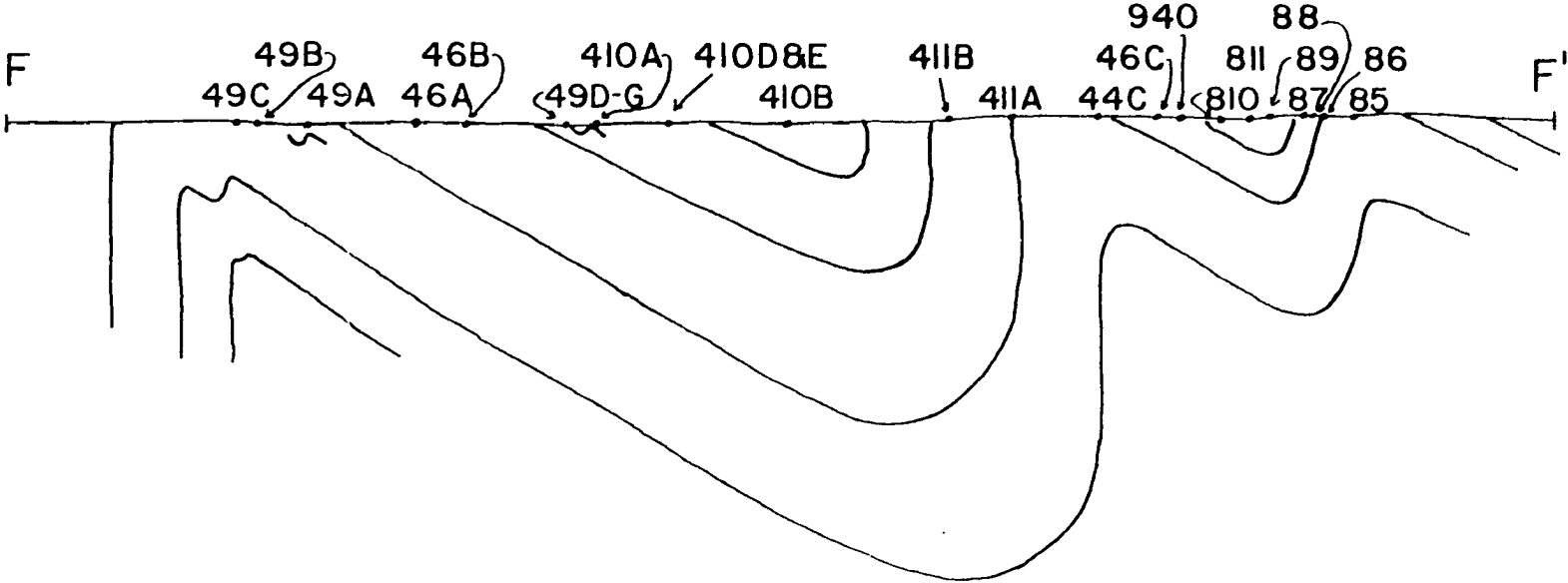
Chapel Run - Pigeon Hill



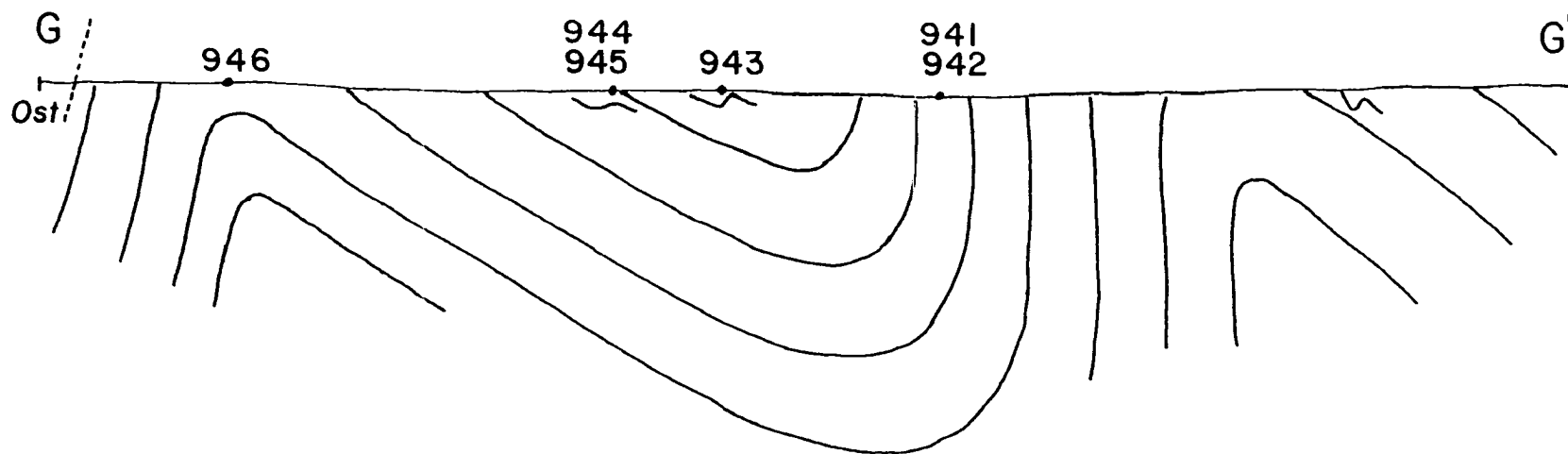
Craig Run



Long Marsh Run



Bullskin Run



collected on the traverses. These can be used to locate the sample and its contained data on the fold. The cross-sections were prepared by projecting the data from the traverse onto a fold profile plane. The fold axis was determined by using a Fisher and Watson statistical program for orientation data on the sphere (for source listings of the programs used in this paper refer to Appendix A). The projection of the data onto the cross-sections was done using a Summagraphics TD digitizer to locate the data on an orthogonal grid. The data points were then projected onto the plane of cross-section. Orientation data collected in the field were projected onto this plane using trigonometric techniques. The apparent dips of bedding and cleavage plotted were plotted on the traverse sections. The cross-sections were prepared in two steps. The first step was to project equally spaced lines through the data so that the surface data points were honored. The fold, in morphology, was patterned after folds seen in the field on that traverse and after folds seen in thin-section. Steep limb attenuation was estimated by measuring attenuation on 6 folds which were found in thin-section. The cross-sections represent expressions of the fold geometry and relations in the field and can be used to locate samples for the comparison of accumulated and incremental strain histories across individual folds to cleavage geometries in collected samples on the folds.

The data for these comparisons were collected from the oriented thin-sections using the following procedures.

Estimation of Accumulated Strain

The use of deformed ooids in the determination of finite strain axes is well documented (Cloos, 1947, 1971; Ramsay, 1967; Elliott 1968, 1970; Dunnet, 1969; Dunnet and Siddans, 1971; LeTehoff, 1979; DePoar, 1980; Siddans, 1980). In most studies oriented samples are cut on three planes which are usually but not always orthogonal. This allows the estimation of strain in three dimensions. The fluctuation of axial ratio and axial orientation is a function of the amount of strain and of the initial shape distribution of the particles being deformed

(Cloos, 1947, 1971; Ramsay, 1967; Elliott, 1970, Dunnet, 1969). The maximum variance of axial orientation (as much as 90 degrees in areas of low strain) decreases with increasing strain (Cloos, 1947; Ramsay, 1967; Elliott, 1970).

In this study the cut plane of the thin-sections is normal to the local fold axis and the view is down plunge. Deformation in the region of sample collection is approximated by plane strain so the deformed ooids in this section will only show the variance of initial population shape. In the samples studied, the fluctuation is relatively low and well within the sample preparation error margins. For sample populations of 50 or more the ooid long axis measured should correspond to the axis of maximum bulk elongation. Accumulated strain was measured in 7 thin sections, where each thin section contained a population of deformed ooids large enough to insure reproducibility of the data set. The estimation of accumulated strain involved two steps.

Preparation of Oriented Thin Sections. Samples were oriented by marking strike and dip and north on a surface. The plane of section was then identified as the plane normal to the local fold axis. This plane was located on the sample using standard rotation techniques with a Schmidt Equal Area stereonet. A thin section was prepared whose base faced down the plunge of the fold on which it was collected.

Measurement of Axial Ratios and Orientations. Photographs were prepared of the oriented thin sections using Kodak Technical Pan film and a Bolens Illumitron slide copier with a Bolens macro lens. The resultant high contrast negatives were projected orthogonally onto a Summagraphics digitizing tablet. The orientation of the projector and digitizer were checked by projecting a square grid onto the tablet and correcting any distortion by moving the projector. Distortion due to spherical aberration of the lenses used was negligible. The use of high contrast negatives allowed for the easy identification of deformed ooids in the samples.

To simplify calculation of axial ratios and long axis orientation the Summagraphics digitizer was connected to a Tektronix computer with a plotter. The data were stored in memory as endpoints of line segments with each ooid comprising 4 endpoints. Long axis orientations

were plotted and the mean and standard deviation of axial ratios and long axis orientation were calculated. The resultant plots for each thin section can be seen in Figures 8a-j. Strain ellipsoids with the appropriate axial ratios were plotted on the traverse cross-sections.

Estimation of Incremental Strain

Preserved particle displacement paths in progressive deformation can be used to calculate the orientation and magnitude of the principal strain axes for each point on the displacement path (Wickham, 1973; and Ramberg, 1975). The displacement path can be divided into a series of line chords of arbitrary length each with definable end points. The orientation of the principal strain axes can be calculated for each incremental line chord relative to an arbitrary rotating reference frame by:

$$\tan 2\theta = \frac{2(x'y' - xy)}{x'^2 - y'^2 - x^2 + y^2} \quad (1)$$

where θ = angle from the arbitrary reference frame to the principal strain axis, x, y is the initial location of a point, and x', y' is the final location of that point.

The transformation constants of each strain increment can be estimated by:

$$\begin{bmatrix} e_{11} & e_{12} \\ e_{21} & e_{22} \end{bmatrix} = \begin{bmatrix} \cos\theta & -\sin\theta \\ \sin\theta & \cos\theta \end{bmatrix} \begin{bmatrix} E_1 & 0 \\ 0 & E_2 \end{bmatrix} \begin{bmatrix} \cos\theta & \sin\theta \\ -\sin\theta & \cos\theta \end{bmatrix} \quad (2)$$

where θ = angle to principal strain axis, e_{11} , e_{12} , e_{21} , and e_{22} are transformation constants, $E_1 = x'/x$ in the rotated reference frame, and $E_2 = y'/y$ in the rotated reference frame.

The incremental strain matrix and the corresponding strain measures can be estimated in a system which preserves displacement paths. Fibrous growths of calcite on quartz grains in the Conococheague Formation preserve a displacement path for the sample in which they occur (Wickham, 1973). The incremental strain history of a sample can be accumulated over time to estimate finite strain. Wickham (1973) tested the validity of the process briefly outlined above by comparing the accumulated strain calculated by this process with the finite strain calculated from deformed ooids within the samples

Figure 8(a-h): Plots of ooid axial ratios, accumulated strain ellipse and statistical values for samples containing deformed ooids. These plots are not oriented in space but are presented as they were digitized.

81078 D31

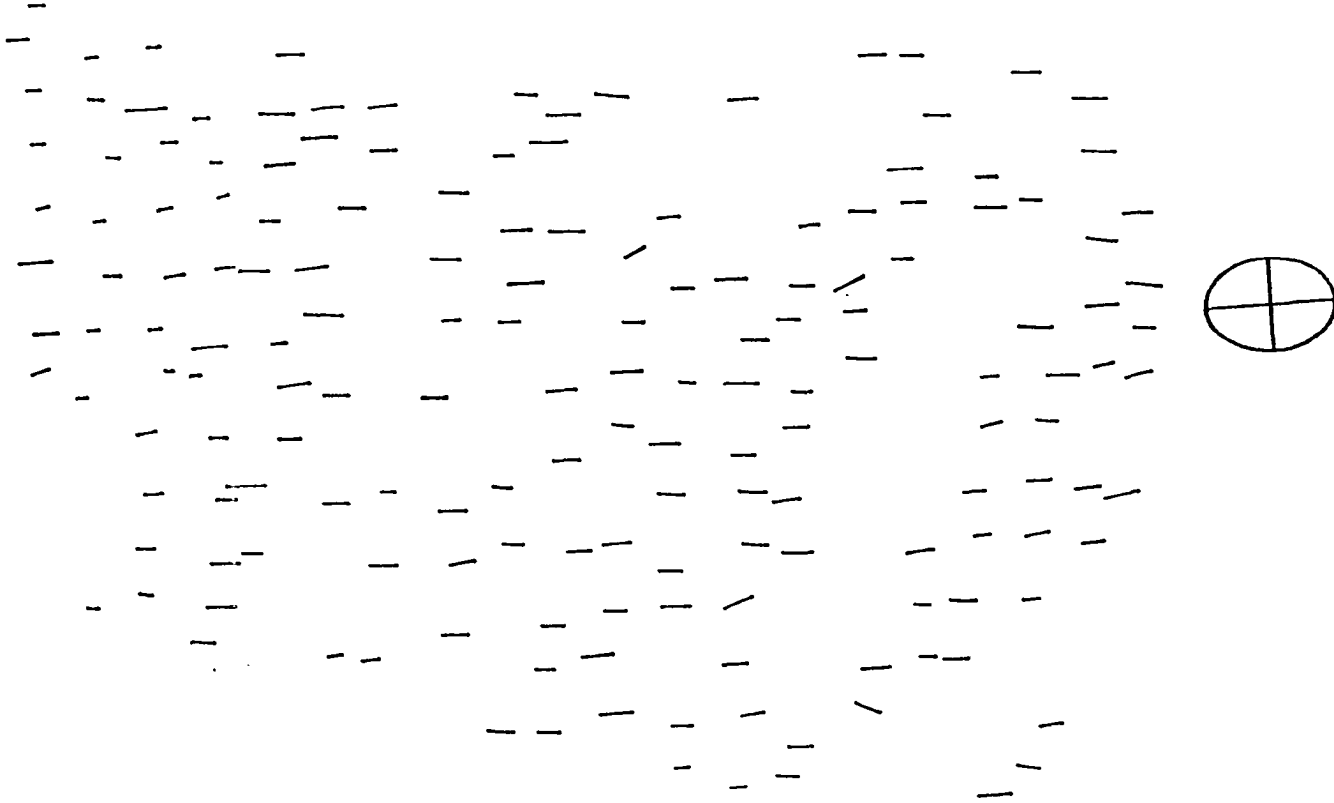
AXIAL RATIO MEAN = 1.58

STANDARD DEVIATION = 0.28

ORIENTATION MEAN = 3.02

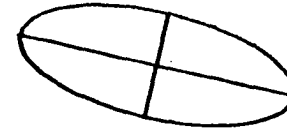
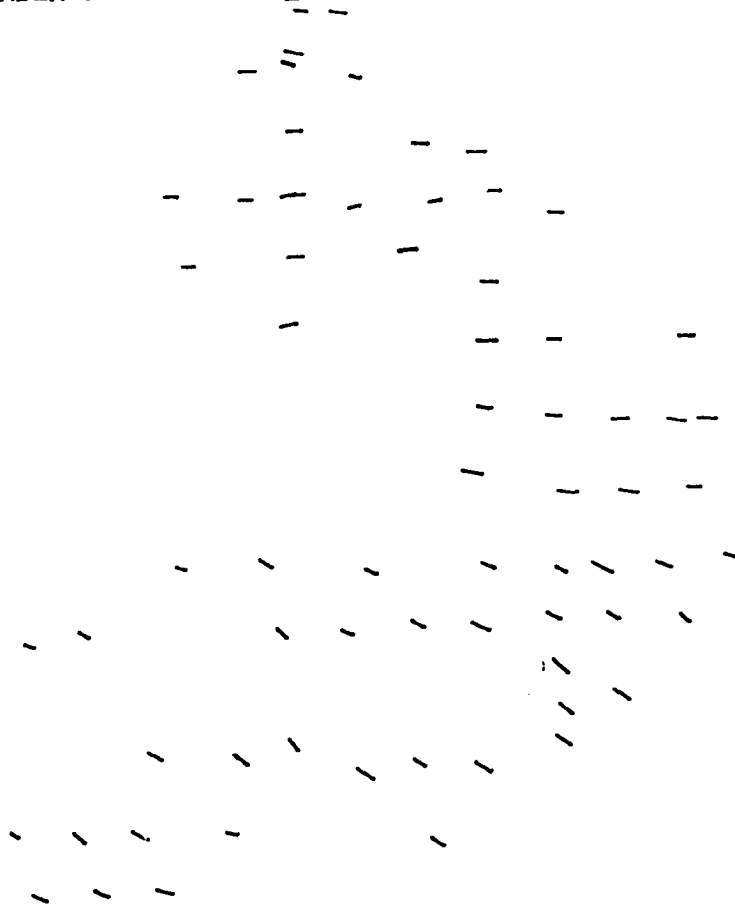
STANDARD DEVIATION = 6.39

NUMBER OF OOLDS = 169



CRAIG RUN D 45 CLOSEUP
AXIAL RATIO MEAN = 3.01
ORIENTATION MEAN = -15.26
NUMBER OF OIDS = 70

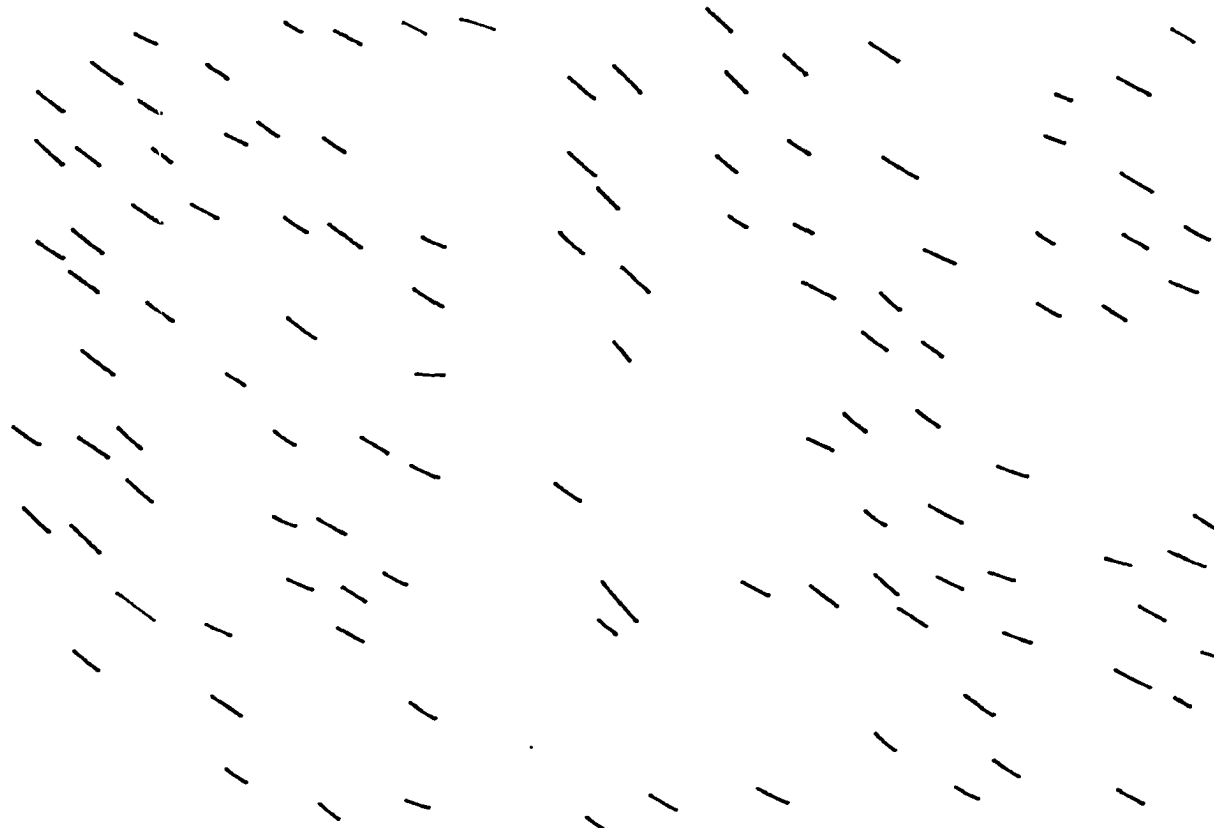
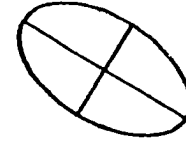
STANDARD DEVIATION = 1.15
STANDARD DEVIATION = 16.33



924

AXIAL RATIO MEAN = 2.04
ORIENTATION MEAN = -31.23
NUMBER OF OOLDS = 117

STANDARD DEVIATION = 0.37
STANDARD DEVIATION = 7.15



928

AXIAL RATIO MEAN = 2.10
ORIENTATION MEAN = 46.70
NUMBER OF OIDS = 83

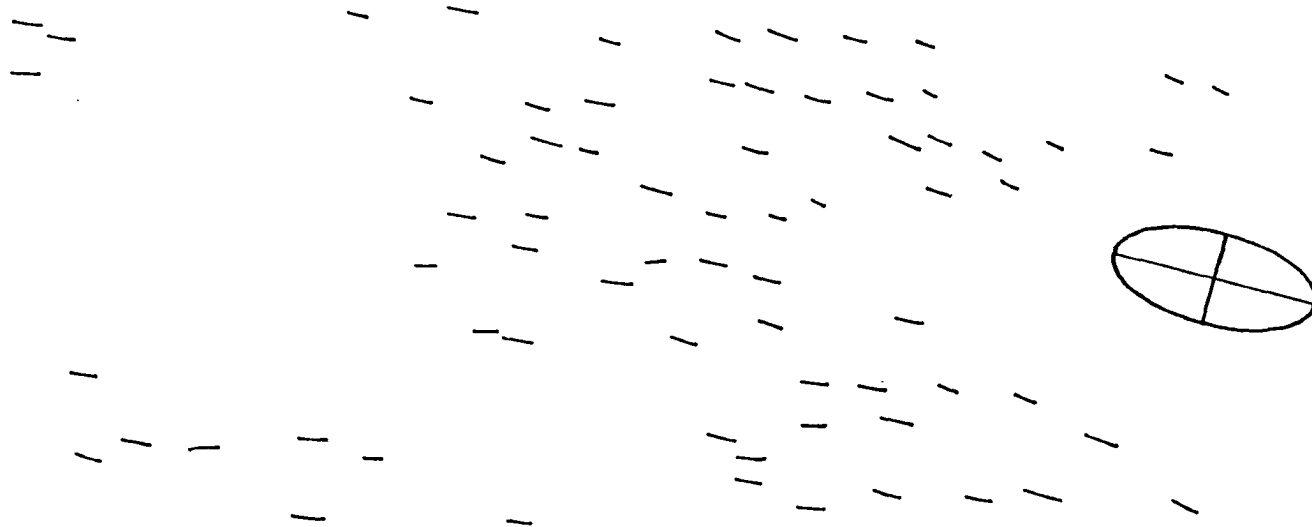
STANDARD DEVIATION = 0.49
STANDARD DEVIATION = 8.40



930

AXIAL RATIO MEAN = 2.55
ORIENTATION MEAN = -14.09
NUMBER OF OIDS = 71

STANDARD DEVIATION = 0.64
STANDARD DEVIATION = 7.32



933

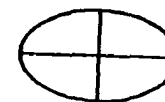
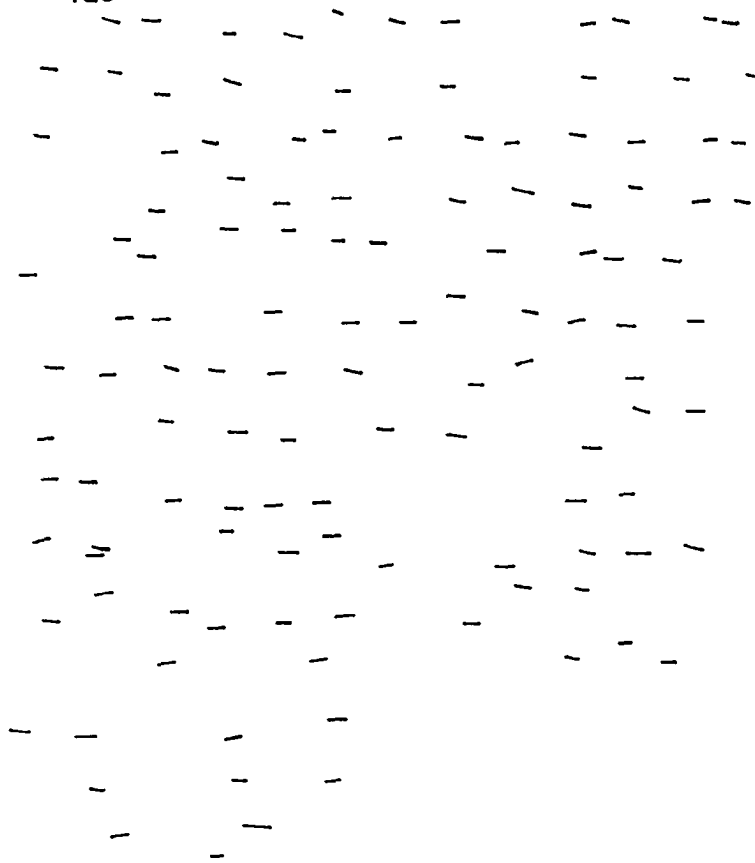
AXIAL RATIO MEAN = 1.92

STANDARD DEVIATION = 0.36

ORIENTATION MEAN = -3.26

STANDARD DEVIATION = 7.72

NUMBER OF OIDS = 125



936 MICRITE

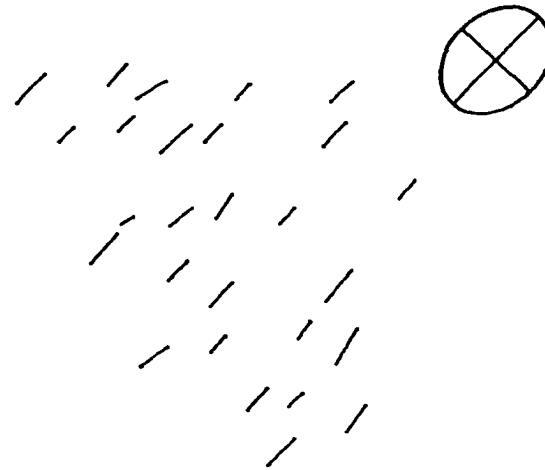
AXIAL RATIO MEAN = 2.15
ORIENTATION MEAN = 62.45
NUMBER OF OIDS = 66

STANDARD DEVIATION = 0.47
STANDARD DEVIATION = 20.55



936 NODULE
AXIAL RATIO MEAN = 1.51
ORIENTATION MEAN = 45.48
NUMBER OF OIDS = 27

STANDARD DEVIATION = 0.20
STANDARD DEVIATION = 6.58



CRAIG RUN 938

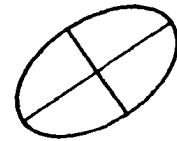
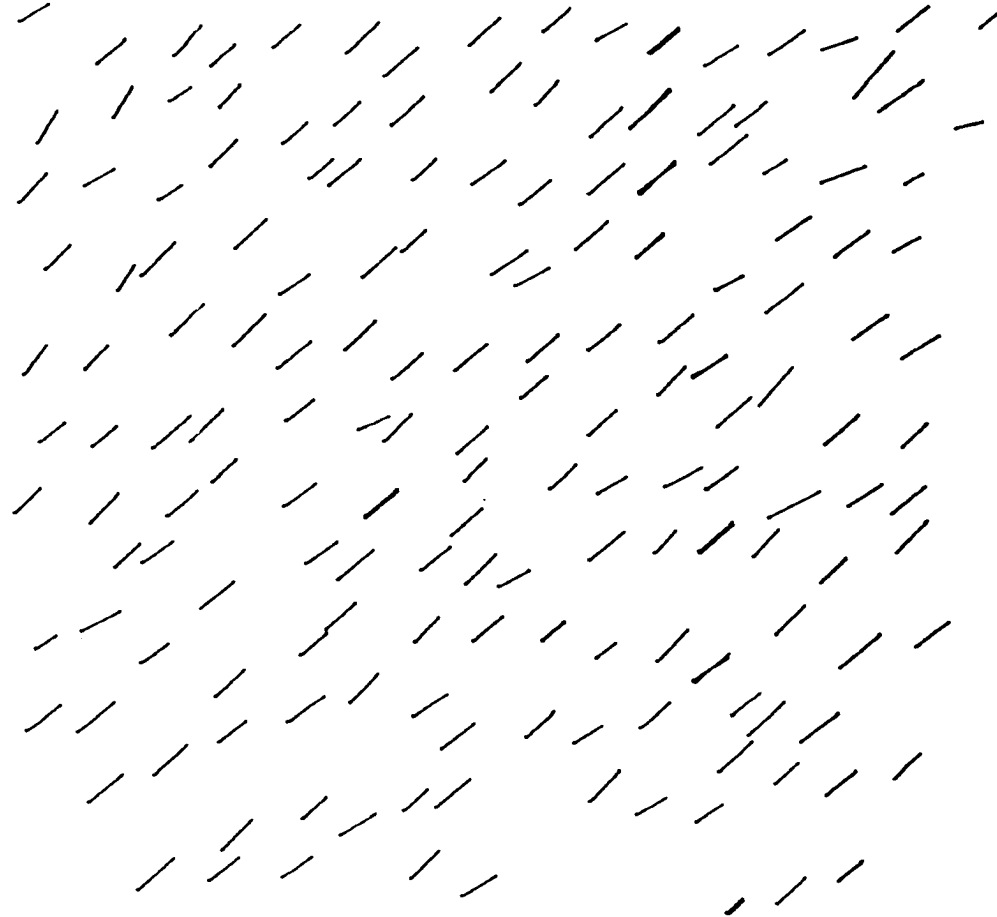
AXIAL RATIO MEAN = 1.93

STANDARD DEVIATION = 0.28

ORIENTATION MEAN = 33.31

STANDARD DEVIATION = 6.11

NUMBER OF OIDS = 199



collected. In that test the calculated accumulated strain closely approximated the measured finite strain.

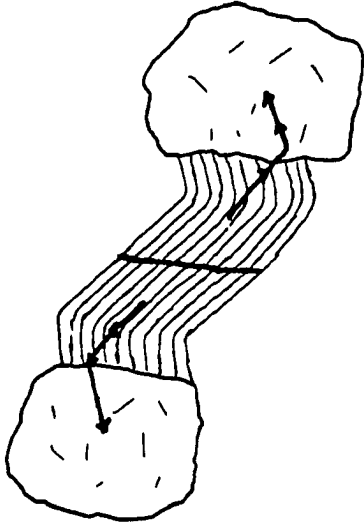
There has been some debate about the displacement path assumed from the fiber sets used for incremental strain estimation (Wickham, 1973, 1978; Durney and Ramsay, 1973). Figure 9 shows two different displacement paths. Displacement path A assumes that crystal growth occurs at the grain boundary. The particle displacement path will match the pressure shadow geometry. In case A the fibers will be oldest at the suture and youngest at the grain boundary. Displacement path B assumes that crystal growth occurs at the suture. The particle path in case B will mirror the pressure shadow fibers. In case B the fibers will be oldest at the grain boundary and youngest at the suture. The paths in Figure 10 assume that the grain centroids are displaced as point masses. The true displacement can be determined from the sense of rotation of the orientation of maximum principal shortening that would be expected on a fold limb during progressive deformation. Figure 10 shows this sense of rotation. From Figure 10 it is apparent that fiber growth at the grain boundary gives the proper sense of rotation of shortening around a fold.

Incremental strain paths were calculated from photomicrographs of oriented thin-sections. The thin sections were cut with the plane of the thin-section normal to the local fold axis and so the observer is looking down plunge on the fold. The data from the thin-sections can then be rotated into any reference frame desired to show the deformation as it would be observed in that reference frame as it rotates during the deformation. Grain centroids of fiber sets were marked on the photographs. The fiber sets were then divided as closely as possible into chords of equal length. The marked photos were digitized on a Summagraphics TD digitizing tablet. The data were rotated so that the reference frame used corresponded to the present day dip of bedding and stored on disk. The data were analyzed using the Tektronix 4051, and a plot of the incremental strain path was prepared and compiled into composite paths for each sample.

These plots are shown in Figure 11a-d. These strain paths are an

Figure 9: Possible displacement paths drawn for a pair of quartz grains. The paths show the path for each grain centroid relative to the suture. The paths represent the two possible interpretations of displacement path based on the assumptions that A) fiber growth occurs at the grain boundary and B) fiber growth occurs at the suture.

a.



b.

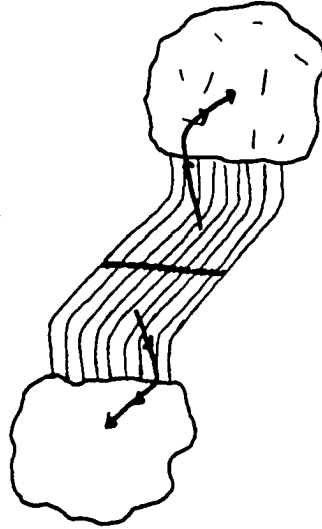


Figure 10: Incremental strain path for shallow and steep limbs of a fold. This figure illustrates the sense of range of orientation for incremental shortening that an observer standing on the bedding plane would see through time during folding. This figure is drawn assuming that fiber growth is at the grain boundary.

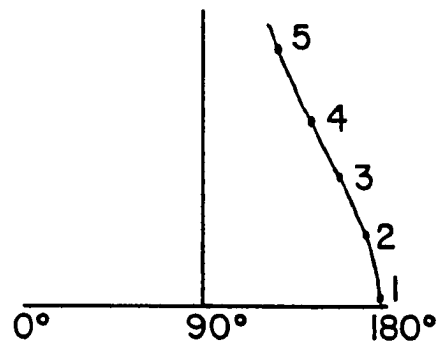
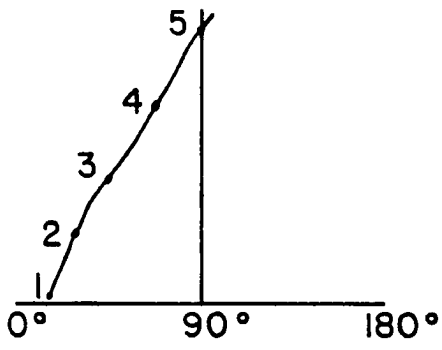
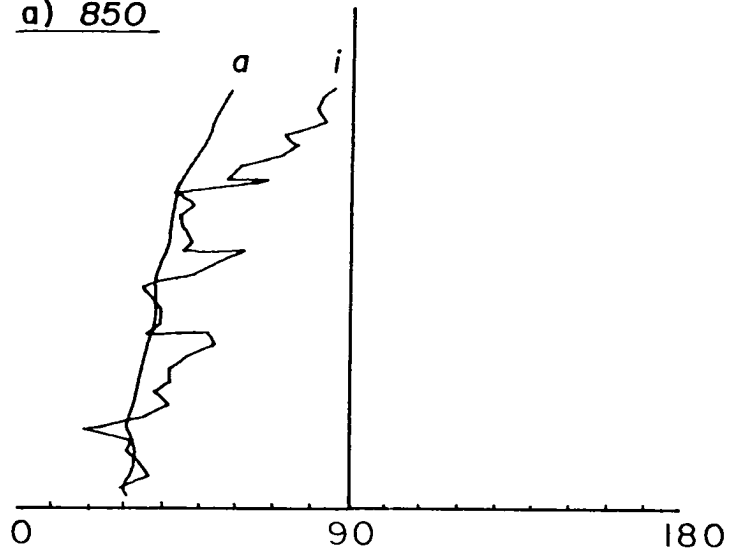
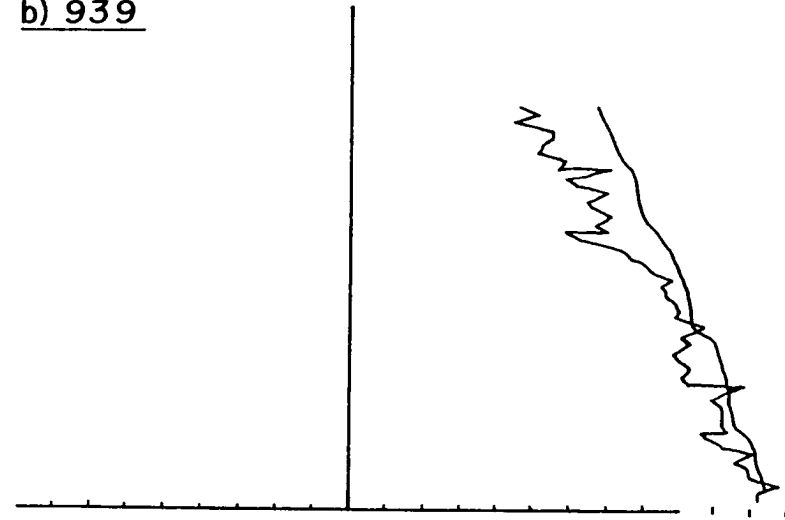


Figure 11: Composite strain paths for samples 816, 850, 937 and 950. These paths were prepared using the techniques described in this section. Horizontal axis is orientation of maximum shortening relative to bedding. Vertical axis is time.

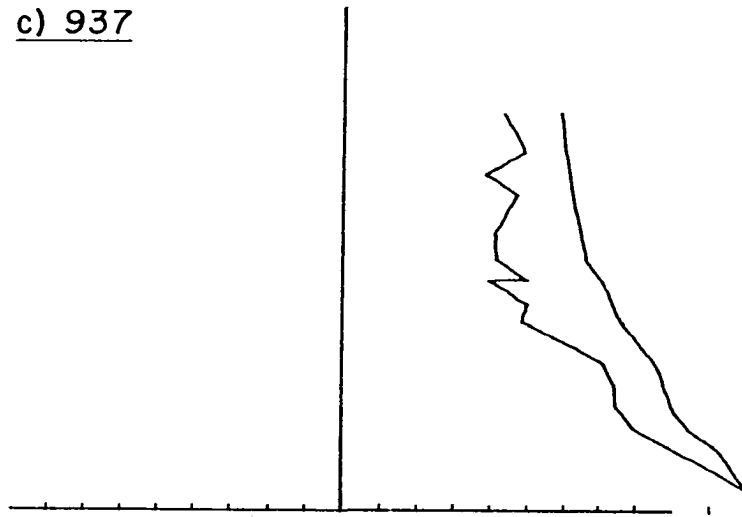
a) 850



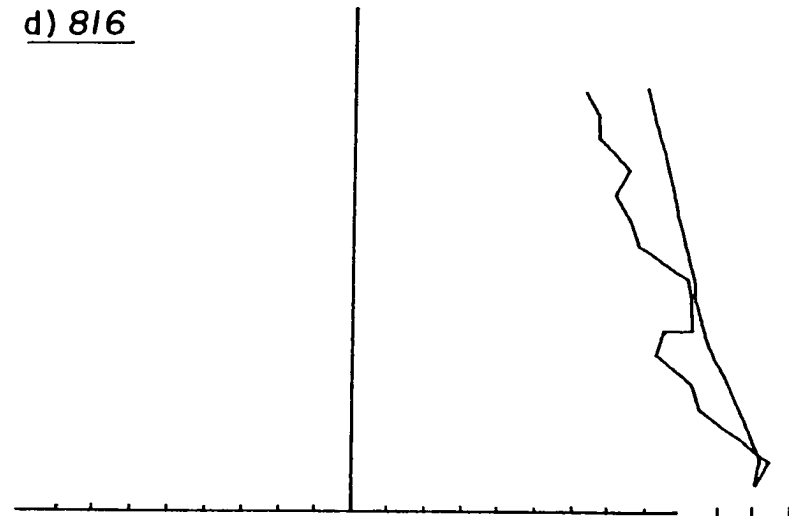
b) 939



c) 937



d) 816



expression of the orientation of simple quadratic shortening through time. The horizontal axis of the plots represents the angle to principal strain, measured clockwise, for that increment (as measured from an arbitrary reference frame in the deforming material which is rotating with bedding on the fold limb). The true amount of rotation cannot be measured, but an approximation of this rotation can be made by comparing the orientation of bedding to assumed initial horizontality. The strain paths can therefore be thought of as a measure of the orientation of simple shortening through time as seen by an observer standing on the bedding plane during deformation. The strain path depicted shows the orientation of maximum shortening for that period of time preserved by the pressure shadows.

Derivation of equations

Basic concepts of infinitesimal strain. Let R be a closed region in a progressively deforming continuous medium which contains a homogeneous material body. At some time t the body is deformed and displaced into some region R' . The region R can be described by one system of Euclidean curvilinear coordinates (x,y) . The region R' can be described by a second system of Euclidean curvilinear coordinates (x',y') . A point $P(x,y)$, in region R , is transformed into a point $P'(x',y')$, in region R' , during the deformation event and may be described in terms of coordinates (x,y) or x',y' . If R is initially undeformed, the final configuration in R' may be described as

$$\begin{aligned}x' &= x'(x,y;t) \\ y' &= y'(x,y;t)\end{aligned}\tag{3}$$

if the functions (x',y') are continuous and differentiable. This necessary condition is satisfied if the material does not fail during the deformation. Since there is a one to one correspondence between points in the two regions, x and y may be described as

$$\begin{aligned}x &= x(x',y';t) \\ y &= y(x',y';t)\end{aligned}\tag{4}$$

For a deformation starting at $t=0$ and ending at $t=\text{constant}$ then the time factor may be left out of equations (3) and (4).

The displacement of the point P can be represented by the displacement vector, q , such that

$$q = iu + jv \quad (5)$$

The components of the displacement vector, u and v , are expressed as

$$\begin{aligned} u &= x' - x \\ v &= y' - y \end{aligned} \quad (6)$$

Mathematically, the necessary condition that there exists a one to one correspondence of points between the two regions can be written as

$$J = \begin{vmatrix} \frac{\partial x'}{\partial x} & \frac{\partial x'}{\partial y} \\ \frac{\partial y'}{\partial x} & \frac{\partial y'}{\partial y} \end{vmatrix} > 0 \quad (7)$$

or in terms of the displacements.

$$J = \begin{vmatrix} 1 + \frac{\partial u}{\partial x} & \frac{\partial u}{\partial y} \\ \frac{\partial v}{\partial x} & 1 + \frac{\partial v}{\partial y} \end{vmatrix} > 0 \quad (8)$$

When the displacement field (u,v) satisfies the condition in equation (8) the deformation is continuous and proper.

The elements of the determinant characterize the gradients of the displacement vector, q , with respect to x and y , such that

$$\begin{aligned} \text{grad } q &= i i \frac{\partial u}{\partial x} + i j \frac{\partial v}{\partial x} + \\ & j i \frac{\partial u}{\partial y} + j j \frac{\partial v}{\partial y} \end{aligned} \quad (9)$$

This can be written in matrix notation as

$$\text{grad } q = \begin{bmatrix} \frac{\partial u}{\partial x} & \frac{\partial v}{\partial x} \\ \frac{\partial u}{\partial y} & \frac{\partial v}{\partial y} \end{bmatrix} \quad (10)$$

Since this gradient is a second order tensor, it may be represented as the sum of a symmetric tensor, corresponding to the pure strain components, and an antisymmetric tensor, corresponding to the rigid rotation of the volume:

$$\text{grad } q = \begin{bmatrix} e_{11} & e_{12} \\ e_{21} & e_{22} \end{bmatrix} + \begin{bmatrix} 0 & \omega_{12} \\ \omega_{21} & 0 \end{bmatrix} \quad (11)$$

Therefore, any deformation can be thought of as a component of pure strain and a component of rotation.

For simplicity, the location of a point after deformation (x',y') may be expressed in terms of the initial location (x,y) and a set of transformation constants which describe the strain of the region from a non-rotating reference frame. As such,

$$\begin{aligned} x' &= ax + by \\ y' &= cx + dy \end{aligned} \quad (12)$$

Where a,b,c , and d are the transformation constants. Substituting equation (12) into equation (6), the displacement components can be expressed in terms of the initial location and the transformation constants:

$$\begin{aligned} u &= (a-1)x + by \\ v &= cx + (d-1)y \end{aligned} \quad (13)$$

It is possible to write all of the measures of strain (such as quadratic elongation, shear, rotation, principal directions etc.) in terms of the transformation constants. Likewise, the gradient of the displacement vector, q , can be written in terms of the transformation constants:

$$\text{grad } q = \begin{bmatrix} \frac{\partial u}{\partial x} & \frac{\partial u}{\partial y} \\ \frac{\partial v}{\partial x} & \frac{\partial v}{\partial y} \end{bmatrix} = \begin{bmatrix} (a-1) & b \\ c & (d-1) \end{bmatrix} \quad (14)$$

Since the displacements can be factored into two components, a symmetric, pure strain component and an antisymmetric, pure rotation component, the transformations in equations (12), (13), and (14) can be factored into pure strain followed by pure rotation (Biot, 1965):

$$\begin{bmatrix} a & b \\ c & d \end{bmatrix} = \begin{bmatrix} \cos\omega & -\sin\omega \\ \sin\omega & \cos\omega \end{bmatrix} * \begin{bmatrix} e_{11} & e_{12} \\ e_{21} & e_{22} \end{bmatrix} \quad (15)$$

where $e_{12} = e_{21}$ and w is the angle to the rotated reference frame from which the strain matrix is measured.

Incremental nature of progressive strain. So far the time of deformation considered has been from some time $t=0$ to $t=c$ where c is a constant. During this time, P has been displaced to P' . The particle path from P to P' may not be a straight line. In the case of a curved displacement path the orientation and axial ratio of each progressive fraction of the displacement path will be different from the preceding fraction and the following fraction. The total strain for the displacement path over $t=0$ to $t=c$ is path independent. The magnitude and orientation of the strain for each fraction of time along the displacement path is path dependent. When a displacement path is divided into a series of increments, each increment will preserve the orientation and magnitude of strain for that fraction of time, t . For each increment, the location of the point after deformation can be expressed in terms of the initial location and the specific transformation constants, as shown in equation (12). Given a displacement path divided into 'n' increments, the displacement increment can be expressed as:

$$\begin{bmatrix} x_1 \\ y_1 \end{bmatrix} = \begin{bmatrix} a_1 & b_1 \\ c_1 & d_1 \end{bmatrix} \begin{bmatrix} x_0 \\ y_0 \end{bmatrix} \quad (16)$$

An additional property of the individual increments is that they will accumulate multiplicatively, resulting in the final configuration.

$$\begin{bmatrix} x' \\ y' \end{bmatrix} = \begin{bmatrix} a_n & b_n \\ c_n & d_n \end{bmatrix} \dots \begin{bmatrix} a_2 & b_2 \\ c_2 & d_2 \end{bmatrix} \begin{bmatrix} a_1 & b_1 \\ c_1 & d_1 \end{bmatrix} \begin{bmatrix} x \\ y \end{bmatrix} \quad (17)$$

Where (x_0, y_0) is the initial position and (x', y') is the final or nth position.

Estimating orientation and magnitude of incremental strain. In a system which preserves natural particle displacement paths, it is possible to determine the magnitude and orientation of strain for a series of increments along this displacement path. The particle displacement path will preserve the deformation path for the region containing the displacement path assuming that the deformation is

homogeneous, progressive and proper.

From equation (12) and (15) it is known that any homogeneous deformation can be written in terms of transformation constants and can be factored into a pure strain component and a pure rotation component. If a homogeneous deformation is assumed to be irrotational, equation (15) becomes

$$\begin{bmatrix} a & b \\ c & d \end{bmatrix} = \begin{bmatrix} e_{11} & e_{12} \\ e_{21} & e_{22} \end{bmatrix} \quad (18)$$

Substituting this into equation (12),

$$\begin{bmatrix} x' \\ y' \end{bmatrix} = \begin{bmatrix} e_{11} & e_{12} \\ e_{21} & e_{22} \end{bmatrix} \begin{bmatrix} x \\ y \end{bmatrix} \quad (19)$$

If the coordinate frame is rotated to a direction of principal strain the equation simplifies to

$$\begin{bmatrix} X' \\ Y' \end{bmatrix} = \begin{bmatrix} E_1 & 0 \\ 0 & E_2 \end{bmatrix} \begin{bmatrix} X \\ Y \end{bmatrix} \quad (20)$$

where (X',Y') is the final location of the point in the now rotated system and (X,Y) is the initial location of the point in the rotated system. Completing the multiplication,

$$X' = E_1 X \text{ or } E_1 = X'/x \quad (21a)$$

$$Y' = E_2 y \text{ or } E_2 = Y'/y \quad (21b)$$

Multiplying equation(21a) by equation(21b),

$$X'Y' = E_1 E_2 XY \quad (22)$$

Now, by definition $E_1 \cdot E_2 / XY$ is equivalent to

$$\det \begin{bmatrix} E_1 & 0 \\ 0 & E_2 \end{bmatrix} * XY \quad (23)$$

To simplify this equation, it is assumed that there is no area

strain in the region being considered (Wickham, 1973). Therefore,

$$\begin{vmatrix} E_1 & 0 \\ 0 & E_2 \end{vmatrix} = 1 \quad (24)$$

and equation (22) becomes

$$X'Y' = XY \quad (25)$$

The rotated coordinates may be related to the original coordinates by

$$\begin{bmatrix} X \\ Y \end{bmatrix} = \begin{bmatrix} \cos\theta & \sin\theta \\ -\sin\theta & \cos\theta \end{bmatrix} \begin{bmatrix} x \\ y \end{bmatrix} \quad (26a)$$

and

$$\begin{bmatrix} X' \\ Y' \end{bmatrix} = \begin{bmatrix} \cos\theta & \sin\theta \\ -\sin\theta & \cos\theta \end{bmatrix} \begin{bmatrix} x' \\ y' \end{bmatrix} \quad (26b)$$

where θ is the angle of rotation between the principal strain and the original unrotated reference frame. These linear equations can be substituted into equation(25), as follows:

$$\begin{aligned} (x'\cos\theta + y'\sin\theta)*(-x'\sin\theta + y'\cos\theta) = \\ (xcos\theta + ysin\theta)*(-x'\sin\theta + ycos\theta) \end{aligned} \quad (27)$$

Multiplying ,and collecting terms

$$(x'y' - xy)(\cos^2\theta - \sin^2\theta) = (x'^2 - y'^2 - x^2 + y^2)(\cos\theta \sin\theta) \quad (28)$$

Now rearranging terms,

$$\frac{(x'y'-xy)}{(x'^2-y'^2-x^2+y^2)} * \frac{(\cos^2\theta - \sin^2\theta)}{(\cos\theta\sin\theta)} \quad (29)$$

For simplicity let $N = \left[\frac{x'y'-xy}{x'^2-y'^2-x^2+y^2} \right]$

Equation (29) may be rewritten as

$$N * \left[\frac{\cos^2\theta - \sin^2\theta}{\cos\theta\sin\theta} \right] = 1 \quad (30)$$

Substituting the double angle identities shown below,

$$\cos^2\theta - \sin^2\theta = \cos 2\theta = 1 - \tan^2\theta / 1 + \tan^2\theta \quad (31a)$$

$$\cos\theta \sin\theta = \frac{1}{2} \sin 2\theta = \tan\theta / 1 + \tan^2\theta \quad (31b)$$

into equation (30) yields

$$N * \left[\frac{1 - \tan^2\theta / 1 + \tan^2\theta}{\tan\theta / 1 + \tan^2\theta} \right] = 1 \quad (32)$$

Simplifying equation (32),

$$N * \left[\frac{1 - \tan^2\theta}{\tan\theta} \right] = 1 \quad (33)$$

or

$$N = \frac{\tan\theta}{1 - \tan^2\theta} \quad (34)$$

Since

$$\frac{\tan\theta}{1 - \tan^2\theta} = \frac{1}{2} \tan 2\theta \quad (35)$$

Equation (35) can be rewritten as:

$$\tan 2\theta = \frac{2(x'y' - xy)}{x'^2 - y'^2 - x^2 + y^2} \quad (36)$$

Equation (36) corresponds to equation (1).

The orientation of a principal strain axis can be determined if the initial and final endpoints of a single strain increment are known. θ is the angle to a principal strain axis from an arbitrary reference frame which is rotating with bedding.

In order to determine the magnitude of the incremental strain and to calculate the standard strain measurements, it is necessary to know

the transformation constants for that strain increment. A direct consequence of equation (36) is that it is possible to relate the strain matrix,

$$\begin{bmatrix} E_1 & 0 \\ 0 & E_2 \end{bmatrix} \quad (37)$$

back to the original reference system by substituting equations (26a) and (26b) into equation (20), such that:

$$\begin{bmatrix} \cos\theta & \sin\theta \\ -\sin\theta & \cos\theta \end{bmatrix} \begin{bmatrix} x' \\ y' \end{bmatrix} = \begin{bmatrix} E_1 & 0 \\ 0 & E_2 \end{bmatrix} \begin{bmatrix} \cos\theta & \sin\theta \\ -\sin\theta & \cos\theta \end{bmatrix} \begin{bmatrix} x \\ y \end{bmatrix} \quad (38)$$

Now, substituting equation (19) into equation (38),

$$\begin{bmatrix} \cos\theta & \sin\theta \\ -\sin\theta & \cos\theta \end{bmatrix} \begin{bmatrix} e_{11} & e_{12} \\ e_{21} & e_{22} \end{bmatrix} \begin{bmatrix} x \\ y \end{bmatrix} = \begin{bmatrix} E_1 & 0 \\ 0 & E_2 \end{bmatrix} \begin{bmatrix} \cos\theta & \sin\theta \\ -\sin\theta & \cos\theta \end{bmatrix} \begin{bmatrix} x \\ y \end{bmatrix} \quad (39)$$

This equation can be simplified if $\begin{bmatrix} \cos\theta & \sin\theta \\ -\sin\theta & \cos\theta \end{bmatrix}$ is an

invertible matrix. A matrix is invertible if and only if the determinant of that matrix does not equal 0. Since

$$\begin{vmatrix} \cos\theta & \sin\theta \\ -\sin\theta & \cos\theta \end{vmatrix} = \cos^2\theta + \sin^2\theta = 1 \quad (40)$$

the rotation matrix is invertible. The inverse of a matrix is defined as

$$A^{-1} = (\det A)^{-1} \alpha \quad (41)$$

O'Nan (1971). α is the adjunct of A, where

$$\alpha = [A_{ij}]^T \quad (42)$$

In this case

$$A^{-1} = \frac{1}{\cos \sin} \begin{bmatrix} \cos\theta & -\sin\theta \\ \sin\theta & \cos\theta \end{bmatrix} \quad (43)$$

Completing the inversion and cancelling like terms, equation (39) becomes

$$\begin{bmatrix} e_{11} & e_{12} \\ e_{21} & e_{22} \end{bmatrix} = \begin{bmatrix} \cos\theta & -\sin\theta \\ \sin\theta & \cos\theta \end{bmatrix} \begin{bmatrix} E_1 & 0 \\ 0 & E_2 \end{bmatrix} \begin{bmatrix} \cos\theta & \sin\theta \\ -\sin\theta & \cos\theta \end{bmatrix} \quad (44)$$

Equation (44) corresponds to equation (2). From the above equation the transformation constants of each strain increment can be calculated and the magnitude and standard measurements of incremental strain determined.

Discussion of Procedure

Particle displacement paths are preserved in the Conococheague Formation as fibrous growth of calcite. The procedure used to estimate the incremental strain history involves 6 steps which are discussed below.

- 1) Collection of oriented samples: A suite of oriented samples of micritic limestone containing approximately 2% quartz sand was collected. The samples were located on the aerial photograph or topographic map relative to the local fold axis.
- 2) Preparation of oriented thin sections: The oriented samples were thin-sectioned with the plane of section matching, as closely as possible, the plane normal to the local fold axis. In each instance the observer is looking down plunge on the local fold when looking at the thin section.
- 3) Identification and photography of useable fibers: The oriented thin sections were studied using a petrographic microscope with a mounted mechanical slide holder. The slide holder established a reference frame of observation in which the thin section was being studied. The fibrous growths of calcite were most easily identified using plane polarized light. Of the 114 thin sections prepared and studied only 7, or 6% of the thin sections contained well preserved fibers. The fibers selected for study were those fibers that did not show any evidence of internal twinning or

recrystallization, both of which would distort the incremental strain path calculated from them. In addition only those fibers which grew from relatively isolated grains were used to minimize the effect of interference of other grains on the motion of the particles of interest. The effect of grain shape is also a factor in the strain path observed so equant or nearly equant grains were selected preferentially over inequant grains.

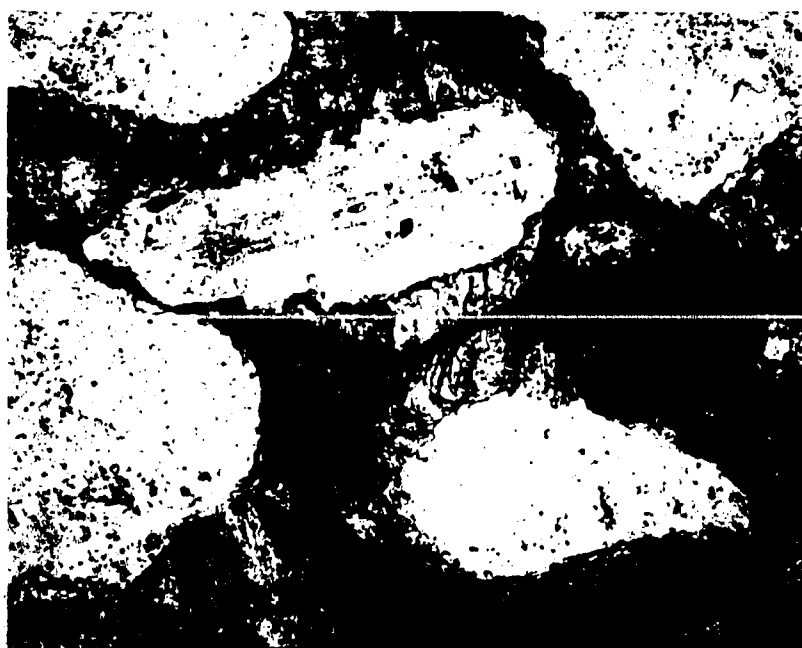
Several sections contained well preserved fibers which fit the above criteria. In some instances, however, only 1 or 2 fiber sets were preserved. An individual fiber set does not necessarily preserve the entire displacement history of the sample in which it forms. Only those sections which contained multiple fiber sets can give a minimum representation of the total displacement path for that sample, assuming that the displacement was approximately homogeneous, continuous and proper on the scale of the thin section. The seven samples used in this study fit the above conditions.

The fibers used in the study fall into two categories: singlets (see Figure 12), and doublets or multiple sets (see Figure 13). When useable fibers were identified they were photographed using either 35 mm Kodak Technical Pan film or 4X5 Polaroid Type 55 film. The orientation of the photographs was noted so the data from the photographs could be rotated. Eleven inch by fourteen inch photographic prints were made of each fiber set. The reference frame of the negative is identical with the reference frame of the positive print in two dimensions. When the fiber sets were larger than could be accommodated on a single negative a composite was made by traversing the fiber set and preparing overlapping prints. The prints were then spliced on a light table so that orientation was preserved across the fiber set.

- 4) Digitizing the data: Each fiber set contains at least one quartz grain and sets of fibers. The centroid of each grain was identified by measuring a series of diameters until a centroid was

Figure 12: Photomicrograph of fiber singlet from sample 816. The field of view is approximately 1.5 mm. The technique used to determine the incremental strain history from singlet fiber sets is described in this section.

Figure 13: Photomicrograph of double fiber set from sample 850. The field of view is approximately 1.5mm. The technique used to determine incremental strain history from these fibers is discussed in this section.



approximated. The final location of the centroid was established by visually determining the center of the zone identified by the measured diameters. The fiber sets were visually divided into equal length line segments. The endpoints of the segments were marked on the photographs. The number of line segments varied depending on the length of the fibers in the photograph. Since the trace of the fiber is a measure of time the actual number of increments, or line segments, along the fiber is arbitrary. The larger the number of increments the greater the accuracy in estimating the actual strain path. However, in many fiber sets the fibers are short enough that using a great number of points was impractical in terms of physically marking the points and in terms of the accuracy of the digitizing system used. Therefore, the results of the calculation of rotation will represent a minimum.

The marked photographs were placed on the digitizing tablet so that the reference frame of the photograph paralleled the reference frame of the digitizer. The endpoints of the increment line segments and the grain centroids were digitized and stored on the Tektronix 4097 floppy disks (see Program Digit, Appendix A). The digitizing scheme is as follows, refer to Figures 12 and 13.

For singlet fibers the motion of the grain centroid relative to the suture was measured for each fiber set. The first point digitized was the suture as the origin. The line segments were digitized toward the centroid. The last point digitized was the grain centroid.

For doublet fiber sets where two grain centroids could be measured from a common suture the digitizing scheme was similar. The suture was digitized as the origin followed by the line segment endpoints and the grain centroid. The cursor was returned to the origin and the process repeated in the opposite direction.

Each data set was labeled with the name of the data file, the number of the specimen, and number of the photograph and whether the data set was a singlet or doublet and right or left.

- 5) Rotation to desired orientation: The data sets stored on the disk

were digitized relative to a known reference system. The data sets could then be rotated to any reference system.

The orientation of each section relative to the horizontal in Virginia was known. The orientation of the data from each thin-section has a known relationship to bedding. It is easiest to think of deformation relative to bedding. The data were rotated so that the resultant strain paths were measured relative to bedding. This preserves the strain measures and the relations derived earlier.

- 6) Calculation of incremental strain measures and orientation: The orientation of a principal strain axis can be determined from equation 1 for the endpoints of an incremental line segment on a displacement path. The measures of the principal strain can be estimated if the transformation constants are known for that strain increment. The transformation constants can be calculated using equation 2. The strain measures calculated are 1) simple quadratic elongation, 2) angle between a reference frame parallel with bedding and the principal strain reference frame, 3) axial ratio of the strain ellipse, 4) area strain, and 5) components of the strain matrix.

The nature of incremental strain in a progressive deformation allows the multiplicative incorporation of each strain increment into the accumulated strain up to that increment. This allows the direct comparison of the incremental strain to accumulated strain up to and including that strain increment.

As shown in text Figure 10 there are two possible displacement paths for each fiber set. The direction of crystallization must be incorporated into calculations of the strain increments. Recall that the digitizing routine used assumed the origin at the suture and progressively digitized away. As seen in text Figure 10 this matches the assumption of crystal growth at the suture. The data sets must be corrected so that the origin is located at the grain centroid. A variety of strain measures were calculated and the orientation of the incremental and accumulated maximum principal shortening were plotted

for 119 fiber sets. These calculations were done using the techniques previously described. These plots are included in Appendix B.

Many of the fiber sets have large axial ratios in the final increment. Those samples which displayed axial ratios greater than 2.0 in the final increment were examined to see if pressure solution had occurred along the boundaries of the developing fiber set. Previous work (Ramsay and Wood, 1972; Wickham, 1973) has shown that an incremental volume loss will effect the strain path for any given specimen. Wickham, 1973, showed that the presence of area change will strongly effect the orientations calculated and the axial ratios. Based on this work those specimens with resultant calculated axial ratios greater than 2.0 which displayed solution activity in the vicinity of the fiber sets were not used in the preparation of the composite paths. The data sets with axial ratio value less than 2.0 can be seen in Appendix C along with the calculated strain attributes for the last increment.

Based on the plots of maximum principal shortening it is apparent that any one fiber set does not preserve the total sense of deformation that the specimen has experienced. One way to approximate the total deformation is to prepare composite paths for the sample. This can be done by superimposing those data sets or those portions of data sets which preserve non-overlapping orientations of the maximum principal shortening axis. During a deformation event the orientation of maximum principal shortening should start nearly parallel with layering and rotate toward bedding normals. In an asymmetric fold system the sense of rotation on a shallowly dipping limb should be from 180° toward 90° . The rotation and steeply dipping limb should be from 0° toward 90° . In the construction of composite paths the relative timing of each fiber set can be determined by the relative position on the fold and the orientation range for that data set. Those data sets with orientations close to parallel with bedding are relatively younger than those data sets with orientations nearly to perpendicular with bedding. The composite paths and its attributes can be calculated by passing the accumulated matrix from the last increment of one data set to the next data set where there is no overlap of orientation. In this way the

final axial ratio for a composite path may serve as an independent check of the validity of that path.

Only 4 of the original 7 samples were used to construct composite paths. These plots can be seen in Appendix C. Of these only sample 816 did not have a gap in orientation between the data sets and therefore has the most reasonable axial ratio. The other samples, 850, 937 and 939 all have gaps between individual data sets making up the composite path. Gaps in orientation between data sets induce apparent area strain and result in large final axial ratios for that composite. These 4 composite paths are seen in Figures 11a-d. These data will be used to compare cleavage orientations to and will give information regarding the deformation history of this region in the following sections.

RESULTS

Folds

General Observations

The field area is on the southeast limb of the Massanutten Synclinorium. Folds in the study area are mostly asymmetric and plunge gently toward the northeast. Fold amplitudes range from 1 km to less than 1 cm.

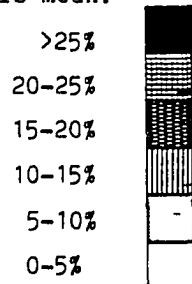
Poles to bedding plot along a narrow girdle on an equal area stereographic lower hemisphere projection (refer to Figure 4 and Figure 14). The best fit bedding pole great circle and the corresponding fold axis for each traverse and for the total Conococheague are compared in Figure 14. The Longwood traverse is not included in this Figure due to lack of sufficient orientation data. The plots in Figure 14 show contour diagrams prepared using standard Kalsbeek counting net routines for planar data. The best fit great circle and fold axis were determined using the techniques described in Ragan (1973). The best fit pole great circles and fold axes have similar orientations throughout the field area.

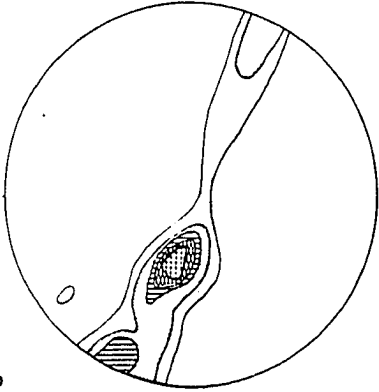
Fold asymmetry and interlimb angles decrease from south to north in the field area. Fold axial surfaces were determined in 6 plots (see Figure 14). The orientation of the fold axial surface does not vary systematically within the field area. The steepest axial surface dips 84°SE in the Craig Run Traverse, the shallowest dipping axial surface, 60°SE , is in the Bullskin Run Traverse. Fold axes determined by the intersection of cleavage and bedding in the hinge of folds and by statistical analysis of orientation data on the sphere are compared in Figure 15. The fold axes plot within a 42 degree radius. All measured and calculated plunges are to the northeast. The fold axes approximated by the contour diagrams are within the cone of

Figure 14: Density contour plots for poles to bedding on traverses in the field area. Lower hemisphere projection. The plots show the local fold axis.

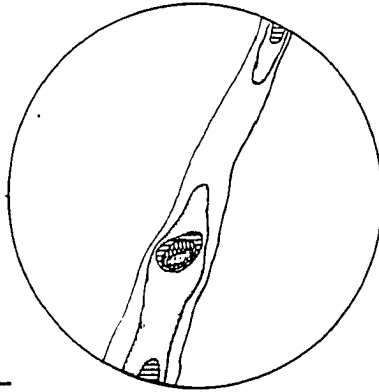
- a) Stone Bridge - Federal Hill
- b) Millwood - Blandy
- c) Chapel Run - Pigeon Hill
- d) Craig Run
- e) Long Marsh Run
- f) Bullskin Run

Symbols mean:

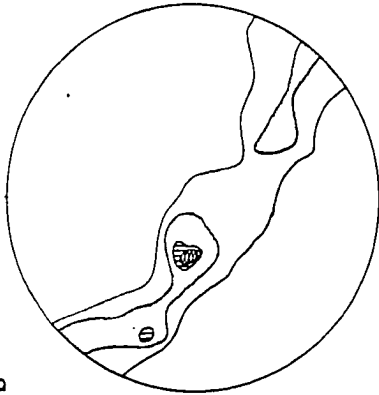




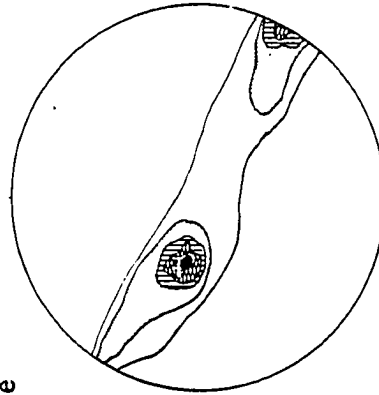
c



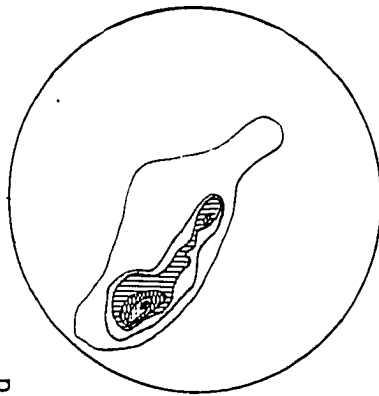
f



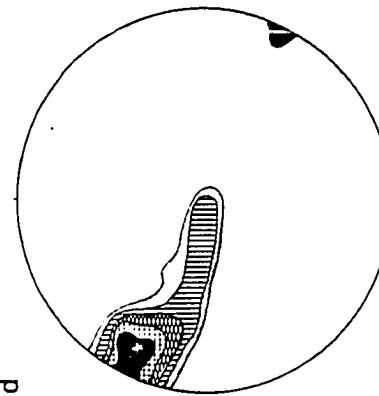
b



e



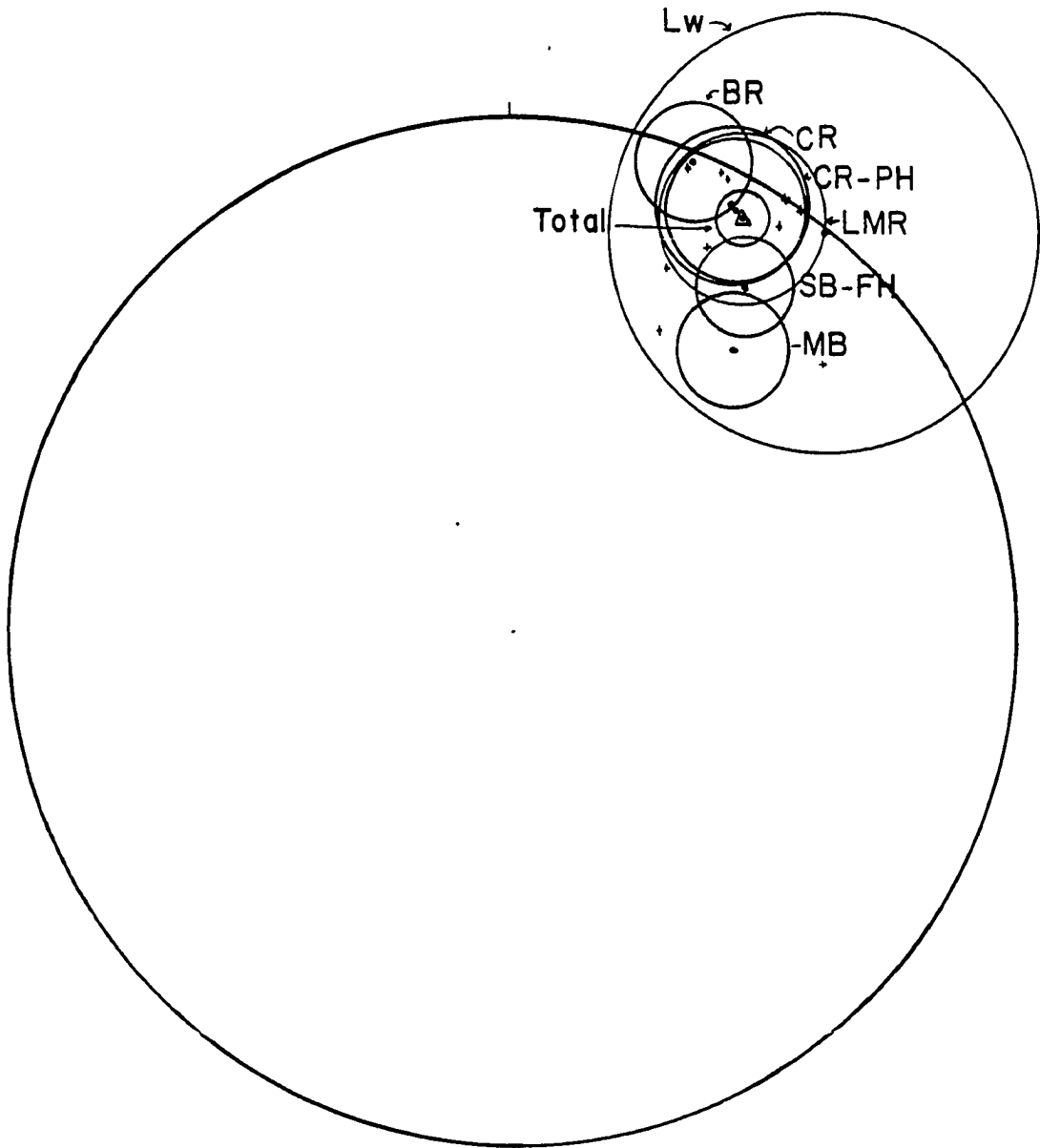
a



d

Figure 15: Lower hemisphere plots of fold axes. Axes marked by a dot are calculated using Fisher and Watson statistical techniques. Axes marked with a + are field measurements. Circles are the radius of cones of confidence. The triangle is the total data pole from the statistical analysis.

- SB-FH = Stonebridge - Federal Hill; 9 degrees radius
- MB = Millwood - Blandy; 13 degrees radius
- LW = Longwood; 42 degrees radius
- CR-PH = Chapel Run - Pigeon Hill; 16 degrees radius
- CR = Craig Run; 14 degrees radius
- LMR = Long Marsh Run; 15 degrees radius
- BR = Bullskin Run; 13 degrees radius
- Total = 6 degrees radius



confidence radius for the statistical analyses.

Fold axial orientation shows a change from south to north across the field area. From south to north the general trend is for shallowing of plunge and rotation of plunge direction toward the north. The similarity of axial surface orientation, bedding pole pattern and fold axes indicate that the folds were formed syntectonically and that they are parasitic on the Massanutten Synclinorium - Blue Ridge Anticlinorium. The presence of locally overturned folds and the variation in symmetry are consistent with the interpretation that the small scale folds are parasitic.

Interlimb angle was measured on 10 folds in the field area. These data are shown in Table 1.

Traverse	Interlimb angle(degrees)	Unit
Stone Bridge - Federal Hill	90	dolomite
	52	limestone-dolomite
	89	dolomite
	59	limestone-dolomite
	65	limestone-dolomite
Millwood - Blandy	40	limestone-dolomite
	85	dolomite
Longwood	71	limestone-dolomite
	50	sandstone-limestone
Craig Run	71	chert-dolomite

Table 1: Interlimb angles from 10 folds in the field area. The folds measured represent a range of fold sizes from outcrop scale to thin section scale.

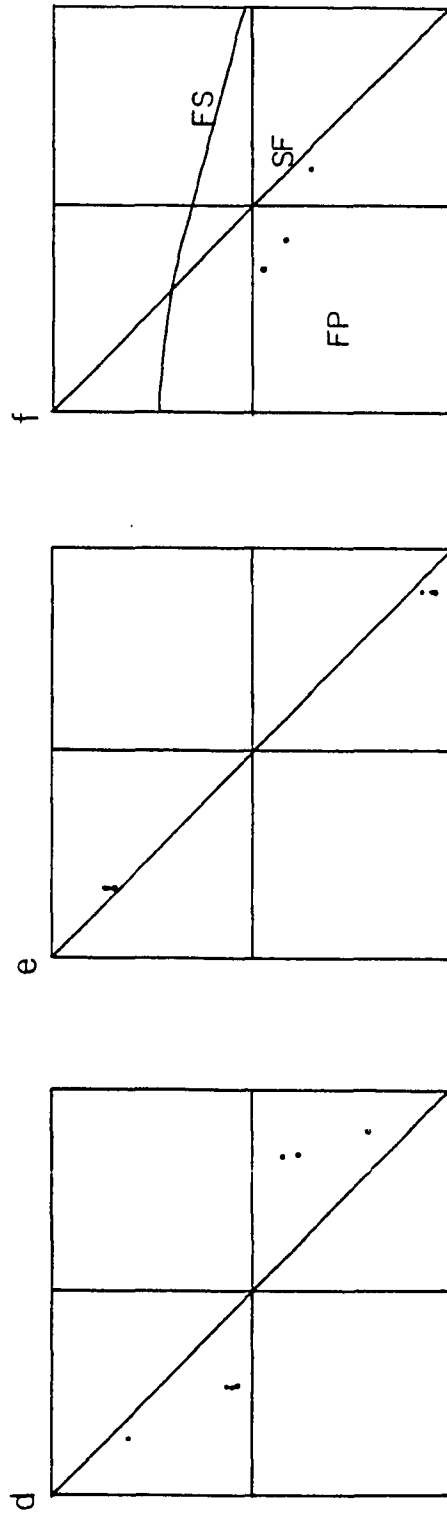
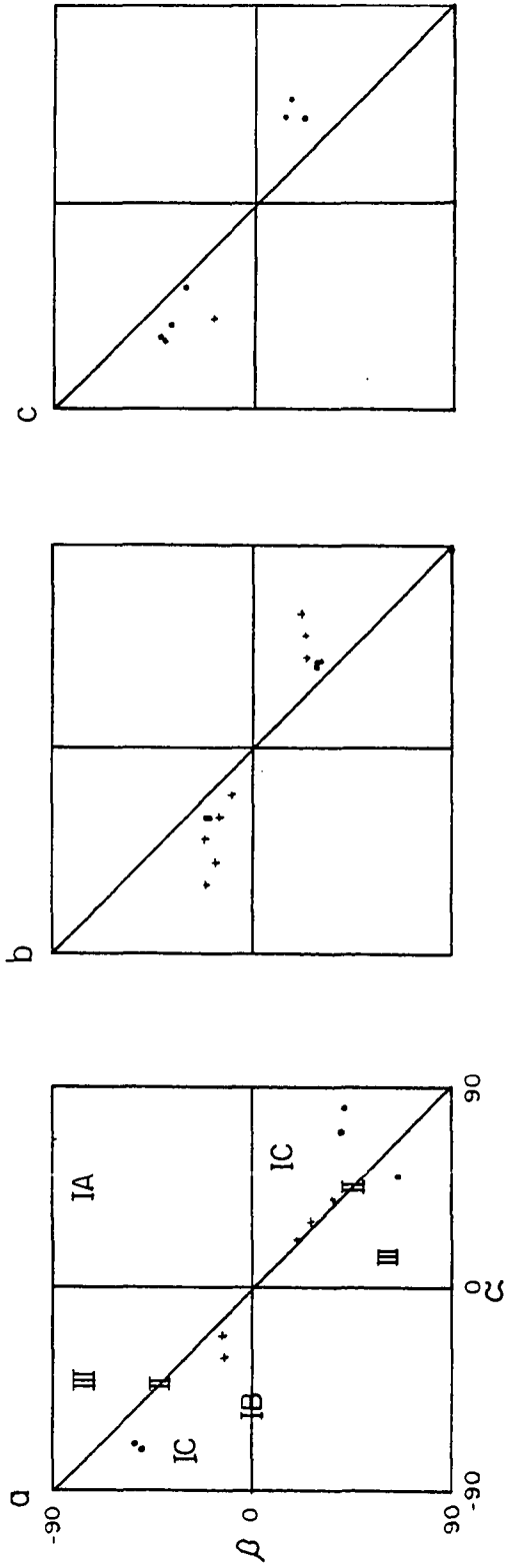
From these data it is apparent that interlimb angle depends on lithology. As a general trend tighter folds are present in interlayered limestones and dolomites and in sandstones. Folds formed in dolomites are more open. Interlimb angles in interlayered limestones and dolomites, here termed 'Ribbon Rock', vary from 40° to 71°. Interlimb angles in dolostones are higher, varying from 85° to 90°. Within the field area there is a general trend towards more open folds from south to north.

The folds in the study area were classified using the modified dip isogon-cleavage classification system (Treagus, 1982). In this classification system the angle of dip and the angle from the dip normal to cleavage are plotted as shown in Figure 16. In these plots

Figure 16: Cleavage - isogon plots for five samples using the techniques described by Treagus (1982).

- a) Sample 817
- b) Sample 842
- c) Sample 845
- d) Sample 95
- e) Sample 843
- f) Plot of elongation direction and dip isogon following the convention of Hudleston (1973) showing the fields of various fold models. In this plot SF is similar folding, FS is flexural slip folding and FP is flattened parallel folding. The measurements in this plot are from samples 842, 843 and 845 and are all in competent layers.

Angular values in all plots are measured according to convention. Beta is the angle between the cleavage trace and the bedding normal. Alpha is the normalized limb dip. The fields labeled IA, IB, IC, II, and III are equivalences of the isogonic 1a, 1b, 1c, 1l, and 1l suggested by Hudleston (1973) and Ramsay (1967).



the left hand side of folds and clockwise angles measured from the dip normal on the left hand side of the fold are negative, following the convention of Hudleston (1973). Standard isogon plots (Hudleston, 1973) were made of three folds where bedding was smoothest. These are superimposed in the plots. From these data it is clear that the folds are dominantly type Ic/1c folds with one sample being type III. This method represents an easy method for determining the fold classification in folded rocks assuming that the cleavage is axial planar at least in the fold hinge. In Figure 16 it is seen that the classification of the folds changes from fold to fold and may change from layer to layer within a multilayer fold. The variation of fold type may be due to viscosity variation between the layers of the fold. Cleavage is refracted at lithologic boundaries. This refraction can be interpreted as resulting from viscosity differences in the multilayer, (Treagus, 1981; 1982). Plots of the elongation axis of ooids found in sample 845 against dip isogon angle, see Figure 16, compromise a B_s plot (Hudleston, 1973; Treagus, 1982). This plot can be superimposed on a diagram showing the classic fold model ranges (Hudleston, 1973; Treagus, 1982). Three samples are plotted on this diagram. Sample 845 represents a true elongation axis plot and is in the flattening field of folding. Samples 817 and 843 were plotted on this diagram as well. Implicit in this plot is the assumption that in samples 817 and 843 the cleavage trace is nearly parallel with the axis of maximum elongation in the fold. From Figure 16 it is apparent that for samples 817 and 843 at least this assumption is valid. In the three cases tested the folds measured are flattening folds where cleavage is oriented close to the axis of maximum elongation. The layers used in the preceding measurements were either dolomite or chert. Measurements were not made in limestone layers.

Based on the preceding observations the following statements can be made regarding the folds within the field area. The tightness of folding diminishes to the northeast within the field area. The overall fold shape changes from south to north in the field area. Fold hinge zones are narrow and are not well exposed in the field. Exposed fold

hinge zones are rounded (see Figure 2). Interlimb angles measured on 10 folds range from 50° to 90° . There is thickening in the hinges and thinning on the steep limbs of folds. The folds are fully described as close to open, plunging, inclined, type Ic/1c, with minor type III folds (Ramsay, 1967; Hudleston, 1973; Treagus, 1981, 1982).

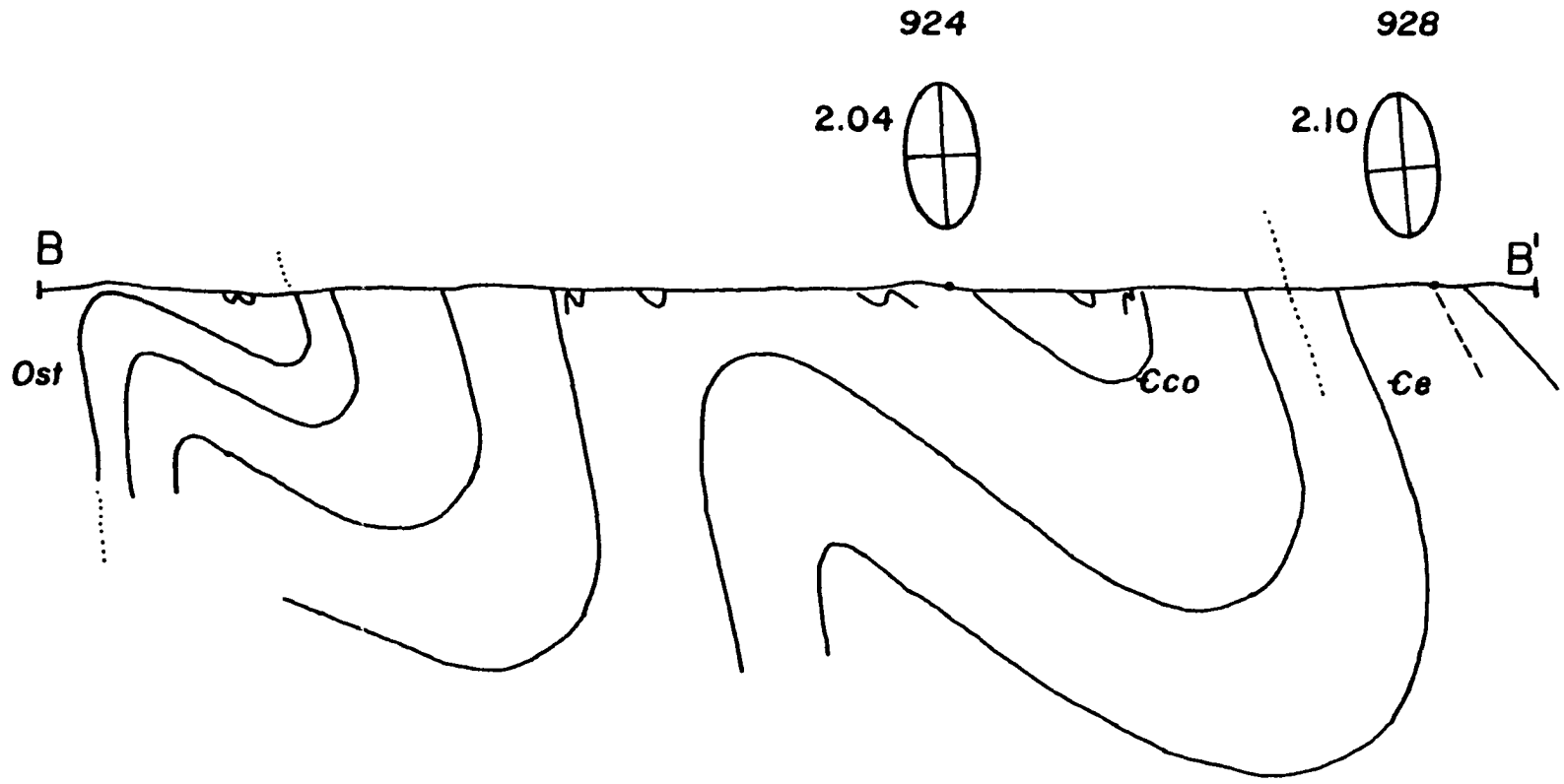
Finite strain ellipse axes (measured from deformed ooids) fan around the fold axes in a similar fashion to cleavage, (see Figure 17). The variation of ooid axial ratios about the folds shows that thinning has occurred on the steep limbs of folds, shortening has been greater on the attenuated steep limbs of the folds, deformation is the greatest in fold hinges and the folds are asymmetric.

Four samples were suitable for the construction of composite strain paths. These paths are shown in Figure 18. These composite paths represent the range in orientation for the principal shortening direction through time. As discussed earlier this range is probably a minimum. In the ideal, the axis of maximum principal shortening will be initially parallel with bedding on opposite limbs of folds (either 0° or 180° in Figures 10,11 and 18) and will rotate toward the bedding perpendicular (90° on Figures 10,11 and 18) with deformation. Strain paths calculated from the fibrous growths of calcite give representations of how folds initiated and grew. Anthony and Wickham (1978) have shown that asymmetric folds in a single layer can develop from symmetric buckles if the layer is inclined to the axis of maximum principal shortening. They concluded that the long limb of the fold will be the limb that was originally down with respect to the shortening direction, that if there is a thickness differential the shallowly dipping limb will be thicker and that the axes of accumulated principal strain will fan asymmetrically about the fold. The origin of folds in the field area has been discussed (Wickham and Anthony, 1978). In their paper Wickham and Anthony conclude that folding in this area initiated with layering inclined as much as 15° to the maximum principal shortening axis.

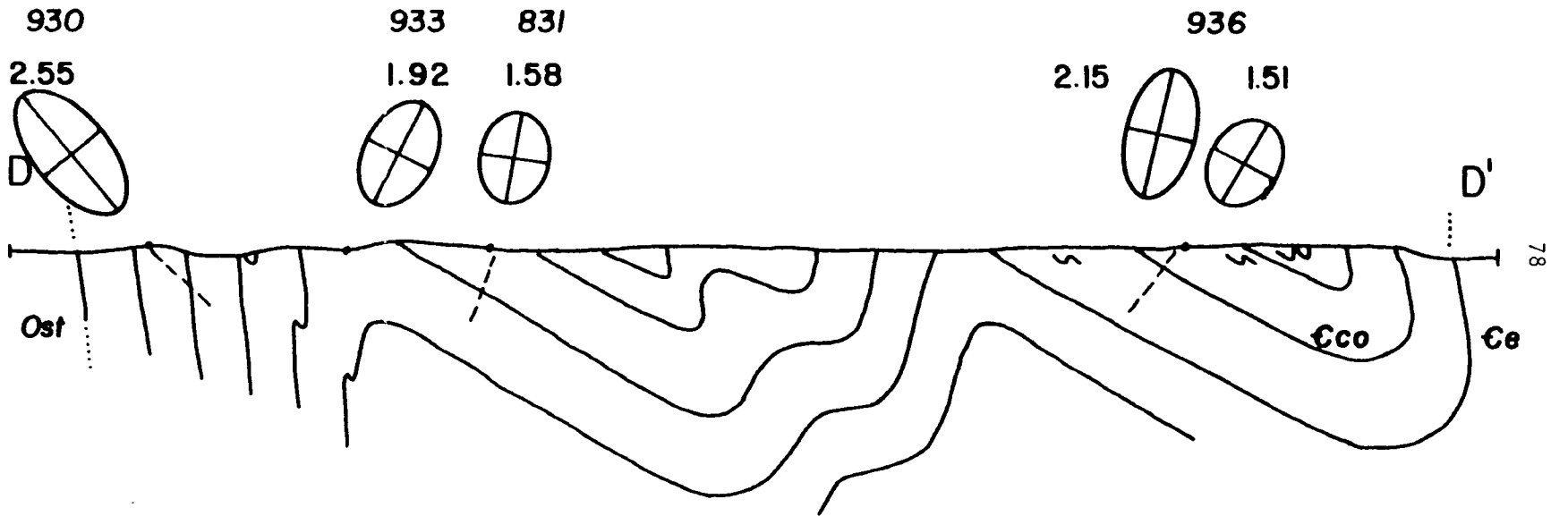
In this study, samples containing useable fibers were collected from both limbs of a fold. Figure 18 shows the composite paths for the fiber sets. The plots show the orientation of maximum principal

Figure 17: Traverse cross-sections with superimposed accumulated strain measures from deformed ooids. The ellipses are oriented in space. Dashed line represents cleavage orientation at that location. Sample number and axial ratios are shown.

Millwood - Blandy



Chapel Run - Pigeon Hill

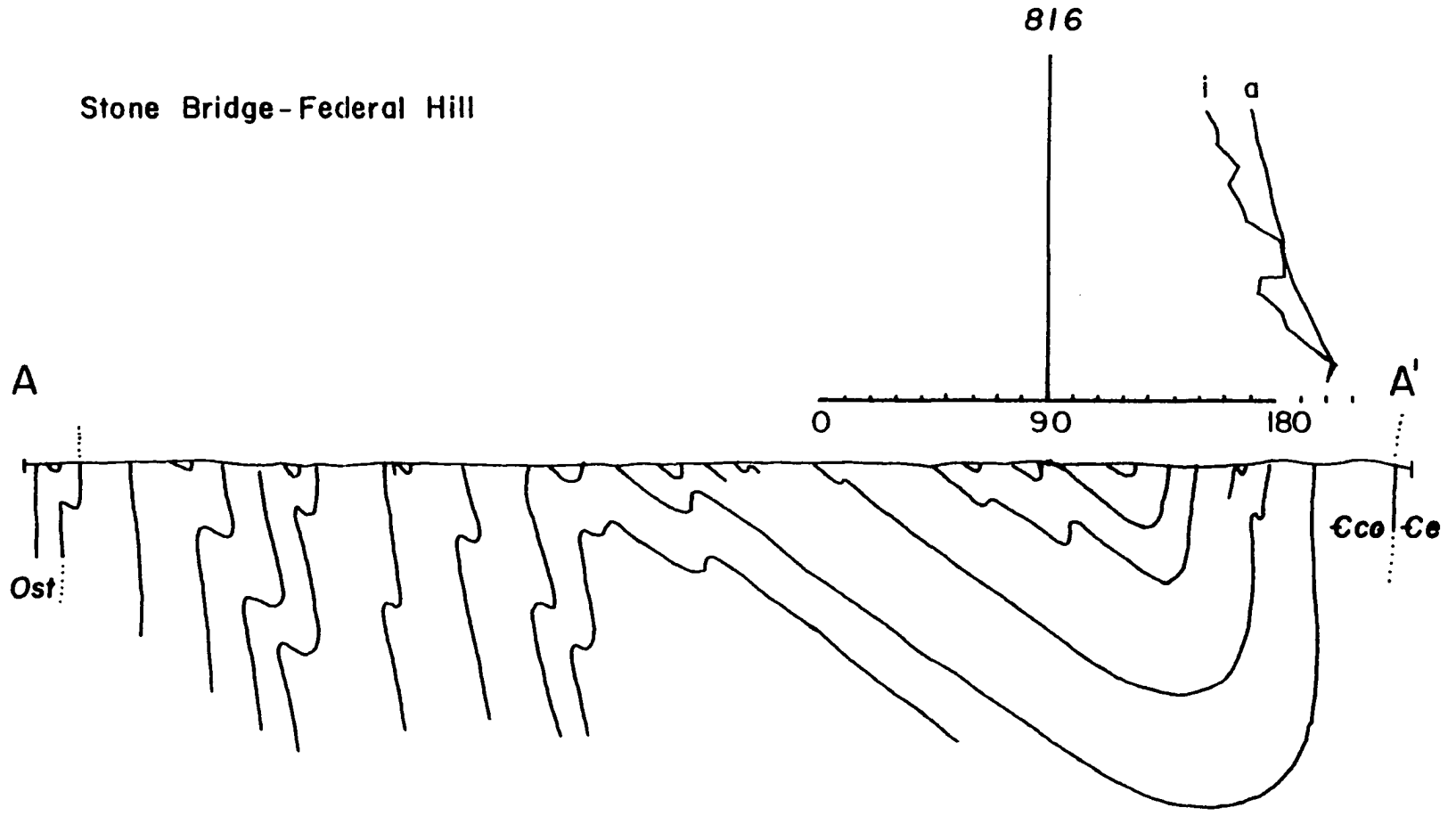


Craig Run

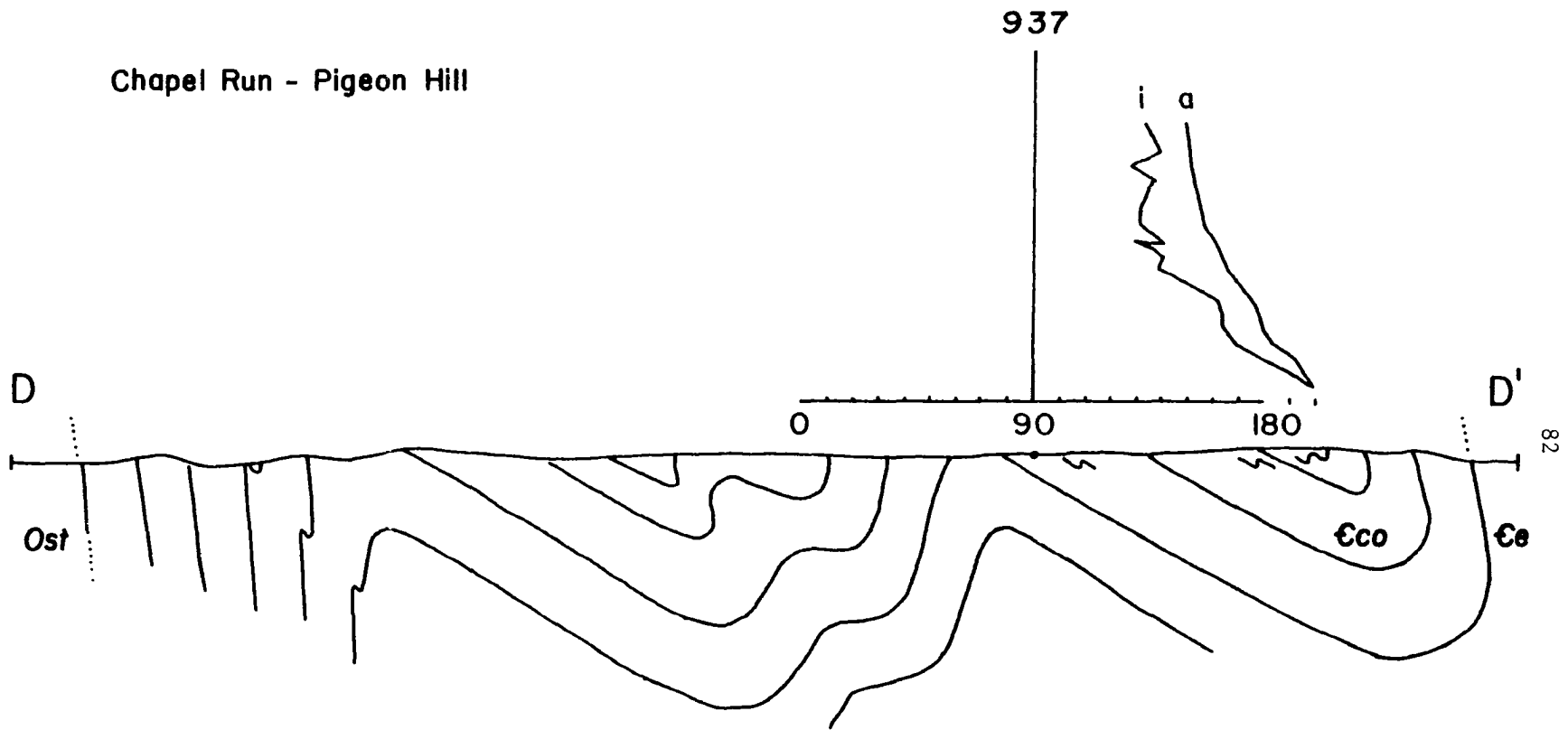


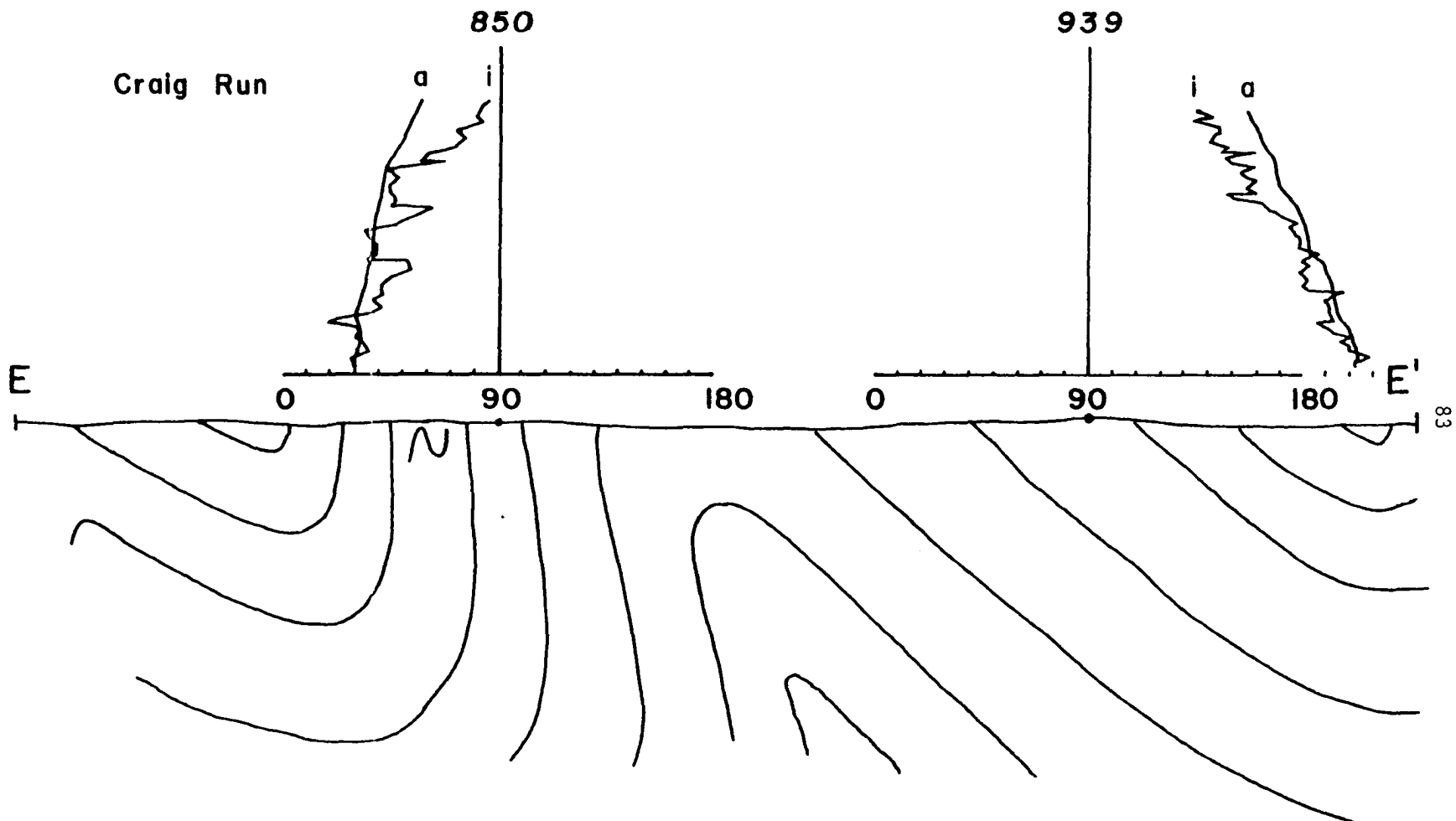
Figure 18: Traverse cross-sections with superimposed incremental strain paths. Plots show orientation of incremental and accumulated shortening axis through time relative to bedding. The horizontal axis represents angle to bedding of the elongation axis. The vertical axis represents time. The incremental strain path is labeled i. The accumulated strain path is labeled a.

Stone Bridge - Federal Hill



Chapel Run - Pigeon Hill





shortening axis relative to bedding through time. Cleavage fabrics in the study area are syntectonic with folding and the formation of tension gashes. It is assumed that the calcite fibers used to calculate the incremental strain path are syntectonic. The plots (Figure 18) show the orientation of the maximum principal shortening axis during the folding event.

Samples 850 and 939 are on the steep and shallow limbs of a fold respectively. The strain path calculated for sample 850 shows an initial orientation of the axis of maximum principal shortening of 30 degrees from bedding. During folding the incremental maximum principal shortening axis rotated toward the bedding perpendicular to a final orientation of 85°. This rotation corresponds to a bed rotating in a field of compression. The bed would have an initial dip of 30° and a final dip of 85°, assuming that the axis of maximum principal shortening is horizontal. This is in close agreement with the present day orientation of bedding at 80° overturned. The initial orientation of the maximum principal shortening axis in sample 939 starts 22° below bedding and rotates through the bedding parallel to a final orientation of 43° from bedding. The final orientation of maximum principal strain in sample 939 would correspond to a dip of 43°E, assuming that the axis of maximum principal shortening was horizontal. The present dip in sample 939 is 45°E. The orientation of maximum principal shortening across this fold is in remarkable agreement with the fold originating from an initially symmetric buckle which was inclined approximately 26° to the compression. The composite paths for samples 816 and 937, both from the shallow limbs of folds have the same general shape as sample 939 and are consistent with the interpretation that the folds described in the field area developed from symmetric buckles that were inclined to the axis of bulk finite shortening by as much as 30°.

Discussion

In this section the folds found in the field area have been described as asymmetric flattening type Ic/1c folds that plunge to the northeast. The folds formed from initially symmetric folds which may have been inclined as much as 30° to the direction of bulk shortening.

They were formed primarily by the flattening of parallel folds, in the competent layers. Layer parallel shear in limestone layers may have been locally important. The variation of fold shape in some samples may be due to bedding plane slip (Chapple, and Spang, 1974; Treagus, 1981), or layer parallel shear. There are only minor slickenside surfaces on bedding planes suggesting that flexural slip may have not been important. Cleavage is not axial planar throughout the fold. Cleavage is axial planar only in the fold hinge. Fold transection is defined as where cleavage cuts the fold axial surface at some angle in profile and along bedding. It is caused by the inclination of bedding to bulk shortening during folding (Borradaile, 1978; Treagus and Treagus, 1981; Gray, 1982). It may be possible to determine the orientation of bedding in three dimensions using the composite strain paths as well as transection of fold axes by cleavage.

The shape and nature of the folds described fit a flattening origin with some layer parallel shear in less competent members. The refraction of cleavage and variation of fold style within multilayers is compatible with models of folds using viscous materials (Chapple and Spang, 1974; Anthony and Wickham, 1978, Treagus, 1981; Treagus and Treagus, 1981). Features seen in the field area formed in a single deformation event with the axis of compression inclined as much as 30° to bedding. The rocks behaved as viscous materials during deformation. The nature and origin of the fabrics present in the map area will be described in the following sections.

Cleavage

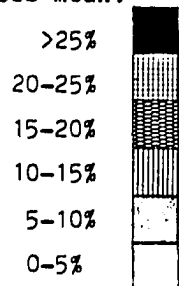
General Observations

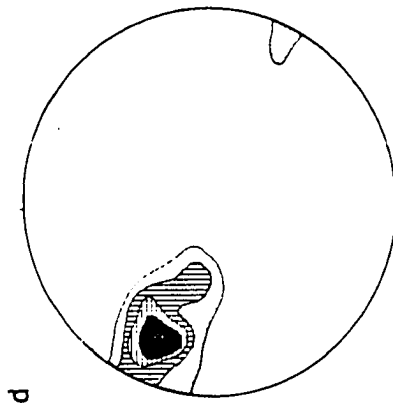
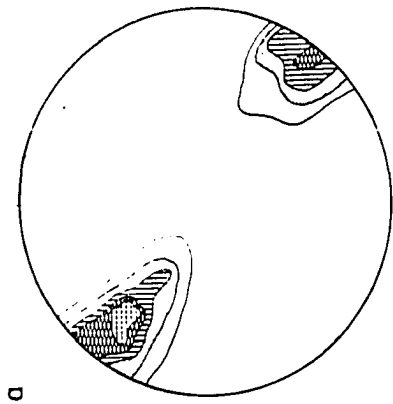
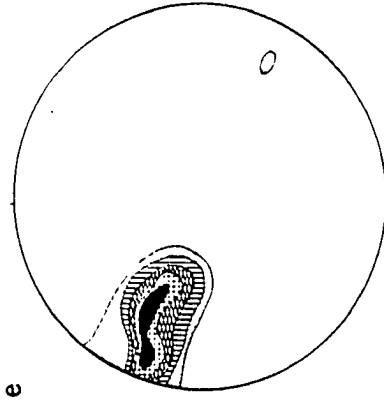
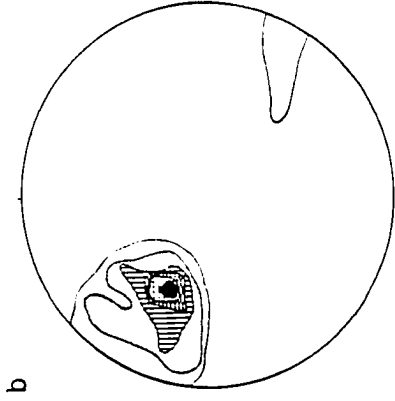
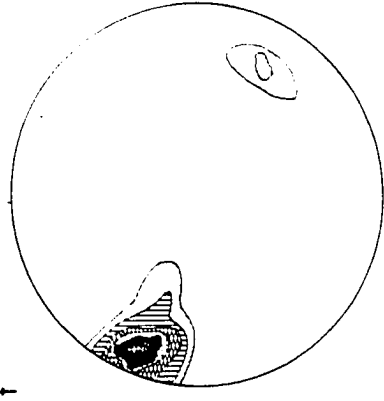
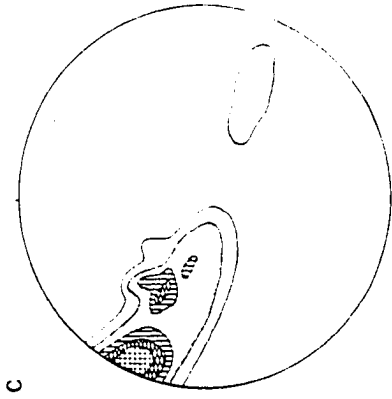
Cleavage surfaces nearly parallel fold hinge surfaces in the fold hinge zone. The similarity of cleavage and fold hinge surface orientation is observed on all scales of folding. The persistence of this relation on all observed scales of folding shows that cleavage fabrics observed are synchronous with fold formation. Cleavage fans around fold hinge surfaces (see Figure 19). Figure 19 shows Kalsbeek plots for poles to cleavage surfaces on all traverses except the

Figure 19: Density plots of poles to cleavage on traverses.
Lower hemisphere projection. Plots show local fold
axis.

- a) Stone Bridge - Federal Hill
- b) Millwood - Blandy
- c) Chapel Run - Pigeon Hill
- d) Craig Run
- e) Long Marsh Run
- f) Bullskin Run

Symbols mean:





Longwood traverse (for reasons discussed earlier) and for all observations in the field area. From these plots it is clear that cleavage fans asymmetrically about the fold hinges and that there is considerable scatter in the orientation of cleavage relative to the local fold axes as well as the calculated fold axes. Fanning of cleavage about the hinge surface is related to viscosity differences in the multilayer folds or to slip along the more incompetent limestone layers of the fold (Treagus, 1982).

Cleavage in the study area is the result of a progressive deformation, approximated by plane strain, that is synchronous with folding. There are two distinct cleavage fabrics present in the study area: penetrative cleavage(Sp) and spaced cleavage(Ss). In the field Sp is expressed as a preferred direction of rupture and weathering, as well as a preferred alignment of rock constituents. In many cases Sp is visible only on weathered surfaces where it forms a grooved appearance. On fresh surfaces Sp is expressed by the preferred alignment of rock constituents such as ooids or pebbles. Penetrative cleavage is observed only in the limestone layers of the Conococheague Formation.

The near parallelism of Sp with the hinge surfaces of folds in fold hinge zones and the expression of Sp by aligned rock constituents suggests that Sp formed by shortening during the folding process.

The second cleavage type present in the field area is a spaced cleavage(Ss), consisting of regularly spaced clay seams. On weathered surfaces Ss seams stand in 1 to 2 mm positive relief above the surrounding rock material. On fresh surfaces Ss appears as dark seams of clay in the lighter rock material. The rock material in between the Ss surfaces does not appear to be deformed. Ss is curved, the curvature is more marked in fold profile than on bedding surfaces. Ss is present primarily in the sucrosic dolomite units of the Conococheague Formation. In the 'ribbon rock' facies of the Conococheague Formation the change from Sp to Ss is visible.

Sp and Ss are not parallel within the same lithology and show refraction at lithologic boundaries of up to 14°. The refraction of cleavage at lithologic boundaries is away from the fold hinge surface

indicating that the limestone layers have a component of layer parallel shear. Cleavage refraction at lithologic boundaries may be an important factor in the study of fold transection. Refraction or curvature of cleavage in a non-coaxially deformed multilayer material with viscosity contrasts between layers may lead to misinterpretation of transection by giving a large range of cleavage orientations (Borradaile, 1974; Treagus and Treagus, 1981; Gray, 1982).

Two distinct syntectonic cleavage fabrics occur in the field area. Cleavage formation and folding were synchronous. The deformation can be approximated by plane strain with the formation of flattening folds that may have undergone some layer parallel shear in viscous multilayers. The two cleavage types will be discussed in the following sections.

Penetrative Cleavage(Sp)

General Observations. Sp is a dimensional fabric consisting of elongate calcite microspar as seen in thin-section and at high magnifications in SEM images (see Figure 20). Sp is present only in limestone layers of the Conococheague Formation. Sp does not refract around rock constituents whose material properties are similar to microspar, such as micritic ooids and pebbles, but does refract around detrital dolomite grains (Figure 21) and other rigid rock constituents. Cleavage refracts at the boundaries of micrite and sucrosic dolomite layers as much as 140° where Sp connects with Ss (see Figure 22). It should be noted, however, that as defined, Sp does not occur in the sucrosic dolomite layers. The cleavage trace is continuous, but refracted, at lithologic boundaries. In some samples Ss cuts Sp (see Figure 23). Sp is formed by an interlocking mosaic of microspar crystals which have an overall dimensional orientation (Figure 20).

The orientation of Sp varies throughout any one specimen (see Table 2). Sp is not associated with strict alignment of platy particles such as randomly dispersed phyllosilicates (see Figure 24). Sp is limited to the phyllosilicate-poor microspar layers of the Conococheague Formation. Sp is a sinuous curvilinear fabric formed by

Figure 20: Scanning Electron Photomicrograph of dimensional fabric (Sp) in sample 817. Scale bar is 10 microns long.

Figure 21: SEM image of refraction of Sp around detrital dolomite grain in sample 815. Magnification is 250X.

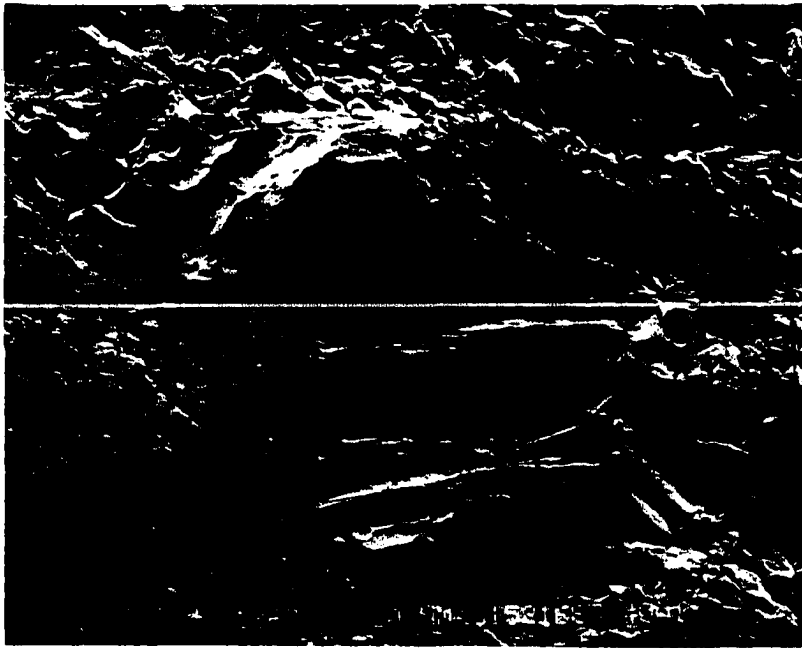
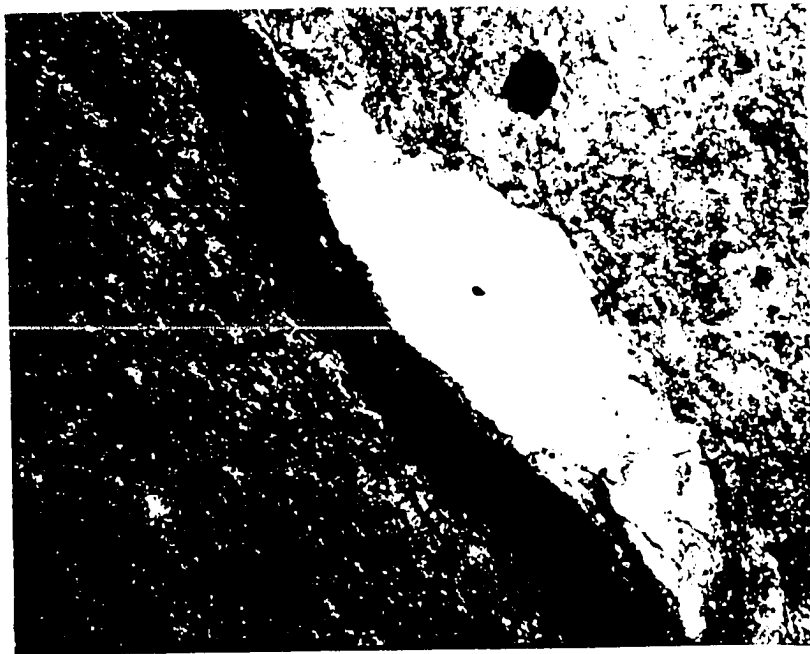


Figure 22: SEM image of cleavage refraction at a lithologic boundary where Sp and Ss connect in sample 809. The upper portion of the photograph is sucrosic dolomite with 1% phyllosilicates by volume. The lower portion is calcite microspar. Magnification is 500X.

Figure 23: Photomicrograph of truncation of quartz grain and calcite pressure shadow as well as truncation of Sp (left) by Ss. Sample 807.



an interlocking mosaic of microspar crystals. Sp is not associated with high angle crystal boundaries or with the in-situ growth of new minerals. The surfaces of rigid particles in the microspar are pitted, indicating that material has been removed by pressure solution. Figure 25 shows the pitted surface of a quartz grain within the microspar layers.

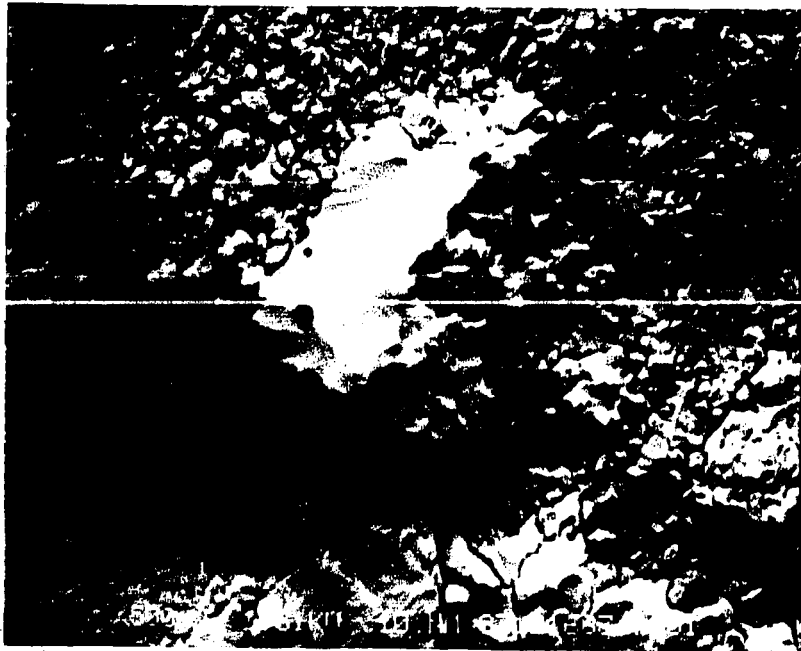
Sp is well developed in specimens with deformed ooid axial ratios of 1:1.4 and greater. Five samples containing deformed ooids had well developed Sp surfaces. Thirty orientations of Sp were measured in each of these 5 samples as well as in 4 other samples that had well developed Sp. Table 2 is a compilation of the mean, standard deviation and orientation range of Sp as well as the orientation of the long axis and axial ratios of deformed ooids.

Discussion. The deformation event which formed the cleavage is non-coaxial. Bedding was locally inclined to the axis of principal shortening throughout the deformation. A cleavage formed in this environment by physical processes should have an orientation similar to that of accumulated strain markers within the same rock volume. The orientation of the cleavage should not change significantly across the area, ignoring local strain inhomogeneity. Cleavage would refract at lithologic boundaries (Treagus, 1981; 1982). Cleavage should not be axial planar but should transect the axial plane of the folds (Treagus and Treagus, 1981). Rock textures associated with plastic flattening or passive rotation of elongate elements should be observed.

Table 2 contains orientation data gathered from deformed ooids and from Sp orientations in a suite of samples containing well developed Sp. Five samples contained deformed ooids. Orientations and orientation ranges for Sp relative to bedding were measured in these samples and in 4 other samples in which Sp was well developed. Measurements were made in samples from both the steep and shallow limbs of folds as well as in the core of a fold. From Table 2 it is apparent that the orientation of Sp is similar to the orientation of the deformed ooids in the respective samples and that the orientation of Sp relative to bedding is similar for sample groups on the steep limb or

Figure 24: SEM photomicrograph of sample 809 showing non-alignment of platy rock constituents on Sp. The platy material is muscovite. Large crystals are dolomite. Magnification is 500X.

Figure 25: SEM photomicrograph of solution pitting of quartz grain on Sp. Cleavage is poorly developed. Sample 831. Magnification is 500X.



on the shallow limbs of folds.

The ranges of Sp orientation are less than the ranges of orientation for the strain increments calculated by the calcite fibers (refer to Figures 11 and 18). The orientation of Sp varies significantly across the samples. The range of orientations for Sp is lower than Ss in any one specimen. The orientation of Sp is close to the orientation of elongation axis of accumulated strain.

Cleavage refracts at lithologic boundaries. At boundaries where micrite is in contact with sucrosic dolomite Sp is continuous with Ss. Sp does not continue into the sucrosic dolomite. Sp therefore is limited to a specific lithology. The refraction of cleavage at lithologic boundaries is not sufficient evidence to support or disprove any interpretation of the cleavage forming mechanism. A cleavage formed by any deformation mechanism will show refraction across lithologic boundaries. The stress field and the accumulating strain field have different orientations in layers of different competence in asymmetric and symmetric folds (Treagus, 1981).

A penetrative cleavage formed by a physical mechanism will have a texture characteristic of that mechanism. Two physical mechanisms have been suggested as being capable of forming cleavage. The mechanisms (plastic flattening and physical rotation) will be discussed separately.

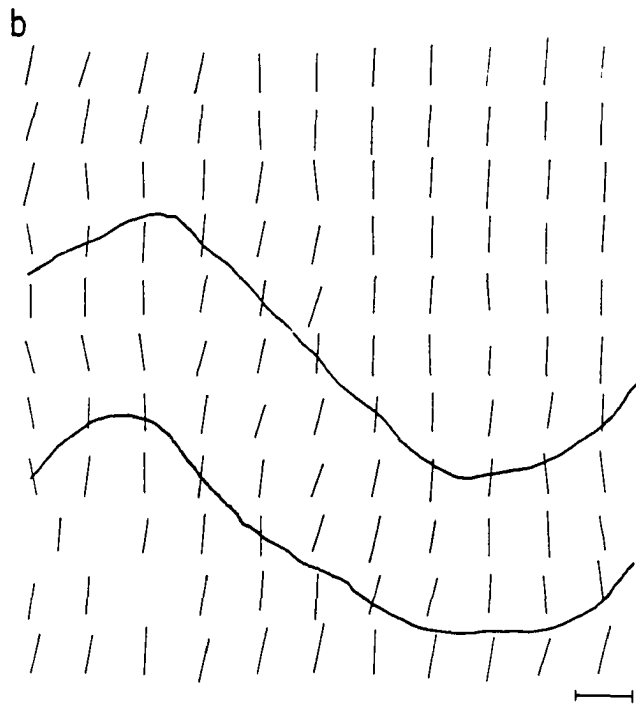
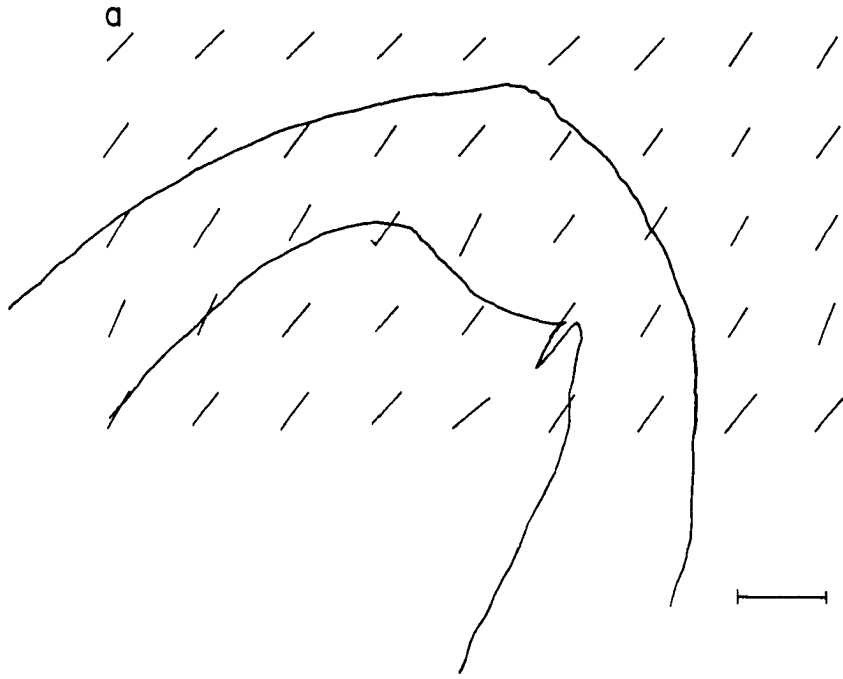
Physical rotation of rigid particles in a deforming material will result in the formation of a cleavage fabric which is statistically perpendicular to the axis of maximum principal shortening. The rotation of platy particles in a viscous material has been considered theoretically and has been shown to be a viable mechanism for the formation of cleavage. In rocks where physical rotation has taken place the orientation the long dimension of the particle should be statistically perpendicular to the maximum principal shortening axis. The samples collected from the field area contain randomly dispersed phyllosilicates. In the micritic layers of the Conococheague the phyllosilicates are minor, making up less than 1% of the sample by volume. The phyllosilicates in the micrites are not oriented along the cleavage trace (Figure 24), indicating that physical rotation is not a

Sample	axial ratio	mean orientation of ooid long axis	standard deviation	mean orientation of Sp	standard deviation	range of Ss orientations	range of Sp orientations	sample location
924	2.0	59	7.2	57	7.4	47	30	shallow limb
928	2.1	44	8.4	44	5.9	50	23	shallow limb
930	2.6	76	7.3	77	3.9	48	16	steep limb
936	2.15	28	20.5	28.9	6.6	83	20	shallow limb
938	1.9	57	6.1	52	5.9	53	28	shallow limb
819				5.8	3.5		26	steep limb
914				2.6	2.4		16	steep limb
919				63.4	3.4		12	shallow limb
931				26.4	3.1		11	steep limb

Table 2: Mean and standard deviation of ooid long axis orientation, mean standard deviation and range of Sp orientation, range of ss orientation and location on fold for 9 samples containing well developed Sp. All measurements are in degrees. Orientations are in degrees relative to bedding.

Figure 26: Sketches of cleavage orientation across two folds showing that cleavage does not transect the folds. The folds have a central dolomite layer that has Ss cleavage. The upper and lower units are limestones with Sp cleavage. Neither Ss or Sp transect the fold axis. Note cleavage refraction. Scale bar represents 2 millimeters on sample.

- a) Sample 817
- b) Sample 843



feasible mechanism of formation for Sp. The cleavage morphology present is not consistent with passive rotation as a dominant mechanism.

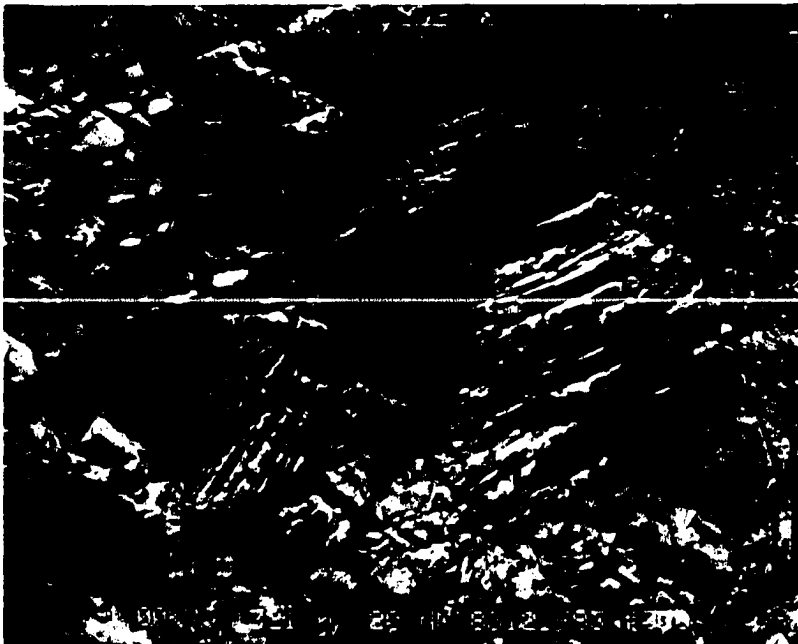
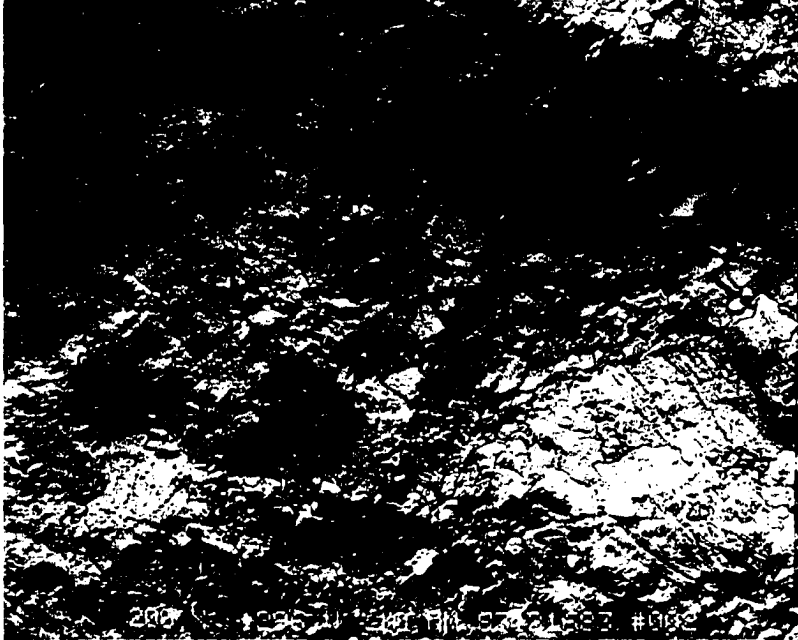
Cleavage may be formed by plastic flattening. Deformation by plastic flattening may involve slip or twin gliding at low temperatures and dislocation creep or glide at high temperatures or rapid strain rates (Rutter, 1976). Experimental and theoretical studies on limestone show that for geologic strain rates dislocation creep or dislocation glide are not active below temperatures necessary to induce recrystallization (Rutter, 1974, 1976). In limestones subject to geologic strain rates this temperature may be as high as 400°C (Rutter, 1974). Evidence of high temperatures has not been found. The highest grade metamorphic mineral present is chlorite. Detrital biotite showing rim reaction and alteration to chlorite is present in many samples. Deformation by twin gliding can occur at low temperatures and confining pressures. Some samples show evidence of limited deformation by twinning (see Figures 27, 28). In these samples twinning is present in detrital dolomite grains and in sparry calcite cement. Twinning within crystals will be visible on almost all scales if this is the primary mechanism of deformation. Twinned crystals are minor and are limited to the dolomitic cores of deformed ooids (see Figure 27) and calcite crystals that are greater than 120 microns in diameter. There is no evidence that indicates deformation by twinning in crystals smaller than 120 microns in diameter. Rutter (1976) calculated the stability fields for pressure solution, Nabarro-Herring Creep, dislocation creep and dislocation glide for calcite and quartz where the mean crystal size was 100 microns. The samples are in the stability field of pressure solution as the dominant deformation mechanism for crystal less than 100 microns in diameter.

Deformation in the specimens is inconsistent with the mechanism of twin gliding alone.

Cleavage may form by chemical mechanisms. Cleavage associated with recrystallization or neo-crystallization should have high temperature textures and mineral assemblages. There is no evidence of

Figure 27: SEM photomicrograph of deformation by twinning and wedging of dolomite core of ooid in sample 831. Magnification is 200X.

Figure 28: SEM image of twinned dolomite grains is sample 831. Magnification is 1000X.



high angle boundaries or new, optically oriented mineral growth. Sp is not related to a recrystallization or neo-crystallization process. The absence of high angle boundaries and new mineral growth along the cleavage trace are inconsistent with these mechanisms. The pressure and temperature conditions of deformation in this area are within the calculated stability field of pressure solution (Rutter, 1974, 1976). There is evidence of pressure solution within the samples. Along contacts of more rigid particles within the microspar matrix there is suturing and pitting of the rigid particle surface.

Pressure solution in a crystalline material will be at points of highest stress. Within the matrix, these points will be at crystal contacts. In a clean system, impurities will not be concentrated by pressure solution. A cleavage formed by pervasive pressure solution in a clean system may not form zones of material accumulation but may form a dimensional fabric of elongate crystals where the long axis is nearly parallel with the elongation axis of the accumulated strain.

Ooids have been used to measure accumulated strain. Examination of individual ooids shows that they may have been deformed, in part, by pressure solution. Sp is nearly parallel with the elongation axis of accumulated strain.

The similarity of orientation of Sp with deformed ooids still remains an apparent contradiction. There are several types of ooids recognized in the study area, these have been described fully by Cloos (1971). Mantled ooids have been deformed by wedging and twinning of the dolomite core (see Figure 27). The mantles of these ooids show the same textural features and orientation of the micrite grains as Sp. The dolomitic cores of the mantled ooids have sutured contacts between crystals and through-going solution surfaces (see Figure 27, 29 and 30). Non-mantled ooids in the samples contain through-going solution surfaces and have the same texture as Sp (see Figure 31). The presence of pressure solution surfaces within the deformed ooids and the similarity of textures between the mantles of the mantled ooids and the non-mantled ooids support the conclusion that the similarity of orientation between Sp and the deformed ooids reflects a common deformation mechanism. In this instance, deformed ooids do not

Figure 29: Photomicrograph of ooids that have been deformed by pressure solution in sample 936. The ooids are mantled ooids with dolomitic cores. The cores have been deformed by twinning and pressure solution.

Figure 30: SEM photomicrograph of sample 936 showing truncation of deformed ooid by pressure solution zone. Magnification is 100X.

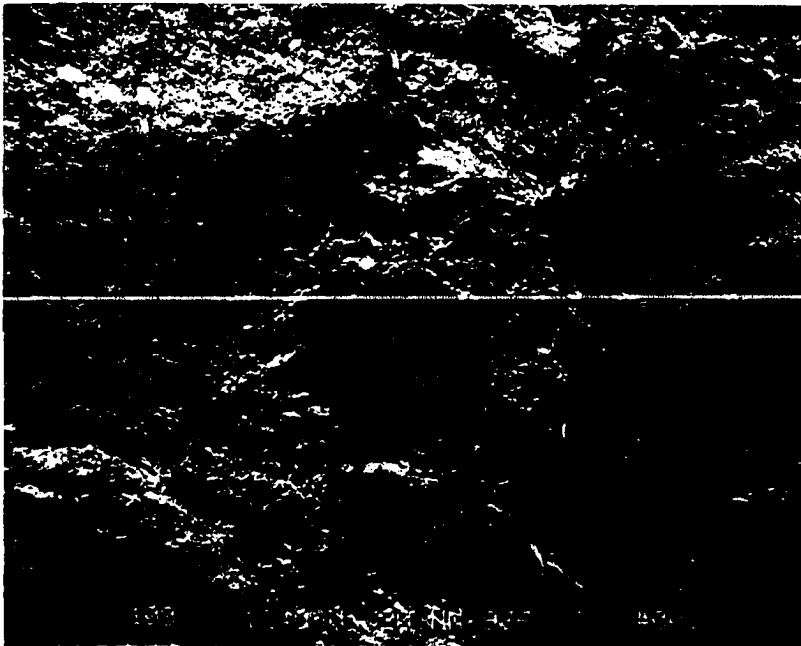
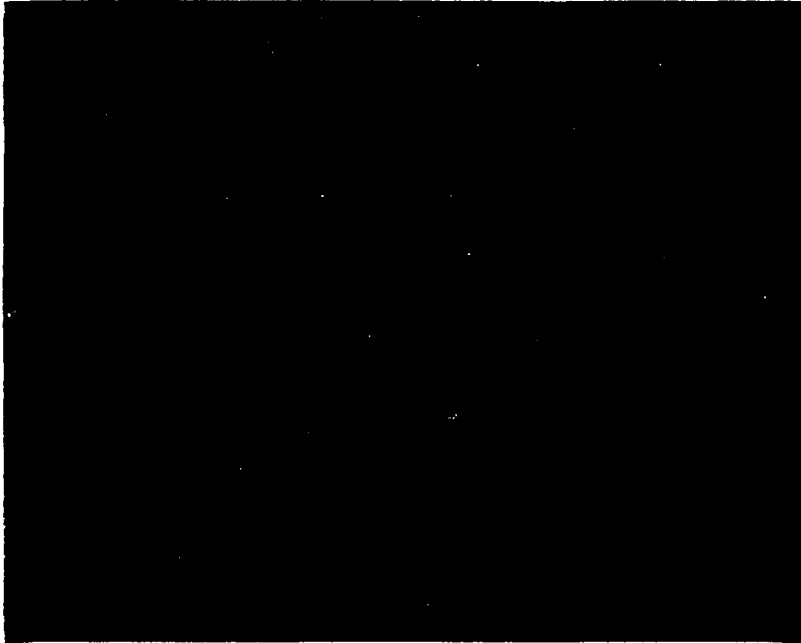
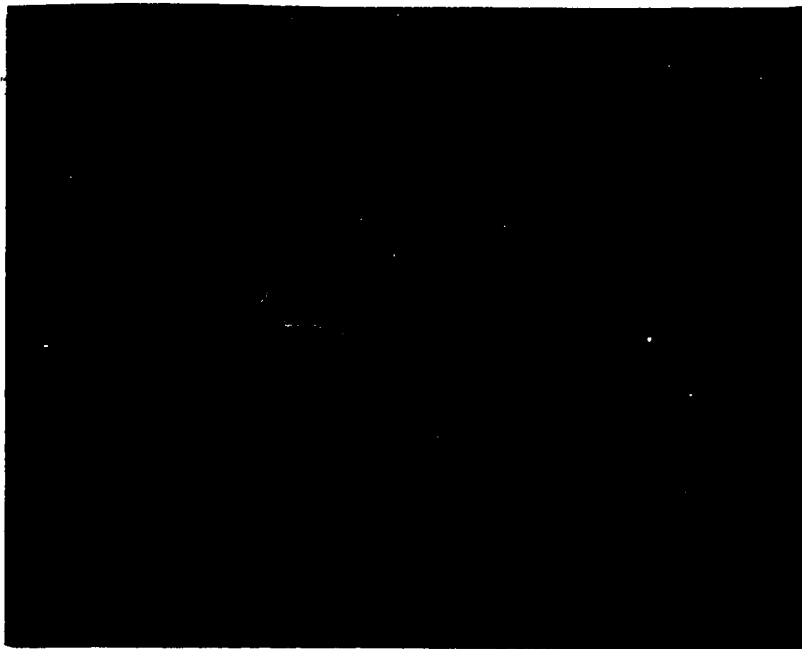


Figure 31: Photomicrograph of sample 928 showing non-mantled ooids that have the same dimensional fabric as Sp and have been cut by solution zones.



represent plastically flattened rock constituents, but represent rock constituents deformed primarily by pressure solution.

The data presented suggest that Sp was not formed by a physical process alone. Based on the textures, relationships of Sp to the local fold axes and the similarity of Sp orientations to the elongation axis of accumulated strain it is concluded that Sp formed by an interaction of twinning and pressure solution at crystal boundaries. The presence of twinned calcite crystals and dolomitic ooid cores suggest that pressure solution and plastic deformation occurred simultaneously. Crystals larger than 120 microns in diameter deformed by twinning and pressure solution. Crystals smaller than 120 microns in diameter deformed by pressure solution alone.

Sp is interpreted as having resulted from pervasive pressure solution at crystal contacts in the phyllosilicate-poor microspar layers of the Conococheague Formation. Examination of deformed rock constituents show similar crystal morphologies indicating that the elliptical shape of the ooids is due in part to deformation by pressure solution and twinning.

Spaced Cleavage(Ss)

General Observations. Ss consists of macroscopic zones or bands of phyllosilicates formed by coalesced microsurfaces of phyllosilicates (see Figure 32), or stringers of phyllosilicates (see Figure 33). Ss forms in the presence of phyllosilicates. Ss is found in phyllosilicate-rich dolomite layers (approximately 1% phyllosilicates by volume) and extends into phyllosilicate-poor limestones (less than 1% phyllosilicates by volume) at lithologic boundaries where they connect with Sp (Figure 22). Rock constituents are truncated along Ss (see Figure 23 and 34). Layers that are inclined to the cleavage trace are offset along Ss (see Figure 35).

The orientation of Ss changes across samples (see Figure 36). Figure 36 shows the curvature of Ss in sample 937. In this sample Ss shows a small range of curvature in the sucrosic dolomite layers and a large range of curvature in a sandy limestone layer where it rotates to a bedding parallel orientation. The change in Ss orientation in

Figure 32: Photograph of thin section of sample 808 in plane polarized light. The thin section is 2"x3". This figure shows how solution zones curve and how they are formed by coalescing microspheres. The solution zones tend to terminate at boundaries between dolomite (dark) and limestone (light).

Figure 33: Photomicrograph of undulating Ss zone in sample 937.

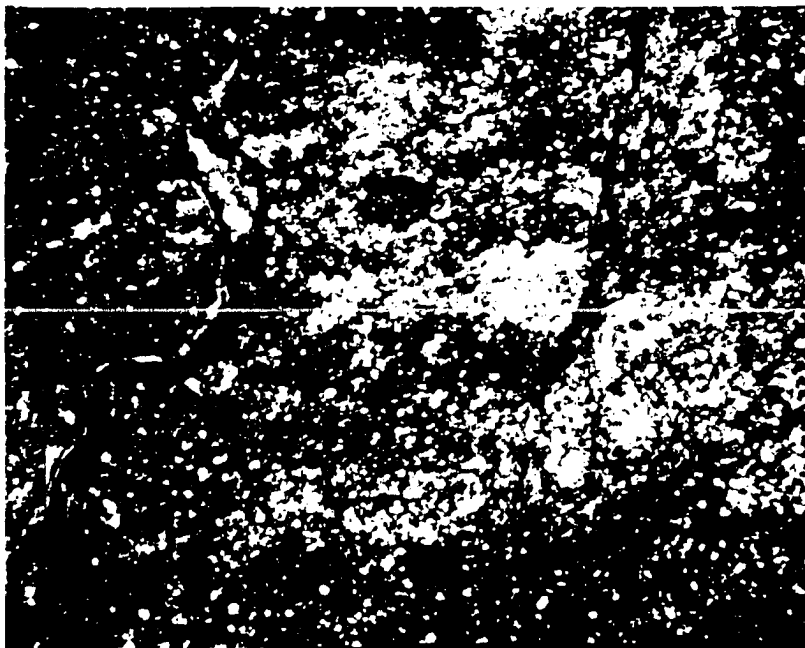
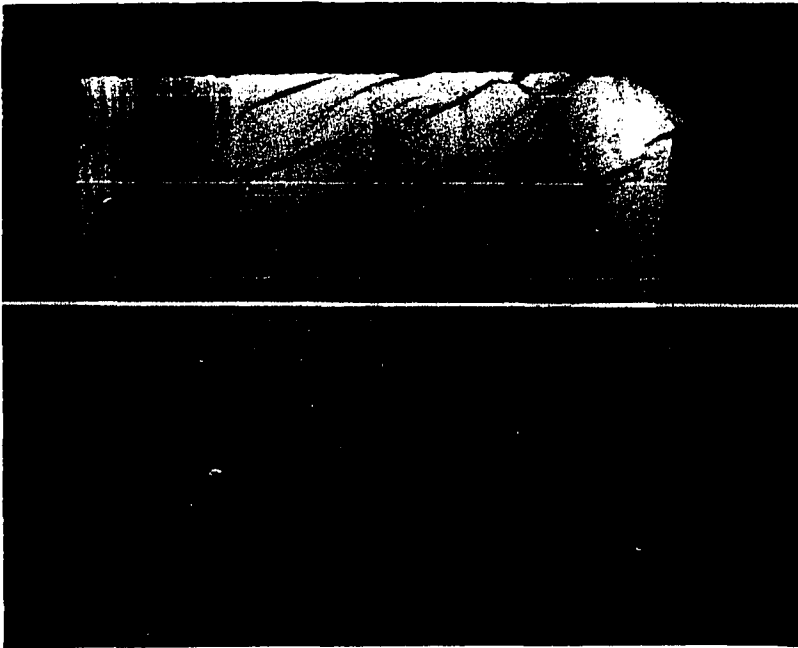
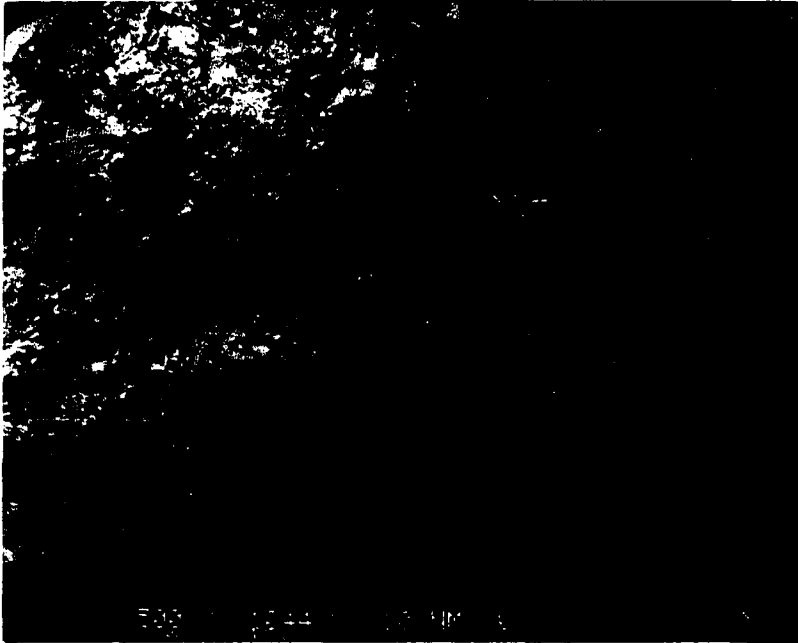


Figure 34: SEM photograph of sample 809 showing truncation of dolomite in Ss. Note phyllosilicates accumulated on the zone are wrapped around the dolomite crystal. Magnification is 1500X.

Figure 35: Photograph of 2"x3" thin section of sample 814 showing variation of apparent offset direction and amount on Ss.



dolomite layers is similar to the range of incremental maximum elongation axes relative to bedding as measured by the calcite fibers (refer to Table 3). Ss is present in 5 samples that contain deformed ooids. The orientation range of Ss is shown in Table 2. The range of orientation of Ss in samples where composite strain paths were prepared is shown in Table 3. Ss has a wider range of orientation than Sp. Samples with large axial ratios have lower orientation ranges of Ss and Sp. The range of orientations for Ss is greater than the range of the elongation axis orientation for incremental and accumulated strain. This may indicate that the total strain path is not preserved, or that strain is locally inhomogeneous. Most of the measured orientations for the spaced zones fall within one standard deviation unit of the range of orientations of calculated elongation axis orientation.

Ss is associated with accumulation of insoluble minerals and with the truncation of rock constituents. Ss connects with fibrous calcite and quartz which fill syntectonic tension gashes (see Figure 37). Ss is present along boundaries of deformed ooids and quartz grains from which calcite fibers have grown (see Figures 38 and 30), and in the cores of deformed ooids (Figures 29 and 31). Ss connects with Sp at lithologic boundaries. The cleavage trace is refracted at these boundaries. Ss cuts Sp in some samples (refer to Figure 23). These relationships will be discussed in the following section.

Discussion. In the previous section it was shown that Sp was formed by twinning and pressure solution. The origin of Ss will be discussed in this section.

The orientations of Ss are not consistent with the range of orientations expected for a cleavage formed by a physical process. The range of Ss orientations is greater than the range of orientation of incremental elongation. Measured initial and final orientations of Ss are shown in Table 3. The measurements assume that Ss initiates at a point near the center of layering and propagates away from that point as deformation progresses (refer to Fletcher and Pollard, 1981). It is further assumed that the point of initiation is near the center of a layer and that the direction of propagation is toward the layer

Figure 36: Photograph of 1"x2" thin section of sample 937 showing the curvature of Ss within the dolomites. Ss becomes nearly parallel with bedding in the limestone layer indicating that slip along limestone layers has occurred.

Figure 37: SEM photomicrograph of sample 809 showing the relationship between Ss and tension gashes. The crystals in the lower right are fibrous calcite infilling a tension gash. The sharp change in elevation in the center of the picture is a solution zone. The solution zone ends in the tension gash. Materials dissolved on the solution zone are precipitated in the tension gash. Magnification is 100X.

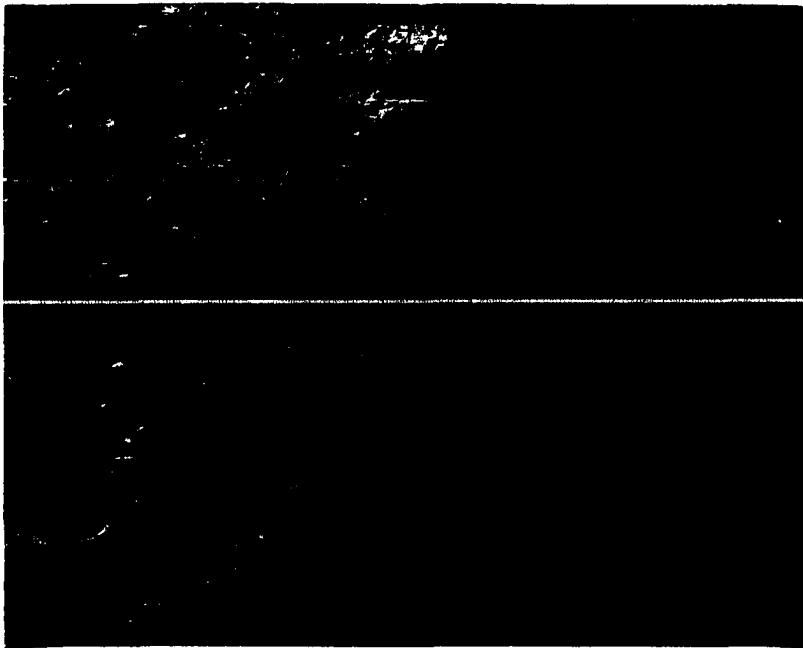
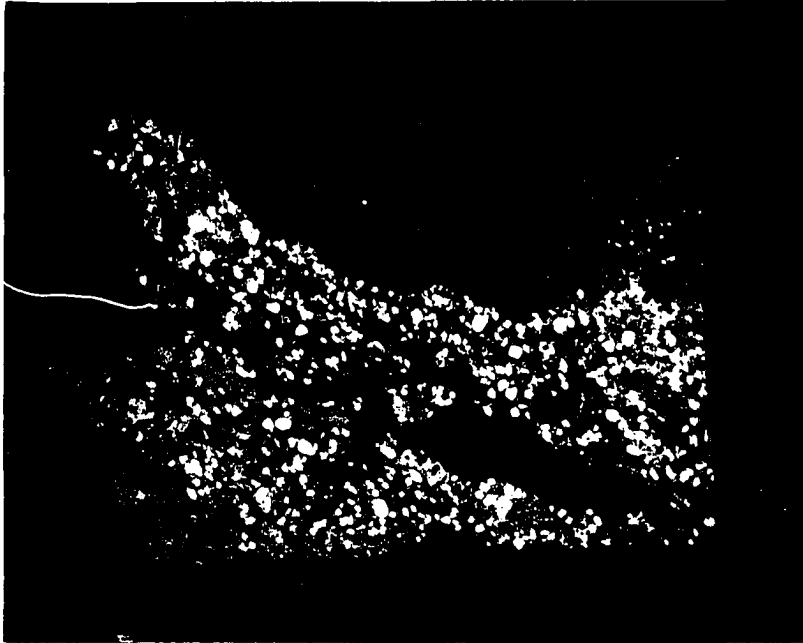


Figure 38: Photomicrograph of sample 816 showing truncation of pressure shadow by pressure solution zone.



Sample	initial incremental elongation axis orientation	final incremental elongation axis orientation	final accumulated elongation axis orientation	difference	refraction at lithologic boundary	initial Ss orientation	final Ss orientation	difference
816	110	62	80	48,30	14	112 101	65 54	47 47
850	30	86	58	56,28				
937	110	32	60	78,66		31	82	51
939	112	46	68	66,44				
814						101 116 110	91 93 100	10 13 10
808						52 49 46	70 47 62	18 1 16

Table 3: Initial, final and ranges of orientations of incremental and accumulated strain and Ss. All measurements are relative to bedding and are in degrees.

boundary. Four samples possessed well developed Ss where it is assumed that no layer parallel shear has occurred. The zones are in dolomitic layers to insure that layer parallel shear or local strain inhomogeneity are minimal (see Figure 36). Layer parallel shear will increase the range of Ss orientation and will result in an erroneous interpretation of the amount of layer rotation in the compressive field. If layer parallel shear has occurred in a layer, Ss within that layer will rotate towards the bedding parallel (Treagus, 1981). Figure 36 demonstrates the effect of layer parallel shear in incompetent layers on the orientation range of Ss.

In samples 816 and 937 the initial and final orientation of the zones are remarkably close to the initial and final orientation of the incremental elongation axis. The initial and final orientations of Ss in sample 814 are not compared to a composite strain path. Sample 814 is in the core of a syncline. A composite strain path is not available for the core of a fold. The difference between the initial and final orientation in sample 814 is small, as would be expected for the core of a fold. During fold development, the hinge sees little rigid rotation and deformation paths are coaxial.

The initial and final orientation of Ss in samples 816 and 937 are nearly identical to the initial and final orientation of the incremental elongation axis relative to bedding. This similarity is consistent with the interpretation that Ss is a solution cleavage. The remarkable agreement of the assumed initial and final orientation of the macroscopic Ss zones and the incremental elongation axis serves as an independent check of the technique used to generate the composite paths and the assumption that pressure solution surfaces form at a point and propagate away. These results give strong support to the validity of treating pressure solution surfaces as anti-cracks.

Recrystallization and neo-crystallization have been ruled out based on arguments put forth in the previous section. The same observations are applicable for Ss. There are no high angle boundaries associated with the formation of Ss. The formation of chlorite does not represent neo-crystallization formation of cleavage. Chlorite replaces some detrital phyllosilicates. The orientation of chlorite is

identical to that of the material being replaced.

Based on physical evidence and orientation data it is concluded that Ss is a pressure solution cleavage. This conclusion is supported by the lack of textures attributable to physical mechanisms within the sucrosic dolomite layers and the presence of textures associated with pressure solution. There is no evidence of deformation by twinning within the sucrosic dolomites. The orientation of phyllosilicates along Ss is not related to a physical whole rock deformation mechanism. Ss zones are zones of material removal. As soluble materials are removed the insoluble materials will accumulate in the solution zone. As phyllosilicates are concentrated they may be passively rotated so their orientations match the orientation of the boundaries of the solution zone.

The textural evidence for pressure solution has been described. Materials are truncated along Ss, indicating that there has been material removal. Layers that are not perpendicular to Ss have been offset on Ss. Slip cleavage or fracture cleavage can be ruled out. If slip occurred on Ss the slip would be uniform along the surface and would have to be compensated across the sample. Figure 35 shows the offset of layering in sample 814. The sense of offset is not uniform across samples and the offset is not compensated across the samples. The sense of offset best fits a material removal process where the orientation of layering relative to the solution zone effects the amount and direction of the apparent slip (Groshong, 1975).

The morphology of the spaced cleavage is not consistent with a physical process. The truncation of rock constituents by the cleavage surfaces and the accumulation of insoluble material on the cleavage surface indicate that pressure solution is the primary mechanism of deformation for the spaced cleavage. If pressure solution is the deformation mechanism in the sucrosic dolomites there should be a corresponding increase in material concentration in the hinge zone of folds and on the attenuated steep limb of folds. This is reflected by the spacing of solution surfaces in the various portions of the folds. Measurements of cleavage spacing in thin section are shown in

Table 4.

Location	Sample	Spacing (cm)	Material
Hinge	811	.42	dolomite
	814	.48	dolomite
	842	.35	limestone
	911	.48	dolomite
Steep limb	808	.57	dolomite
	809	.85	dolomite
	829	.64	limestone
Shallow limb	816	1.27	dolomite

Table 4: Spacing of solution zones in 8 samples from various portions of folds. Spacing was measured perpendicular to the solution zone trace. Measurements are in centimeters.

These values were derived by counting the number of macroscopic solution zones on traverses perpendicular to the Ss trace. In the hinge zones of folds the spacing of Ss is less than 4.8mm. On the shallow limb, sample 816, the spacing is 1.3cm. On the steep limb, the spacing is between 5.7mm and 8.5mm. The spacing of macroscopic solution surfaces is related to the amount of shortening. Spacing diminishes with increased shortening and strain rate. The spacing of solution surfaces has been studied by Fletcher and Pollard (1981), who treat solution surfaces as anticracks. Spacing of solution zones is dependent on strain rate, pressure, temperature, effective stress, chemical character of the solids in the system and the thickness of the film of material transport. The spacing of pressure solution surfaces may be important in understanding the folding process and the associated fabric development.

Both Sp and Ss have been documented as having formed by pressure solution. These two cleavage fabrics have different textural signatures which can be used to determine their relationships. Sp is a dimensional fabric of elongate calcite micrite to microspar that formed by pressure solution at points of high stress. The micritic matrix in which Sp formed is relatively free of impurities. The lack of accumulated material prohibited the formation of macroscopic surfaces. The range of orientation of Sp reflects local inhomogeneity of strain, such as refraction around rigid rock constituents or lithologic boundaries and possibly some preservation of the last strain increment.

Ss preserves the strain history of the region. Ss is characterized by the formation of macroscopic solution zones by coalesced microspheres. Pressure solution originated at points of highest stress at crystal boundaries in the same manner as Sp. In the presence of accumulated material a solution zone would develop. As shortening continued pressure solution occurred perpendicular to the maximum stress component on the pressure solution zone. Microspheres forming at adjacent crystal boundaries coalesce as shortening continues. Macroscopic zones develop and begin to control the shortening in the local area of the pressure solution zone. Materials that are removed by the surface are transported along the surface and deposited locally in tension features. The formation of macroscopic zones controls the orientation ranges of Ss. Sp does not form a macroscopic zone of accumulation, its orientation reflects, for the most part, the elongation axis of accumulated strain. The presence of phyllosilicates is one factor which may control the style of pressure solution in the samples observed.

Cleavage formation is intimately associated with folding. The geometric and textural relationships of cleavage can be used to interpret the origin of cleavage. The relationships of cleavage to folds give valuable information regarding the folding process. Both Ss and Sp are axial planar within the hinge zone of folds. Previous workers (Borradaile, 1978; Treagus and Treagus, 1981; Gray, 1982) have examined fold transection by cleavage and used it to infer that transected folds formed initially as symmetric folds where the enveloping surfaces were inclined relative to the shortening direction. In this study two cleavage fabrics have been described that formed during a folding event similar to those described by the above mentioned authors. It has been shown that layering was initially inclined to the direction of shortening, resulting in asymmetric folds with attenuated steep limbs. The cleavage in this system does not transect the fold axis. The cleavages described have been formed predominantly by pressure solution. The principal axis of extension in an asymmetric fold will parallel the axial surface in the hinge of the fold. This conclusion is drawn from observation of the results of

finite element models constructed of asymmetric folds by Wickham and Anthony (1978) not from the text of that article. Conclusions regarding the relations of folds and cleavage in systems where the mechanism and nature of deformation is not known should be carefully drawn.

As previously stated the folding in the region is dominantly asymmetric with an attenuated steep limb. Deformation by pressure solution has been interpreted as following a modified linear, incompressible flow law (Fletcher, 1982). The data agree with results of linear, incompressible, viscous finite element models of fold form and cleavage relations (Wickham and Anthony, 1978). Cleavage refraction at lithologic boundaries agrees with the model proposed by Treagus (1982) for viscous materials. Curvature of cleavage in incompetent layers show that some layer parallel shear occurred.

Cleavage in the Conococheague Formation has been formed primarily by pressure solution. The geometry, textures, spacing and occurrence of cleavage indicate that the deformation event which formed the cleavage is one approximated by plane strain. Folding was syntectonic with cleavage formation. Layering was inclined as much as 30° to the shortening direction resulting in asymmetric folds but not in transection of fold axes within the fold hinge zone. The data collected indicate that the deformation experienced by the material on the limbs of folds was non-coaxial and that the deformation as observed from a global reference frame (this reference frame is preserved in the fold axes) was irrotational. Conclusions based solely on the relationships of cleavage to fold axes should be made with care unless the deformation history and mechanisms can be documented. The data support a viscous rheology for the materials during deformation. Deformation in carbonate rocks is accomplished primarily by pressure solution with some twinning depending on crystal size.

The concentration of insoluble materials in solution zones suggests that it may be possible of determine the amount of shortening on the macroscopic solution zones by comparing the concentration of materials in the zone with the concentration of materials in the

matrix. This is discussed in the following section.

Estimation of Volume Loss by Pressure Solution

Introduction. The concentration of insoluble material in Ss zones presents a unique opportunity to estimate the amount of local volume loss by pressure solution. Soluble rock constituents (calcite, dolomite and quartz) are removed and insoluble materials (clays and organic material) are concentrated by pressure solution .

Materials in solution zones are accumulated by dissolution and removal of soluble materials at solution zone boundaries. Accumulated insoluble materials are related to insoluble materials in the matrix. The predominant minerals in the solution zones examined are phyllosilicates that are chemically related to the interstitial clays within the matrix. It is possible to determine the volume loss along a solution zone by comparing the concentration of an element in the solution zone to the concentration of that element in the matrix, assuming the element is concentrated by pressure solution of the directly adjoining matrix, the system is closed for that element and the element was homogeneously distributed through the sample prior to pressure solution. The estimation of volume loss on the zone can be made using the following relations:

If

M = Mass of element.
 V = Volume of rock before pressure solution.
 V' = Volume loss due to pressure solution.
 A1 = Concentration of element in solution zone.
 A2 = Concentration of element in matrix.

A1 and A2 can be expressed as

$$A1 = M/(V-V') \quad (1)$$

$$A2 = M/V$$

Since A2 is a function of M and V

$$A1 = (A2*V)/(V-V') \quad (2)$$

simplifying yields

$$A2/A1 = 1 - (V'/V) \quad (3)$$

Now $(1 - (V'/V))$ is a representation of the volume loss by pressure solution. It is possible (using equation 3) to estimate the

volume loss represented by a solution zone by comparing the concentration of an element in the zone to the concentration of that element in the matrix.

Estimation of the volume loss by pressure solution involves the determination of elemental concentrations within solution zones and the adjoining matrix. Wet chemical analysis of bulk samples is not possible due to sampling difficulties. The simplest method involves the measurement of concentrations of elements per unit using surface techniques. It is assumed that the composition of the rock does not change in the third dimension (perpendicular to the surface). Two surface sampling techniques are possible. The concentration of elements can be determined for a spot using the microprobe or for a region using an EDX (Energy Dispersive X-ray Analyzer). For simplicity an EDX was used in this study. The microprobe was used to verify the chemical determinations made using the EDX and to determine the mineralogy of the samples. The procedures and data are discussed below.

With the EDX it is possible to scan large surface areas, averaging out the surface and matrix effects over the specimen. When a material is bombarded by an electron beam, each element in the material gives off a characteristic wavelength and energy of electromagnetic radiation that is dependent on the energy of the beam striking the surface of the material. The microprobe and EDX make use of this phenomenon to determine the chemical makeup of a spot or region under the beam. In EDX analysis the beam scans a certain area on the sample surface. As the beam scans the surface it excites the elements on the material surface. Each element will give off its characteristic wavelength and energy of electromagnetic radiation. The EDX unit can be used to determine the overall elemental composition of a given sample. A scan of sample 809 is shown in Figure 39. An electron dot map is a representation of the sample where each dot represents an excitation site on the sample surface, for a given element. With the electron dot map of the surface it is possible to see the relative concentration or depletion of various elements in the solution zones (refer to Figure 40). In theory each dot on the dot map represents one

Figure 39: Plot of elemental composition of sample 809 using EDX. This sample is representative of the samples analyzed.

LP-2886 SECS

809

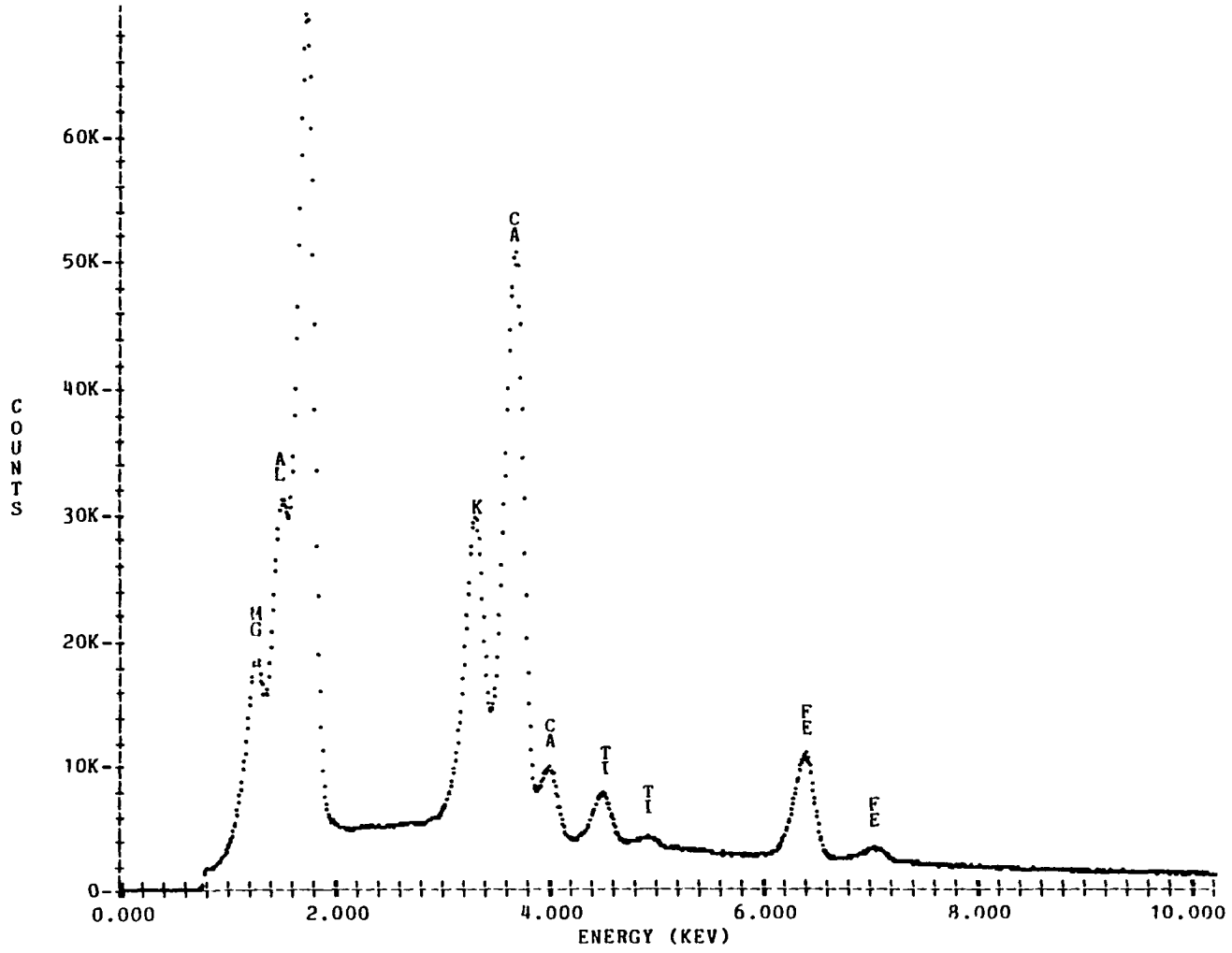
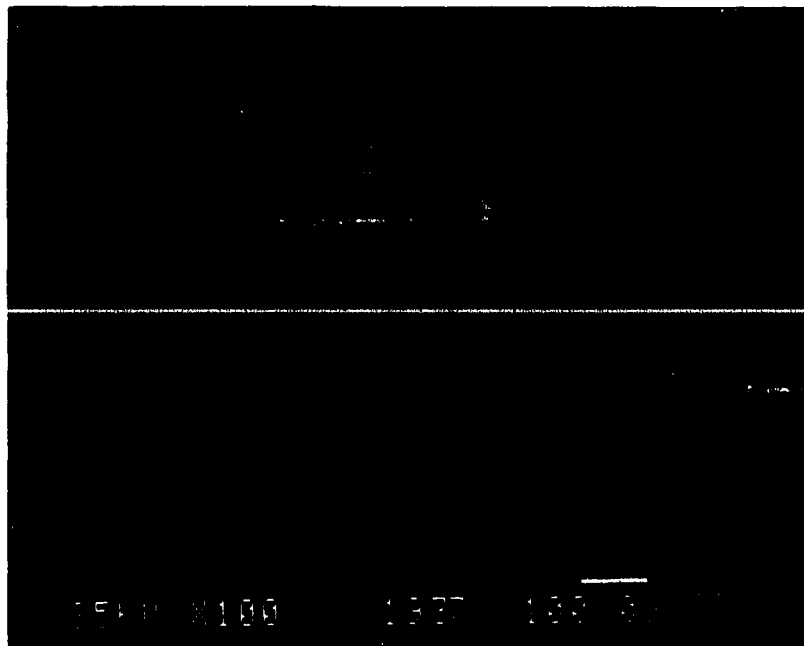
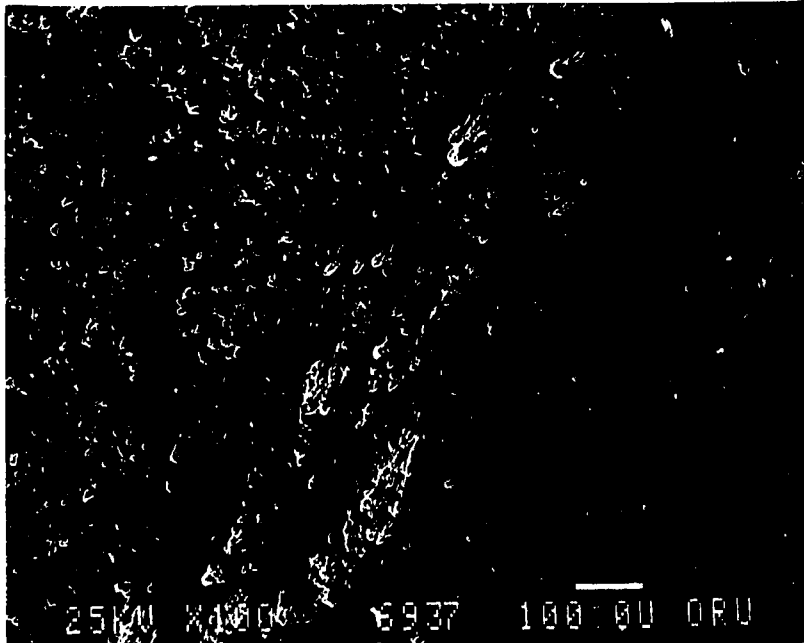
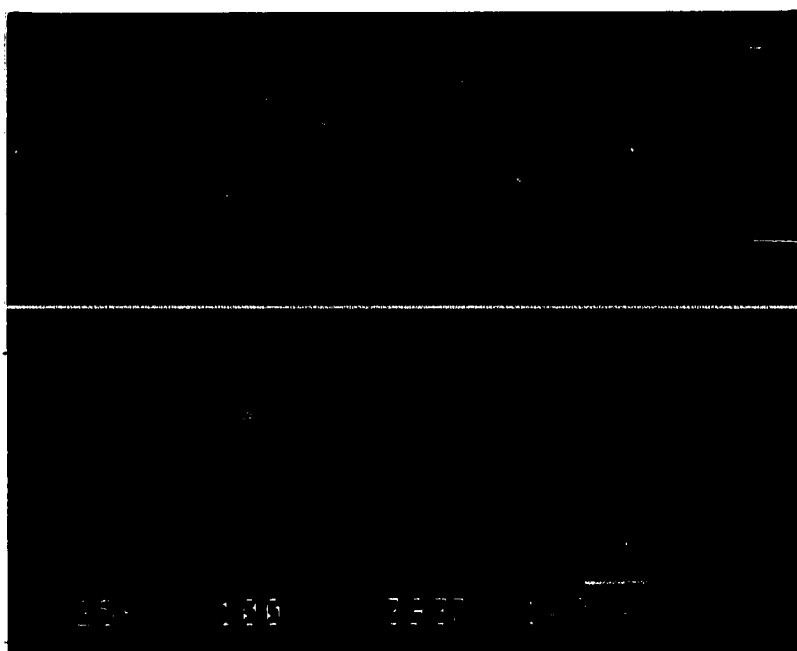
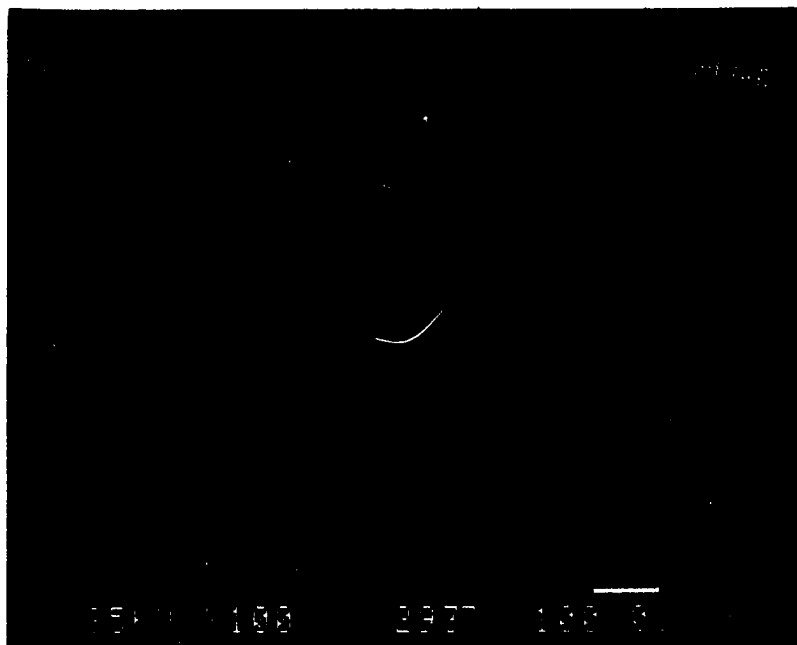
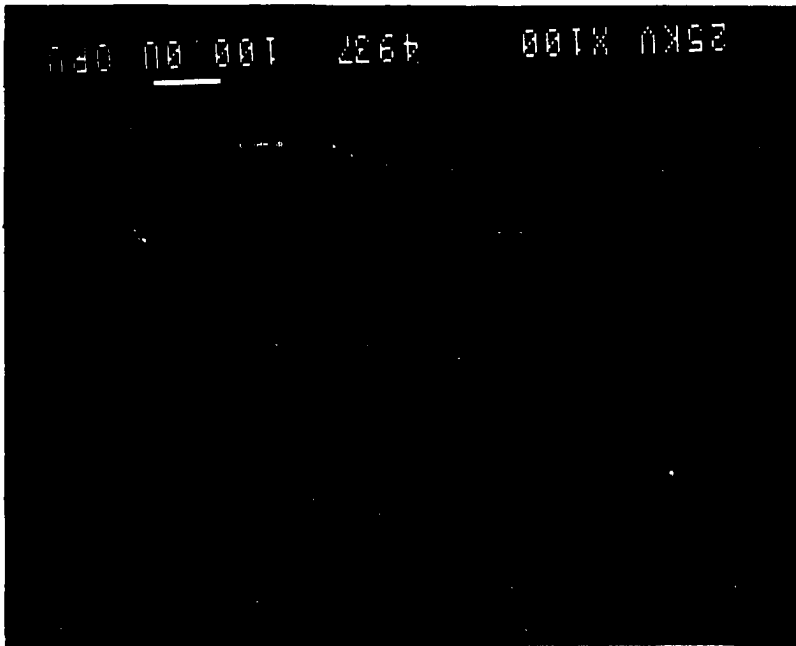
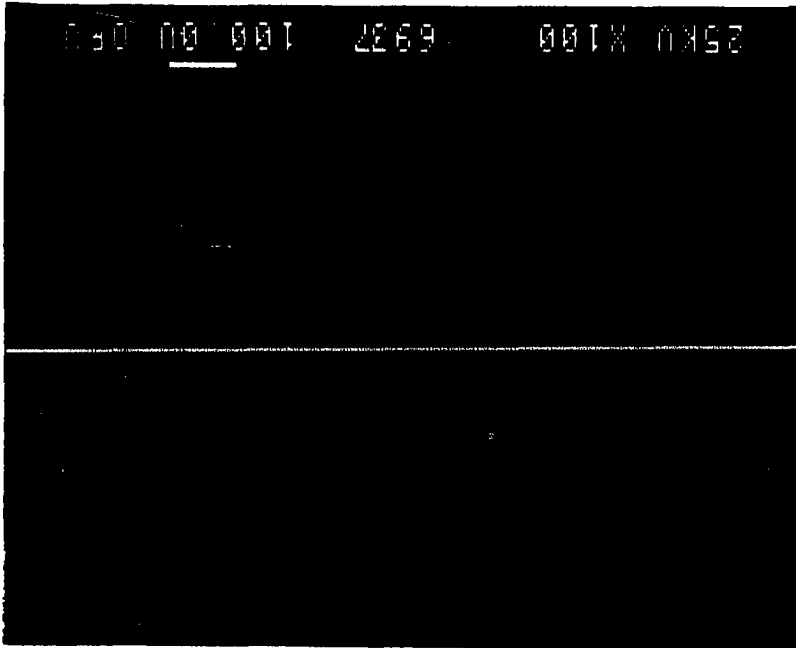


Figure 40(a-f): Representative electron dot map images of sample 937 showing

- a) Secondary electron image of surface.
- b) K alpha for magnesium showing weak accumulation of magnesium in zone.
- c) K alpha for aluminum showing accumulation of aluminum in zone.
- d) K alpha for silicon showing accumulation of silicon in solution zone.
- e) K alpha for potassium showing accumulation in zone.
- f) K alpha for calcium showing depletion in zone.







Location	Sample	Analysis number	Beam diameter	SiO ₂	TiO ₂	Al ₂ O ₃	Fe ₂ O ₃	MgO	CaO	K ₂ O	Total	Mineralogy
Solution zone	814	1	20	40.34	0.20	14.37	1.66	10.67	9.88	8.85	86.01	clay + feldspar
		2	20	43.40	1.26	17.64	3.46	13.60	0.91	8.56	88.63	
		3	20	45.70	1.43	21.98	2.97	12.32	0.10	8.42	92.95	
		4	20	43.48	1.60	20.35	4.78	12.97	0.03	8.90	92.15	
	937	5	20	44.04	1.07	20.56	3.43	13.81	1.16	7.91	92.01	chlorite + illite
		6	20	46.77	1.69	20.66	2.36	9.33	1.46	9.82	92.12	
		13	20	34.89	0.35	16.43	6.32	27.23	0.64	2.88	88.48	
		15	1	33.88	1.79	17.06	7.63	27.78	0.38	0.47	89.04	
		16	10	30.41	3.80	12.04	4.75	24.57	5.07	3.48	84.14	
		17	20	31.94	6.19	16.91	6.07	26.15	0.18	1.31	88.79	
Matrix	814	18	20	31.15	0.01	16.91	7.13	28.52	0.01	0.26	84.03	chlorite + anatase
		23	1	32.09	0.03	11.70	4.43	21.17	0.06	0.37	69.88	
		7	1	44.90	0.00	37.81	2.07	0.47	0.13	8.72	94.10	
		8	1	41.58	0.10	13.06	3.68	26.49	0.13	8.03	93.10	
	937	9	1	38.41	3.05	16.90	12.78	14.60	0.12	6.97	92.43	chlorite phlogopite biotite phlogopite dolomite + clay ferroan dolomite
		10	1	43.05	0.11	14.23	3.06	22.41	0.07	7.72	90.68	
		11	1	7.82	0.02	3.26	2.95	17.74	26.55	0.62	58.99	
		14	10	11.14	0.03	3.62	2.60	17.40	22.00	0.04	57.65	
		20	1	0.10	-	-	0.22	0.43	54.52	-	55.29	
		21	10	0.01	-	-	0.25	0.67	53.59	-	54.53	
Pressure shadow	937	22	1	0.02	-	-	0.18	0.54	56.42	-	57.19	calcite
		19	1	5.78	0.02	0.91	0.60	18.27	32.07	0.44	58.12	calcite + clay
Twinned crystal	937	24	1	-	-	-	0.17	0.47	56.02	-	56.68	calcite

Table 5: Data from microprobe analysis listed as weight percent of 7 elements. The percentages are based on a ZAF correction program. The microprobe was standardized on a 20 micron beam diameter. All beam diameters are in microns. The ZAF correction incorporates adsorption coefficient, takeoff angle and backscatter fluorescence. The program does not correct for CO₂ or H₂O.

atom of a particular element.

Carbon coated thin-sections were used. Beam energy was kept constant throughout the sample runs. A solution zone was selected in six samples. The zone was centered and scanned at a magnification of 100X so that the zone and the matrix could be seen. Dot maps were prepared for magnesium, aluminum, silicon, potassium and calcium. The concentration of dots on the surface corresponds to the concentration of that element on the surface of the sample. Referring to equation 3 of this section it is possible to use the ratio of the number of dots in a certain area on the surface within the solution zone and in the surrounding matrix to estimate the amount of volume loss due to pressure solution in the sample.

The number of dots for each element was counted in a circle of 100 microns diameter (on the surface) in the solution zone and in the matrix. These numerical values correspond to A1 and A2 in equation 3 of this section. The areas where dots were counted were selected at random. Counts were made until values stabilized. In most samples 4 count regions were sufficient for reproducibility.

General Observations.

Two samples were analyzed using the microprobe to determine the mineralogy of accumulated materials in Ss and in the interstices of the adjoining matrix. These data are presented in Table 5. The purpose of these analyses was to determine if the solution zone mineralogy was similar to the mineralogy of the interstitial material in the matrix and if the amount of volume loss along the solution zones could be estimated.

The phases in the spaced cleavage zones are identical to the interstitial material in the matrix (see Table 5). The composition of accumulated material is uniform along the solution zone, (analyses 1-6), consisting of clays (probably illite plus smectite) and feldspar. The composition of the interstitial material in the matrix is similar, (analyses 11 and 12). Detrital muscovite and biotite are present as well as phlogopite (analyses 8,9 and 10). In sample 937 the material on the solution zone has been altered to chlorite (analyses 13, 15, 16,

17, 18, and 23). The interstitial material in the matrix has also been altered to chlorite (analysis 14).

Pressure shadows do not show change in composition along the fiber (analysis 20-22). Fibrous growths of calcite on quartz are syntectonic. Elements that are not accumulated on the solution zone would be free in the system and may be incorporated in the pressure shadows if a stable phase could grow. The pressure shadows serve as independent checks of the assumption that the system is closed to certain elements. The pressure shadow examined does not show contamination along its trace, indicating that calcium is being removed along the solution zones and that aluminum, potassium, silicon, magnesium, iron are locally concentrated in the solution zone, at least during the formation of the pressure shadow. Microprobe analysis indicates that it is possible to determine the amount of volume loss represented by the solution zones.

EDX scans for magnesium, aluminum, silicon, potassium and calcium were made. These elements were the most abundant elements found in both the microprobe analysis and in the EDX scans. Iron was present in some of the scans. Electron dot maps were not prepared for iron because iron is mobile in carbonate rocks, concentrating locally in hematite pods or limonitic stains within the matrix as well as in the solution zones. Titanium was present in some of the specimens as rutile both in the matrix and on Ss. Electron dot maps of titanium were not prepared because the concentrations of titanium were not significantly above background. The numerical values in Table 6 are estimates of the volume loss by pressure solution on Ss. These values are best estimates from dot maps of excitation sites on the surface prepared with an EDX. A value of 1 represents zero material removal by pressure solution. Fractional numbers represent some material removal with smaller ratios representing greater volume loss due to pressure solution. The elements used in the dot maps were present in sufficient concentration to be detected above background. The data in Table 6 are best estimates of the volume loss due to pressure solution assuming one dot in the matrix represents the same mass abundance of the element

as one dot in the solution zone. Each metallic element will be discussed below.

Magnesium is a free ion formed by the dissolution of dolomite and a fixed ion in clays. Magnesium is present in detrital biotite and muscovite. The availability of free magnesium to the system by dissolution of dolomite implies that magnesium may not be useful as an indicator of volume loss by pressure solution. Magnesium is not incorporated into syntectonic pressure shadows. Magnesium is incorporated in chlorite and substitutes freely in clays.

The variation of magnesium is large. In sample 811 the solution zone is depleted in magnesium relative to the matrix. This sample shows a high degree of alteration. Chlorite is present indicating that this sample has been subject to fluid migration and ion exchange of at least magnesium. The variance in magnesium values across the samples is great enough to eliminate the use of magnesium as an indicator of volume loss.

Aluminum is present in clays and feldspar. The abundance of feldspar is small (less than .1%). Some samples contain euhedral, authigenic feldspar. Dissolution of these crystals would provide a small amount of free aluminum to the system. Most of the aluminum is fixed in clays. Aluminum is conserved in metamorphic reactions (Beach, 1982). The deviation in aluminum concentrations is small. This variation is a good indicator of different amounts of volume loss by pressure solution in different parts of a fold. Sample 937 shows the smallest volume loss, sample 814 the largest volume loss.

Silicon is present in the system as a fixed ion in clays and a free ion by dissolution of quartz and feldspar. Silicon is mobile in the system. Tension gashes are filled with syntectonic quartz, indicating that dissolution of quartz has occurred and that silicon has been free to migrate in the system.

Potassium is present in the system in clays and feldspar. The availability of potassium in the system should be similar to aluminum. The behavior of potassium is more variable than aluminum (refer to Table 6).

Discussion. Samples 808 and 809 were collected from the steeply

dipping limb of a fold. Samples 811 and 814 were collected from the hinge zone of a syncline. Samples 816 and 937 were collected from the gently dipping limb of a fold. Samples 811 and 814 show the greatest volume loss. These two samples are from the hinge zones of synclines where the spacing of pressure solution surfaces is the closest. As discussed earlier the hinge zone of a fold is the region of greatest volume loss and the greatest strain rate during fold formation. The values for 808 and 809 are less than the values of 811 and 814. Samples 808 and 809 are from the steep limb of a fold. The spacing of solution surfaces in these samples is intermediate between the core and the shallowly dipping limbs of the folds. The volume loss calculated in samples 816 and 937 (from the shallowly dipping limbs of folds) are the lowest. These samples also have the largest spacing of solution surfaces.

Sample	Magnesium	Aluminum	Silicon	Potassium	Location
808	.43	.40	.56	.83	steep limb
809	.63	.38	.68	.67	steep limb
811	2.17	.37	.43	.63	hinge
814	.52	.35	.41	.47	hinge
816	.82	.42	.31	.47	shallow limb
937	.65	.59	.58	.86	shallow limb

Table 6: Estimates of volume loss due to pressure solution using $A_2/A_1 = (1 - (V'/V))$. Fractional numbers represent samples that show volume loss for that element. The procedure used is discussed in the text.

Aluminum shows the least variance in the calculated values.

Aluminum is conserved in metamorphic reactions and has been used as the basis for general reaction describing pressure solution in greywackes (Beach, 1982). The reactions involve removal of quartz, feldspar and calcite and the growth of muscovite. The system under investigation contains calcite and dolomite with minor quartz, feldspar and phyllosilicates. Muscovite and biotite are present as detrital grains and show reaction to chlorite and phengite in some samples. The accumulated materials in solution zones show alteration to chlorite in some samples. The chlorite is oriented in the same manner as the other phyllosilicates. The formation of chlorite may be synchronous with

pressure solution. Chlorite will incorporate magnesium from dissolving dolomite. Pressure shadows in the samples studied are pure calcite, indicating that calcium has the greatest mobility in the conditions of deformation. The variation of compositions in the samples, especially the presence or absence of chlorite, precludes the preparation of reaction equations describing pressure solution in this system. Chlorite may have formed simultaneously with pressure solution and served as a sink for magnesium, or may have formed later. The alignment of chlorite does not necessarily indicate a syntectonic origin. Chlorite simply assumes the orientation of the mineral being replaced.

The variability of compositions between samples suggests that elements other than aluminum reacted differently in each sample studied. Some samples show formation of chlorite while others do not. The chemical data collected are interpreted as indicating that solution zones are zones of material accumulation. Metamorphic reaction may occur on the solution zones. The degree of metamorphism will depend on the chemistry of the materials accumulating and the movement of water through the system. The variability of magnesium, calcite, silicon and potassium in the samples suggests that these elements are not conserved and are not reliable as indicators of volume loss by pressure solution. Aluminum is preserved in reactions (Beach, 1982) and represents the best element for the determination of volume loss by pressure solution. Pressure solution cleavage zones have acted as zones of accumulation of aluminum, magnesium, potassium and silicon and as zones of depletion of calcium. Metamorphic reactions may occur on the zones during deformation or after deformation. The other elements studied are not conserved in reactions. Pressure shadows of calcite and tension gash infill of calcite and quartz indicate that calcium and silicon were mobile during the deformation. Aluminum, potassium and magnesium were concentrated in the solution zones.

Estimation of strain rate from solution zone spacing

Using the relation derived by Fletcher and Pollard (1981) for the spacing of solution zones it is possible to estimate strain rate. The spacing in Table 4 can be used to calculate the strain rate in portions

of folds in the field area. The expression for the strain rate as a function of effective stress, solution zone spacing, and mineralogy is

$$\dot{\epsilon}_{xx} = 6(C_0/RT)V_0^2(Dk/d^3)(\sigma_{xx}-\sigma_{yy}) \quad (4)$$

where C_0 is the mean concentration of the solid in the fluid film
 V_0 is the specific volume of the solid
 D is the diffusivity of the solute in water
 k is the effective film thickness
 R is the gas constant
 T is absolute temperature
 d is the spacing of the solution zones
 $\sigma_{xx}-\sigma_{yy}$ is the deviatoric stress.

The values used for these variables are as follows. The mean concentration of the solid in the fluid film for calcite is taken from Fletcher and Pollard (1981). Syntectonic growths of calcite fibers indicates that as dolomite is dissolved magnesium is removed from solution within the solution zone. Magnesium is easily incorporated into clays that directly adjoin the point of pressure solution. It is assumed therefore that magnesium does not remain in solution and need not be considered in deriving the mean concentration of the solid in solution. The value used is $3 \times 10^{-7} \text{M/cm}^3$. The specific volume of dolomite is $64.35 \text{ cm}^3/\text{M}$. The diffusivity of the solute is 10^{-5} s (Fletcher and Pollard, 1981). The effective film thickness is 10^{-3} cm (Fletcher and Pollard, 1981). The gas constant is $83.147 \text{ bar cm}^3/\text{deg. KM}$. The absolute temperature is 373°K or 100°C . The values for spacing are taken from Table 5. The effective stress is 30 bars (Fletcher and Pollard, 1981). The calculated strain rates are shown in Table 7.

Location	Sample	Spacing	Strain rate
Core	811	.42 cm.	$9.73 \times 10^{-11}/\text{sec.}$
Core	814	.48 cm.	$6.52 \times 10^{-11}/\text{sec.}$
Core	842	.35 cm.	$1.68 \times 10^{-10}/\text{sec.}$
Core	911	.48 cm.	$6.52 \times 10^{-11}/\text{sec.}$
Steep limb	808	.57 cm.	$3.89 \times 10^{-11}/\text{sec.}$
Steep limb	809	.85 cm.	$1.70 \times 10^{-11}/\text{sec.}$
Steep limb	829	.64 cm.	$2.57 \times 10^{-11}/\text{sec.}$
Shallow limb	816	1.37 cm.	$3.28 \times 10^{-12}/\text{sec.}$

Table 7: Calculated strain rates using equation 4 (from Fletcher and Pollard, 1981). The strain rates are for solution cleavage spacings measured in samples from different parts of folds.

The above values were calculated for temperatures of 100°C . The

effect of raising the temperature to 200° will be to multiply the strain rate by 0.79. The presence of chlorite in the samples does not imply elevated temperatures during deformation, it may simply be replacement of existing clays. The strain rates calculated for either temperature are in the stability field of pressure solution for calcite with crystal sizes of 100 microns in diameter or smaller. The presence of twinned crystals larger than 120 microns in diameter suggests that the values used in the calculation are reasonable. Rutter (1976) shows that under geologic conditions, deformation of crystals smaller than 100 microns in diameter will occur by pressure solution and, for crystals larger than 100 microns, the deformation will be by plastic mechanisms. The values listed in Table 7 are approximations of the conditions of deformation and should not be treated as absolute numbers.

The values in Table 7 are for spacing of solution zones measured in dolomite layers of the Conococheague Formation. Both the limestone and dolomite have deformed primarily by pressure solution. In this case the difference in spacing of solution surfaces or zones may be an important clue in the understanding of the formation of the fabrics and structural elements seen in the units. As previously stated Sp is not marked by the formation of discrete solution zones or surfaces. Pressure solution forming Sp has occurred at crystalline boundaries so the spacing of Sp is the crystal size or approximately 100 microns. Substituting this value into equation 4 of this section along with the appropriate molar volume results in strain rates of 2.36×10^{-9} and 1.86×10^{-9} for deformation at 100° and 200° respectively. The strain rates calculated are within the range of geologic strain rates quoted in the literature (Hobbs, Means and Williams, 1976,; Fletcher and Pollard, 1981). The strain rates are greatest in the hinges of folds and least on the shallowly dipping limbs of folds. Strain rates are greater within the less competent limestone layers. The result of this difference in strain rate is readily visible in the character of the pressure solution and the spacing of solution surfaces as well as in the nature of the folds. The stiffer dolomite layers are the buckling

members that control the fold formation. The limestone layers flowed around the dolomite layers. The dolomite layers deform by the slower process of buckling while the limestone layers deform by the more rapid process of flow. As a generality the difference in strain rates can be thought to represent the difference in kinematic viscosity of the two materials being deformed.

The data indicate that the conditions of deformation which caused the formation of cleavage in the field area was within the stability field of pressure solution for fine grained material and may have been in the stability field of plastic flattening for more coarsely crystalline materials as shown by the textures discussed earlier. The data indicate that volume loss and strain rate was greatest in the hinge zone of folds and least in the shallowly dipping limbs of folds.

CONCLUSIONS

The Conococheague Formation contains two distinct syntectonic cleavage fabrics. A penetrative cleavage(Sp) formed in clean limestone layers, and a spaced cleavage(Ss) formed in sucrosic dolomite layers containing phyllosilicates. Both cleavages formed predominantly by pressure solution. The different appearances of these two types of pressure solution is a function of strain rate (at a given stress) and material property. The presence of impurities such as phyllosilicates may help to localize discrete solution zones.

Pressure solution zones originate at a point and propagate away, curving as the stress field changes orientation relative to bedding during deformation. Impurities are concentrated in discrete solution zones. The orientation of these solution zones track the orientation of maximum principal extension as the zone propagates away from its point of origin. If impurities are not present, discrete solution zones do not develop. In impurity-free systems pressure solution occurs at crystal or grain contacts. As the orientation of maximum compressive stress changes relative to bedding the points of highest stress on crystal or grain boundaries change. This forms a dimensional fabric by the selective removal of asperities. Cleavage fabrics formed by pervasive pressure solution parallel the axis of accumulated elongation. The spacing of pressure solution surfaces or zones depends on the strain rate (for a given stress) which varies with location on folds and with material property. Materials with the closest spacing (limestone) flowed, while dolomite layers buckled. Both materials were deformed primarily by pressure solution.

Incremental strain markers show that layering was not initially horizontal with respect to the applied stress field. The angle of inclination may have been as much as 30° from the applied stress. This

resulted in the formation of asymmetric folds with asymmetrically fanned cleavage nearly parallel with the hinge surface of the folds, in the hinge zone.

The morphology of cleavage in deformed ooids indicates that pressure solution was the dominant deformation mechanism of the ooids. Ooids with dolomitic cores are twinned and show evidence of pressure solution indicating a combination of deformation mechanisms. Crystals larger than 120 microns in diameter are twinned.

Calculation of volume loss by pressure solution shows that volume loss was greatest in the hinge zones of folds and least in the shallowly dipping limbs of folds. Strain rates calculated from solution zone spacing show that the strain rate is the greatest in the hinge of folds and the least in shallowly dipping limbs. Strain rates in limestones are greater than strain rates in dolomites. Calculated strain rates are in the stability field of pressure solution as a deformation mechanism for crystals smaller than 100 microns in diameter under the conditions assumed. Deformation of crystals larger than 120 microns occurred by plastic mechanisms. These results are verified by the presence of twinning in crystals larger than 120 microns in diameter.

Folds are type Ic/1c with minor III folds. In multilayers the competent members are type Ic/1c flattening folds. Dolomite layers rotated and flattened during folding while limestone layers experienced layer parallel shear and flow. Deformation style, cleavage refraction, variation of fold type and deformation mechanism all indicate that the materials deformed viscously.

The following statements can be made from the data.

- 1) The maximum principal shortening axis, measured by incremental strain markers, shows an initial orientation inclined as much as 30° to bedding. There is no evidence to indicate whether the units were tilted relative to the horizontal or whether the compression was tilted relative to horizontal layering.
- 2) The primary deformation mechanism is pressure solution. Crystals larger than 120 microns in diameter deformed by twinning and some

pressure solution. Strain rates calculated from solution cleavage spacing place the deformation near the pressure solution - dislocation glide boundary (Rutter, 1976) for temperatures between 100 and 200°C and crystals approximately 100 microns in diameter.

- 3) The presence of insoluble materials in some layers of the Conococheague caused the formation of solution zones which initiate at crystalline boundaries and coalesce into spaced solution zones. The spacing of these solution zones is dependent on location in the fold and is a function of strain rate. Discrete solution zones do not form in the limestone layers of the Conococheague Formation. Pressure solution in the limestones occurs at crystal boundaries at a spacing of approximately 100 microns. The orientation of the spaced cleavage zones indicate change in bedding orientation relative to the stress field during fold formation. The orientation of bedding relative to the applied stress field and the resultant strain field can be approximated from the analysis of syntectonic fibrous growths of calcite which preserve particle path in the deforming matrix.
- 4) Aluminum is conserved and is useful as a volume loss indicator. Magnesium, potassium, silicon and calcium are not conserved and are not useful as volume loss indicators. The dissolution of dolomite is not followed by the precipitation of dolomite. Magnesium is concentrated in the solution surfaces. Calcite is precipitated in pressure shadows and tension gashes. Silicon is concentrated in the solution zones and to a degree in tension gashes. Magnesium may be concentrated in clays or may be used in the formation of chlorite in the solution zones.

It has been shown that preserved strain paths can be used along with careful observations of cleavage morphology to determine the deformation history of an area. Analysis yields information regarding deformation mechanisms that formed cleavage within the region and allows the estimation of volume loss due to pressure solution.

The deformation history of a small portion of the Virginia Great Valley has been described. Pressure solution was the dominant mechanism that acted to form two geometrically distinct cleavages. The

interpretations derived in this paper are valid for the deformation of any carbonate sequence under similar conditions. Pressure solution is an important deformation mechanism that is responsible rock fabrics in fine grained carbonate rocks deformed under low temperature, low confining pressure and low strain rate conditions.

REFERENCES

- Alterman, I. B., 1973, Rotation and dewatering during slaty cleavage formation: some new evidence and interpretations: *Geology*, v. 1, p. 33-36.
- Alvarez, W., Engelder, T., and Geiser, P. A., 1978, Classification of solution cleavage in pelagic sediments: *Geology*, v. 6, p. 263-266.
- Anthony, M., and Wickham, J., 1978, Finite element simulation of asymmetric folds: *Tectonophysics* v. 47, p. 1-14.
- Beach, A., 1979, Pressure solution as a metamorphic process in deformed terrigenous sedimentary rocks: *Lithos*, v. 12, p. 51-58.
- Beach, A., 1982, Deformation mechanisms in some cover thrust sheets from the external French Alps: *Journal of Structural Geology*, v. 4, p. 137-150.
- Bell, T. H., 1981, Foliation development: the contribution, geometry, and significance of progressive, bulk inhomogeneous shortening: *Tectonophysics*, v. 75, p. 273-296.
- Beutner, E. C., 1978, Slaty cleavage and related strain in Martinsburg slate, Delaware Water Gap, New Jersey: *Amer. Jour. Sci.*, v. 278, p. 1-23.
- Beutner, E. C., 1980, Slaty cleavage unrelated to tectonic dewatering: The Siamo and Michigamme slates revisited: *Geol. Soc. Amer. Bull.*, v. 91, p. 171-178.
- Biot, M. A., 1965, Mechanics of Incremental Deformation: John Wiley & Sons, Inc., New York, 504 pp.
- Borradaile, G. J., 1978, Transected folds: A study illustrated with examples from Canada and Scotland: *Geol. Soc. America Bull.*, v. 89, p. 481-493.
- Boulter, C. A., 1974, Tectonic deformation of soft sedimentary clastic dikes from the Precambrian rocks of Tasmania, Australia, with particular reference to their relations with cleavages: *Geol. Soc. Amer. Bull.*, v. 81, p. 589-609.
- Chapple, W. M., and Spang, J. H., 1974, The importance of layer-parallel slip during folding of layered sedimentary rocks: *Geol. Soc. America Bull.*, v. 85, p. 1523-1534.
- Clark, B. R., 1970, Origin of slaty cleavage in the Coeur d'Alene District, Idaho: *Geol. Soc. Amer. Bull.*, v. 81, p. 3061-3072.
- Clark, B. R., 1974, Mechanical formation of preferred orientation in clays: *Amer. Jour. Sci.*, v. 269, p. 250-266.

- Cloos, E., 1947. Oolite deformation in the South Mountain fold, Maryland: Geol. Soc. Amer. Bull., v. 58, p. 843-918.
- Cloos, E., 1971, Microtectonics along the western edge of the Blue Ridge, Maryland and Virginia: Johns Hopkins Press, Baltimore, Studies in Geology no. 20, 234 pp.
- de Boer, R. B., 1977, On the thermodynamics of pressure solution Interaction between chemical and mechanical forces: Geochim. Cosmochim Acta, v. 41, no. 2, p. 249-256.
- de Poar, D. G., 1980, Some limitations of the Rf/0 technique of strain analysis: Tectonophysics, v. 64, no. 1/2, p. T/29-T/31.
- Dieterich, J. H., 1969, Origin of cleavage in folded rocks: Amer. Jour. Sci., v. 267, p. 155-165.
- Dieterich, J. H., and Carter, N. L., 1969, Stress history of folding: Amer. Jour. Sci., v. 267, p. 129-154.
- Dunnet, D., 1969, A technique of finite strain analysis using elliptical particles: Tectonophysics, v. 7, p. 117-136.
- Dunnet, D., and Siddans, A. W. B., 1971, Non-random sedimentary fabrics and their modification by strain: Tectonophysics, v. 12, p. 307-325.
- Durney, D. W., 1972, Solution transfer, an important geological deformation mechanism: Nature, v. 235, p. 315-317.
- Durney, D. W., 1976, Pressure-solution and crystallization deformation: Phil. Trans. Royal soc. London, Ser. A., v. 283, no. 1312, p. 229-240.
- Durney, D. W., 1978, Early theories and hypotheses on pressure-solution-redeposition: Geology, v. 6, no. 6, p. 369-372.
- Durney, D. W., and Ramsay, J. G., 1973, Incremental strains measured by syntectonic crystal growths In: K. A. DeJong and R. Scholten (eds.), Gravity and Tectonics, Wiley, New York, p. 67-96.
- Edmundson, R. S., and Nunan, W. E., 1973, Geology of the Berryville, Stephenson, and Boyce quadrangles, Virginia: Report of Investigations, no. 34, Virginia Division of Mineral Resources, Charlottesville, Virginia, 112 pp.
- Elliott, D., 1968, Determination of finite strain and initial shape from deformed elliptical objects: Geol. Soc. Amer. Spec. Paper, no. 115, 57 pp.
- Elliott, D., 1970, Determination of finite strain and initial shape from deformed elliptical objects: Geol. Soc. Amer. Bull., v. 81, no. 8, p. 2221-2236.
- Elliott, D., 1972, Deformation paths in structural geology: Geol. Soc. Amer. Bull., v. 83, p. 2621-2638.
- Elliott, D., 1973, Diffusion flow laws in metamorphic rocks: Geol. Soc. Amer. Bull., v. 84, p. 2645-2662.
- Epstein, J. B., and Epstein, A. G., 1969, Geology of the Valley and Ridge Province between Delaware Water Gap and Lehigh Gap, Pennsylvania, In: Subitzky, S. (ed.), Geology of selected areas in New Jersey and eastern Pennsylvania and guidebook of excursions, 1969, Ann. Mtg. Geol. soc. Amer., Atlantic City, N.J., New Brunswick Rutgers Univ. Press, p. 132-205.

- Etheridge, M. A., 1973, Experimentally produced slaty and crenulation cleavage during a single deformation: *Geol. Soc. Aus. Jour.*, v. 20, p. 223-227.
- Etheridge, M. A., and Hobbs, B. E., 1974, Chemical and deformation controls on recrystallization of mica: *Cont. Min. Pet.*, v. 43.
- Fletcher, R. C., 1982, Coupling of diffusional mass transport and deformation in a tight rock: *Tectonophysics*, v. 83, p. 275-291.
- Fletcher, R. C., and Pollard, D. D., 1981, Anticrack model for pressure solution surfaces: *Geology*, v. 9, p. 419-424.
- Gibbs, J. W., 1876, On the equilibrium of heterogeneous substances: *Trans. Conn Acad.*, III, p. 108-248. (Also published in 1961 in *The Scientific Papers of J. W. Gibbs*, Dover, 460pp.)
- Geiser, P. A., 1974, Cleavage in some sedimentary rocks of the central Valley and Ridge Province, Maryland: *Geol. Soc. Amer. Bull.*, v. 85, p. 1399-1412.
- Geiser, P. A., 1975, Slaty cleavage and the dewatering hypothesis, an examination of some critical evidence: *Geology*, v. 3, no. 12, p. 717-720.
- Gill, G. E., 1980, Deformation history and origin of slaty cleavage in the Martinsburg Formation near Harrisburg, Pennsylvania: *Northeastern Geology*, v. 2, no. 2, p. 62-67.
- Gray, D. R., 1977, Differentiation associated with discrete crenulation cleavages: *Lithos*, v. 10, p. 89-101.
- Gray, D. R., 1978, Cleavages in deformed psammitic rocks from southeastern Australia: their nature and origin: *Geol. Soc. Amer. Bull.*, v. 89, p. 577-590.
- Gray, D. R., 1981, Cleavage-fold relationships and their implications for transected folds: and example from southwest Virginia, U.S.A.: *Jour. Struct. Geol.*, v. 3, p. 265-277.
- Gregg, W. J., 1979, The redistribution of pre-cleavage clastic dikes by folding at New Paltz, New York: *Jour. Geol.*, v. 87, p. 99-104.
- Groshong, R. H., 1975, Strain, fractures, and pressure solution in natural single layer folds: *Geol. Soc. Amer. Bull.*, v. 86, p. 1363-1376.
- Groshong, R. H., Jr., 1975, "Slip" cleavage caused by pressure solution in a buckle fold: *Geology*, v. 3, p. 411-413.
- Groshong, R. H., Jr., 1976, Strain and pressure solution in the Martinsburg slate, Delaware Water Gap, New Jersey: *Amer. Jour. Sci.*, v. 276, p. 1131-1146.
- Groves, G. W., and Kelley, A., 1969, Change of shape due to dislocation climb: *Phil. Mag.*, v. 19, p. 977-986.
- Helmstaedt, H., and Greggs, R. G. 1980, Stylolitic cleavage and cleavage refraction in lower Paleozoic carbonate rocks of the Great Valley, Maryland: *Tectonophysics*, v. 66, p. 99-114.
- Hobbs, B. E., 1966, Microfabric of tectonites from the Wyangala Dam area, New South Wales, Australia: *Geological Society of America Bulletin*, v 77, p 685-706.
- Hobbs, B. E., 1968, Recrystallization of single crystals of quartz: *Tectonophysics*, v. 6, p 353-401.

- Hobbs, B. E., Means, W. D., and Williams, P. F., 1976, An outline of structural geology: John Wiley and Sons, New York, 577 p.
- Holeywell, R. C., and Tullis, T. E., 1975, Mineral reorientation and slaty cleavage in the Martinsburg Formation, Lehigh Gap, Pennsylvania: *Geol. Soc. Amer. Bull.*, v. 86, p. 1296-1304.
- Hudleston, P. J., 1973, Fold morphology and some geometrical implications of theories of fold development: *Tectonophysics*, v. 16, p. 1-46.
- Jeffery, G. B., 1923, The motion of ellipsoidal particles immersed in a viscous fluid: *Royal Soc. London Proceedings, Ser. A.*, v. 192, p. 161-179.
- Kamb, W. B., 1959, Theory of preferred orientations developed by crystallization under stress: *Jour. Geol.*, v. 67, p. 153-170.
- Knipe, R. J., 1979, Chemical changes during slaty cleavage development, In: *Mecanismes de deformation des mineraux et des roches*, Nicholas, A. et al. (compiler), Soc. Fr. Mineral Cristallogi., Bull. v. 102, no. 2-3, p. 206-209.
- Knipe, R. J., 1981, The interaction of deformation and metamorphism in slates: *Tectonophysics*, v. 78, p. 249-272.
- Le Tehoff, B., 1979, Non-coaxial deformation of elliptical particles: *Tectonophysics*, v. 53, p. T/7-T/14.
- March, A., 1932, Mathematische theorie der regelung nach der korngestalt bei affiner deformation: *Zeitschrift Kristallographie*, v. 81, p. 285-298.
- Maxwell, J. C., 1962, Origin of slaty and fracture cleavage in the Delaware Water Gap area, New Jersey and Pennsylvania: *Geol. Soc. Amer. Bulletin* Volume, p. 281-311.
- Merino, E., and Ortoleva, P., 1980, Temporal development of fabric in uniaxially stressed polycrystalline media: a theory: *Contributions to Mineralogy and Petrology*, v. 71, p. 429-435.
- O'Nan, M., 1971, Linear Algebra: Eagle Mathematics Series, Volume 2A, Harcourt Brace Jovanovich Inc., New York, 385 p.
- Plessman, von W., 1964, Gesteinlösung, ein Hauptfactor beim Schieferungsprozess: *Geol. Mitt.*, v. 4, p. 69-82.
- Plessman, von W., 1966, Solution, deformation, transportation and structure (in German): *Z. Deut. Geol. Ges.* v. 115, pt. 2-3, p. 650-663.
- Powell, C. McA., 1969, Intrusive sandstone dikes in the Siamo Slate near Negaunee, Michigan: *Geol. Soc. Amer. Bull.*, v. 80, p. 2585-2594.
- Powell, C. McA., 1972a, Tectonic dewatering and strain in the Michigamme Slate, Michigan: *Geol. Soc. Amer. Bull.*, v. 83, p. 2149-2158.
- Powell, C. McA., 1972b, Tectonically dewatered slates in the Ludlorian of the Lake District, England: *Geol. Jour.*, v. 8, p. 95-110.
- Powell, C. McA., 1973, Clastic dikes in the Bull Formation of Cambrian age, Taconic Allochthon, Vermont: *Geol. Soc. Amer. Bull.*, v. 84, p. 3045-3050.
- Powell, C. McA., 1974, Timing of slaty cleavage during folding of Precambrian rocks, northwest Tasmania: *Geol. Soc. Amer. Bull.*, v. 85, p. 1043-1060.

- Powell, C. McA., 1979, A morphological classification of rock cleavage: *Tectonophysics*, v. 58, p. 21-34.
- Ragan, D. M., 1973, Structural geology: an introduction to geometrical techniques: second edition, John Wiley and Sons, New York, 208 pp.
- Ramberg, H., 1975, Particle paths, displacement and progressive strain applicable to rocks: *Tectonophysics*, v. 28, p. 1-38.
- Ramsay, J. G., 1967, Folding and Fracturing of Rocks: McGraw Hill Book Co., New York, 568 pp.
- Ramsay, J. G., and Wood, D. S., 1973, The geometric effects of volume change during deformation processes: *Tectonophysics*, v. 16, p. 263-277.
- Robin, P. Y. F., 1978a, On the thermodynamics of pressure solution, interaction between thermal and mechanical forces: discussion: *Geochim. et Cosmochim. Acta*, v. 31, no. 3, p. 333-336.
- Robin, P. Y. F., 1978b, Pressure solution at grain to grain contacts: *Geochim. Cosmochim. Acta*, v. 42, no. 9, p. 1383-1389.
- Roy, A. B., 1978, Evolution of slaty cleavage in relation to diagenesis and metamorphism: A study from the Hunsruckschiefer: *Geol. Soc. Amer. Bull.*, v. 89, p. 1775-1785.
- Rutter, E. H., 1974, The influence of temperature, strain rate and interstitial water in the experimental deformation of calcite rocks: *Tectonophysics*, v. 22, p. 311-334.
- Rutter, E. H., 1976, The kinetics of rock deformation by pressure solution: *Phil. Trans. Roy. Soc. London, Ser. A.*, v. 283, no. 1312, p. 203-219.
- Rutter, E. H., and Rusbridge, M., 1977, The effect of non-coaxial strain paths on crystallographic preferred orientation development in the experimental deformation of a marble: *Tectonophysics*, v. 39, p. 73-86.
- Siddans, A. W. B., 1972, Slaty cleavage - a review of research since 1815: *Earth Sci. Rev.*, v. 8, p. 205-232.
- Siddans, A. W. B., 1980, Analysis of three-dimensional, homogeneous, finite strain using ellipsoidal objects: *Tectonophysics*, v. 64, no. 1/2, p. 1-16.
- Sprunt, E. S., and Nur, A., 1977, Destruction of porosity through pressure solution: *Geophysics*, v. 42, no.4, p. 726-741.
- Spry, A., 1969, Metamorphic Textures: Pergamon Press, Oxford, 350 pp.
- Treagus, S. H., 1981, A theory of stress and strain variations in viscous layers and its geologic implications: *Tectonophysics*, v. 72, p. 75-103.
- Treagus, S. H., 1982, A new isogon-cleavage classification and its application to natural and model folds: *Geol. Jour.*, v. 17, p. 49-64.
- Treagus, J. E., and Treagus, S. H., 1981, Folds and the strain ellipsoid: a general model: *Jour. Struct. Geol.*, v. 3, p. 1-17.
- Tullis, T. E., 1976, Experiments on the origin of slaty cleavage and schistosity: *Geol. Soc. Amer. Bull.*, v. 87, p. 745-753.

- Tullis, T. E., and Wood, D. S., 1975, Correlation of finite strain from both reduction bodies and preferred orientation of mica in slate from Wales: *Geol. Soc. Amer. Bull.*, v. 86, p. 632-638.
- Wagner, F., Wenk, H. R., Kern, H., Van houtte, P., and Esling, C., 1982, Development of preferred orientation in plane strain deformed limestone: Experiment and Theory: *Contributions to Mineralogy and Petrology*, v. 80, p. 132-139.
- Wenk, H. R., and Shore, J., 1975, Preferred orientation in experimentally deformed dolomite: *Contributions to Mineralogy and Petrology*, v. 50, p. 115-126.
- Wenk, H. R., Venbitasubramanyan, C. S., and Baker, D. W., and Turner, F. J., 1973, Preferred orientation in experimentally deformed limestone: *Contributions to Mineralogy and Petrology*, v. 38, p. 81-114.
- Weyl, P. K., 1959, Pressure solution and the force of crystallization a phenomenological theory: *Jour. Geophy. Res.*, v. 64, no. 11, p. 2001-2025.
- White, S. H., and Knipe, R. J., 1978, Microstructure and cleavage development of selected slates: *Cont. Min. Pet.*, v. 66, no. 2, p. 165-174.
- Wickham, J. S., 1969, Structural Geology of the western slope of the Blue Ridge near Front Royal, Virginia: PhD. Dissertation, Johns Hopkins Univ., 129 pp.
- Wickham, J. S., 1972, Structural geology of a portion of the Blue Ridge, northern Virginia: *Geol. Soc. Amer. Bull.*, v. 83, p. 723-760.
- Wickham, J. S., 1973, An estimate of strain increments in a naturally deformed carbonate rock: *Amer. Jour. Sci.*, v. 273, p. 23-47.
- Wickham, J. S., and Anthony, M., 1978, Strain paths and folding of carbonate rocks near Blue Ridge, central Appalachians: *Geol. Soc. Amer. Bull.*, v. 88, p. 920-924.
- Williams, P. R., 1972, Development of metamorphic layering and cleavage in low grade metamorphic rocks at Bermagui, Australia: *American Journal of Science*, v. 272, p. 1-47.
- Willis, D. G., 1977, A kinematic model of preferred orientation: *Geol. Soc. Am. Bull.*, v. 88, p. 883-894.
- Wintsch, R. P., 1978, A chemical approach to the preferred orientation of mica: *Geol. Soc. Am. Bull.*, v. 89, p. 1715-1718.
- Wood, D. S., 1974, Current views of the development of slaty cleavage: *Ann. Rev. Earth Planet. Sci.*, v. 2, p. 309-401.

APPENDIX A
PROGRAMS

PROGRAM DIGIT

```

100 PAGE
110 PRINT "Data transfer program from Summagraphics to disk"
120 PRINT
130 PRINT
140 PRINT "Mount the disk you will store data on. This program will"
150 PRINT "load data in discrete packs onto disk. The data files will be"
160 PRINT "created by the program on your command and will be titled."
170 PRINT "Turn on the hard copy unit for a copy of your data "
180 PRINT
190 PRINT "To hook up the digitizer, plug light gray cord into modem on"
200 PRINT "Summagraphics and into RS232 on Tectronix. This program is "
210 PRINT "set to receive at 1200 baud. The data format is for 7 data "
220 PRINT "bits and 2 stop bits with even parity and no parity error"
230 PRINT "action. These parameters can be changed in the program or"
240 PRINT "in the Summagraphics. See Tectronix Communication Interface"
250 PRINT "manual or Summagraphics Technical Information. If data"
260 PRINT "format does not match program, no transmission will occur."
270 PRINT
280 PRINT "Digitize using the following format:"
290 PRINT
300 PRINT "Suture, first data point use flag#1 (WHITE) on cursor F=3"
310 PRINT " The suture will be the origin"
320 PRINT "Fiber points use flag#Z (YELLOW) F=1"
330 PRINT "To end data set, make a copy of the data and go on to a new "
340 PRINT "data set and file use, centroid flag#3 (GREEN) F=2"
350 PRINT "To end the program, close all files, reset all parameters"
360 PRINT "and copy the screen use flag#2 (BLUE) F=4"
370 PRINT
380 PRINT "Press RETURN to continue"
390 INPUT Z$
400 REM
410 PAGE
420 PRINT "Enter file identifier."
430 INPUT C$
440 PRINT "Input file size."
450 INPUT C1
460 CREATE C$,"auct";C1,0
470 OPEN C$:1,"F",M$
480 CALL "rewind",1
490 PRINT
500 PRINT "The file had been created and is ready for data "
510 PRINT
520 PRINT "Press RETURN TO BASIC key. The terminal is ready for data"
530 REM SET UP MICROPROCESSOR AND SEND PROMPT TO SUMMAGRAPHICS
540 CALL "TERMIN"
550 PRINT
560 PRINT "Enter the title of this data set"
570 INPUT E$
580 PAGE
590 PRINT E$
600 PRINT #1:E$
610 REM SET BAUD RATE, EVEN PARITY AND NO PARITY ERROR ACTION
620 CALL "RATE",1200,0,0
630 REM SET UP FLAG CONTROL AND DATA MANIPULATION
640 REM
650 INPUT @40:F,X,Y
660 IF F=4 THEN 910
670 PRINT F,X,Y
680 REM SET UP HARD COPIER TO COPY ON PAGE FULL CONDITION
690 PRINT @32,26:3
700 PRINT #1:F,X,Y
710 IF F=2 THEN 730

```

```
720 GO TO 650
730 CLOSE 1
740 COPY
750 PAGE
760 PRINT "__INPUT NEW FILE NAME__"
770 INPUT B$
780 PRINT "INPUT FILE SIZE"
790 INPUT C3
800 CREATE B$,"AUCN";C3,0
810 OPEN B$;1,"F",M$
820 CALL "REWIND",1
830 PRINT "READY FOR DATA ___"
840 PRINT
850 PRINT "INPUT TITLE OF DATA SET"
860 INPUT F$
870 PAGE
880 PRINT F$
890 PRINT #1:F$
900 GO TO 640
910 REM RESTORE ALL PARAMETERS TO ORIGINAL POWER UP CONDITION
920 COPY
930 PRINT @37,0:13,255,255
940 PRINT @32,26:0
950 INIT
960 END
```

PROGRAM DRAFT

```

1230 PRINT "_"
1240 PRINT "-"
1260 REM -- SET UP DIGITIZER INTERFACE
1270 GOSUB 6000
2000 PRINT "--"
2010 PRINT "DEPRESS 'ORIGIN' BUTTON AND SIMULTANEOUSLY"
2020 PRINT "  DIGITIZE THE LOWER LEFT CORNER OF MAP"
2030 INPUT @40:F,X0,Y0
2040 PRINT "--"
2050 PRINT
2060 PRINT "DIGITIZE THE UPPER RIGHT CORNER OF MAP      "
2070 INPUT @40:F,X9,Y9
2080 PRINT "--"
2120 DIM X(500),Y(500)
2230 I=1
2240 INPUT @40:F,X(I),Y(I)
2250 REM GET SECOND AND SUBSEQUENT POINTS
2260 I=2
2270 INPUT @40:F,X(I),Y(I)
2280 REM IF X<0 THEN WE ARE DONE WITH THIS CURVE
2290 REM ELSE, KEEP GETTING POINTS
2300 IF X(I)<0 THEN 3000
2310 I=I+1
2320 GO TO 2270
3000 REM COMPUTE LENGTH AND AREA OF CURVE, AND PLOT IT IF LAST Y WAS >0
3010 N=I-1
3220 REM -- PLOT CURVE
3230 GOSUB 4000
3240 REM DIGITIZE ANOTHER CURVE
3250 PRINT "-";
3260 GO TO 2230
4000 REM SUBROUTINE TO PLOT A CURVE
4030 WINDOW 0,150,0,100
4040 VIEWPORT 0,150,0,100
4100 U=X(1)
4110 V=Y(1)
4120 REM SCALE X AND Y (U AND V)
4130 GOSUB 5000
4140 MOVE @1:U,V
4150 FOR I=2 TO N
4160 U=X(I)
4170 V=Y(I)
4180 GOSUB 5000
4190 DRAW @1:U,V
4200 NEXT I
4210 MOVE @1:0,0
4220 @=1
4230 RETURN
5000 REM -- SCALES X AND Y
5010 REM X9, Y9, ARE MAX VALUES IN X AND Y DIRECTIONS
5020 U=U/X9*150
5030 V=V/Y9*100
5040 RETURN
6000 REM SET UP DIGITIZER INTERFACE"
6010 PRINT
6020 PRINT "HIT 'RETURN TO BASIC' KEY"
6030 CALL "TERMIN"
6040 CALL "RATE",1200,0,0
6050 RETURN

```

PROGRAM ELLIPSE

```
100 PAGE
110 PRINT "Input long axis dimension of ellipse, A=";
120 INIT
130 INPUT A
140 PRINT "Enter short axis dimension of ellipse, B=";
150 INPUT B
160 PRINT "Enter location of center of ellipse, H,K ";
170 INPUT H,K
180 PAGE
190 VIEWPORT 0,150,0,100
200 WINDOW -15,15,-10,10
210 DIM X(148),Y(148)
220 FOR I=0 TO 2*PI STEP PI/72
230 Z=I*72/PI+1
240 X(Z)=A*COS(I)+H
250 Y(Z)=B*SIN(I)+K
260 NEXT I
270 GOSUB 300
280 HOME @1:
290 END
300 REM SUBROUTINE TO draw ELLIPSE
310 MOVE @1:X(1),Y(1)
320 FOR J=1 TO 145
330 DRAW @1:X(J),Y(J)
340 NEXT J
350 MOVE @1:-A,0
360 DRAW @1:A,0
370 MOVE @1:0,-B
380 DRAW @1:0,B
390 HOME @1:
400 PRINT @1:"AXIAL RATIO = ":A
410 RETURN
```

PROGRAM FISH

**** TSO FOREGROUND HARDCOPY ****
 DSNAME=AA0041.FISH.PORT

```

C LAST ACCESS 5-18
C   MAIN PROGRAM
C
C   ROGER FEENSTRA, MODIFIED BY GAYLE TAPP(1979)
C   FISHER AND WATSON ANALYSIS OF DIRECTIONAL DATA ON THE
C   SPHERE
C
C   NOTE: INCLINATION OUTPUT IS FOR TOTAL SPHERE -
C         NOT JUST THE LOWER HEMISPHERE OF THE
C         STEREONET -- CONSEQUENTLY, NEGATIVE
C         INCLINATIONS POINT UPWARD INTO UPPER
C         HEMISPHERE AND POSITIVE POINT DOWNWARD
C         INTO LOWER HEMISPHERE.
C
C THIS PROGRAM USES THE SAME DATASET AS THE KALSBECK PROGRAM
C THE FIRST CARD OF THE DATASET IS READ BUT IGNORED
C THE PROGRAM HAS BEEN CHANGED TO READ ONLY STRIKE AND DIP
C THE PROGRAM WILL READ ONLY ONE DATASET AT A TIME
C
CCCCCCCCCCCCCCCCCCCCCCCCCCCCCCCCCCCCCCCCCCCCCCCCCCCCCCCCCCCC
  DIMENSION X(3,3),K2(3),Y(3),D(3),RR(3,3),TITLE(60),
  1DUMMY(40)
  COMMON/ONE/AZC(500),ROEC(500)
  EQUIVALENCE (Y(1),XL), (Y(2),XM), (Y(3),XN)
  DATA K2/'L','M','N'/
  DATA ID17, ID26, ID31, ID35/1HE, 1HN, 1HS, 1HW/
  READ (5,993) (DUMMY(I),I=1,40)
993  FORMAT(40A1)
C   NCASE = NUMBER OF DATA SETS
  DATA KODE,NCASE/1,1/
C   READ(5,2) NCASE
  2   FORMAT(I2)
  IF (NCASE.LE.0) STOP
  DO 92 LCSE=1,NCASE
  C   SITE = NAME OF DATA SET
  READ(5,14) KODE
  14  FORMAT(I1)
  C   WRITE(6,998) LCSE
998  FORMAT(//,1X,'**CASE ',I4)
  READ(5,997) N,(TITLE(I),I=1,60)
  997  FORMAT(I4,60A1)
  C   WRITE(6,997)
  READ(5,702) N
  702  FORMAT(I4)
  C   WRITE(6,777) N
  777  FORMAT(1H1,/,I4)
  SXL=0.0
  SYX=0.0
  SYN=0.0
  CL=0.10
  ZERO=0.0
  DO 16 I=1,3
  DO 16 J=1,3
  16  X(I,J) = 0.0
  SUM = 0.0
  KOU = 0

```

```

C      CHECK KODE FOR TYPE OF DATA SET.
150  IF (KODE.EQ.2) GO TO 17
      CALL POLE2(ID17, ID26, ID31, ID35, N)
      GO TO 20
17    READ(5, 86) THE, PHI
86    FORMAT(2P10.3)
      IF (THE + 900.0) 20, 40, 20
20    CONTINUE
      DO 701 II = 1, N
          RPHI = ROEC(II) * 0.0174533
          RTHE = AZC(II) * 0.0174533
          KOU = II
C      COMPUTE DIRECTION COSINES, IRVINGS CONVENTIONS
          XL = COS(RPHI) * COS(RTHE)
          XM = COS(RPHI) * SIN(RTHE)
          XN = SIN(RPHI)
          IPHI = IFIX(ROEC(II))
          ITHE = IFIX(AZC(II))
          DO 25 K=1, 3
          DO 25 I=1, 3
25    X(K, I) = X(K, I) + Y(K) * Y(I)
          SXL = SXL + XL
          SXM = SXM + XM
          SXN = SXN + XN
701  CONTINUE
40    XKOU = KOU
      WRITE (6, 888) (TITLE(I), I=1, 60), N
888  FORMAT (1H1, 60A1, 5X, I4, 14H OBSERVATIONS///)
      WRITE(6, 38) SXL, SXM, SXN
38    FORMAT(3X, 6HTOTALS, 22X, 3P11.4)
43    RSQ = SXL*SXL + SXM*SXM + SXN*SXN
      R = SQRT(RSQ)
C      WRITE (6, 44) KOU
44    FORMAT(/3X, 10HNUMBER OBS, I6)
      IF (KOU.LE.2) GO TO 46
      WRITE(6, 45) R
45    FORMAT(/3X, 3HR =, F10.3)
46    CONTINUE
      WRITE(6, 49)
49    FORMAT(/3X, 27H*** EIGENVALUE ANALYSIS ***/)
      WRITE(6, 5)
5    FORMAT(/3X, 24HSUM CROSS PRODUCT MATRIX//12X, 1HL, 11X, 1HM, 12X, 1HN/)
      DO 50 K=1, 3
50    WRITE(6, 6) KP(K), (X(K, I), I=1, K)
6    FORMAT(3X, A3, 3F12.5)
      DO 60 I=1, 3
60    SUM = SUM + X(I, I)
      WRITE(6, 10) SUM
10    FORMAT(/3X, 9HSUM OF SQ, F13.5//)
      CALL EIGEN(X, 3, D, RR, ITER, NER)
      DO 90 I=1, 3
      DO 82 J=1, 3
82    RR(I, J) = -RR(I, J)
      WRITE(6, 83) I, D(I)
83    FORMAT(/, 3X, 12HEIGENVALUE (, I1, 3H) =, F10.5).
      WRITE(6, 85) (RR(I, J), J=1, 3)
85    FORMAT(5X, 12HEIGENVECTORS, 5X, 3P15.5)
      AZ = ATAN2(RR(I, 2), RR(I, 1)) * 57.2957795
      IF (AZ.LT.0.0) AZ = AZ + 360.
      ZIN = ARCSIN(RR(I, 3)) * 57.2957795
      WRITE(6, 87) AZ, ZIN
37    FORMAT(5X, 9HAZIMUTH =, F7.2, 1X, 3HDEG, 3X, 13HINCLINATION =,
&P7.2, 1X, 3HDEG/)
90    CONTINUE
      T = ATAN2(SXM, SXL) * 57.2957795
      IF (T.LT.0.0) T = T + 360.

```

```

P = ARCSIN(SXN/R)*57.2957795
XK = (XKOU - 1.0)/(XKOU - R)
COSA = 1. - (XKOU - R) * ( 1./CL** (1./{XKOU-1.}) - 1.)/R
A = 1.57079633 - ARCSIN(COSA)
A = A*57.2957795
WRITE(6,48) T,P,XK,A
48  FORMAT(/3X,26H*** CLUSTER STATISTICS ***//
      85X,10HT, AZIMUTH,17X,F7.2,1X,3HDEG/
      85X,14HP, INCLINATION,13X,F7.2,1X,3HDEG/
      85X,12HK, PRECISION,15X,F7.2/
      85X,27HA, RADIUS OF CONE OF CONFID,P7.2,1X,3HDEG/)
92  CONTINUE
    IF(NCASE.EQ.1) GO TO 100
100 STOP
    END
SUBROUTINE EIGEN(X,N,D,R,ITER,NER)
C    X=INPUT MATRIX,N=ORDER OF X,D=EIGENVALUES,R(I,J)=EIGENVECTORS
C    FOR D(I) EIGENVALUES, ITER=ITERATIONS,NER=ERROR CODE(IF 0
C    OK, IF 1 CHECK MATRIX NOT AGREE WITH INPUT
C
DIMENSION X(3,3),R(3,3),D(3)
DIMENSION ISAVE(50),JSAVE(50),SINS(50),COSS(50)
MAXIT=100
E=.00001
DO 1 I=1,N
DO 1 J=1,N
1  R(I,J)=X(I,J)
C    SET ITERATION COUNTER
ITER=0
NL=N-1
C    SEARCH FOR LARGEST OFF DIAGONAL ELEMENT
2  BIGH=E
DO 4 K=1,NL
LL=K+1
DO 4 L=LL,N
FREE=ABS (R(K,L))
IF(FREE-BIGH) 4,4,3
3  BIGH=FREE
I=K
J=L
4  CONTINUE
IF (BIGH-E) 10,10,5
C    NOT YET CONVERGED ACCORDING TO 2
5  IF (MAXIT-ITER) 6,6,7
C    DID NOT CONVERGE WITHIN MAXIMUM NUMBER OF ITERATIONS ALLOWED
6  WRITE(6,315)MAXIT
315  FORMAT(1H0,32HPROBLEM DID NOT CONVERGE WITHIN ,I4,
&10HITERATIONS //)
GO TO 15
C    ZERO ELEMENT R(I,J)
C    INCREASE COUNT ON ITERATIONS
7  ITER=ITER+1
C    COMPUTE SIN AND COS
AMBDA=-R(I,J)
U=.5*(R(I,I)-R(J,J))
OMEGA = AMBDA/SQRT (AMBDA**2+U**2)
IF(U) 8,9,9
8  OMEGA=-OMEGA
9  SXN = OMEGA/SQRT (2. * (1.+SQRT (1.-OMEGA**2)))
CXS = SQRT (1.-SXN**2)
ISAVE(ITER) = I
JSAVE(ITER) = J
SINS(ITER) = SXN
COSS(ITER) = CXS
C
C    SUBROUTINE TO PREMULTIPLY BY TRANSPOSE OF TRANSFORMATION MATRIX

```

```

100 DO 101 K=1,N
    RI=R(I,K)
    RJ=R(J,K)
    R(I,K)=CXS*RI-SXN*BJ
101 R(J,K)=SXN*RI+CXS*BJ
C   SUBROUTINE TO POSTMULTIPLY BY TRANSFORMATION MATRIX
200 DO 201 K=1,N
    CI=R(K,I)
    CJ=R(K,J)
    R(K,I)=CXS*CI-SXN*CJ
201 R(K,J)=SXN*CI+CXS*CJ
    GO TO 2
C
C   CONVERGED ACCORDING TO E
C   GENERATE IDENTITY MATRIX AND SAVE EIGENVALUES
10 DO 12 I=1,N
    D(I)=R(I,I)
    DO 11 J=1,N
11 R(I,J)=0.0
12 R(I,I)=1.0
C
C   COMPUTE EIGENVECTORS
C   TEST IF THERE WERE ANY ITERATIONS
IF(ITER) 15,15,13
C   THERE WERE ITERATIONS
13 DO 400 L=1,ITER
    I = ISAVE(L)
    J = JSAVE(L)
    SXN = SINS(L)
    CXS = COSS(L)
    DO 901 K=1,N
    RI=R(I,K)
    RJ=R(J,K)
    R(I,K)=CXS*RI-SXN*BJ
901 R(J,K)=SXN*RI+CXS*BJ
400 CONTINUE
C   COMPUTE CHECK, CHECK WITH INPUT
NER = 0
15 DO 220 I=1,N
    DO 22 J=1,I
    FREE=0.0
    DO 21 K=1,N
21 FREE=R(K,I)*R(K,J)*D(K)+FREE
    IF(ABS((FREE-X(I,J))*2./((FREE+X(I,J)))).GT.0.001) NER=1
22 CONTINUE
220 CONTINUE
    RETURN
    END
C
C   FUNCTION ARCSIN(Y)
C
C   RANGE X GR OR = TO -1 BUT LT OR = 1
X = Y
SIGN = 1.0
IF (X) 10,20,20
10 SIGN = -1.0
X = -X
20 PHI=((((-0.0022959648*X-.0111462294)*X+.0268999482)*X-
&.0488025043)*X+.0887556286)*X-.2145852647)*X+1.57079617
ARCSIN = SIGN * (-PHI * SQRT(1.0 - X) + 1.57079617)
RETURN
END
FUNCTION ANG(ANGL,#ELCRL)
I = ANGL/#RLCRL
X = I
IF (ANGL) 1,2,3

```

```

1  X = ABS(X) + 1.
   GO TO 3
2  X = -X
3  ANG = ANGL + X * WHLCRL
   RETURN
   END
   SUBROUTINE POLE2(ID17, ID26, ID31, ID35, N)
C  ROUTINE FOR PLANAR SURFACES DATA
   COMMON/ONE/AZC(500), ROEC(500)
C  WRITE (6,220)
220 FORMAT (5X,15HDATA ARE PLANES/1H1,3X,6HSTRIKE,7X,3HDIP///)
   DO 221 I=1,N
   READ (5,222) ST,ISD,DIP,IDPD
222  FORMAT (4X,      F3.0,1X,A1,F8.0,1X,A1)
   ROEC(I) = 90.0-DIP
   AZ=270.0+ST
   IF (ISD.EQ.ID35) AZ=270.0-ST
   IF (IDPD.EQ.ID35) AZ=90.0-ST
   IF (IDPD.EQ.ID35.AND.ISD.EQ.ID17) AZ=90.0+ST
   AZC(I)=AZ
221  CONTINUE
   RETURN
   END

```

PROGRAM INCREMENT

```

100 PAGE
110 INIT
120 PRINT "COMPOSITE STRAIN PATH PROGRAM"
130 PRINT "DO YOU WANT PLOTS? Y/N "
140 INPUT Q$
150 PRINT "TOTAL PRINT OUT, FINAL INCREMENT, OR NO PRINT OUT? T/F/N "
160 INPUT P$
170 PRINT
180 CALL "RATE",1200,0,0
190 DELETE D$
200 PRINT "Enter FI of Data file. Enter 'STOP' to end program"
210 INPUT D$
220 IF D$="STOP" THEN 1610
230 REM
240 DELETE Z$,C$,F1,F2,F3,F4,N,X,Y,X0,Y0,X1,Y1,X8,Y8,X9,Y9,T0,D0,S0,C0
250 DEL N0,N1,N2,N3,N4,E1,E2,E3,E4,G1,G2,G3,G4,A1,R1,R2,R3,E5,E6,A0,R0
260 DELETE R6,R7,A2,A3,C1,C2,C3,C5,Q1,Q2,T1,T2,M,G,S2,M$,D8-M,S1,G$,Q
270 PRINT "HOW MANY INCREMENTS OF THIS DATASET DO YOU WANT?"
280 INPUT M
290 OPEN D$:1,"R".M$
300 INPUT #1:C$
310 DIM G(30,2)
320 M=1
330 INPUT #1:F,X,Y
340 IF F=3 THEN 360
350 GO TO 390
360 S1=X
370 S2=Y
380 GO TO 330
390 IF F=1 THEN 410
400 IF F=2 THEN 460
410 REM
420 G(M,1)=X
430 G(M,2)=Y
440 M=M+1
450 GO TO 330
460 CLOSE 1
470 X8=X
480 Y8=Y
490 X9=X8-G(M-1,1)
500 Y9=Y8-G(M-1,2)
510 FOR I=1 TO M-1
520 G(I,1)=G(I,1)+X9
530 G(I,2)=G(I,2)+Y9
540 NEXT I
550 N=1
560 PRINT "INPUT F1,F2,F3,F4, ACCUMULATED STRAIN MATRIX"
570 INPUT F1,F2,F3,F4
580 DIM D8(M-1),G9(M-1)
590 FOR K=1 TO M-2
600 IF K=0 THEN 620
610 GO TO 630
620 K=M-2
630 DELETE X0,Y0,X1,Y1
640 X0=G(K,1)
650 Y0=G(K,2)
660 X1=G(K+1,1)
670 Y1=G(K+1,2)
680 PRINT N:
690 IF P$="N" THEN 790
700 IF P$="T" THEN 730
710 IF KCM=2 THEN 790
720 PRINT 940:D$

```

```

730 PRINT @40:0$1;"_"
740 PRI @40:"*****"
750 PRINT @40: USING 760:" Increment number",N
760 IMAGE /,FA,1$T,FD,/
770 PRINT @40: USING 780:"X0=",X0,"Y0=",Y0,"X1=",X1,"Y1=",Y1
780 IMAGE 10T,FA,FD,3D,20T,FA,FD,3D,30T,FA,FD,3D,40T,FA,FD,3D,/
790 T0=2*(X1*Y1-X0*Y0)/(X1^2-Y1^2-X0^2+Y0^2)
800 IF X1^2-Y1^2-X0^2+Y0^2<0 THEN 830
810 D0=ATN(T0)/2
820 GO TO 840
830 D0=(ATN(T0)+PI)/2
840 REM
850 S0=SIN(D0)
860 C0=COS(D0)
870 N0=X0+C0+Y0*S0
880 N1=-C0*S0+Y0+C0
890 N2=X1+C0+Y1*S0
900 N3=-X1*S0+Y1+C0
910 E1=N2/N0
920 E2=0
930 E3=0
940 E4=N3/N1
950 S0=-S0
960 G1=E1*C0^2-(E2+E3)*S0*C0+E4*S0^2
970 G2=E2*C0^2+(E1-E4)*S0*C0-E3*S0^2
980 G3=E3*C0^2+(E1-E4)*S0*C0-E2*S0^2
990 G4=E4*C0^2+(E2+E3)*S0*C0+E1*S0^2
1000 E1=G1
1010 E2=G2
1020 E3=G3
1030 E4=G4
1040 GOSUB 2000
1050 N=N+1
1060 IF P$="N" THEN 1300
1070 IF P$="T" THEN 1090
1080 IF KCM=2 THEN 1300
1090 PRINT @40:"THE ANGLE TO THE PRINC STRAIN AXIS IN RADIANS=" ";
1100 PRINT @40: USING "FD,5D":A1
1110 PRINT @40:"THE AXIAL RATIO OF THE RESULTING STRAIN ELLIPSE=" ";
1120 PRINT @40: USING "FD,5D":R2
1130 PRINT @40:"THE ANGLE BETWEEN THE COORDINATE SYSTEMS=" ";
1140 PRINT @40: USING "FD,5D":R3
1150 PRINT @40:"_"
1160 PRINT @40: USING 1170:"INCREMENTAL STRAIN MATRIX"
1170 IMAGE 2$T,FA,/
1180 PRINT @40: USING 1190:"E11=";E1,"E12=";E2,"E21=";E3,"E22=";E4
1190 IMAGE 2$T,FA,FD,2D,40T,FA,FD,2D,/2$T,FA,FD,2D,40T,FA,FD,2D,/,/,/
1200 PRINT @40: USING 1210:"SIMPLE ELONGATION",E5,E6,"ORIENTATION",A0,R0
1210 IMAGE FA,3$T,FD,5D,4$T,FD,5D,/,FA,3$T,FD,5D,4$T,FD,5D
1220 PRINT @40: USING 1230:"SIMPLE RECIPROCAL ORIENTATION",A1,R1
1230 IMAGE FA,3$T,FD,5D,4$T,FD,5D
1240 PRINT @40: USING 1250:"ELONGATION",R6,R7
1250 IMAGE FA,3$T,FD,5D,4$T,FD,5D
1260 PRINT @40: USING 1270:"AXIAL RATIO",A2,"RECIP AXIAL RATIO",R2
1270 IMAGE FA,3$T,FD,5D,/,FA,3$T,FD,5D
1280 PRINT @40: USING 1290:"ROTATION",R3,"AREA STRAIN",A3
1290 IMAGE FA,3$T,FD,5D,/,FA,3$T,FD,5D,/,/
1300 G9(K)=A1
1310 G1=E1*F1+E2*F3
1320 G2=E1*F2+E2*F4
1330 G3=E3*F1+E4*F3
1340 G4=E3*F2+E4*F4
1350 F1=G1

```

```

1360 F2=G2
1370 F3=G3
1380 F4=G4
1390 E1=F1
1400 E2=F2
1410 E3=F3
1420 E4=F4
1430 GOSUB 2000
1440 IF P#="N" THEN 1560
1450 IF P#="T" THEN 1470
1460 IF K#-2 THEN 1560
1470 PRINT @40: USING 1480:"ACCUM FINITE STRAIN MATRIX",F1,F2,F3,F4
1480 IMAGE 25T,FA,/,/,25T,FD,2D,45T,FD,2D,/,25T,FB,2D,45T,FD,2D,/,/
1490 PRINT @40: USING 1210:"SIMPLE ELONGATION",E5,E6,"ORIENTATION",A0,R0
1500 PRINT @40: USING 1230:"SIMPLE RECIPROCAL ORIENTATION",A1,R1
1510 PRINT @40: USING 1250:"ELONGATION",R6,R7
1520 PRINT @40: USING 1270:"AXIAL RATIO",A2,"RECIP AXIAL RATIO",R2
1530 PRINT @40: USING 1290:"ROTAION",R3,"AREA STRAIN",A3
1540 PRI @40:"*****"
1550 PRINT @40:"_"
1560 D8(K)=A1
1570 NEXT K
1580 IF U#="N" THEN 1600
1590 GOSUB 3000
1600 GO TO 190
1610 END
2000 REM THIS IS THE SUBROUTINE
2010 C1=E1^2+E3^2
2020 C2=2*(E1+E2+E3+E4)
2030 C3=E2^2+E4^2
2040 T1=C2/(C1-C3)
2050 A0=ATN(T1)/2
2060 IF A0<0 THEN 2080
2070 A0=A0+PI
2080 R0=A0+PI/2
2090 Q1=C1*COB(A0)^2+C2*SIN(A0)*COS(A0)+C3*SIN(A0)^2
2100 Q2=C1*COB(R0)^2+C2*SIN(R0)*COS(R0)+C3*SIN(R0)^2
2110 C3=Q2-Q1
2120 IF C3<0 THEN 2190
2130 C3=Q1
2140 Q1=Q2
2150 Q2=C3
2160 C3=A0
2170 A0=R0
2180 R0=C3
2190 C4=E3^2+E4^2
2200 C5=2*(E1+E3+E2+E4)
2210 C6=E1^2+E2^2
2220 C7=(E1+E4-E2+E3)^2
2230 T2=C5/(C6-C4)
2240 A1=ATN(T2)/2
2250 IF A1<0 THEN 2270
2260 A1=A1+PI
2270 R1=A1+PI/2
2280 R4=(C4*COB(A1)^2-C5*SIN(A1)*COS(A1)+C6*SIN(A1)^2)/C7
2290 R5=(C4*COB(R1)^2-C5*SIN(R1)*COS(R1)+C6*SIN(R1)^2)/C7
2300 C3=R5-R4
2310 IF C3<0 THEN 2380
2320 C3=R4
2330 R4=R5
2340 R5=C3
2350 C3=A1
2360 A1=R1

```

```

2370 R1=C3
2380 E5=SQR(Q1)
2390 E6=SQR(ABS(Q2))
2400 A2=E5/E6
2410 R6=SQR(R4)
2420 R7=SQR(R5)
2430 R2=R7/R6
2440 A3=SQR(C7)
2450 R3=A0-A1
2460 IF A0<PI THEN 2480
2470 A0=A0-PI
2480 IF R0<PI THEN 2500
2490 R0=R0-PI
2500 IF A1<PI THEN 2520
2510 A1=A1-PI
2520 IF R1<PI THEN 2540
2530 R1=R1-PI
2540 RETURN
3000 REM DRAFTING SUBROUTINE
3010 DELETE J,K,I,E,H$,W$,Z
3020 PRINT "-----Plot? y/n-----";
3030 INPUT L$
3040 PRINT "ENTER NUMBER OF INCREMENTS  "
3050 INPUT Z
3060 IF L$="N" THEN 3410
3070 HOME @1:
3080 PRINT @1:D$
3090 PRINT @1:"_":C$
3100 WINDOW 0,PI,0,Z
3110 VIEWPORT 30,120,10,30
3120 MOVE @1:0,0
3130 DRAW @1:PI,0
3140 MOVE @1:PI/2,0
3150 DRAW @1:PI/2,Z
3160 T=Z*.01
3170 FOR I=0 TO PI STEP PI/18
3180 MOVE @1:I,0
3190 DRAW @1:I,T
3200 NEXT I
3210 T=PI/180
3220 FOR I=0 TO Z STEP 1
3230 MOVE @1:PI/2-T,I
3240 DRAW @1:PI/2+T,I
3250 NEXT I
3260 MOVE @1:D8(1),1
3270 FOR E=1 TO Q-1
3280 DRAW @1:D8(E),E
3290 NEXT E
3300 PRINT @1:" A"
3310 GOSUB 3330
3320 MOVE @1:G9(1),1
3330 FOR E=1 TO Q-1
3340 DRAW @1:G9(E),E
3350 NEXT E
3360 PRINT @1:"_I"
3370 GO TO 3470
3380 MOVE @1:0,0
3390 PRINT @1:"_0"
3400 MOVE @1:PI/2,0
3410 PRINT @1:"_PI/2"
3420 MOVE @1:PI,0
3430 PRINT @1:"_PI"
3440 MOVE @1:PI/4,0

```

3450 HOME 01:
3460 RETURN
3470 RETURN

PROGRAM KALSB


```

INTEGER T,S
DATA ID1, ID2, ID17, ID26, ID31, ID35/1HR, 1HL, 1HE, 1HN, 1HS, 1HW/
C CHANGE FOLLOWING CARD FOR PRINTER PLOT OR SCREEN PLOT
DATA NCOL, NROW/71, 57/
JM(1) = NCOL
JM(2) = 1
JM(3) = IFIX(FLOAT(NCOL/2))
IF (MOD(NCOL, 2) .GE. 0.5) JM(3) = JM(3) + 1
JM(4) = JM(3)
JM(5) = JM(3)
IM(1) = IFIX(FLOAT(NROW/2))
IF (MOD(NROW, 2) .GE. 0.5) IM(1) = IM(1) + 1
IM(2) = IM(1)
IM(3) = IM(1)
IM(4) = NROW
IM(5) = 1
C DO LOOP TO INITIALLY FILL CTPC MATRIX
DO 990 I=1, NROW
DO 990 J=1, NCOL
990 CTPC(I, J) = 0.0
S=6
T=5
C DATA DUMMY/'1', '0', '-', '1', '2', '3', '4', '5', '6', '7', '8',
C '9', 'A', 'B', 'C', 'D', 'E', 'F', 'G', 'H', 'I', 'J', 'K', 'L',
C 'M', 'N', 'O', 'P', 'Q', 'R', 'S', 'T', 'U', 'V', 'W', 'X', 'Y',
C 'Z', '*', 'B' /
DATA DIPLIM/0.16/
READ (T, 299) (DUMMY(I), I=1, 40)
299 FORMAT (40A1)
DATA INDEX, IND/1, 2/
105 READ (T, 100) N, (TITLE(I), I=1, 60)
100 FORMAT (I4, 60A1)
777 IF (INDEX.EQ.0) GO TO 101
WRITE (S, 115) (TITLE(I), I=1, 60), N
115 FORMAT (60A1, 5X, I4, 14H OBSERVATIONS/)
C POLE1 IS LINEATIONS SUBROUTINE
IF (IND.EQ.1) CALL POLE1(ID1, ID2, ID17, ID26, ID31, ID35)
C POLE2 IS PLANAR SURFACES SUBROUTINE
IF (IND.EQ.2) CALL POLE2(ID1, ID2, ID17, ID26, ID31, ID35)
173 DO 106 I=1, N
RODIN=SIN(ROEC(I))
XV(I)=SIN(AZC(I))*RODIN
YV(I)=COS(AZC(I))*RODIN
ZV(I)=COS(ROEC(I))
106 CONTINUE
XN=N
C ROUTINE TO PERFORM POINT COUNT AND FILL THE CTPC MATRIX
C WITH PERCENT POPULATION PER UNIT AREA
102 DO 107 I=1, N
RAD=TAN(ROEC(I)/2.0)
X=RAD*SIN(AZC(I))*{(3.0*FLOAT(NCOL))/2.0}+{(3.0*FLOAT(NCOL))/2.0}
Y=RAD*COS(AZC(I))*{(3.0*FLOAT(NCOL))/2.0}+{(3.0*FLOAT(NCOL))/2.0}
COUNT=0.0
DO 301 J=1, N
DOTP=ABS(XV(I)*XV(J)+YV(I)*YV(J)+ZV(I)*ZV(J))
IF (DOTP.GE.1.0.AND.DOTP.LT.1.001) DOTP=0.999
ANG=ARCOS(DOTP)
IF (ANG.LE.DIPLIM) COUNT=COUNT+1.0
301 CONTINUE
COTPC=COUNT*100.0/XN
K=FLOAT(NROW+1)-Y*0.2
M=X*0.333333+0.5
IF (K.LT.1) K=1
IF (M.LT.1) M=1
IF (COTPC.GT.CTPC(K, M)) CTPC(K, M) = COTPC
107 CONTINUE

```

```

104 CONTINUE
C ONE QUARTER OF A CIRCLE IS PLACED ONTO THE CTPC MATRIX
C WHILE THE REMAINDER IS GENERATED BY SYMMETRY
XXX=-999.9
DO 150 I=1,5
K=IM(I)
M=JM(I)
IF (CTPC(K,M).LE.0.0) CTPC(K,M)=XXX
150 CONTINUE
DO 151 I = 1,90
ANG = 360.0 - FLOAT(I)
ANG = ANG *0.0174533
X = JM(3) * COS(ANG)
Y = IM(1) * SIN(ANG)
X = JM(3) + X
Y = IM(1) - Y
IF (X.LT.1.0) X = 1.0
IF (Y.LT.1.0) Y = 1.0
J1 = IPIX(X)
I1 = IPIX(Y)
J2 = NCOL+1 - J1
I2 = NROW+1 - I1
IF (CTPC(I1,J1).LE.0.0) CTPC(I1,J1)=XXX
IF (CTPC(I1,J2).LE.0.0) CTPC(I1,J2)=XXX
IF (CTPC(I2,J2).LE.0.0) CTPC(I2,J2)=XXX
IF (CTPC(I2,J1).LE.0.0) CTPC(I2,J1)=XXX
151 CONTINUE
C ROUTINE TO CONVERT THE CTPC MATRIX FROM NUMERICAL VALUES TO
C PRINT SYMBOLS
DO 812 I=1,NROW
DO 812 J=1,NCOL
IF (CTPC(I,J).LE.(-999.9)) GO TO 814
IF (CTPC(I,J).LE.0.0) GO TO 810
IF (CTPC(I,J).LT.0.5) GO TO 811
M=3
813 MM=M-2
XMM=MM
IF (CTPC(I,J).LT.XMM) GO TO 815
M=M+1
IF (M.LE.37) GO TO 813
CTPC(I,J)=DUMMY(38)
GO TO 812
815 CTPC(I,J)=DUMMY(M)
GO TO 812
814 CTPC(I,J)=DUMMY(39)
GO TO 812
810 CTPC(I,J)=DUMMY(1)
GO TO 812
811 CTPC(I,J)=DUMMY(2)
812 CONTINUE
DO 886 J=1,100000
886 CONTINUE
WRITE (S,110)
C CHANGE 35 TO NCOL/2 FOR PRINTER PLOT
110 FORMAT (1H1,35X,1H*)
DO 111 I=1,NROW
WRITE(S,112) (CTPC(I,J),J=1,NCOL)
C CHANGE 71 TO NCOL FOR PRINTER PLOT
112 FORMAT (1X,71A1)
DO 111 J=1,NCOL
CTPC(I,J)=0.0
111 CONTINUE
CALL PRINT1(ID1,ID2,ID17,ID26,ID31,ID35)
C ROUTINE FOR PRINT SYMBOL TABLE
INDEX = 0
GO TO 777

```

```

101 STOP
    END
    SUBROUTINE POLE1(ID1, ID2, ID17, ID26, ID31, ID35)
C   ROUTINE FOR LINEATION DATA
    DIMENSION AZC(500), ROEC(500), DUMMY(40)
    COMMON AZC, ROEC, T, S, N, DUMMY
    INTEGER T, S
C   WRITE (S, 201)
201 FORMAT (5X, 19HDATA ARE LINEATIONS/1H1, 3X, 6HSTRIKE, 4X, 6HPLUNGE//)
    DO 202 I=1, N
    READ (T, 200) ISDR, ST, ISD, DIP
C   WRITE (S, 200) ISDR, ST, ISD, DIP
200 FORMAT (3X, A1, F3.0, 1X, A1, F8.0)
    ROEC(I) = (90.0 - DIP) * 0.01745332
    AZ = ST
    IF (ISDR.EQ.ID31) AZ = 180.0 - ST
    IF (ISD.EQ.ID35) AZ = 180.0 + ST
    IF (ISD.EQ.ID35.AND.ISDR.EQ.ID26) AZ = 360.0 - ST
    AZC(I) = AZ * 0.01745332
202 CONTINUE
    RETURN
    END
    SUBROUTINE POLE2(ID1, ID2, ID17, ID26, ID31, ID35)
C   ROUTINE FOR PLANAR SURFACES DATA
    DIMENSION AZC(500), ROEC(500), DUMMY(40)
    COMMON AZC, ROEC, T, S, N, DUMMY
    INTEGER T, S
    WRITE (S, 220)
220 FORMAT (3X, 6HSTRIKE, 5X, 3HDIP/)
    DO 221 I=1, N
    READ (T, 222) ST, ISD, DIP, IDPD
    WRITE (S, 223) ST, ISD, DIP, IDPD
223 FORMAT (4H N, F3.0, 1X, A1, F8.0, 1X, A1)
222 FORMAT (4X, F3.0, 1X, A1, F8.0, 1X, A1)
    ROEC(I) = DIP * 0.01745332
    AZ = 270.0 + ST
    IF (ISD.EQ.ID35) AZ = 270.0 - ST
    IF (IDPD.EQ.ID35) AZ = 90.0 - ST
    IF (IDPD.EQ.ID35.AND.ISD.EQ.ID17) AZ = 90.0 + ST
    AZC(I) = AZ * 0.01745332
221 CONTINUE
    RETURN
    END
    SUBROUTINE PRINT1(ID1, ID2, ID17, ID26, ID31, ID35)
C   ROUTINE FOR PRINT SYMBOL TABLE
    DIMENSION AZC(500), ROEC(500), DUMMY(40)
    COMMON AZC, ROEC, T, S, N, DUMMY
    INTEGER T, S
    DO 887 J=1, 100000
887 CONTINUE
    WRITE (S, 550) (DUMMY(I), I=1, 4)
550 FORMAT (28H1 SYMBOLS ON STEREO-NET MEAN////5X, 6HSYMBOL, 7X, 13HPERC
1ENT RANGE//8X, A1, 9X, 9H0 OR LESS/8X, A1, 9X, 1H0, 3X, 3H1/2/8X, A1, 8X,
23H1/2, 4X, A1)
    DO 551 I=4, 37
    MBO = I - 3
    MTO = I - 2
551 WRITE (S, 552) DUMMY(I), MBO, MTO
552 FORMAT (8X, A1, 8X, I2, 4X, I2)
    WRITE (S, 553) DUMMY(38)
553 FORMAT (8X, A1, 8X, 14H35 AND GREATER////////)
    RETURN
    END

```

PROGRAM OOID

```

100 REM bryan tapp 12-21-81
110 PAGE
120 PRINT "          ****OOID****"
130 INIT
140 PRI "This program calculates the axial ratio and axial orientation"
150 PRINT "of deformed ooids. The long axis of each ooid is plotted and"
160 PRI "the mean and standard deviation for the sample is calculated "
170 PRINT "for both axial ratio and axial orientation."
180 PRINT "Turn on the hard copy unit if you want copies."
190 PRINT @32,26:3
200 SET DEGREES
210 CALL "RATE ",1200,0,0
220 PRINT "PRESS RETURN TO BASIC_"
230 CALL "TERMIN"
240 GO TO 280
250 PRINT "ANOTHER SAMPLE?___ Y/N";
260 INPUT A$
270 IF A$="N" THEN 830
280 DELETE F,X,Y,X0,X1,X9,Y0,Y1,Y9,X3,X4,0,L1,L2,R,S1,S2,S3,S4,S5,S6
290 DELETE S7,S8,C$,Z
300 PAGE
310 PRINT "TYPE IN SAMPLE ID."
320 INPUT C$
330 PRINT "ENTER AMOUNT AND DIRECTION OF ROTATION TO ORIENTED SPACE";
340 INPUT Z
350 PRINT "___DIGITIZE LOWER LEFT AS ORIGIN___"
360 INPUT @40:F,X0,Y0
370 PRINT "___DIGITIZE UPPER RIGHT___"
380 INPUT @40:F,X9,Y9
390 DIM X(4),Y(4),X1(400),Y1(400),S3(200),S4(200),R(200),O(200)
400 S2=0
410 S1=0
420 N=1
430 M=1
440 N=1
450 PRINT "___DIGITIZE OIDS___"
460 I=1
470 PRINT "_____"
480 INPUT @40:F,X(I),Y(I)
490 PRINT "___"
500 IF X(I)<0 THEN 540
510 IF I=4 THEN 860
520 I=I+1
530 GO TO 480
540 REM STATISTICS SUBROUTINE SORTA
545 M=M-1
550 PRINT "_____PLOT? Y/N"
560 INPUT D$
570 IF D$="N" THEN 830
580 WINDOW 0,150,0,100
590 VIEWPORT 0,150,0,100
600 FOR J=1 TO N-1 STEP 2
610 MOVE @1:X1(J)/X9*150,Y1(J)/Y9*100
620 DRAW @1:X1(J+1)/X9*150,Y1(J+1)/Y9*100
630 NEXT J
640 HOME @1:
650 X3=S1/M
660 X4=S2/M
670 DIM S7(M),S8(M)
680 FOR J=1 TO M
690 S3(J)=(R(J)-X3)^2
700 S4(J)=(O(J)-X4)^2

```

```
710 S7(J)=S3(J)
720 S8(J)=S4(J)
730 NEXT J
740 S5=SQR(SUM(S7)/(M-1))
750 S6=SQR(SUM(S8)/(M-1))
760 X4=X4+Z
770 PRINT @1:C#
780 PRI @1: USI @10:"_LAXIAL RATIO MEAN =" ;X3;" STANDARD DEVIATION =" ;S5
790 PRI @1: USI @10:"_ORIENTATION MEAN =" ;X4;" STANDARD DEVIATION =" ;S6
800 PRINT @1:"_NUMBER OF COIDS = " ;M
810 IMAGE FA,2X,FD.2D,30T,FA,2X,FD.2D
820 GO TO 250
830 PRINT @32,26:0
840 INIT
850 END
860 REM ASSIGNMENT SUBROUTINE
870 L1=SQR((X(2)-X(1))^2+(Y(2)-Y(1))^2)
880 L2=SQR((X(4)-X(3))^2+(Y(4)-Y(3))^2)
890 R(M)=L1/L2
900 S1=S1+R(M)
910 O(M)=ATN((Y(2)-Y(1))/(X(2)-X(1)))
920 S2=S2+O(M)
930 X1(N)=X(1)
940 Y1(N)=Y(1)
950 X1(N+1)=X(2)
960 Y1(N+1)=Y(2)
970 N=N+2
980 M=M+1
990 IF M=200 THEN 540
1000 GO TO 460
```

```

100 PAGE
110 REM SPROTATE
120 SET DEGREES
130 PRINT "INPUT MASTERFILE FI"
140 INPUT D$
150 OPEN D$:1,"R",N$
160 CALL "REWIND",1
170 DEL A$,B$,E$,F$,G$,H$,I$,Q$,O$,A,B,C,D,E,F,G,H,I,J,K,L,M,M$,N$,X,Y
180 DELETE X1,Y1,Q,N,Z
190 INPUT #1:A$
200 ON EOF (1) THEN 300
210 A=1
220 DIM M$(300)
230 OPEN A$:2,"R",M$
240 CALL "REWIND",2
250 N=POS(M$,"used",1)-6
260 Q$=SEG(M$,N,5)
270 N=VAL(Q$)
280 INPUT #2:E$
290 DIM F(100)
300 DIM X(100)
310 DIM Y(100)
320 INPUT #2:F(A),X(A),Y(A)
330 ON EOF (2) THEN 360
340 A=A+1
350 GO TO 320
360 CLOSE 2
370 PAGE
380 A=A-1
390 PRINT E$
400 FOR L=1 TO A
410 PRINT F(L),X(L),Y(L)
420 NEXT L
430 PRINT
440 PRINT "Angle of rotation, CLOCKWISE OF REFERENCE FROM ORIGINAL"
450 DIM X1(A)
460 DIM Y1(A)
470 INPUT B
490 PRINT
500 FOR K=1 TO A
510  $X1(K)=X(K)*\cos(B)+Y(K)*\sin(B)$ 
520  $Y1(K)=Y(K)*\cos(B)-X(K)*\sin(B)$ 
530 NEXT K
540 PAGE
545 PRINT A$
550 PRINT E$
560 PRINT "Rotated data set",B;" degrees"
570 PRINT
580 FOR L=1 TO A
590 PRINT F(L),X1(L),Y1(L)
600 NEXT L
610 REM
620 PRINT
630 PRINT "To save your rotated data enter FI of rotated data file "
640 INPUT H$
650 PRINT
670 PRINT
680 CREATE H$,"AUCN";N+500,0
690 REM
700 OPEN H$:3,"F",M$
710 CALL "REWIND",3
720 PRINT #3:E$

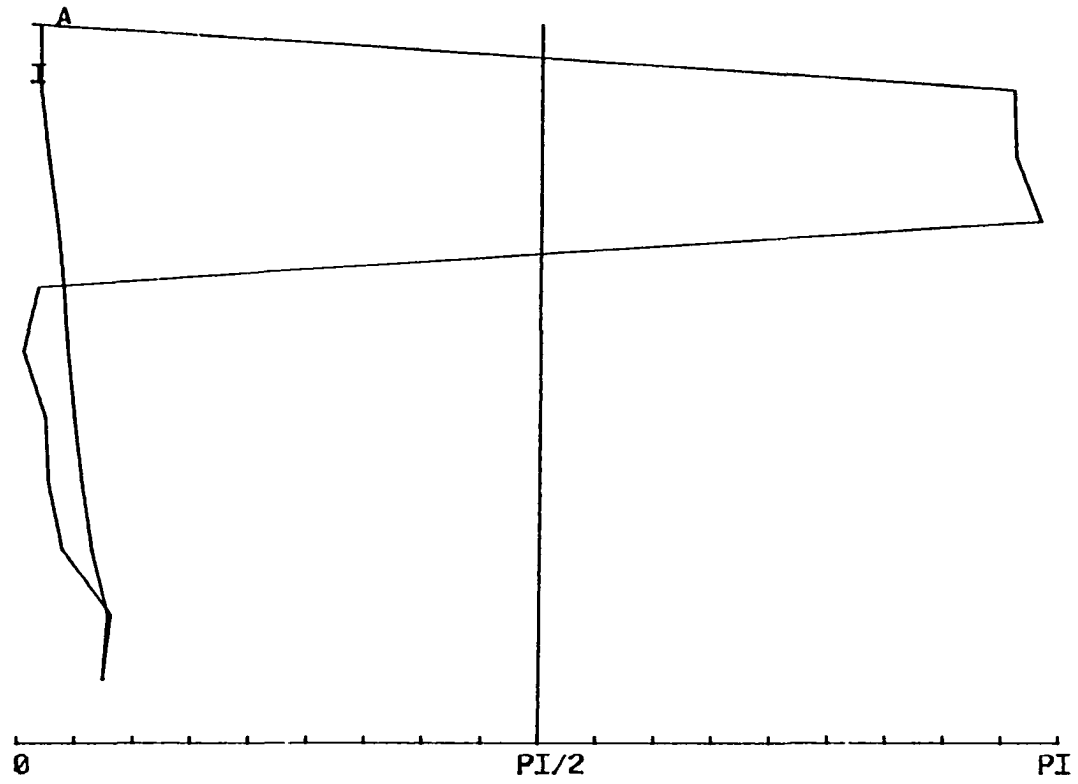
```

```
730 FOR M=1 TO A
740 PRINT #3:F(M),X1(M),Y1(M)
750 ON EOF (0) THEN 770
760 NEXT M
770 CLOSE 3
780 GO TO 170
790 PAGE
800 CLOSE 1
810 END
```

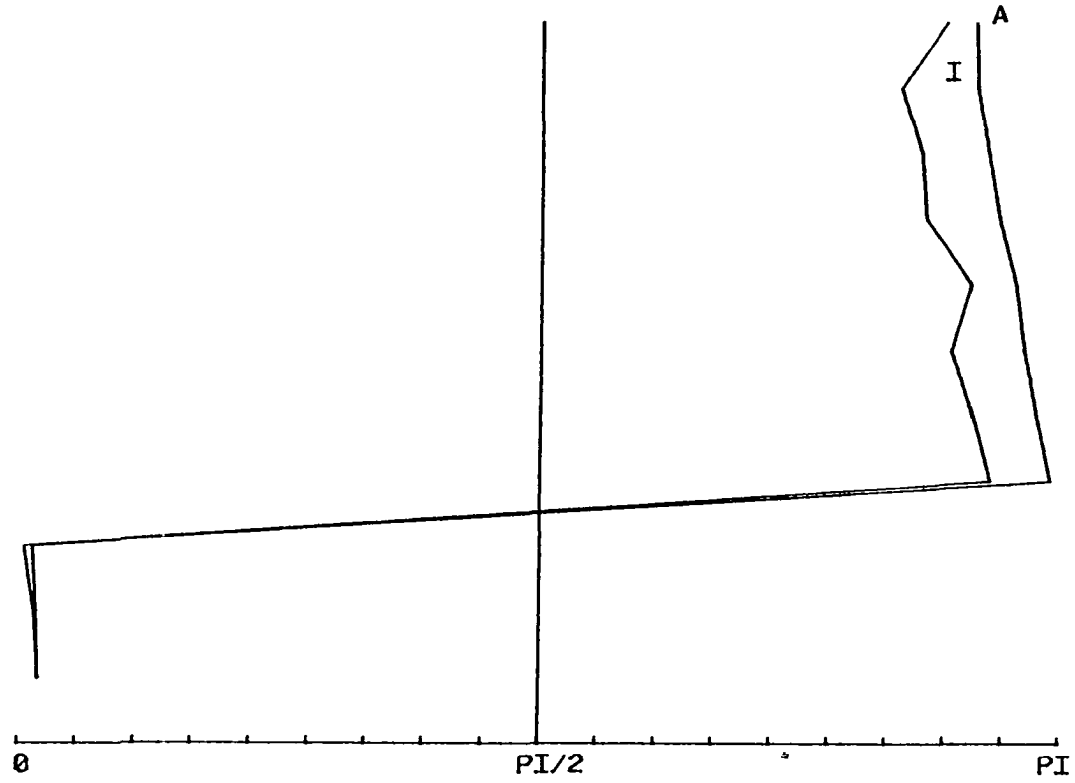
APPENDIX B
STRAIN PATHS FOR SAMPLES
WITH AREA STRAIN < 2.0

SAMPLE 816

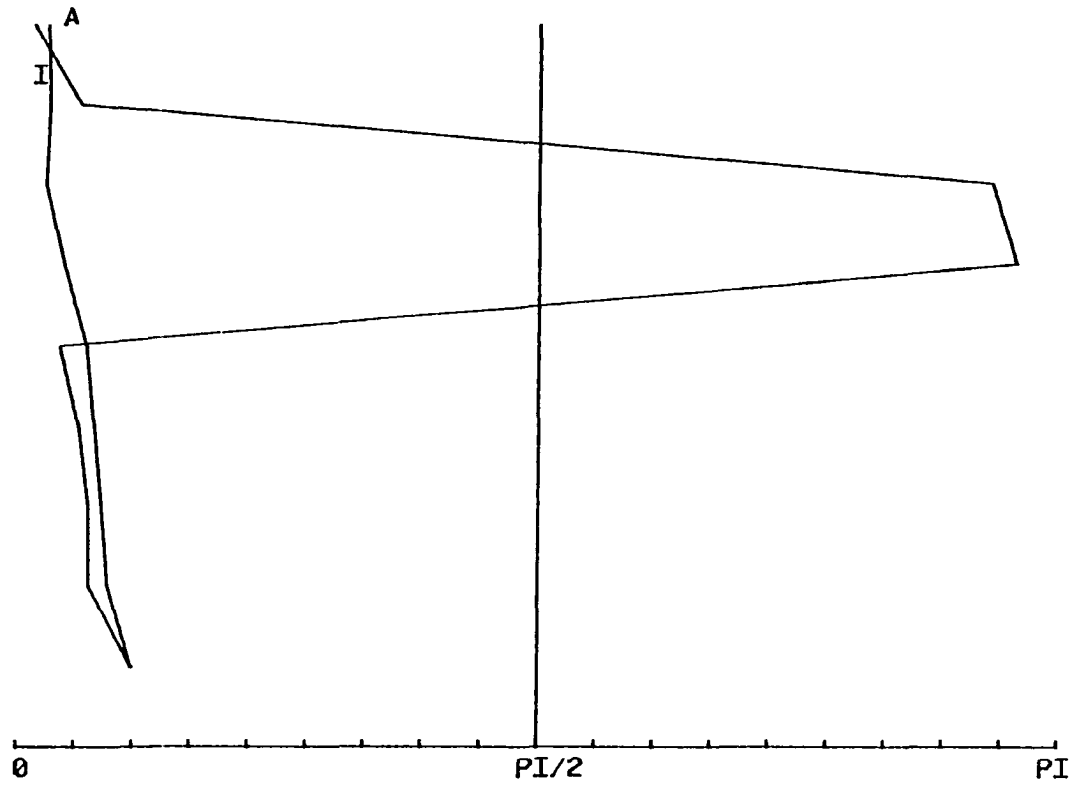
STONE1BE
PHT 1.11.80#5,6,7;SAMPLE 8.8.78 D16 PAIR,LEFT SET,FILE 30



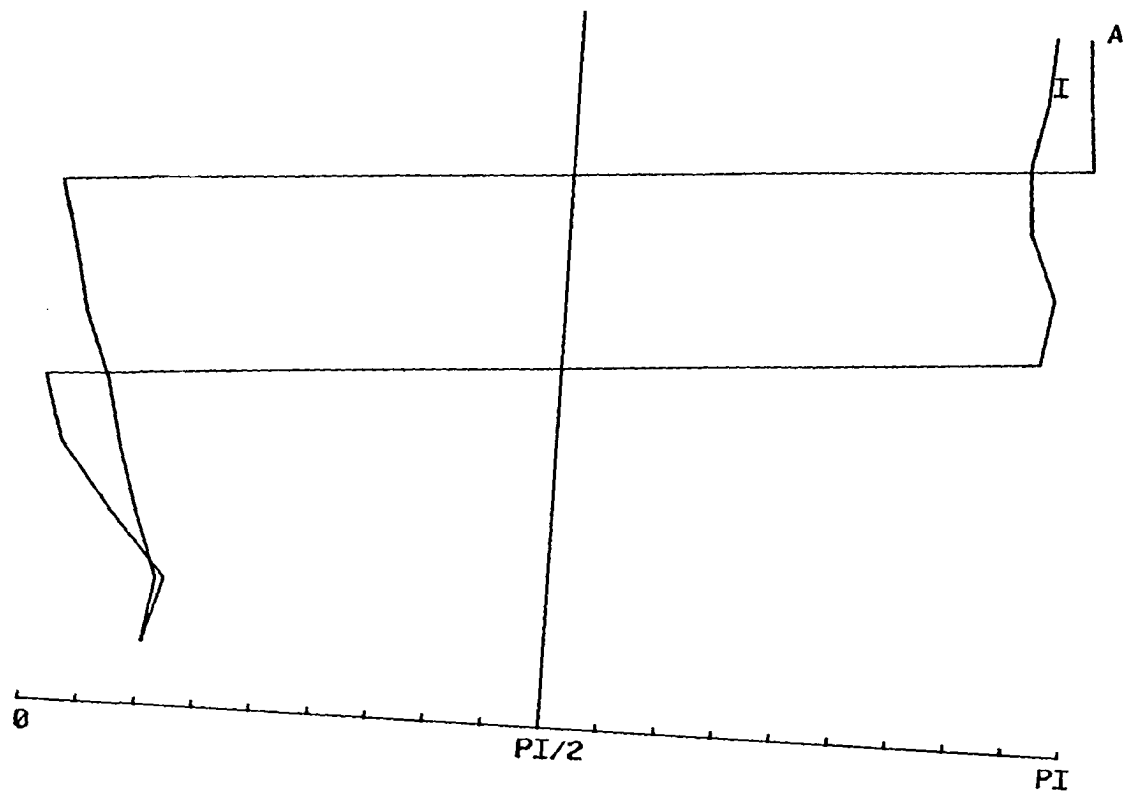
STONE2BE
PHT 1.11.80#5,6,7;SAMPLE 8.8.78 D16,PAIR, RIGHT SET, DATA FILE 31



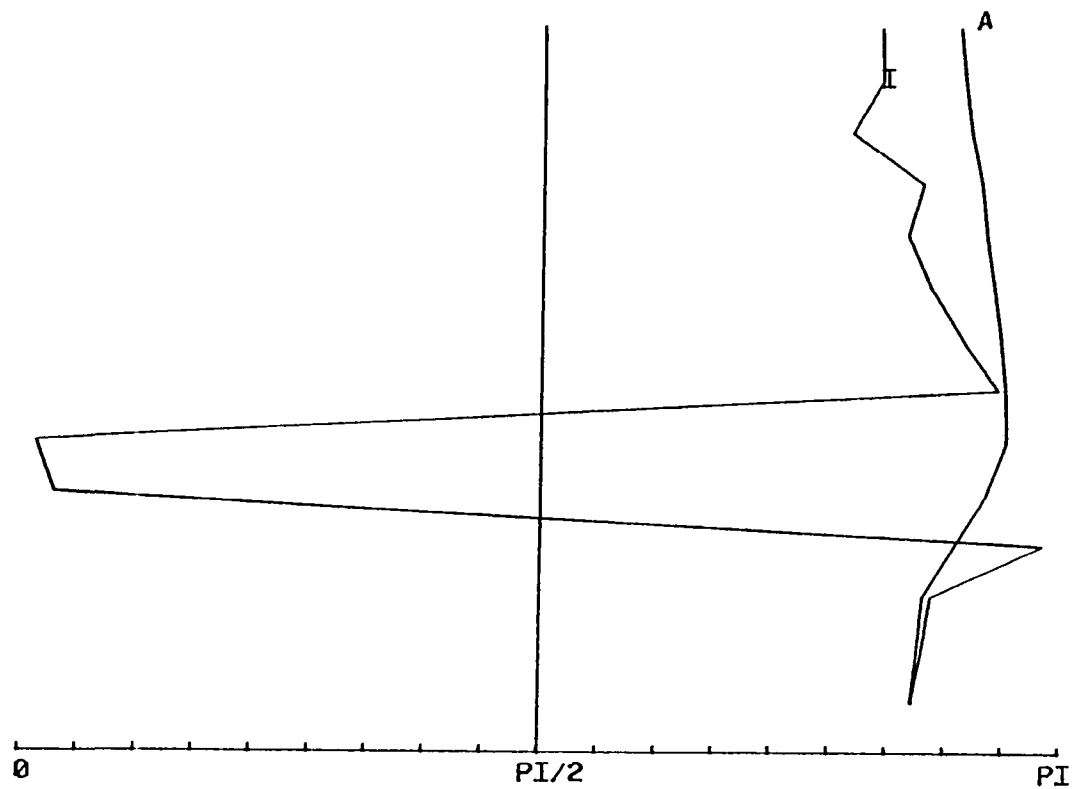
STONE3BE
PHOTO 1.11.80#8; SAMPLE 8.8.78 D16, PAIR, LEFT SET, DATA FILE 32



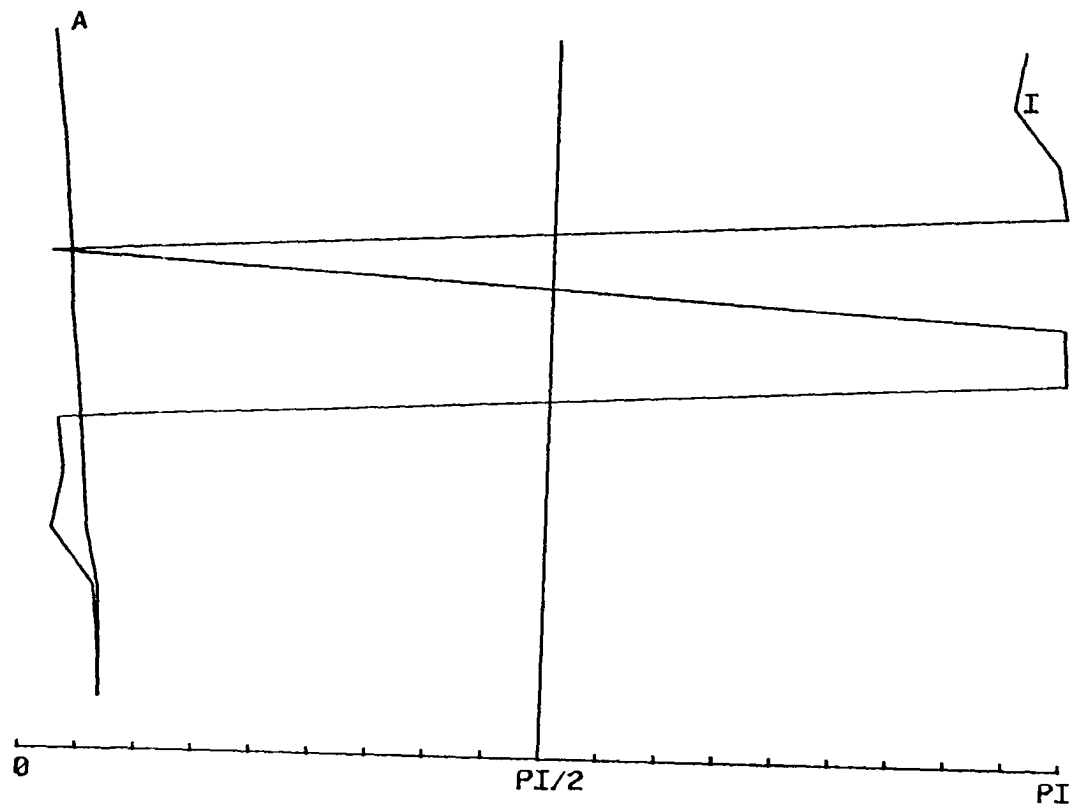
STONE4BE
PHOTO 1.11.8018; SAMPLE 8.8.78 D18, PAIR, RIGHT SET, FILE 33



STONE6BE
PHOTO 1.11.80#9; SAMPLE 8.8.78 D16, PAIR, RIGHT, FILE 35

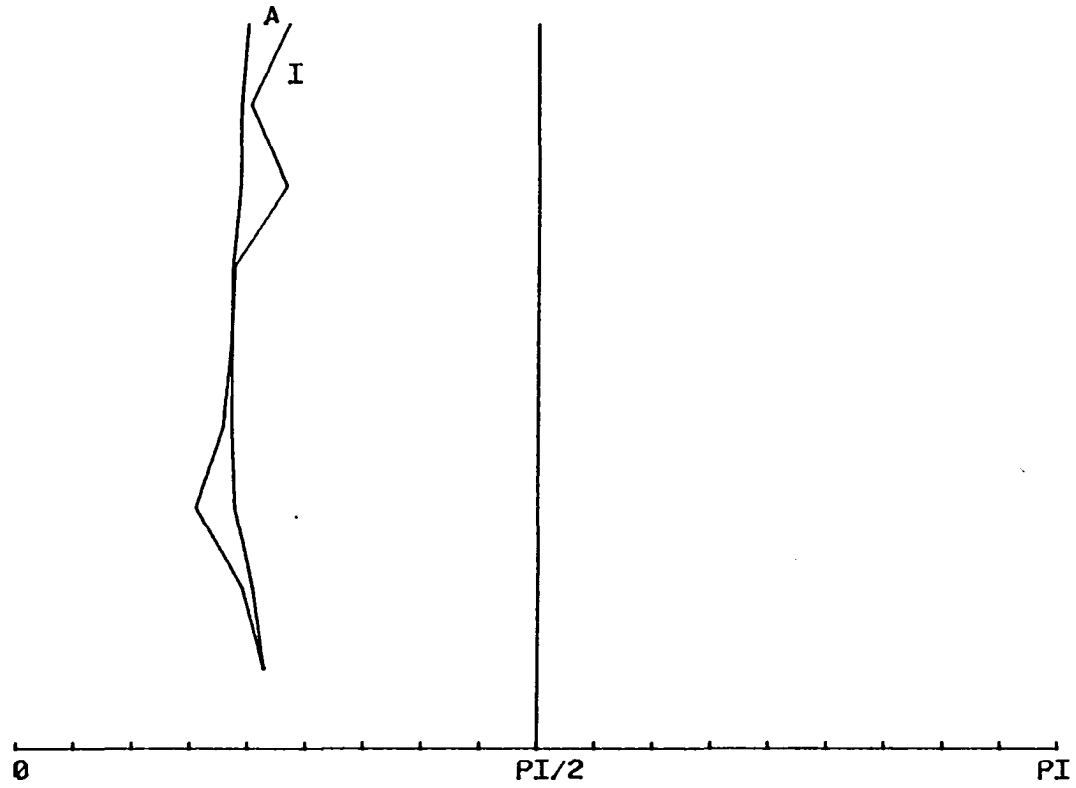


STONE7BE
PHOTO 1.11.80#10; SAMPLE 8.8.78 D16, SINGLET, LEFT, FILE 36

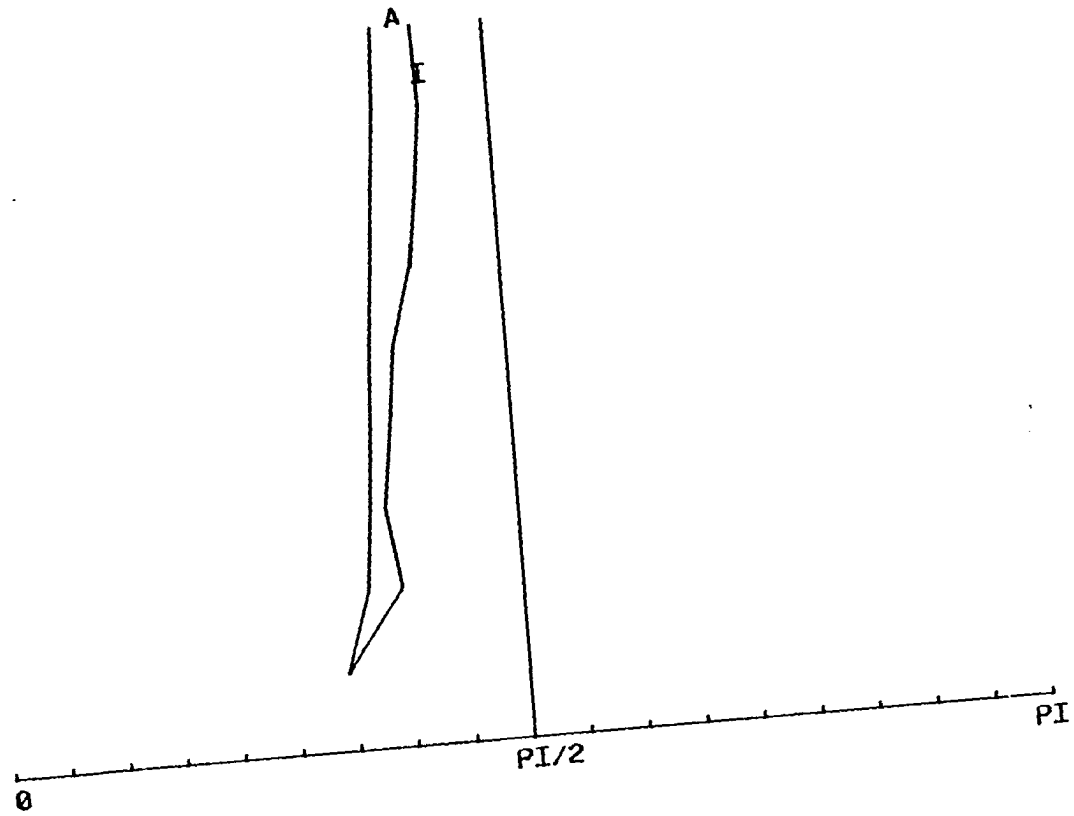


SAMPLE 850

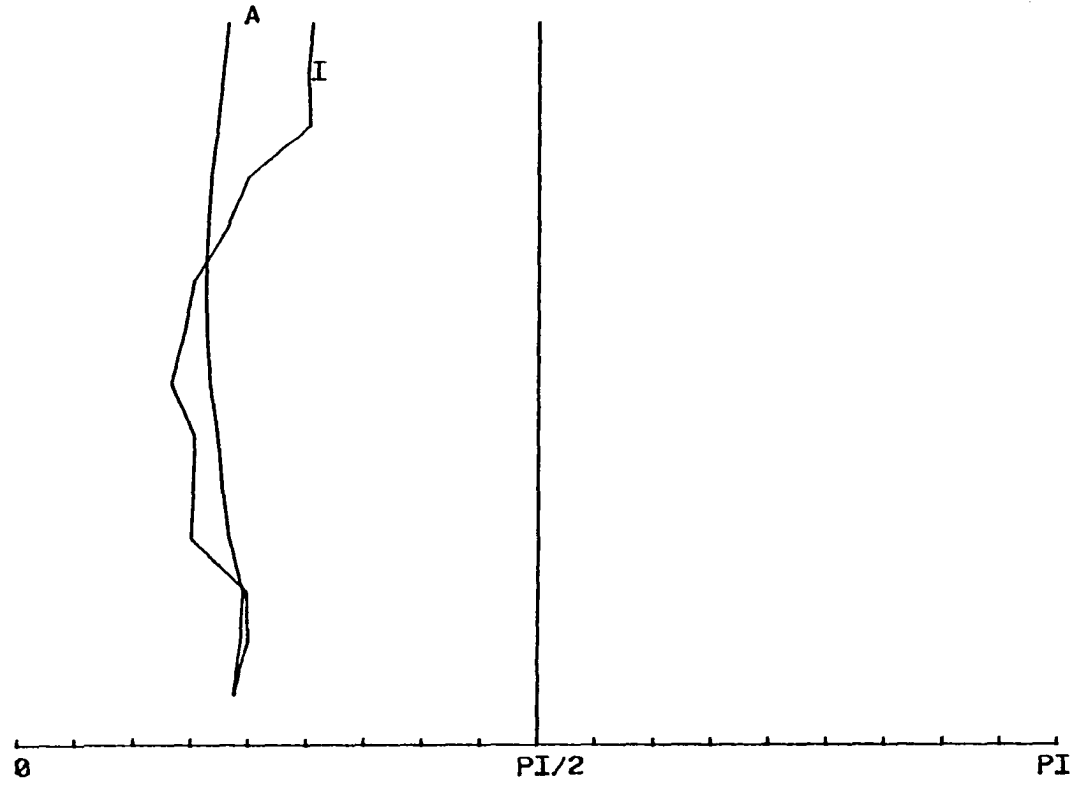
CRAIG7BE
PHOTO 1.11.80#20; SAMPLE 8.14.78 D50, PAIR, LEFT, FILE 46



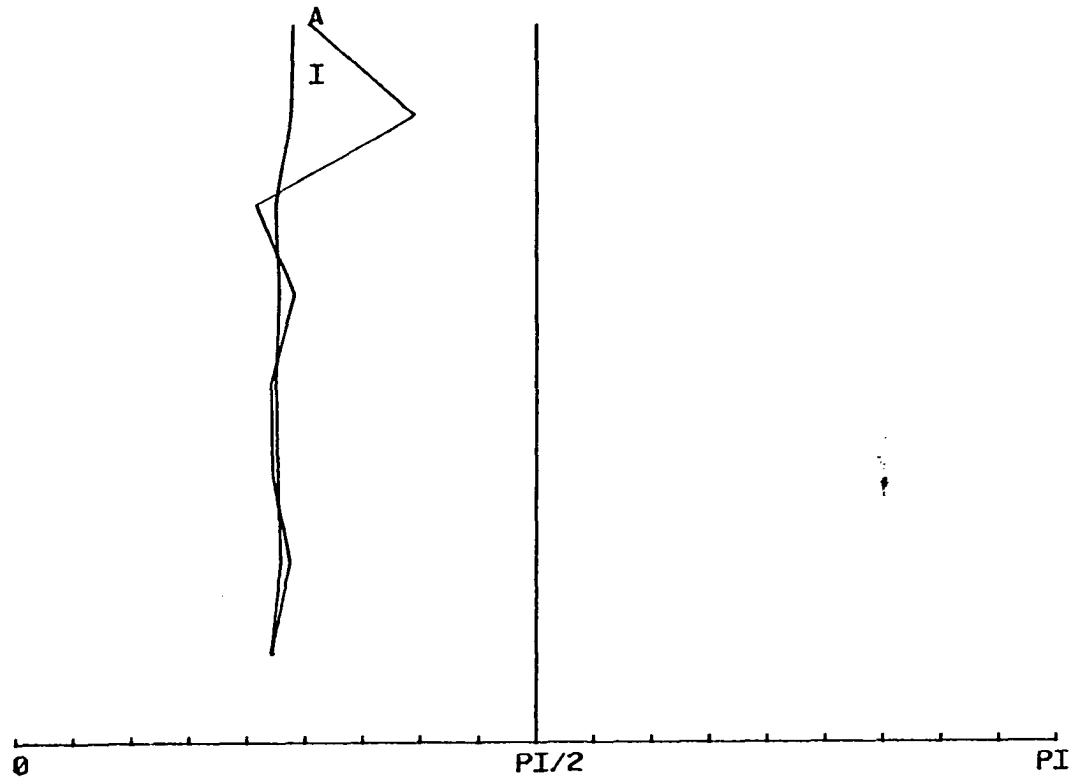
CRAIGIOBE
PHOTO 1.11.80#21,22; SAMPLE 8.14.78 D50; PAIR, RIGHT, FILE 49



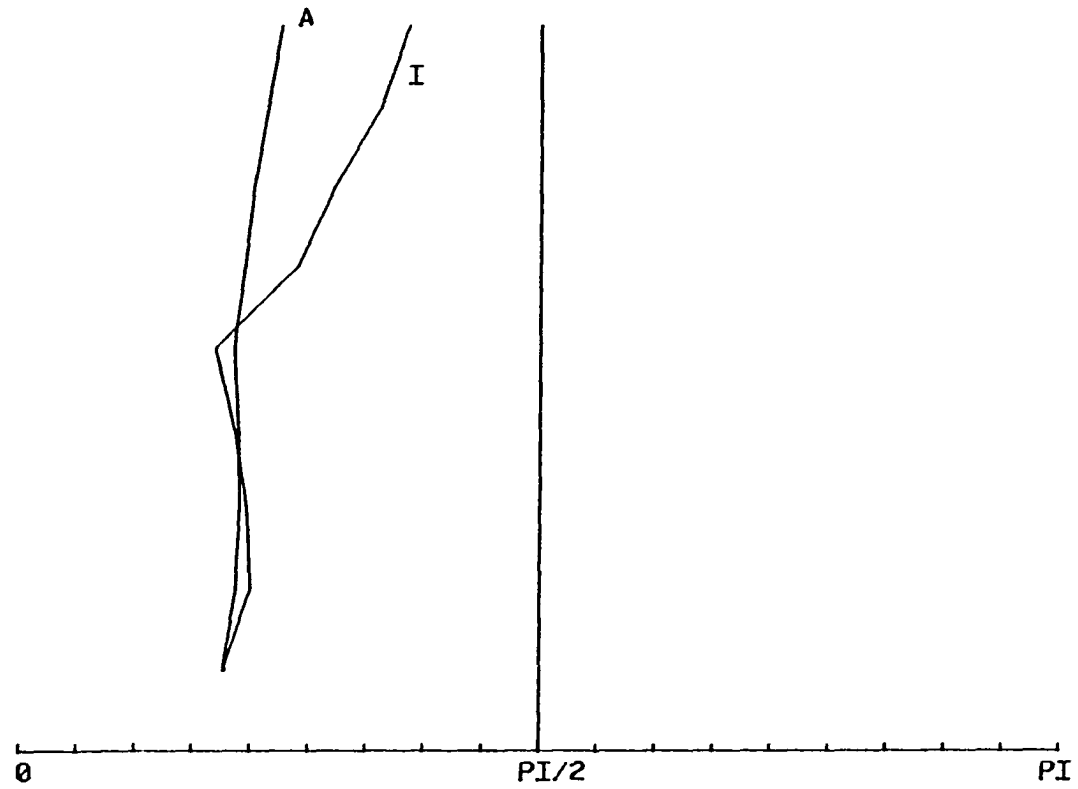
CRAIG11BE
PHOTO 1.11.80#23,24; SAMPLE 8.14.78 D50; PAIR, LEFT, FILE 50



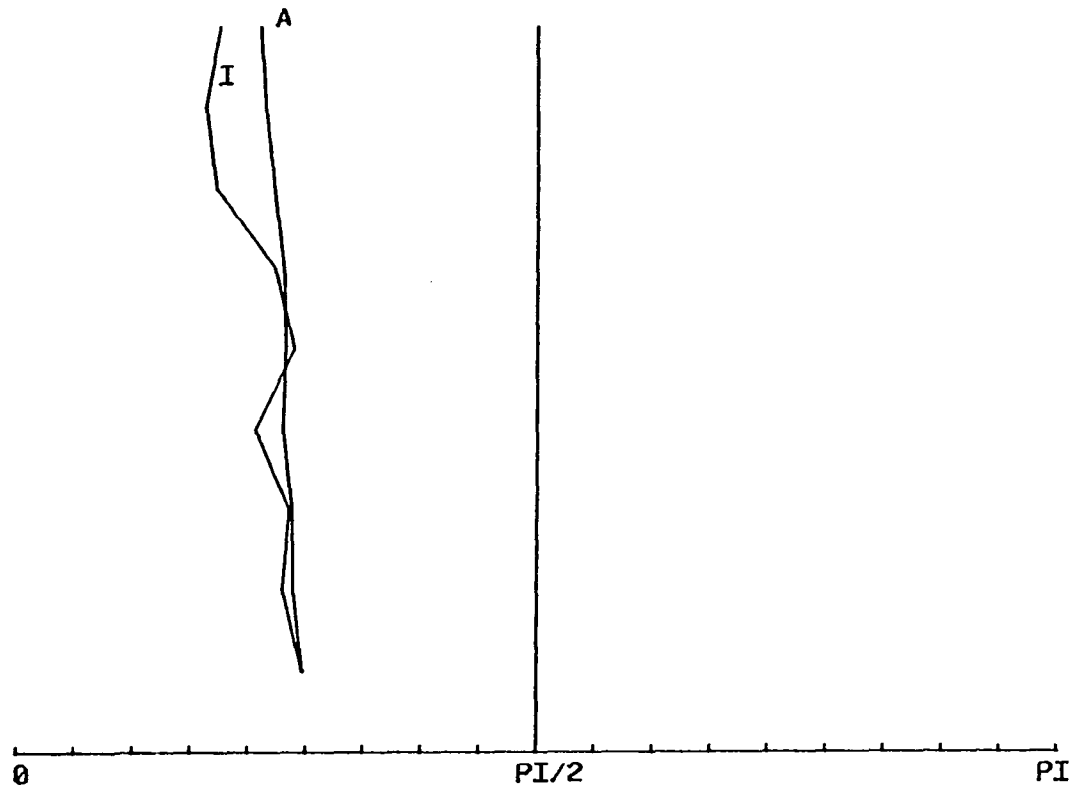
CRAIG13BE
PHOTO 1.11.80#25; SAMPLE 8.14.78 D50, PAIR, LEFT, FILE 52



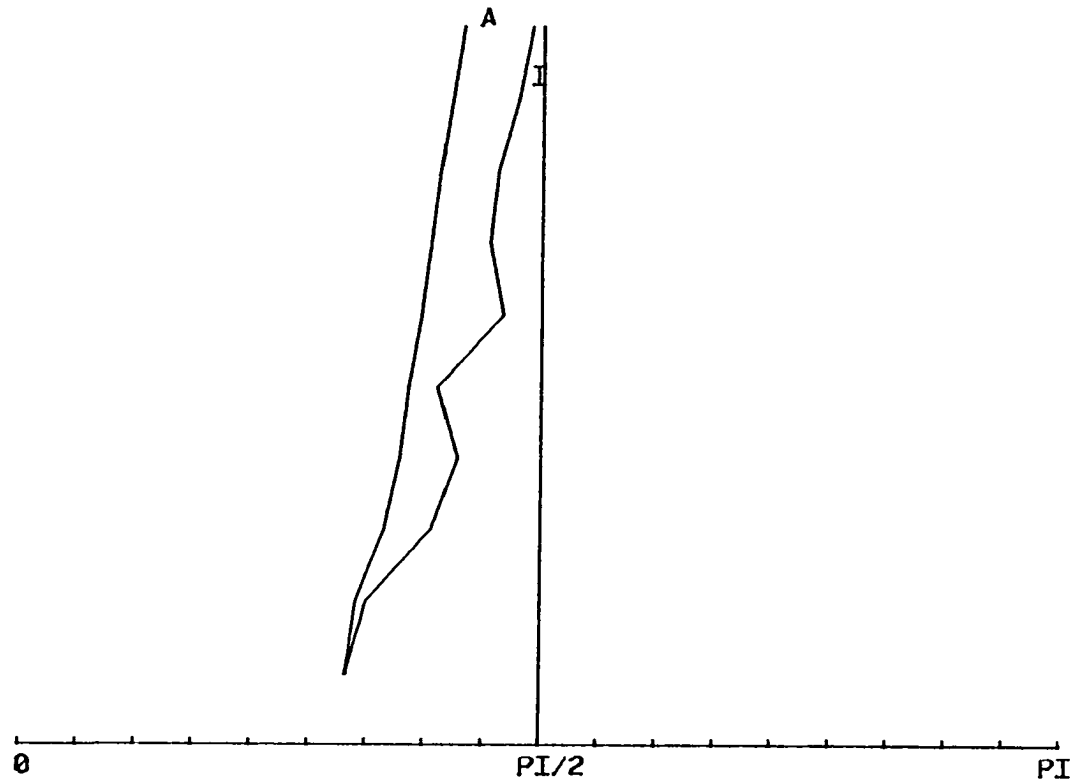
CRAIG14BE
PHOTO 1.11.80#25; SAMPLE 8.14.78 D50, PAIR, RIGHT, FILE 53



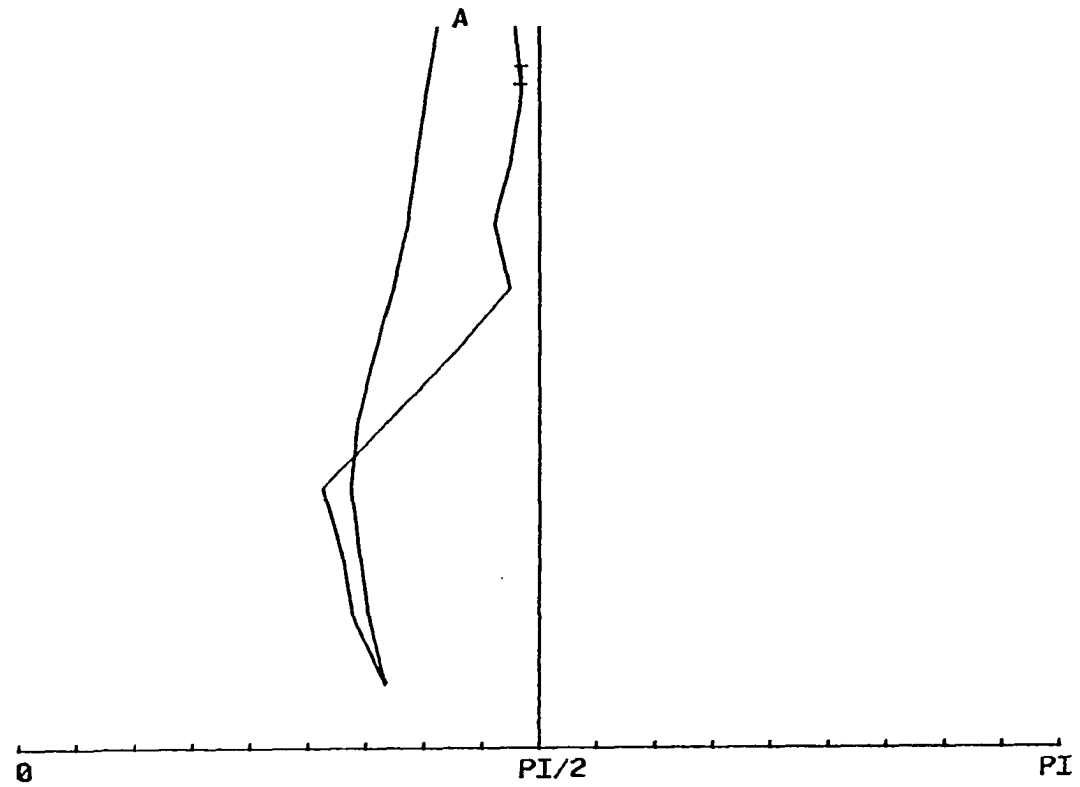
CRAIG17BEP
PHOTO 1.11.80#26-32; SAMPLE 8.14.78 D50; CHAIN, PAIR, RIGHT, FILE 56



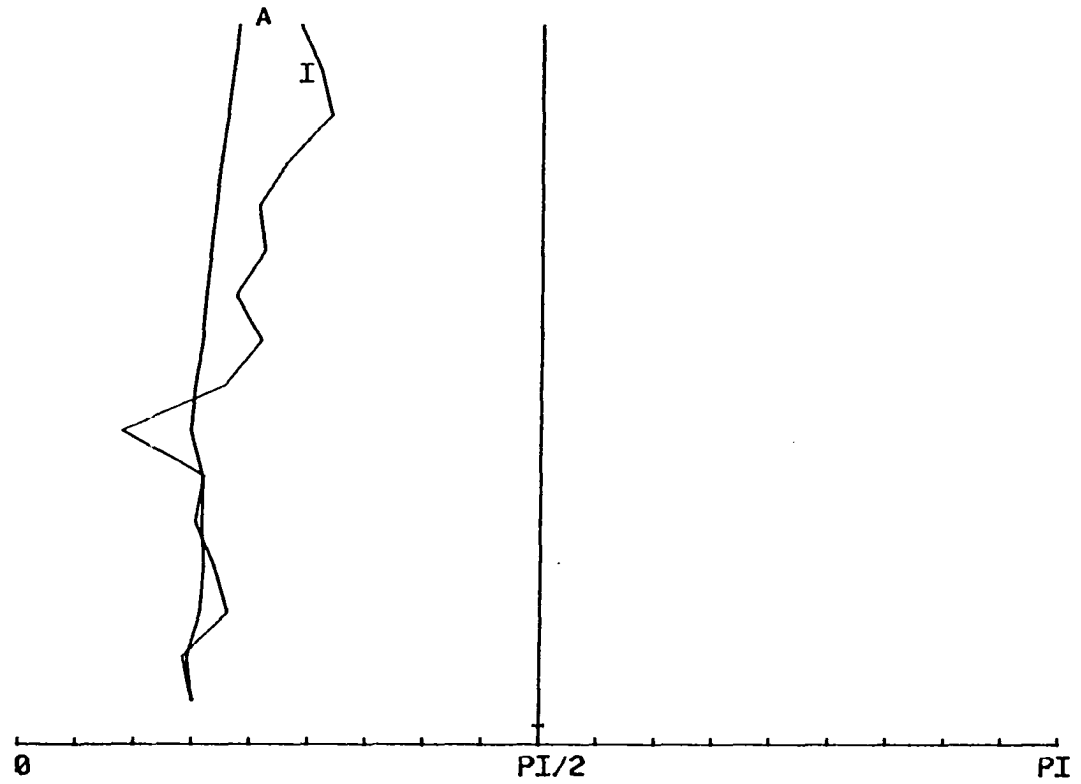
CRAIG20BEP
PHT 1.11.80#26-32; SAMPLE 8.14.78 D50, CHAIN CENTROID 3-4, LEFT, FILE 59



CRAIG21BEP
PHT 1.11.80#26-32; SAMPLE 8.14.78 D50; CHAIN CENTROID 3-4; RIGHT, FILE 60

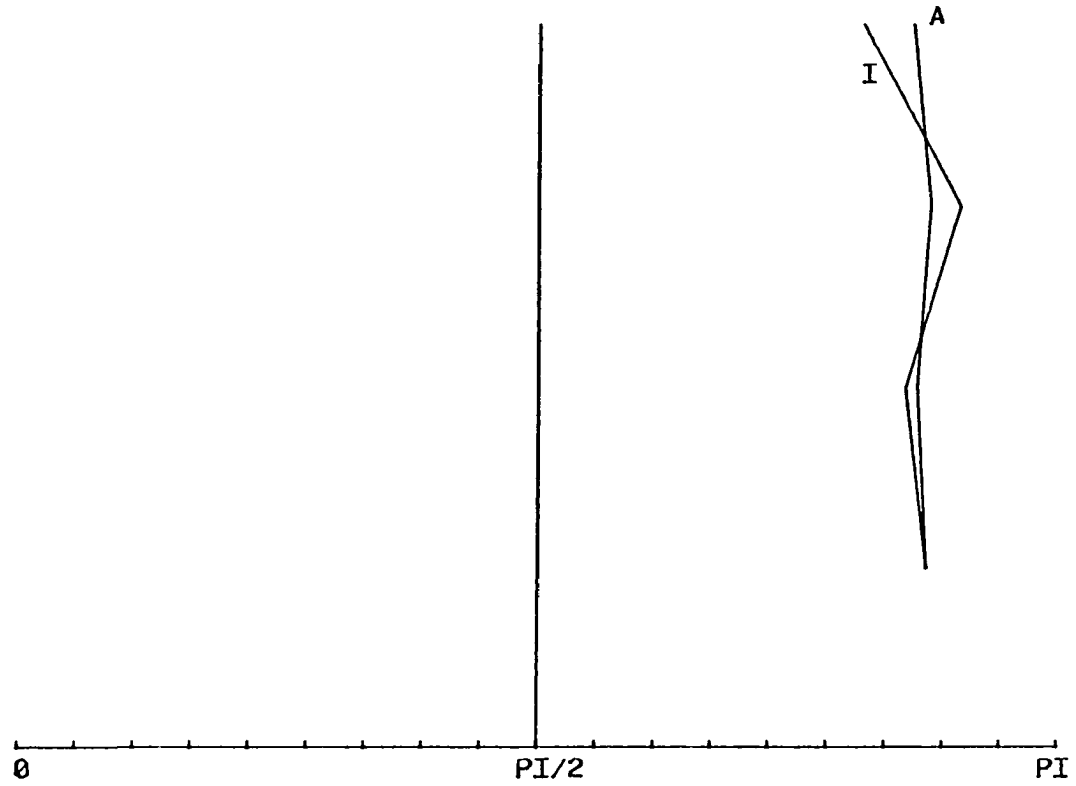


CRAIG22BEP
PHT 1.11.80#26-32; SAMPLE 8.14.78 D50, CHAIN SE SINGLET, FILE 61

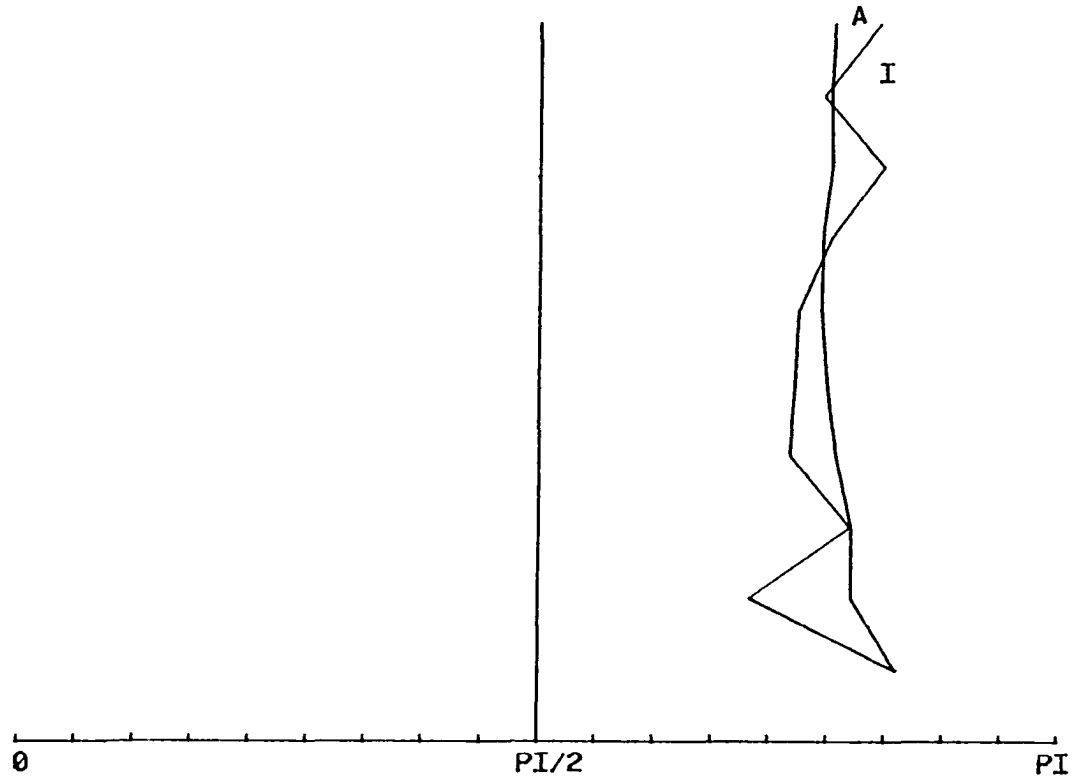


SAMPLE 937

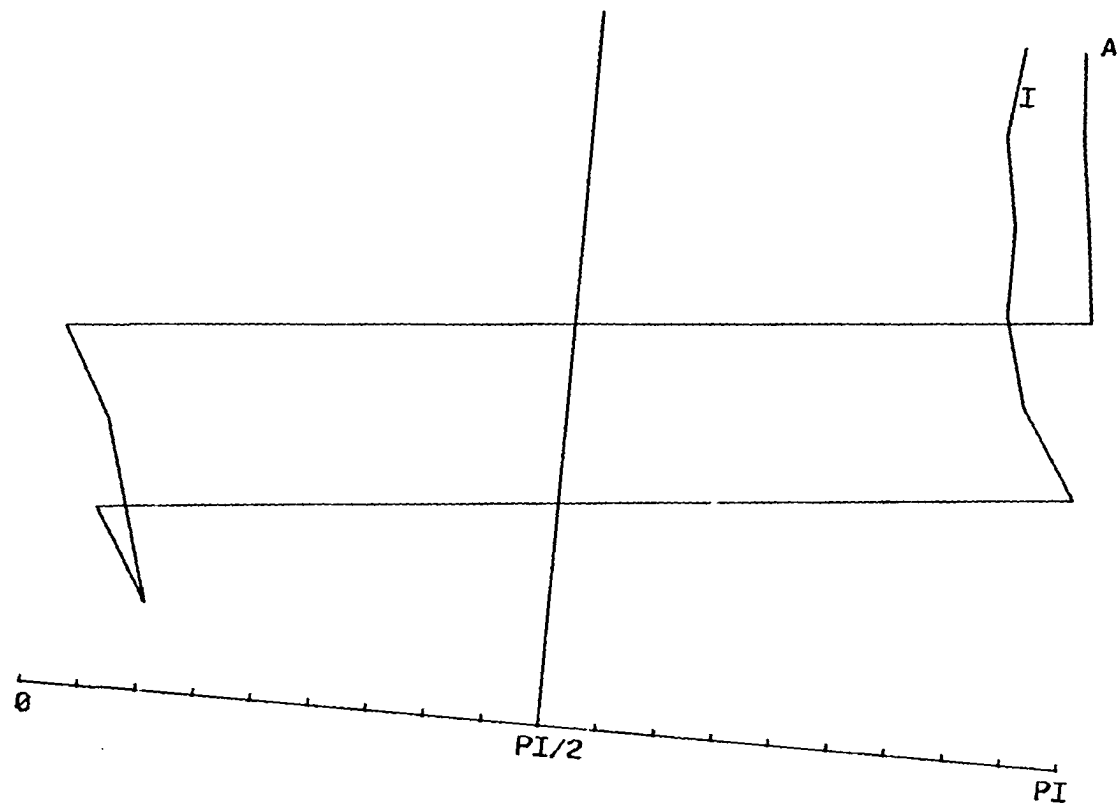
CHAPEL7BE
chapel 7 p3b 937a left left



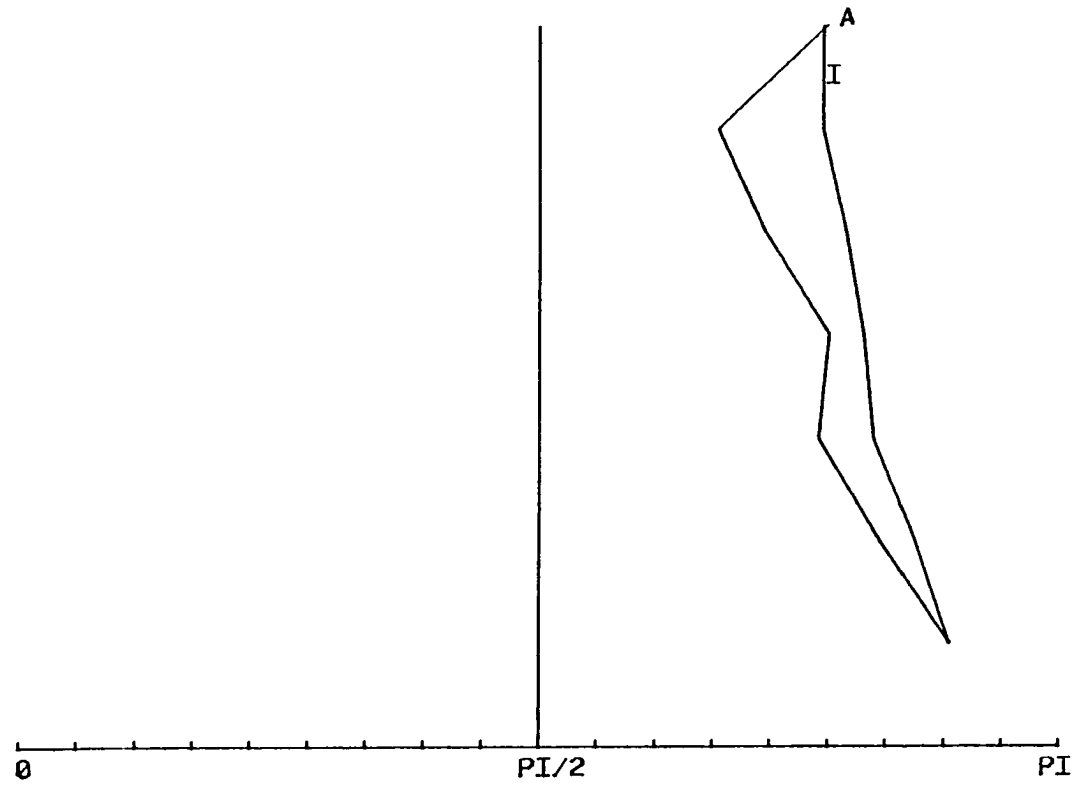
CHAPEL12BE
chapel 12 p2b 937a left right



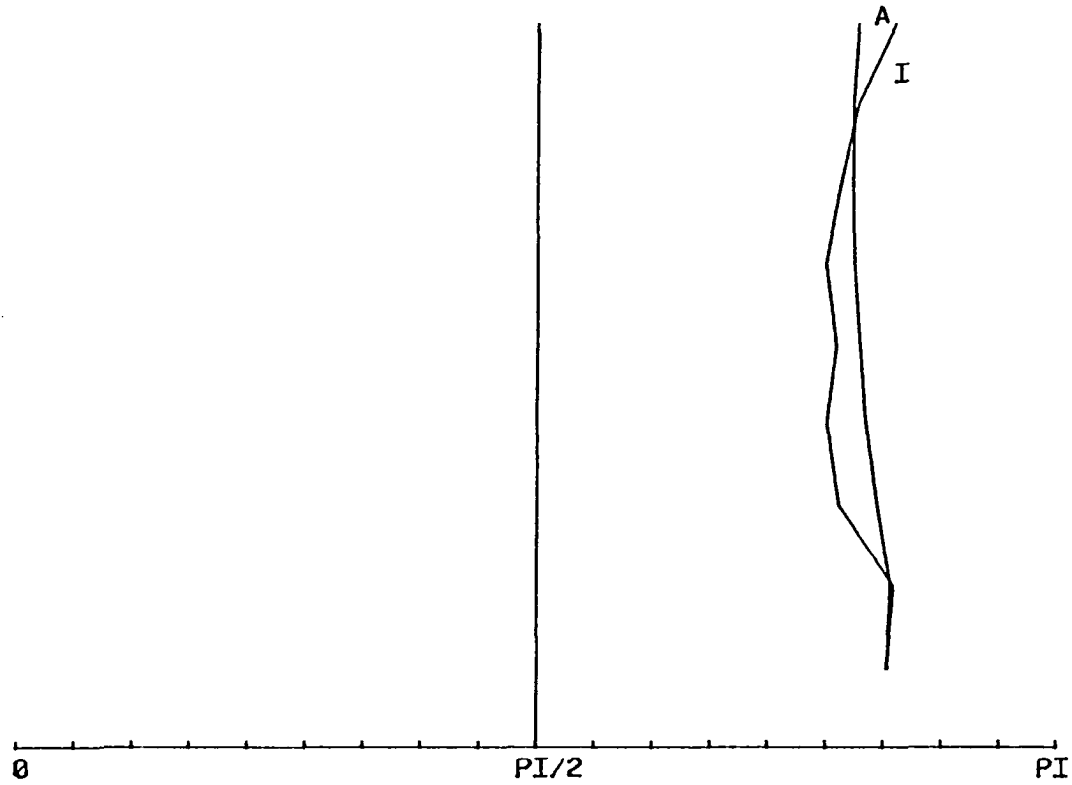
CHAPEL10BE
chapel 10 p3b 937a right right



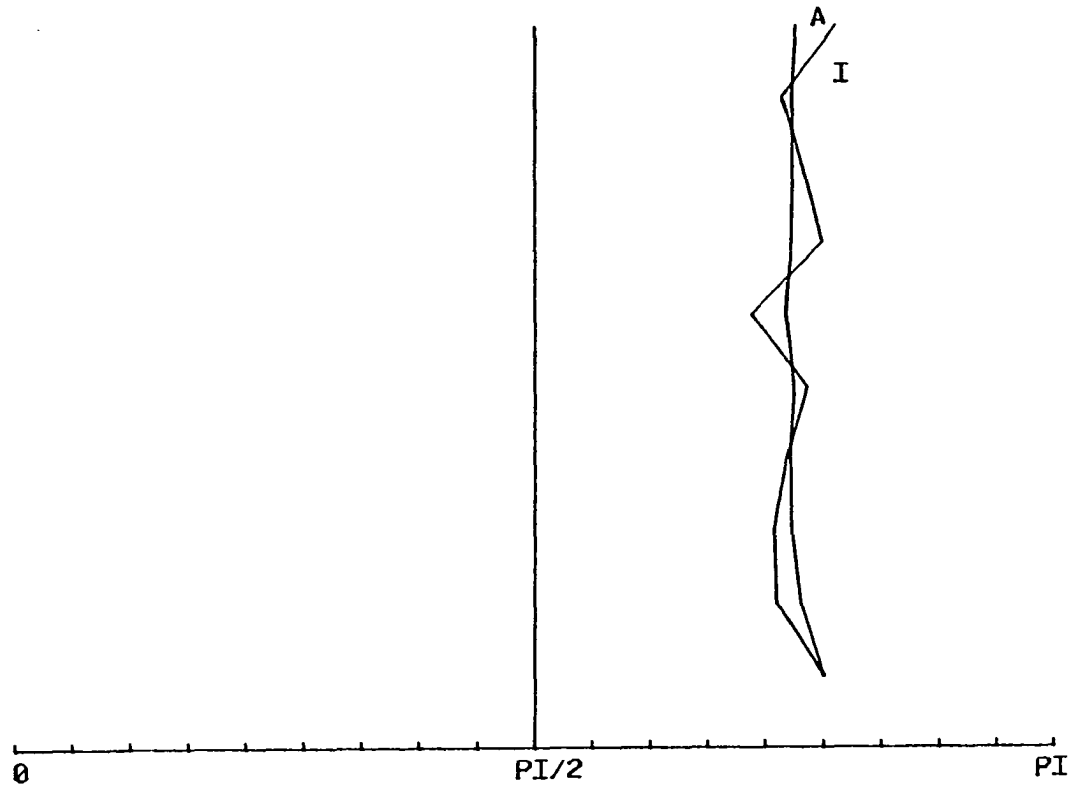
CHAPEL15BE
CHAPEL 15 P6B 937A DOUBLET RIGHT,LEFT



CHAPEL16BE
CHAPEL 16 P6B 937A DOUBLET LEFT,RIGHT

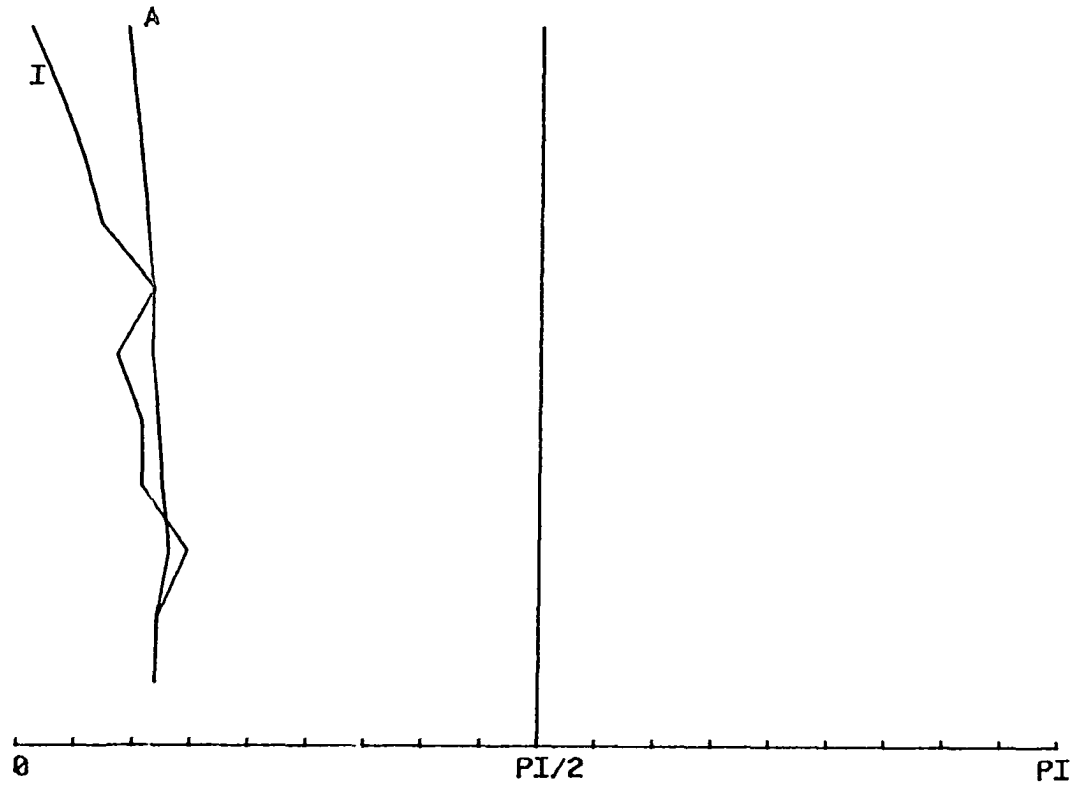


CHAPEL29BE
CHAPEL 29 P1B 937A SINGLET LEFT

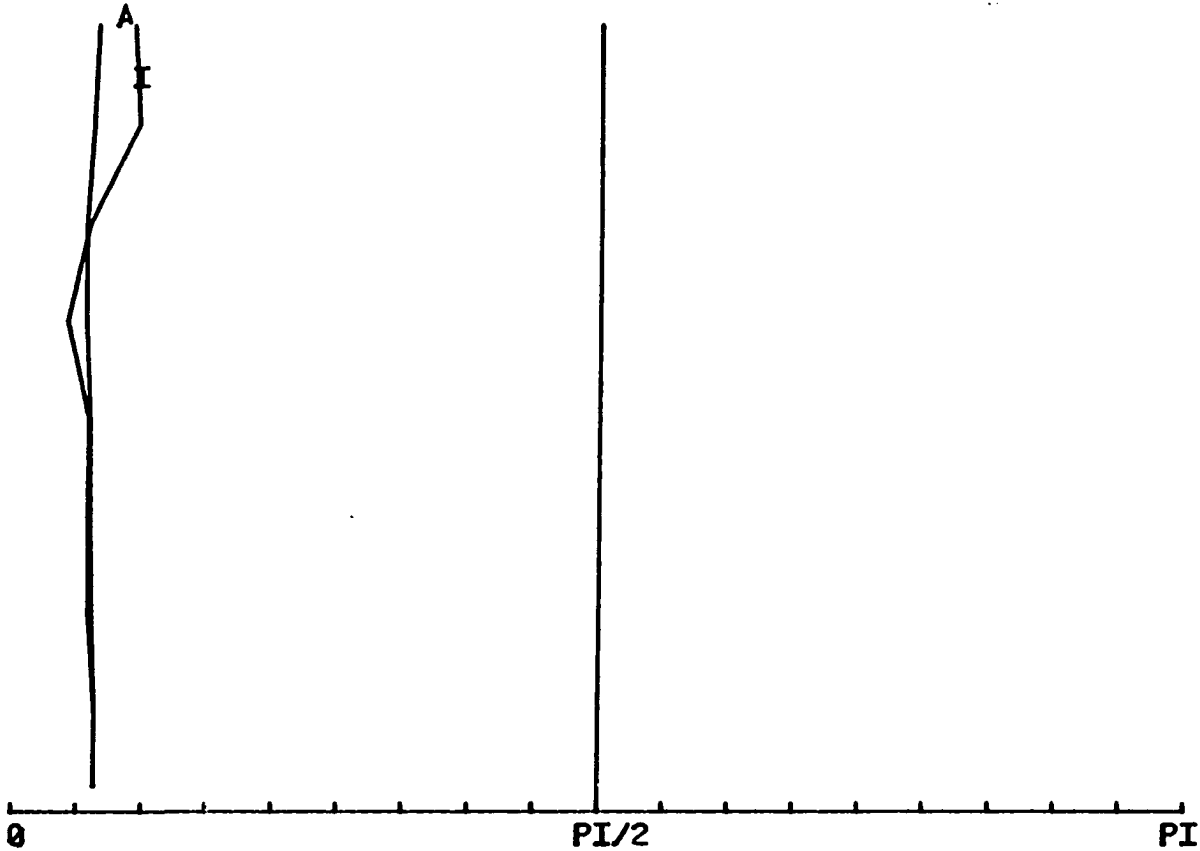


SAMPLE 939

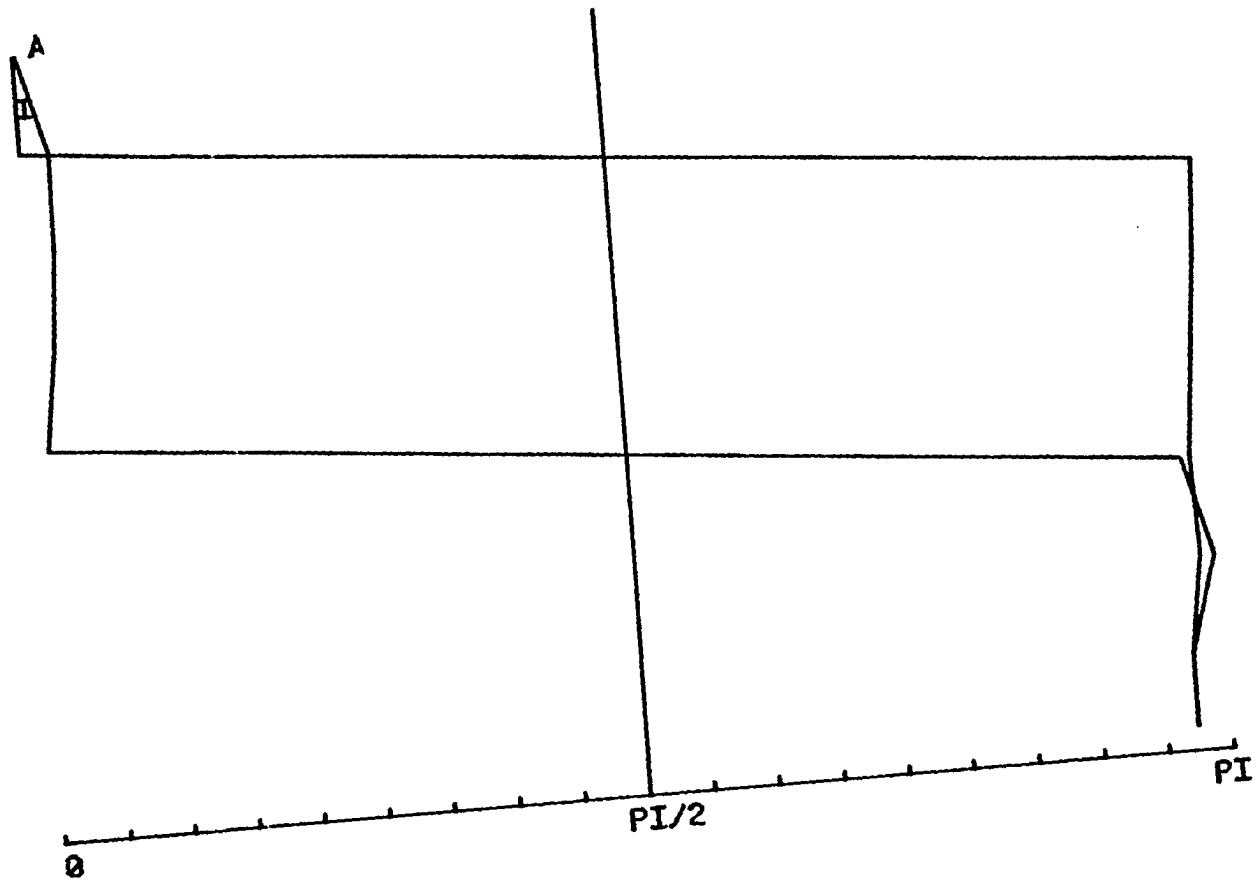
CRAIG23BE
craig run 23 7279-39 9p-10p(6-29) doublet left



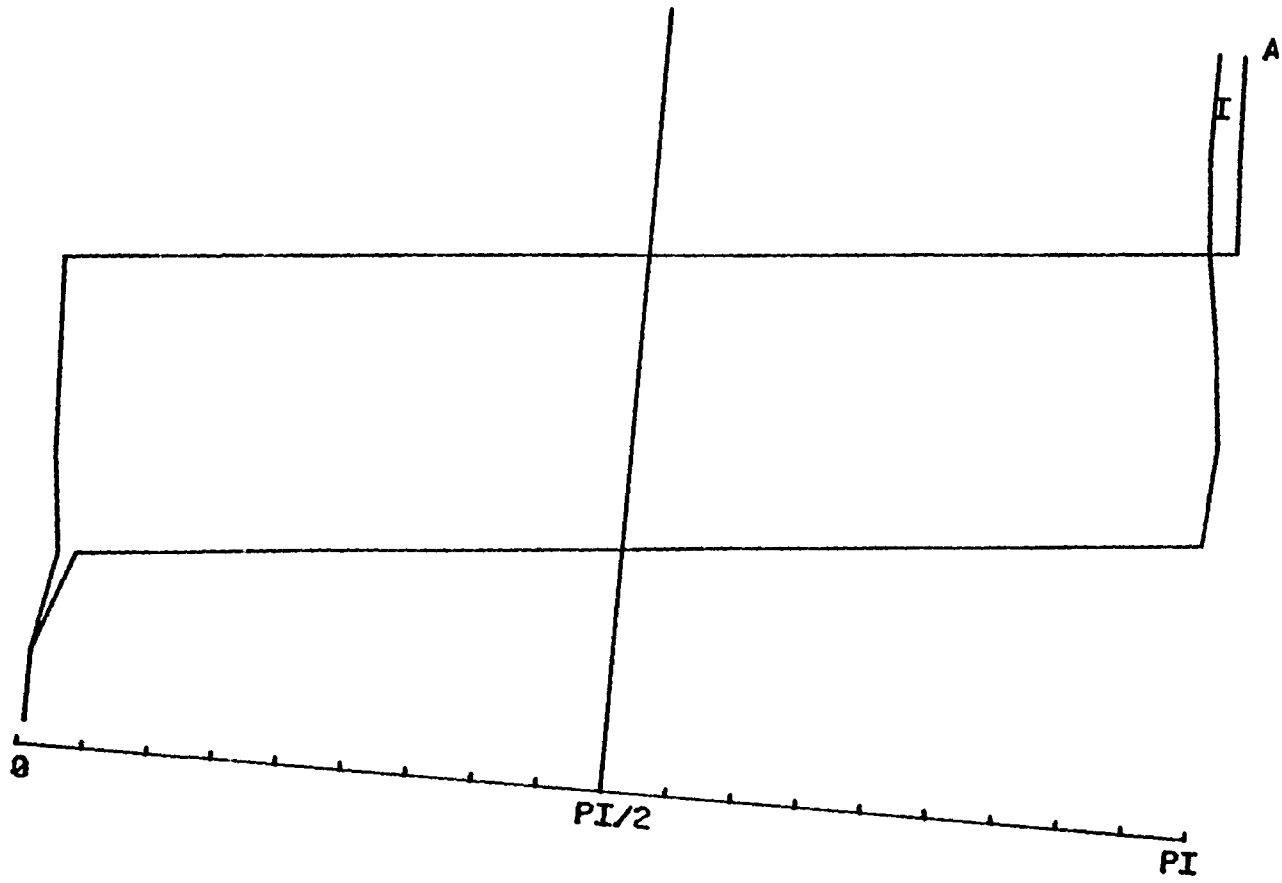
CRAIG26B



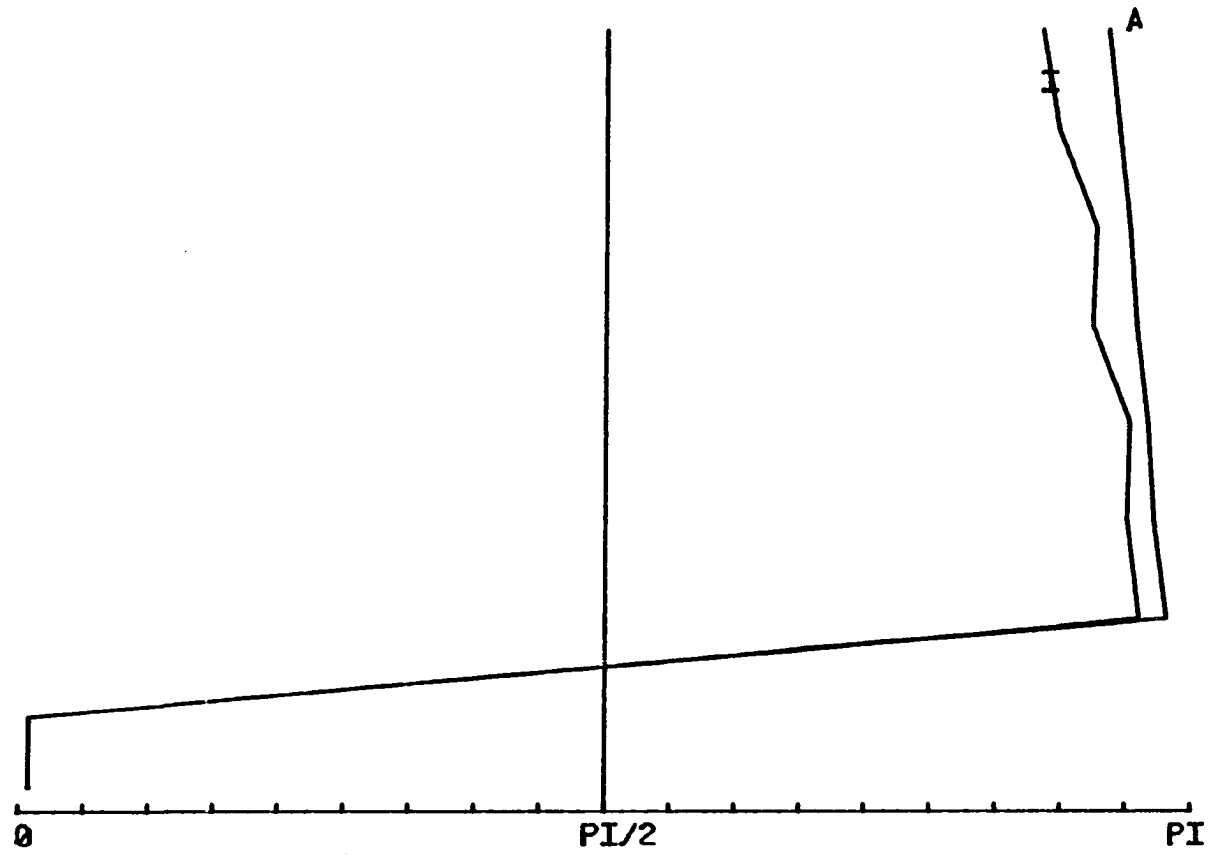
CRAIG27B



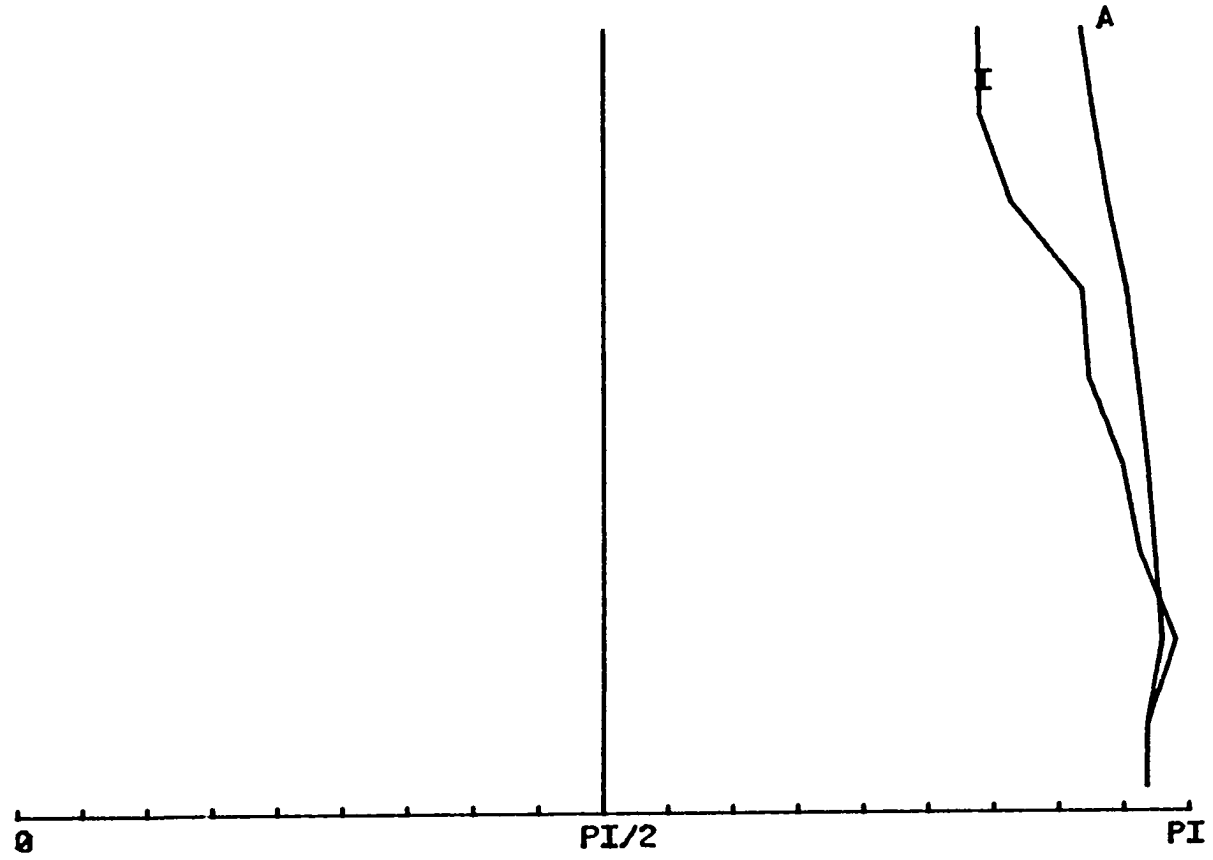
CRAIG28B



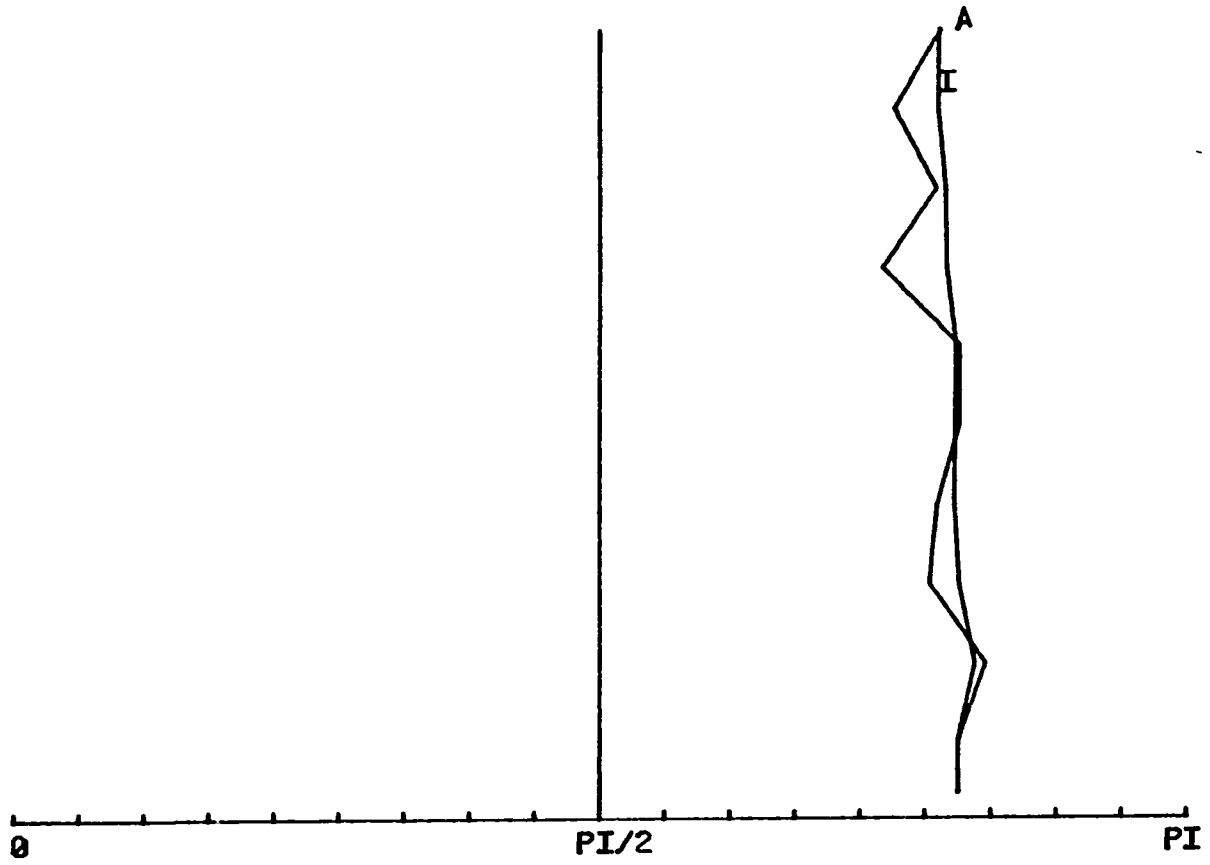
CRAIG30B



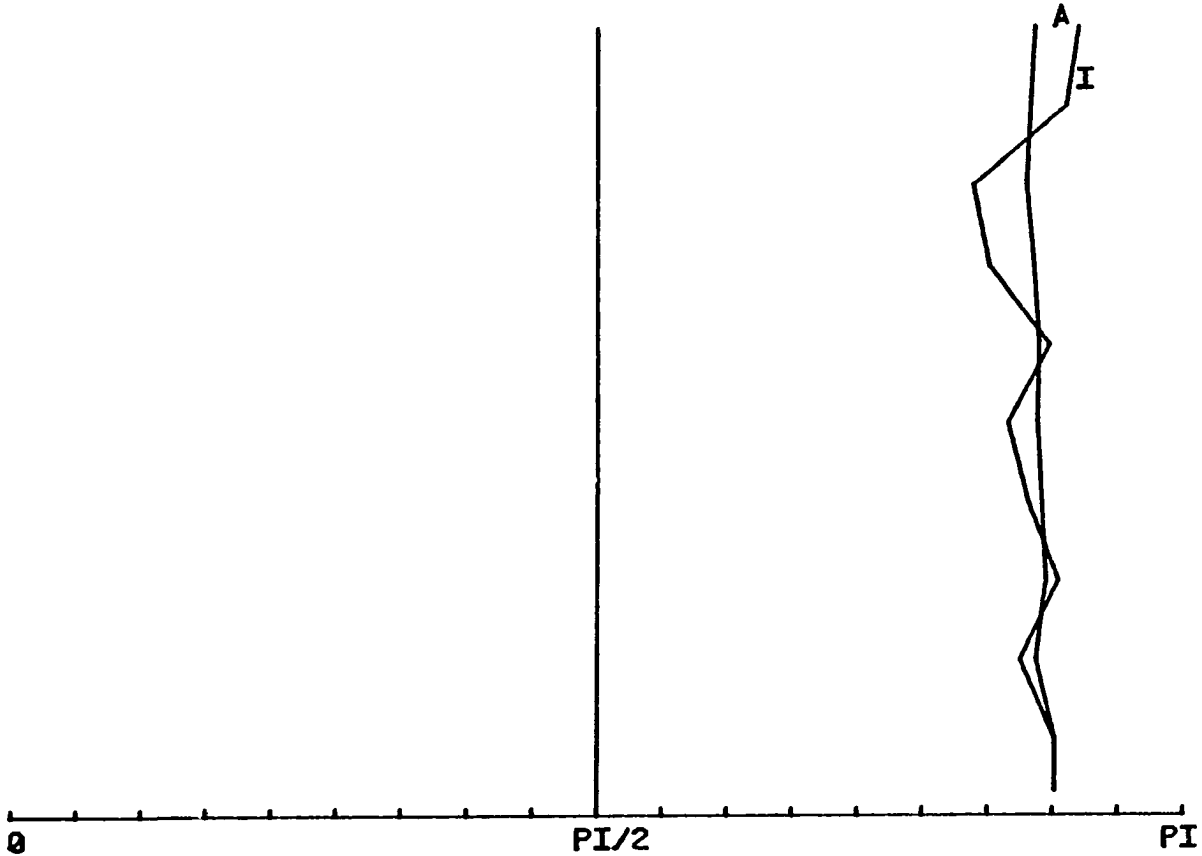
CRAIG31B



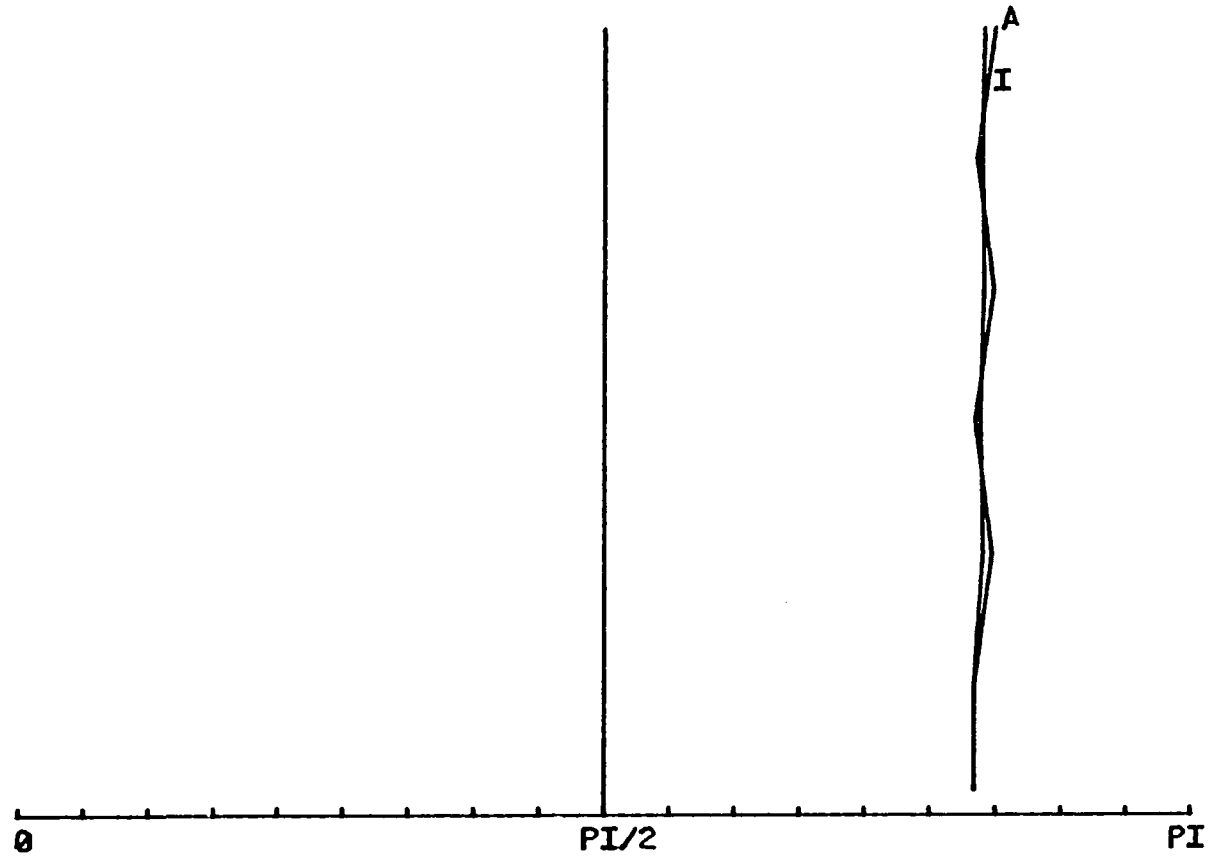
CRAIG32B



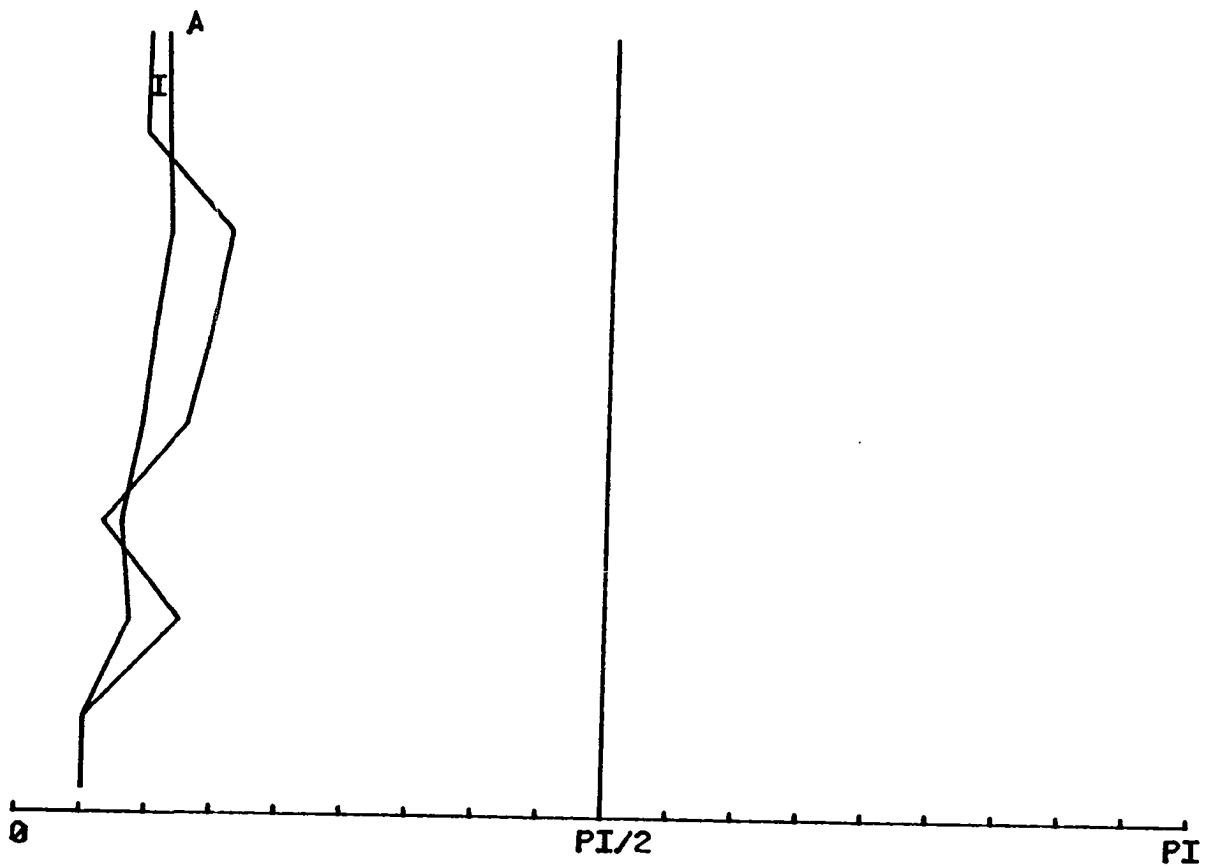
CRAIG34B



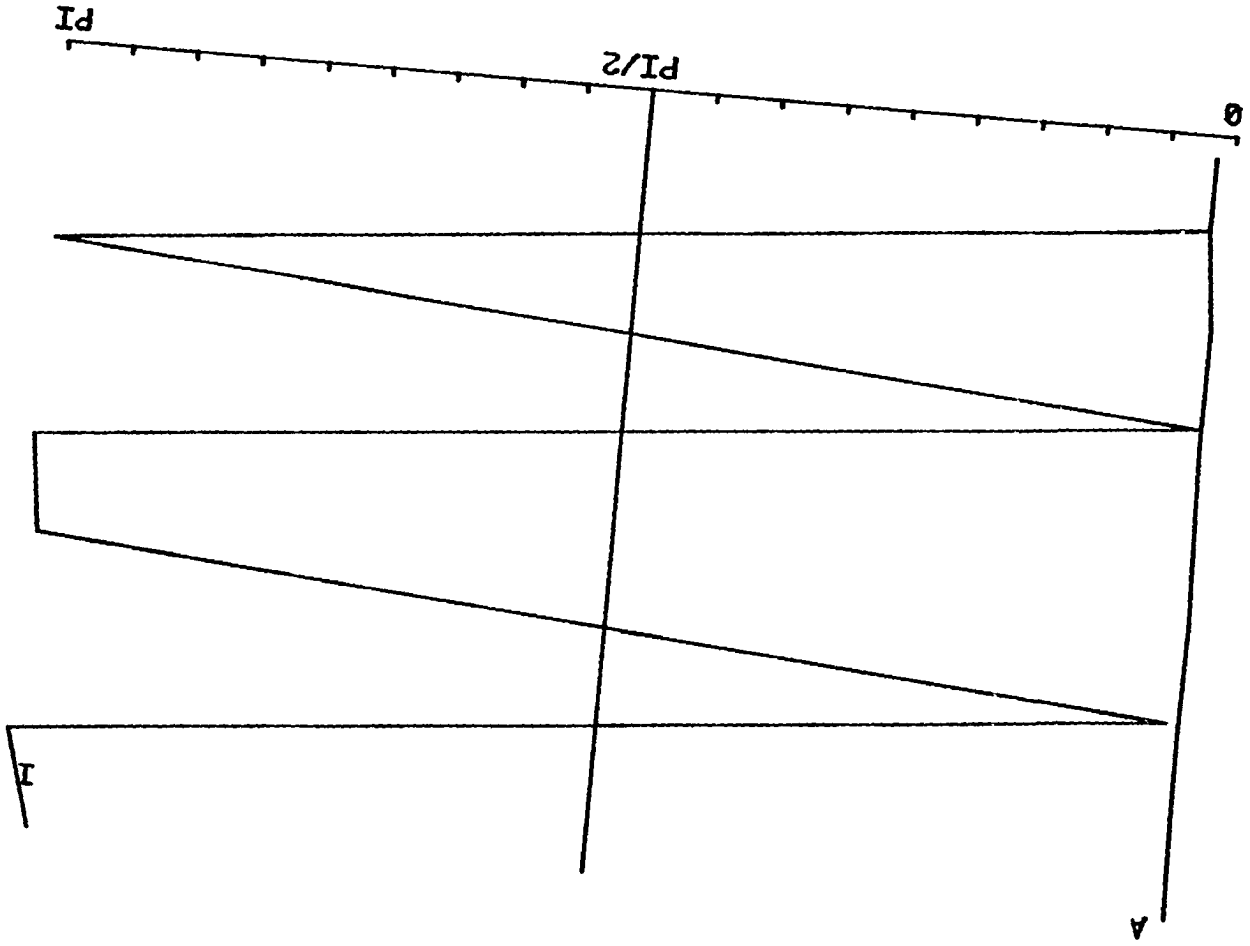
CRAIG35B



CRAIG36B

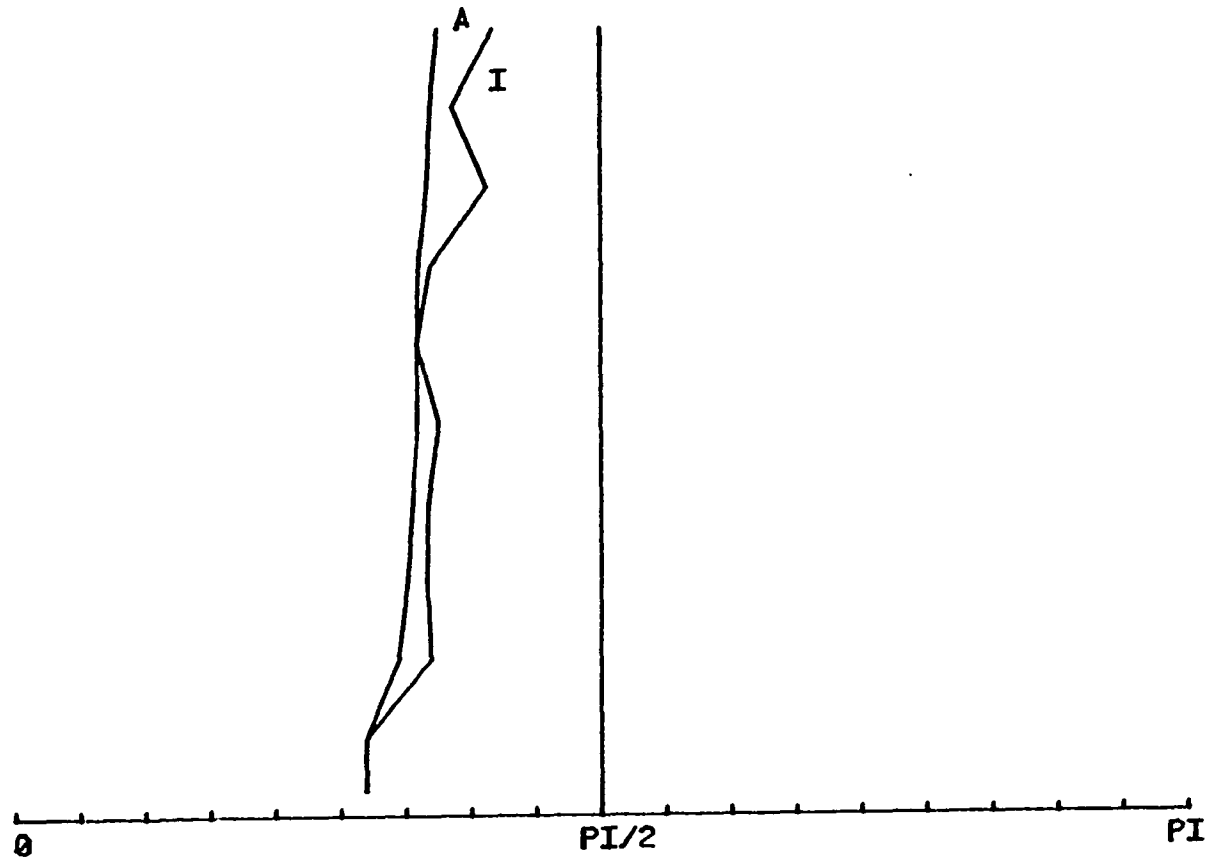


CRAIG37B



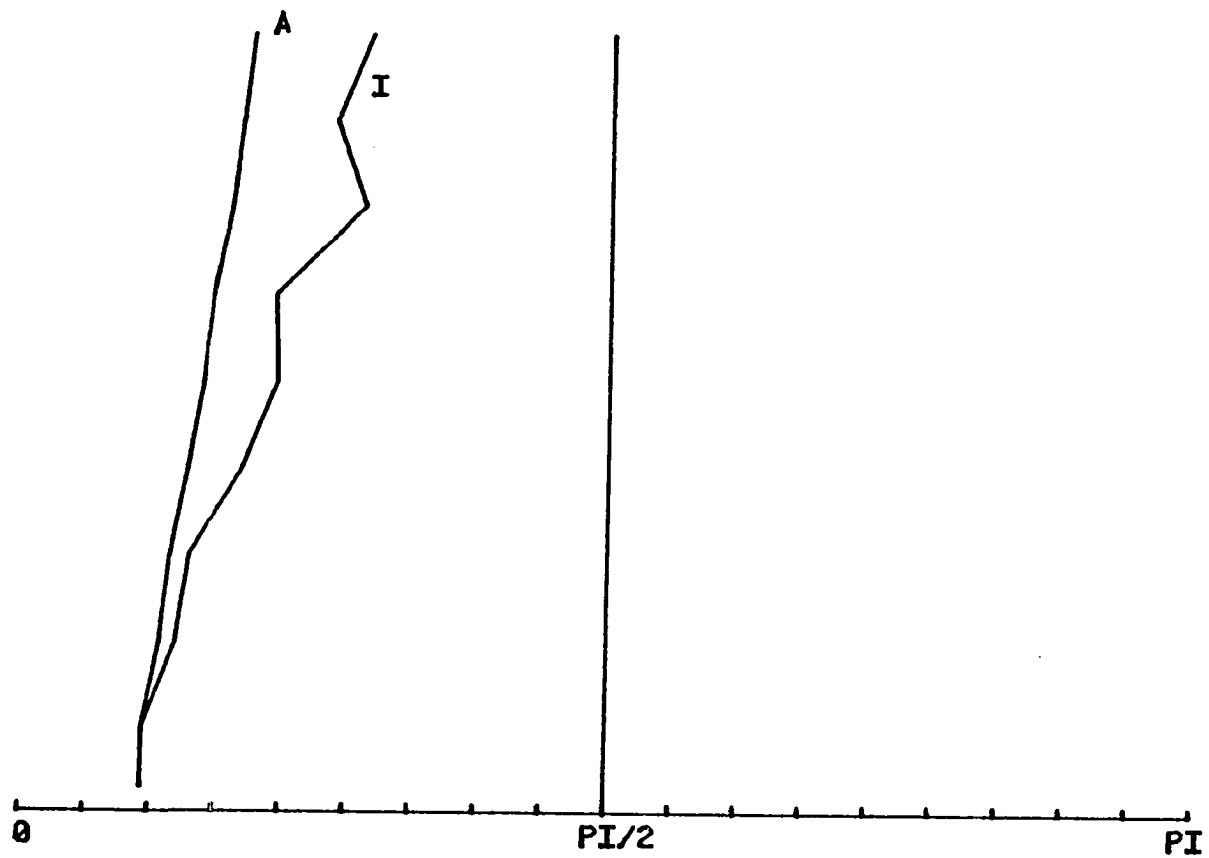
SAMPLE 932

CHAPEL20B



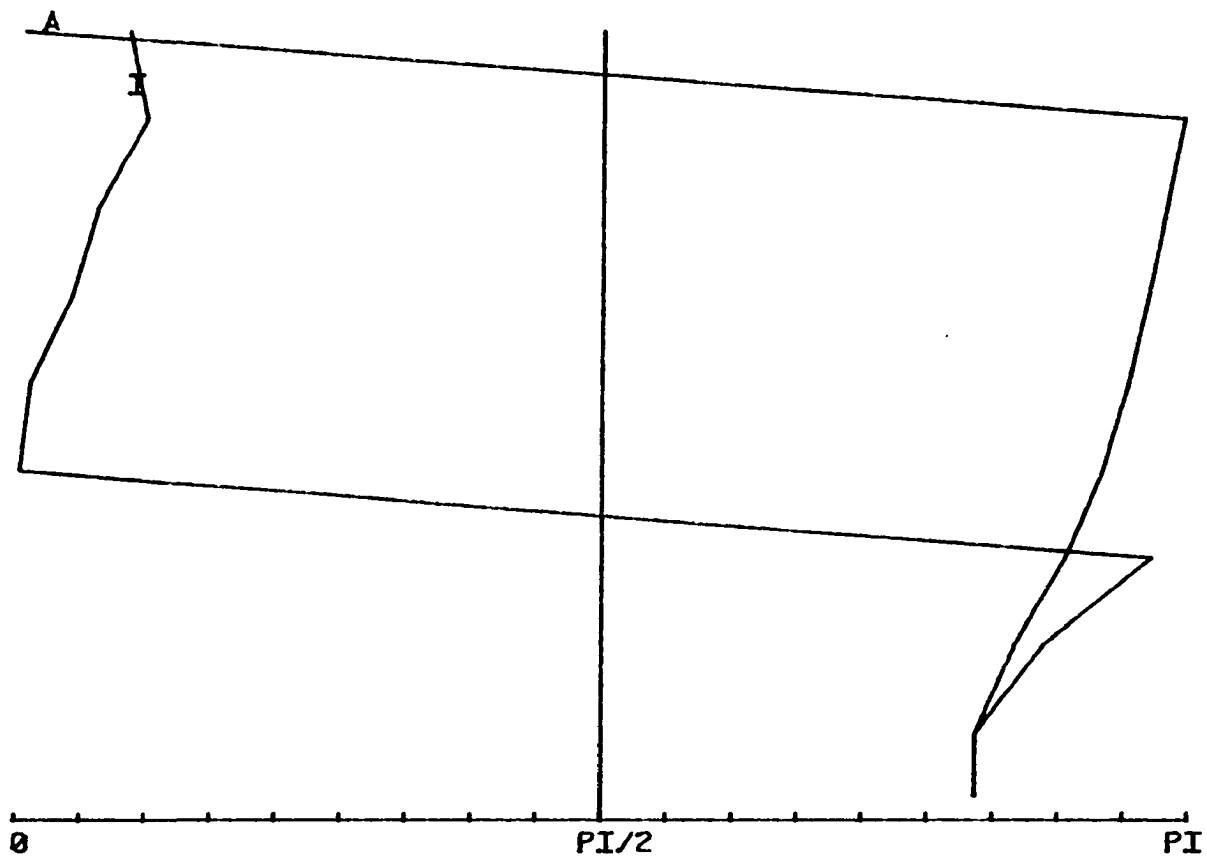
SAMPLE 934

CHAPEL3B



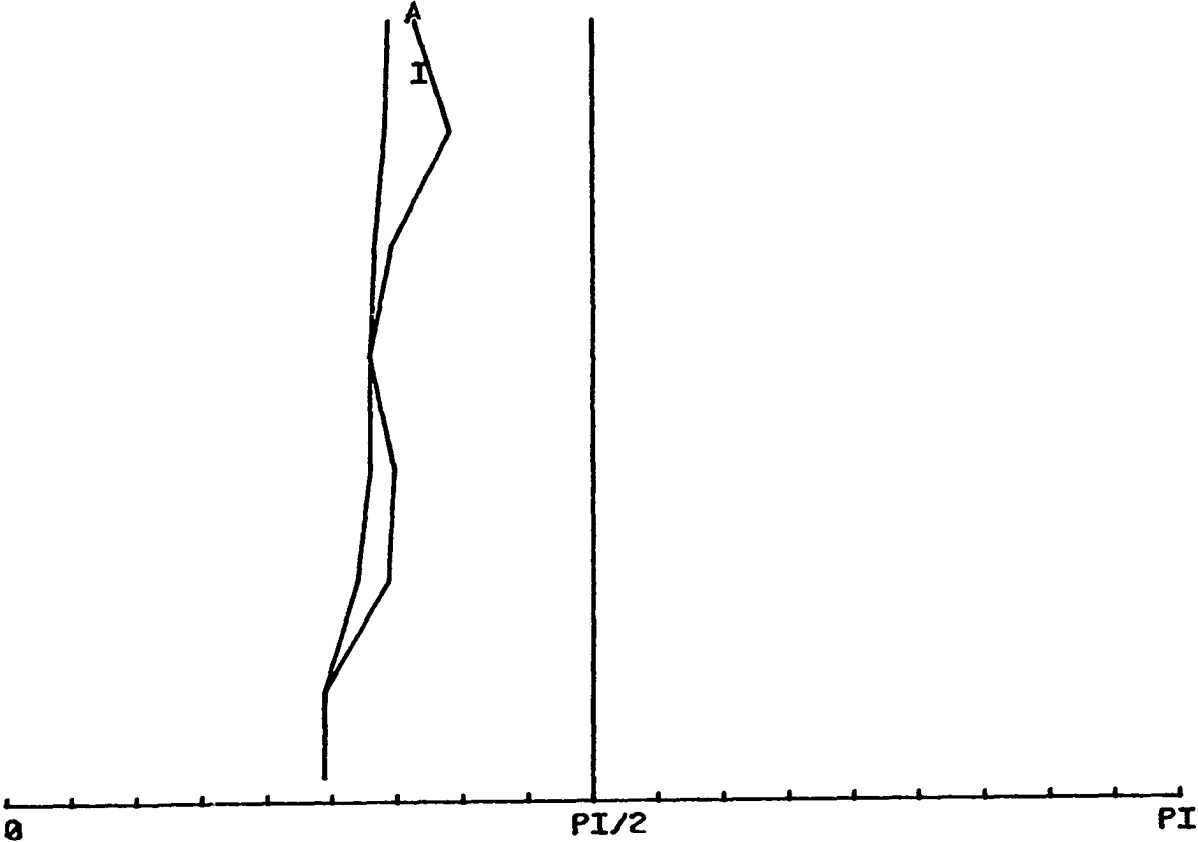
SAMPLE 943

BULL 16B



SAMPLE 944

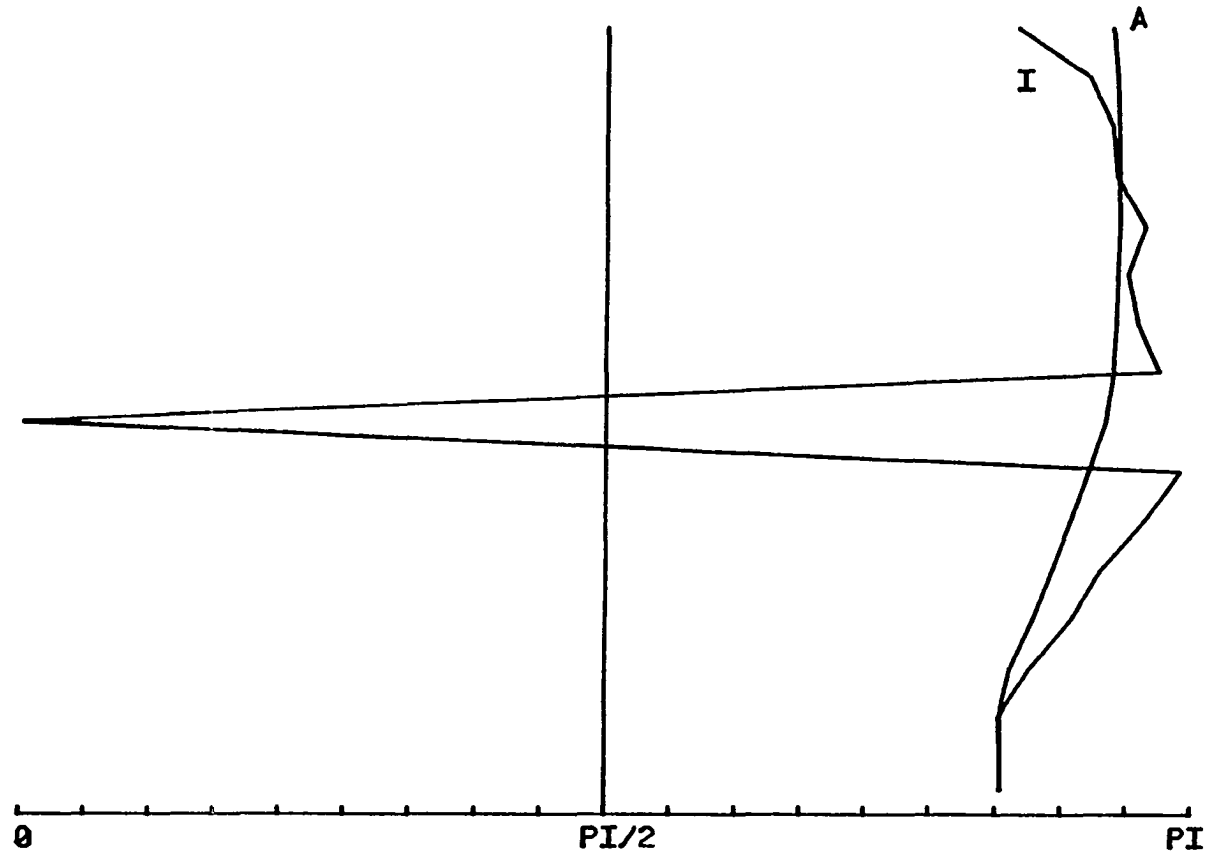
BULL22B



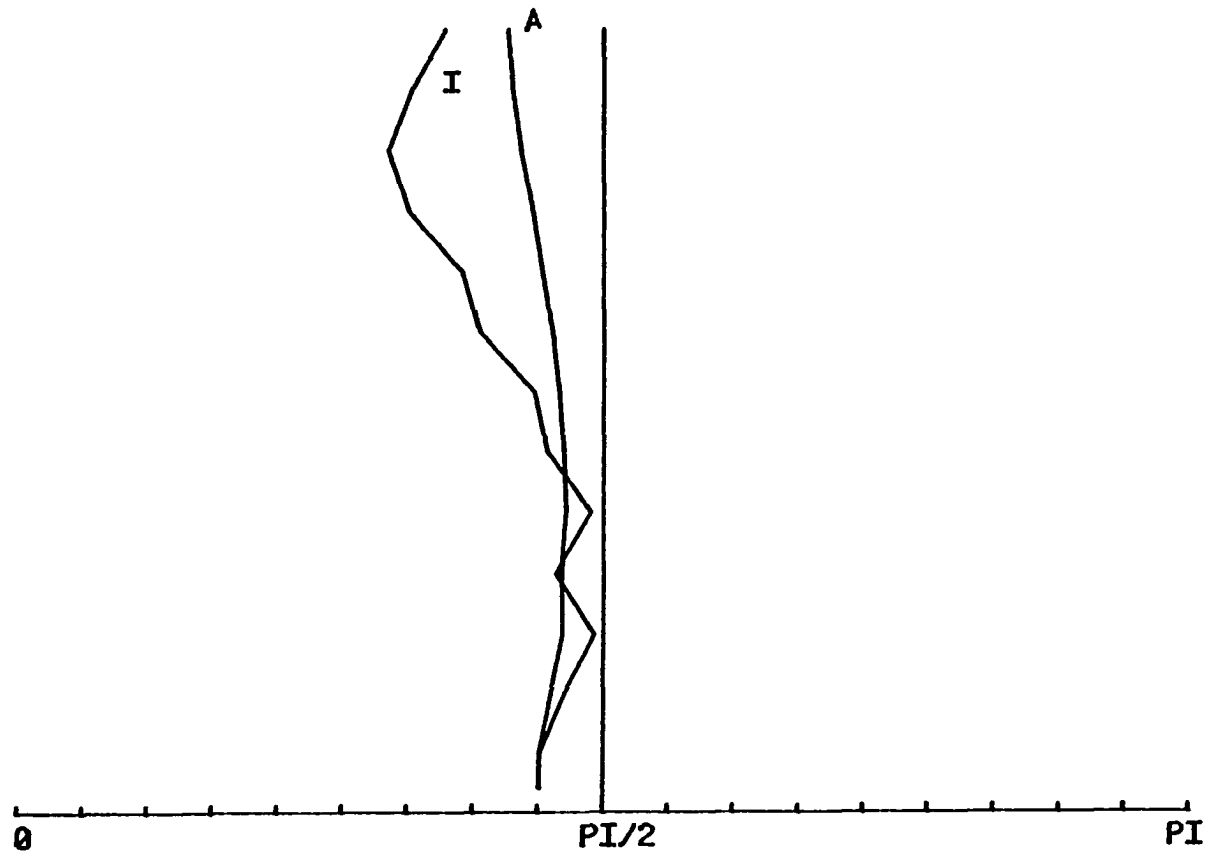
APPENDIX C
STRAIN PATHS WITH
AREA STRAIN >2.0

SAMPLE 816

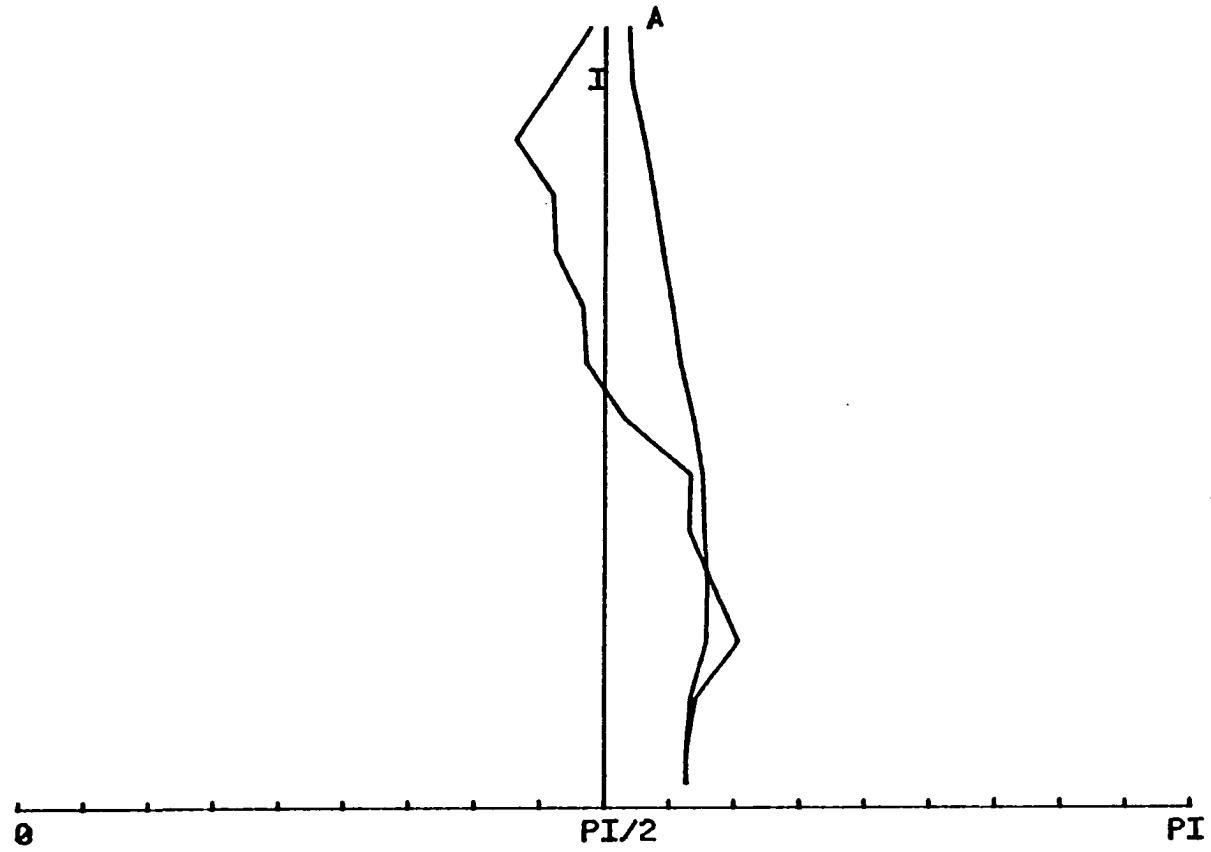
STONE12B



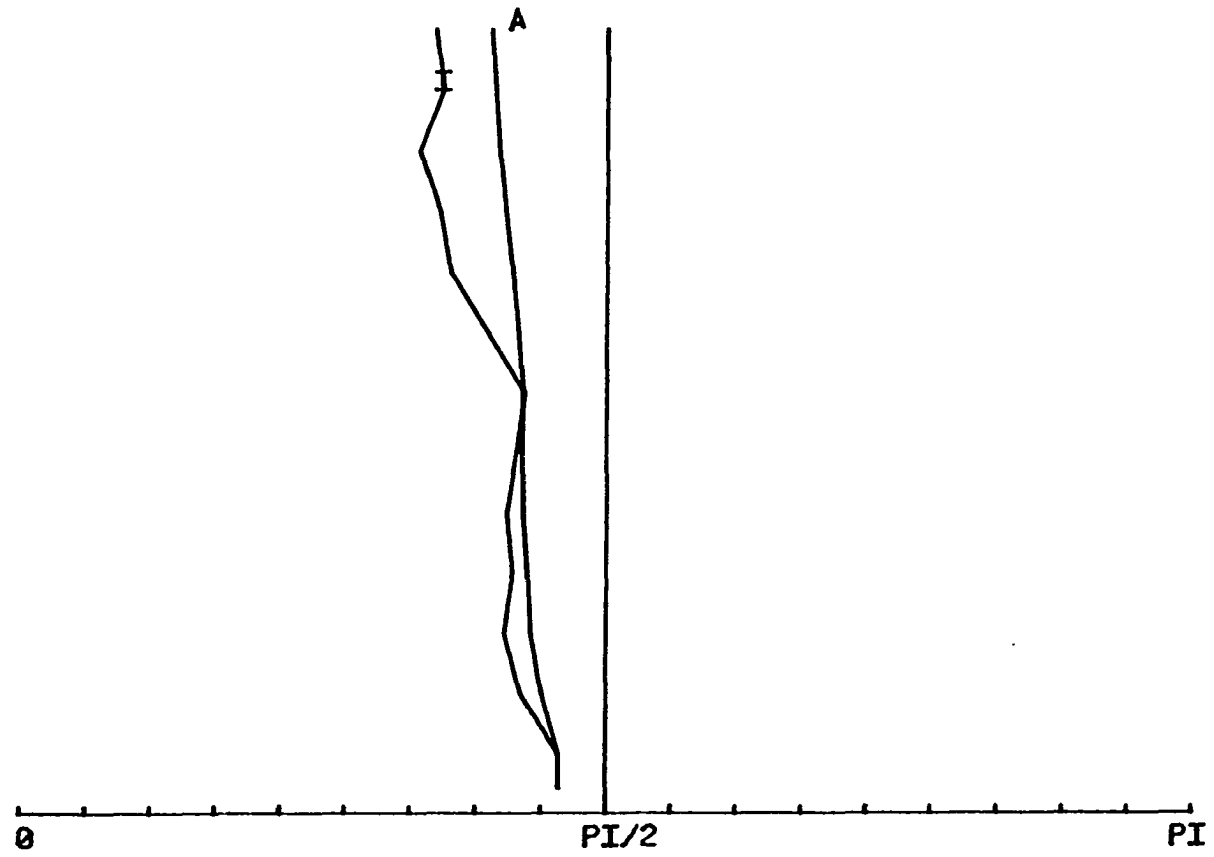
STONE5B



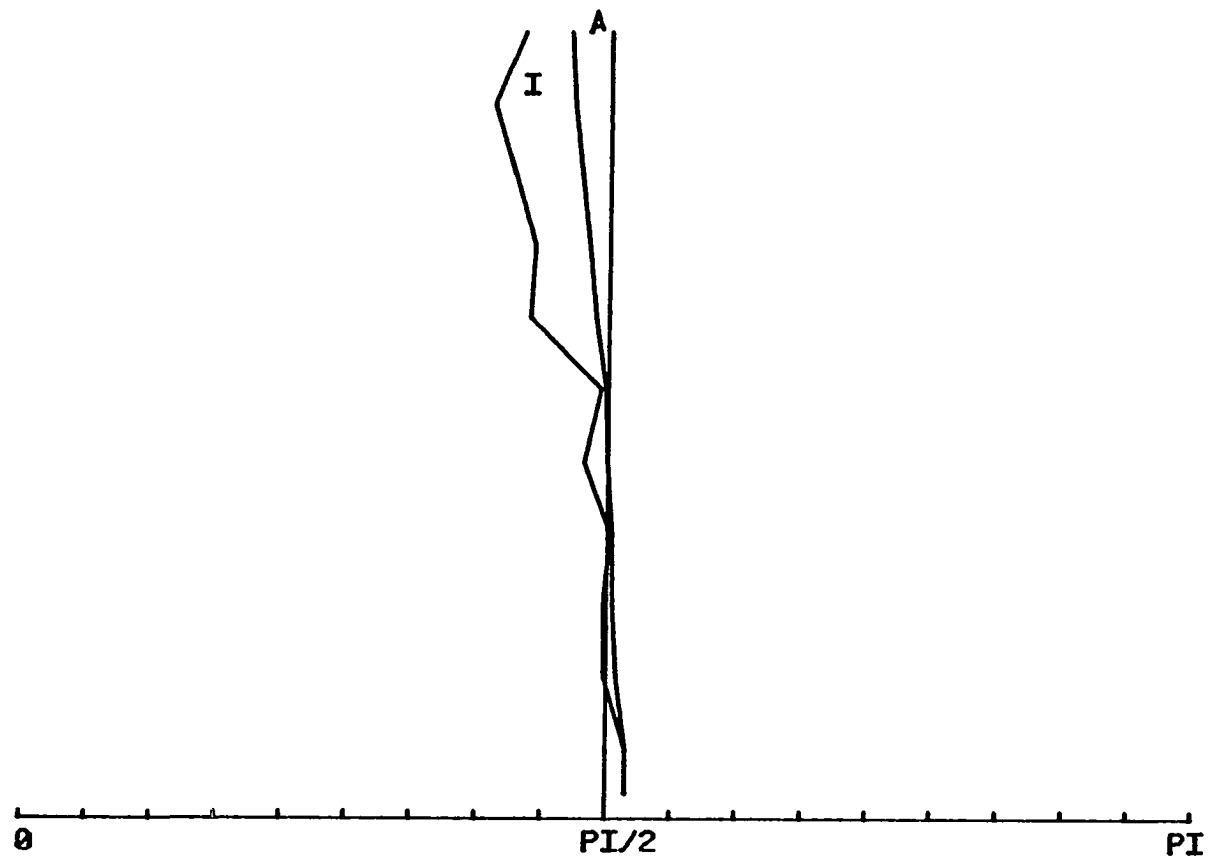
STONE8B



STONE9B

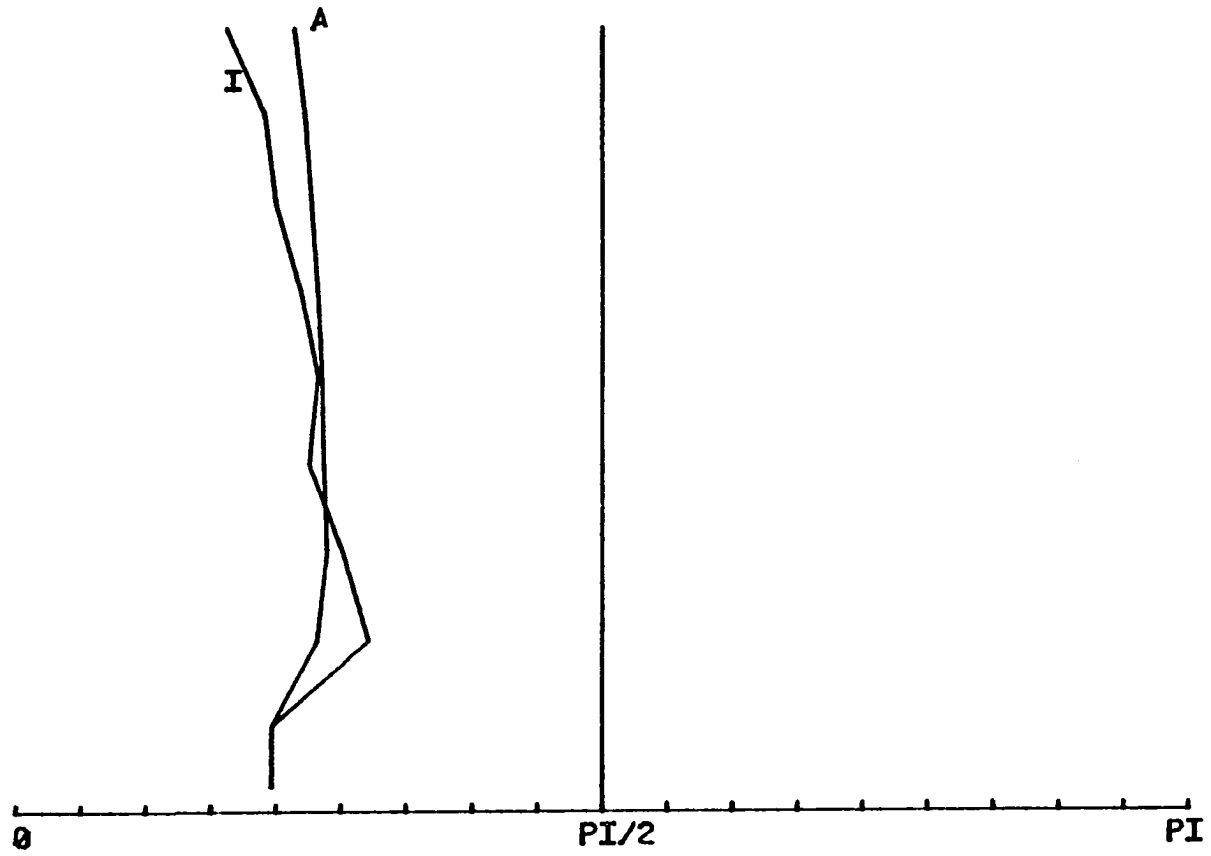


STONE 10B

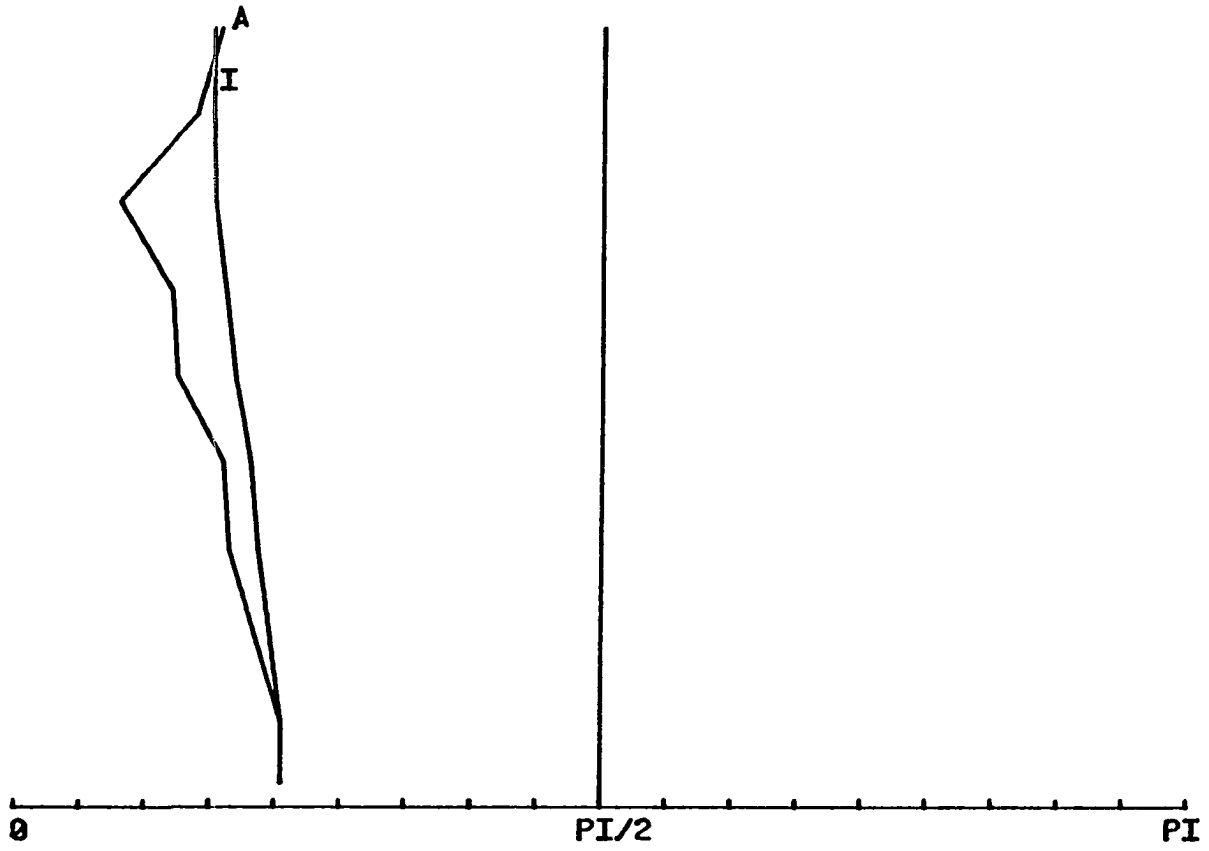


SAMPLE 848

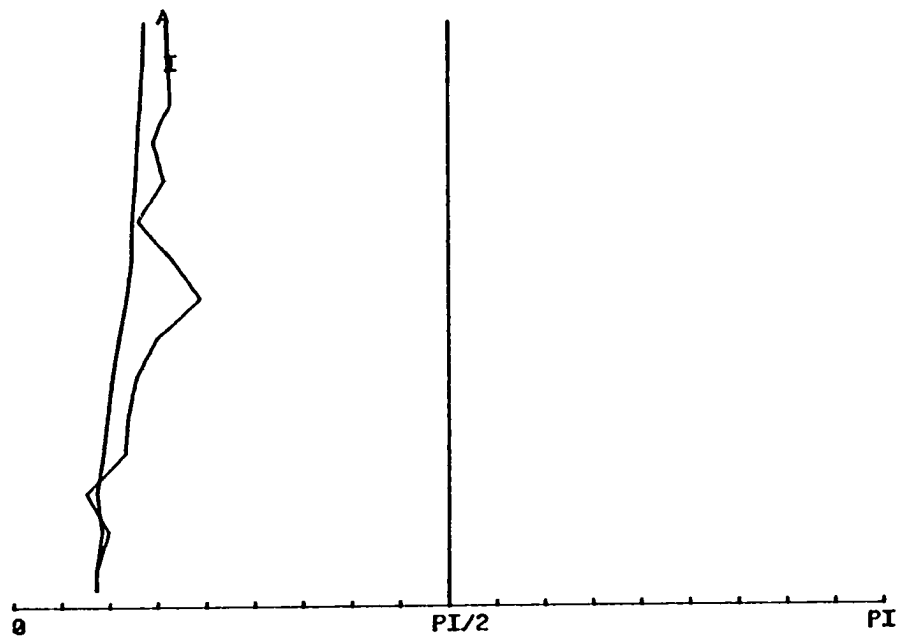
CRAIG1B



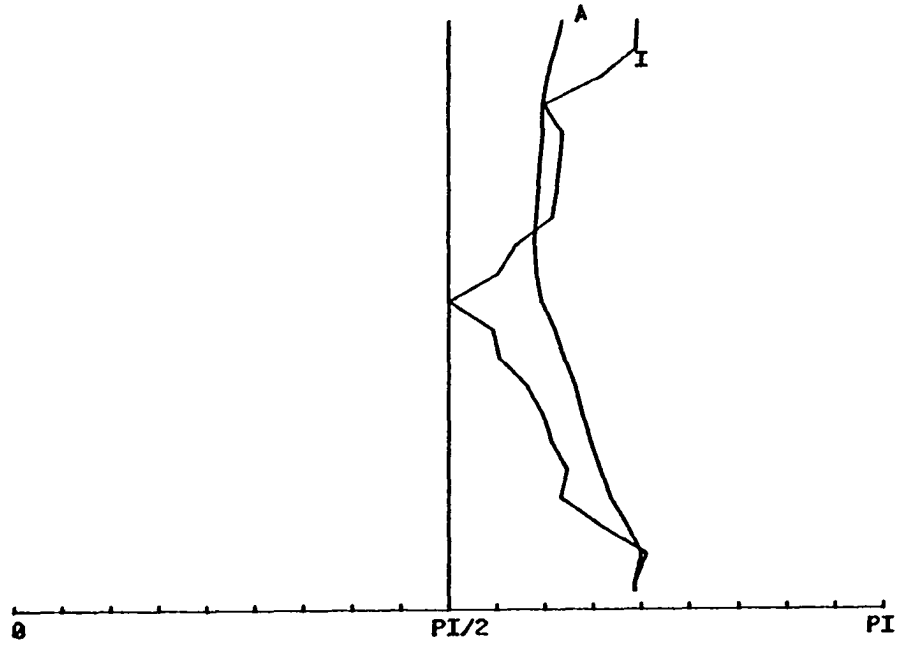
CRAIG2B



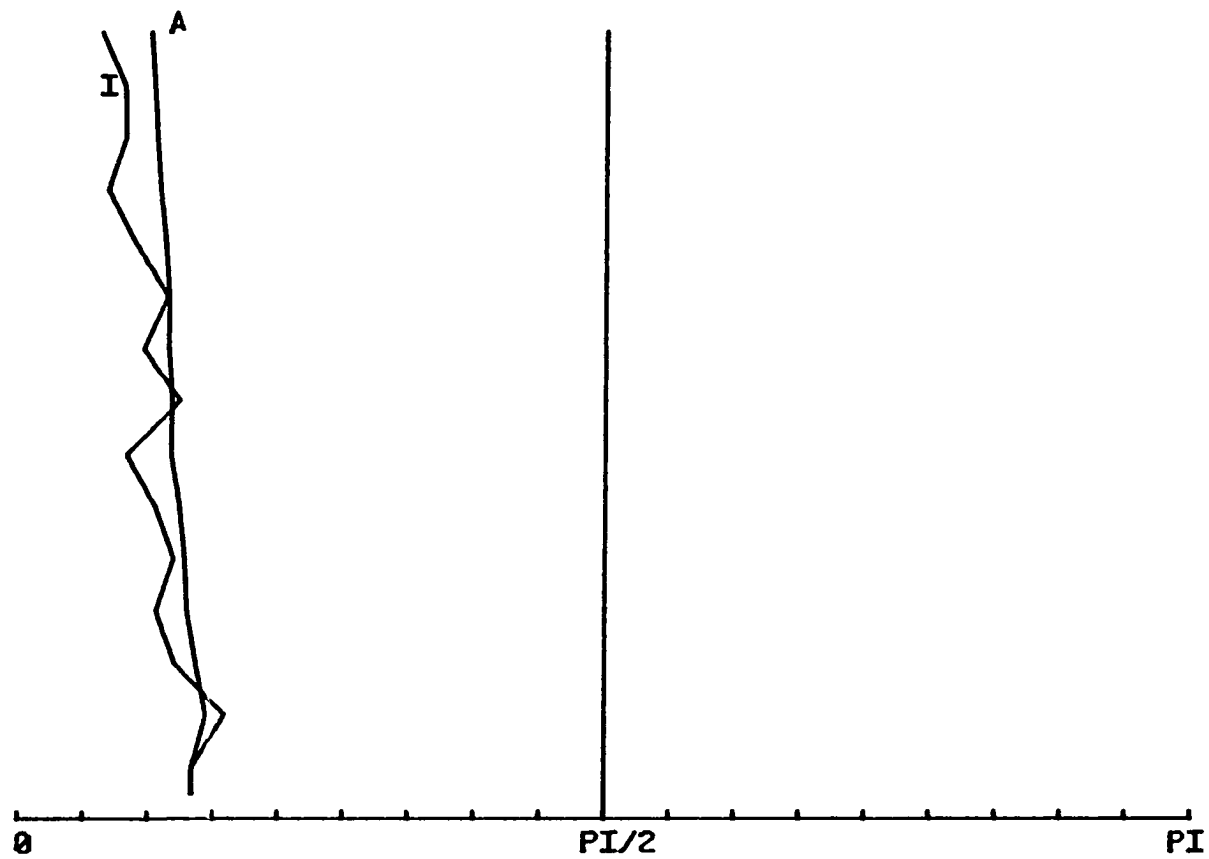
CRAIG3B



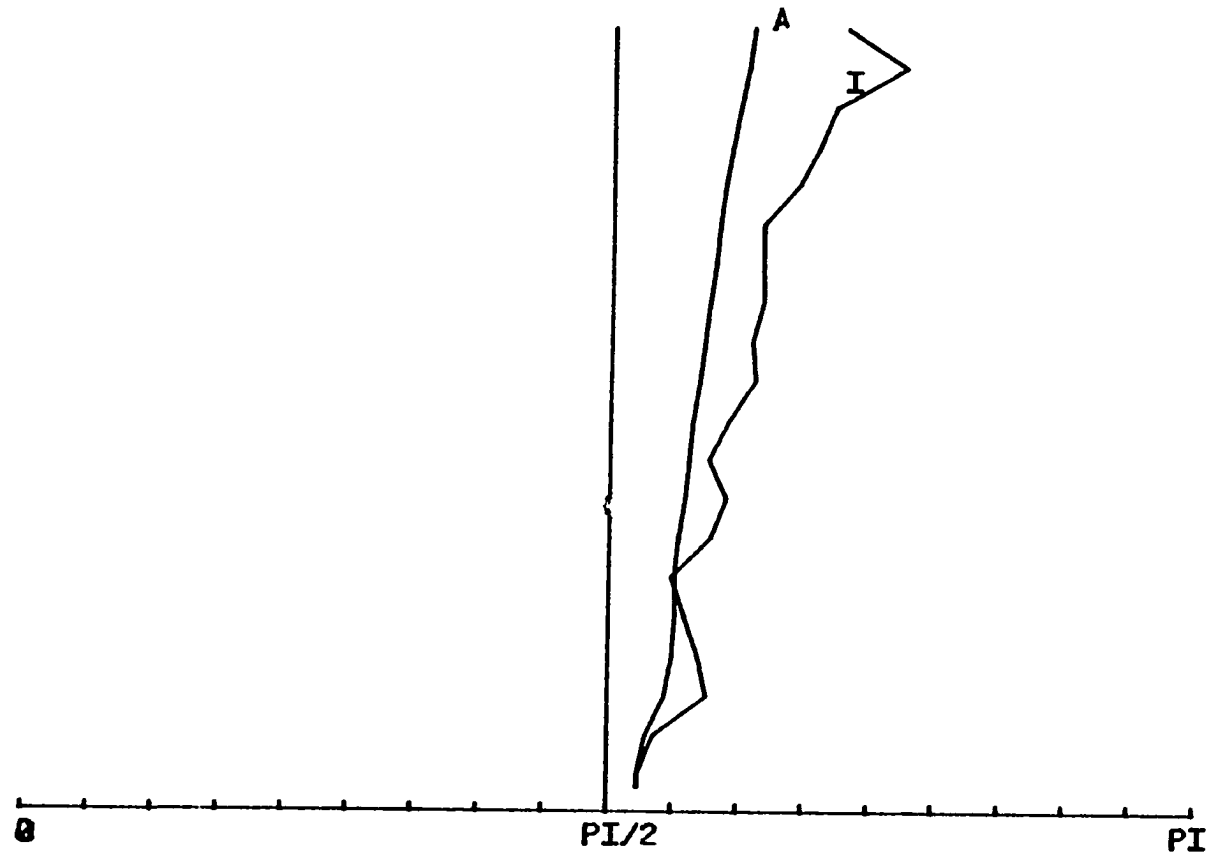
CRAIG4B



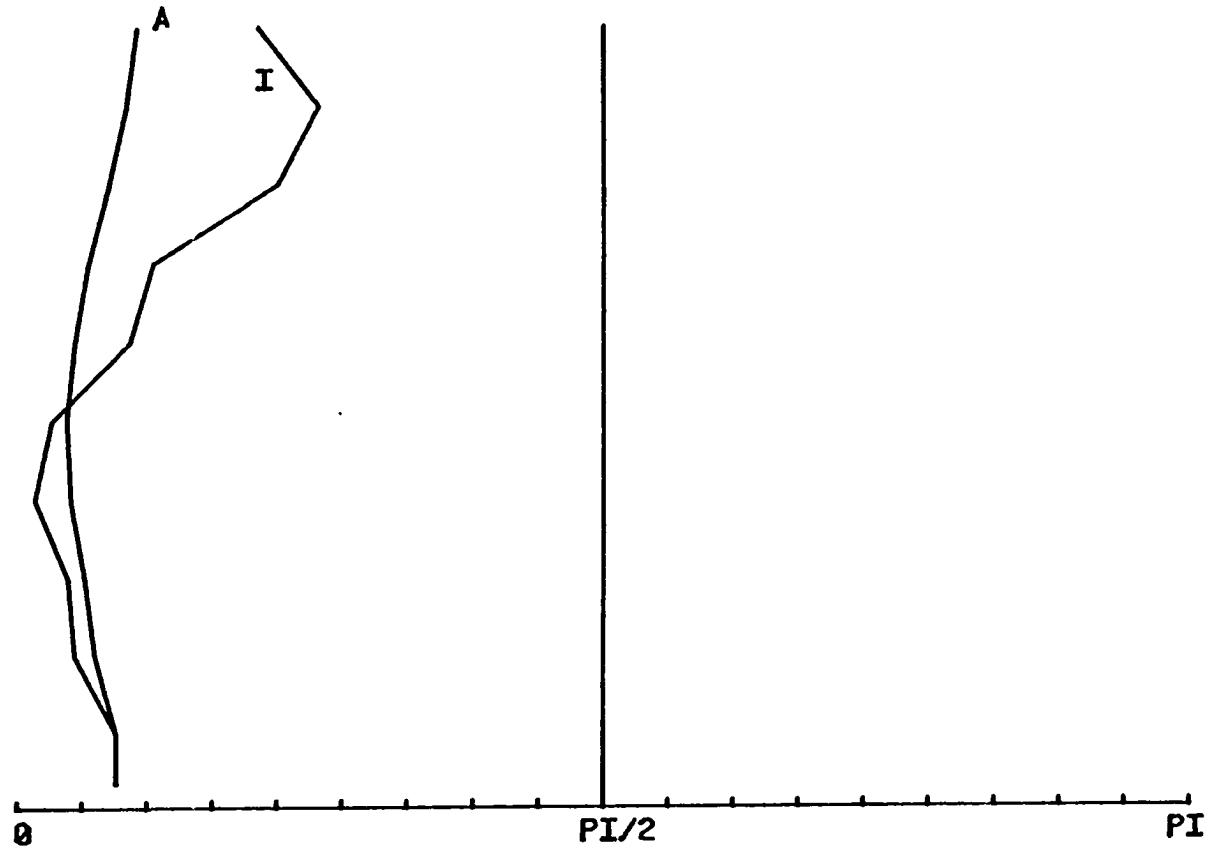
CRAIG5B



CRAIG6B



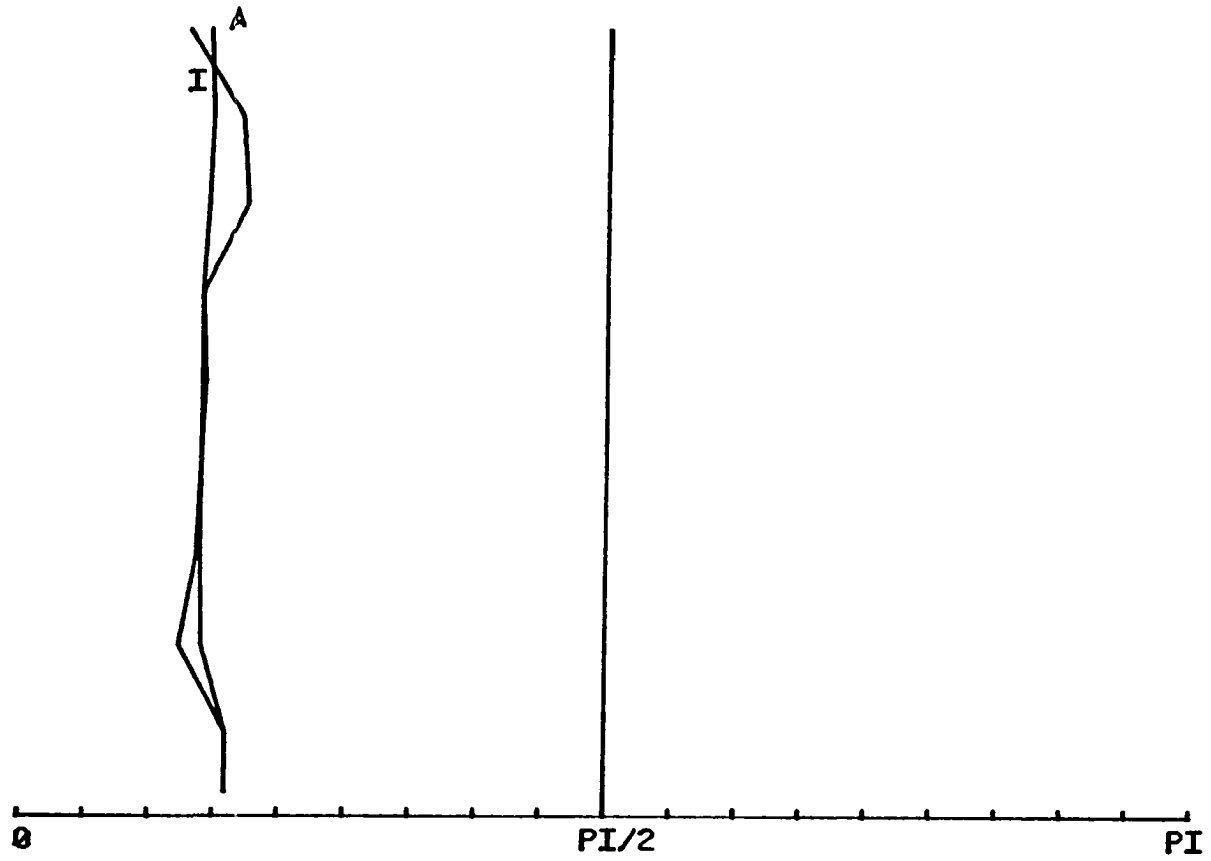
CRAIG8B



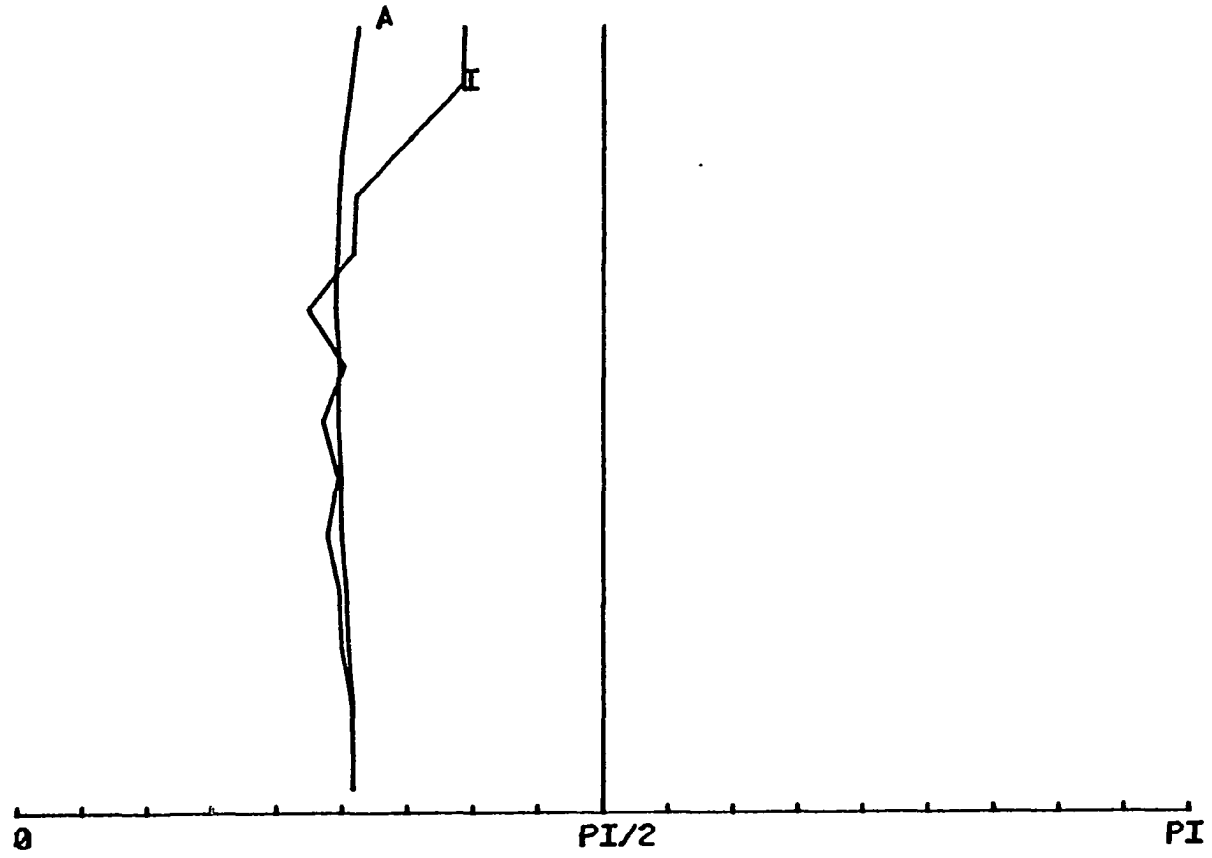
••

SAMPLE 850

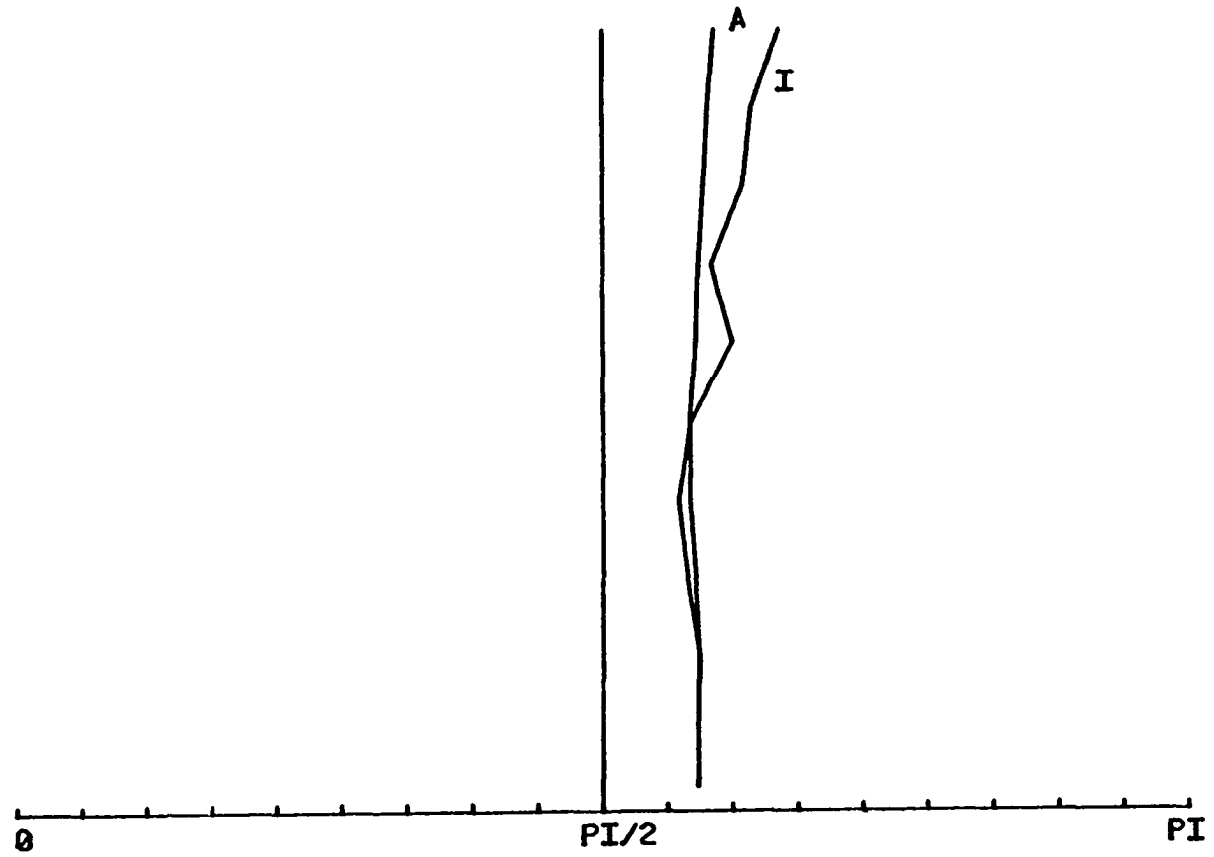
CRAIG9B



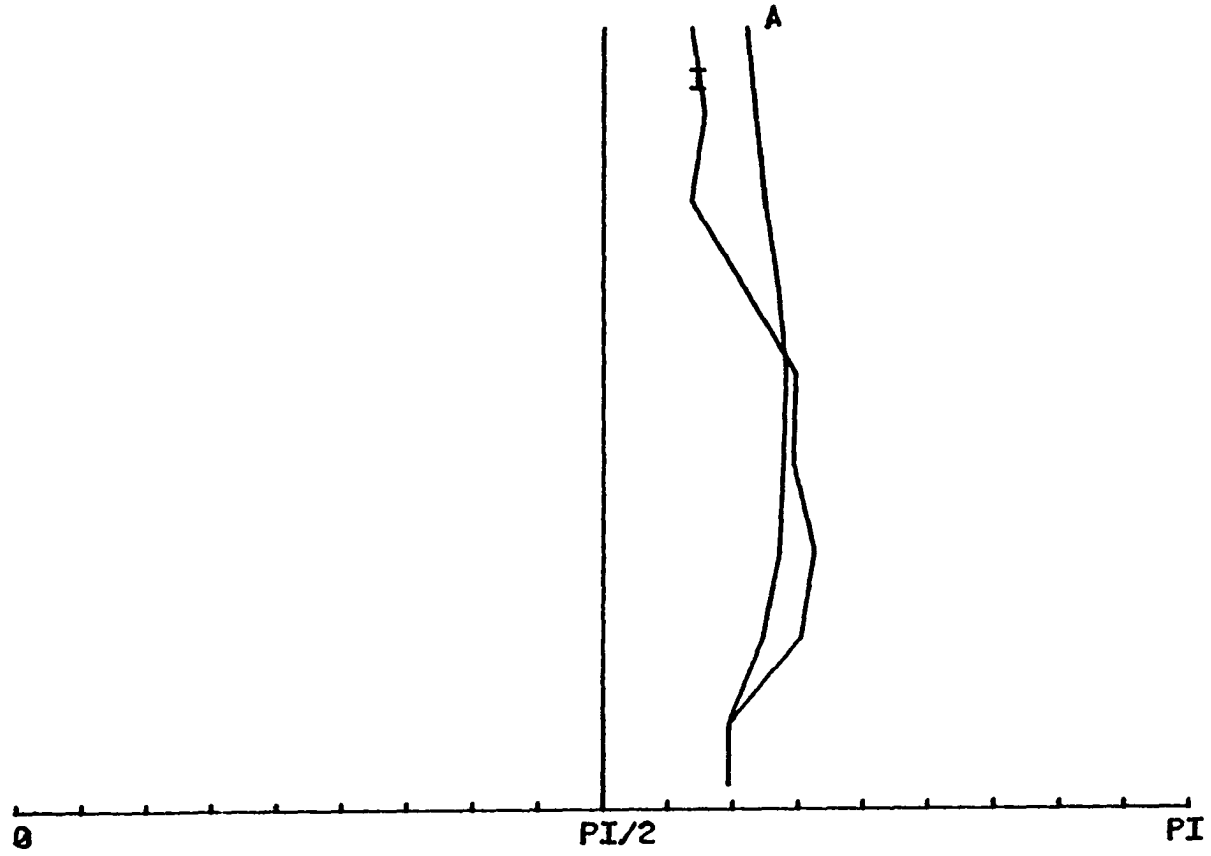
CRAIG12B



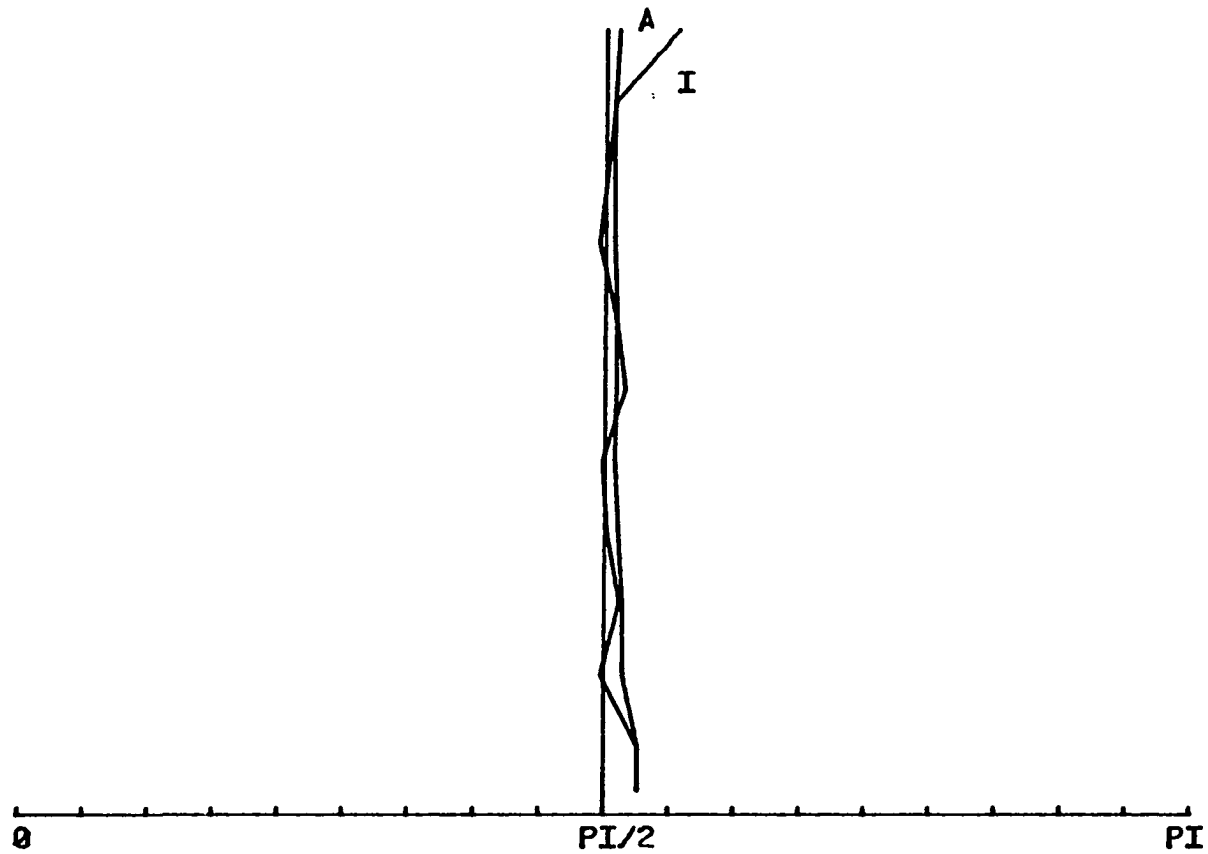
CRAIG15B



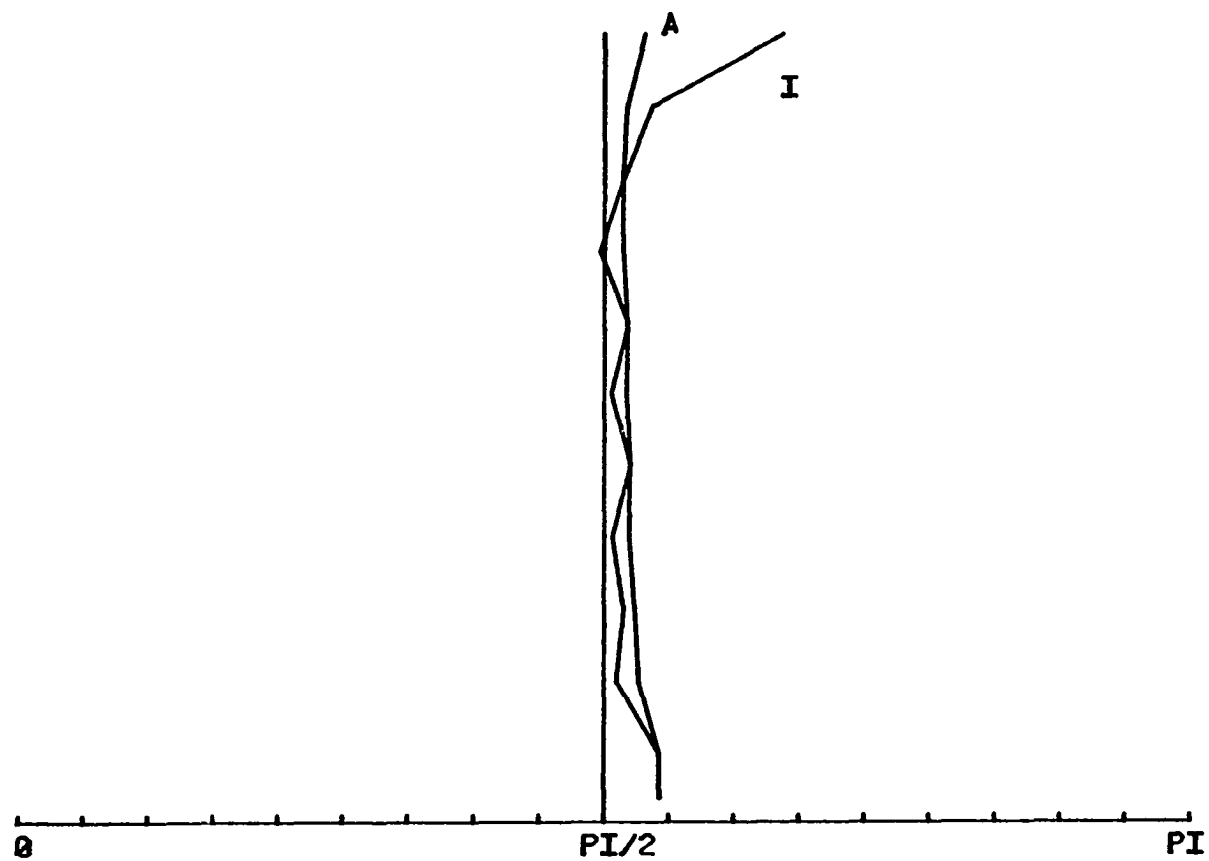
CRAIG16B



CRAIG 18B

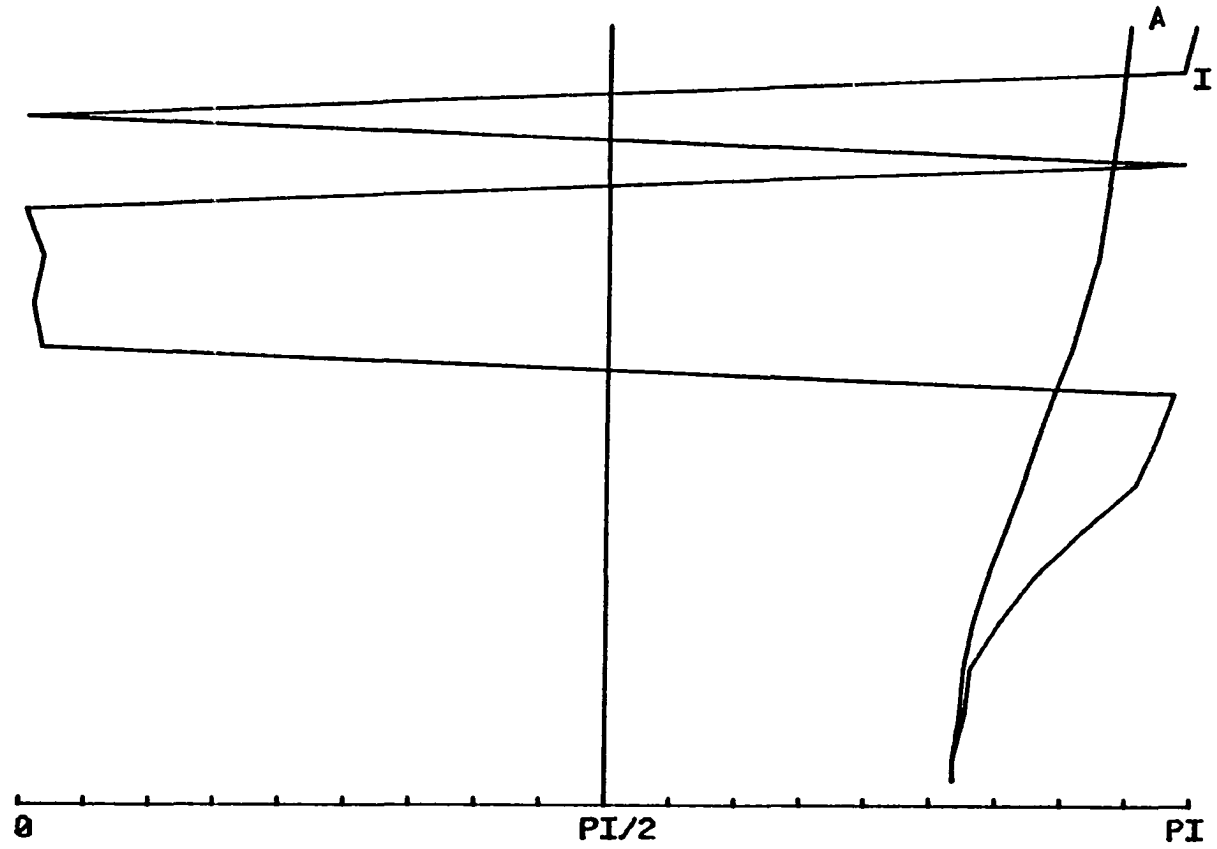


CRAIG19B



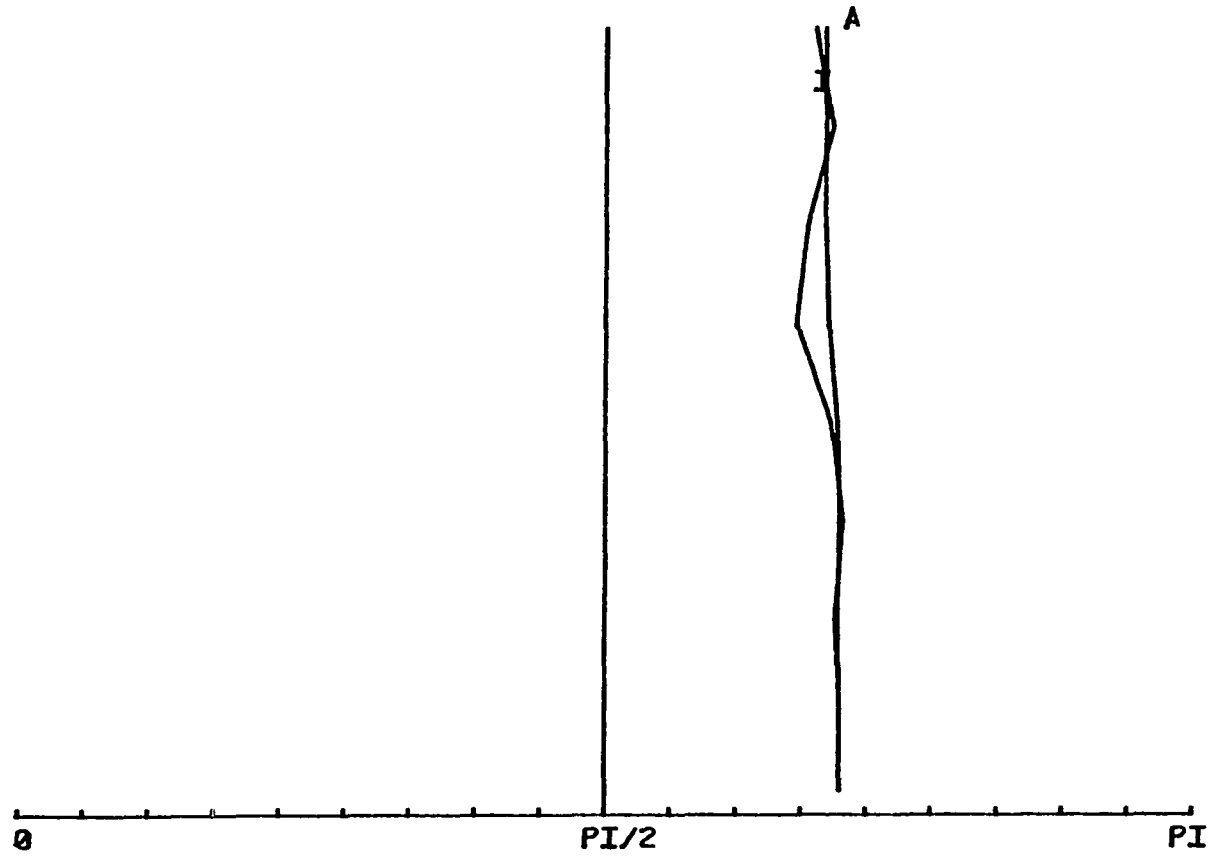
SAMPLE 902

STONE11B

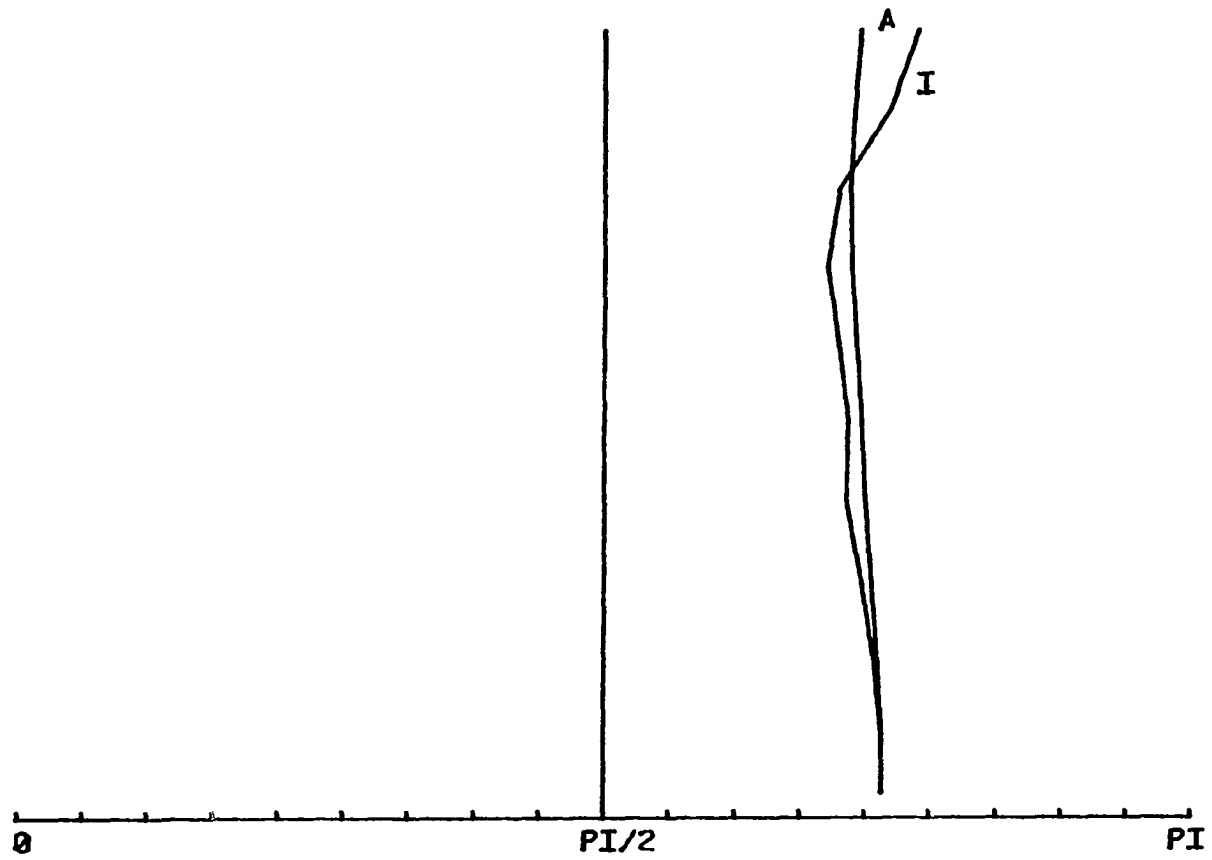


SAMPLE 920

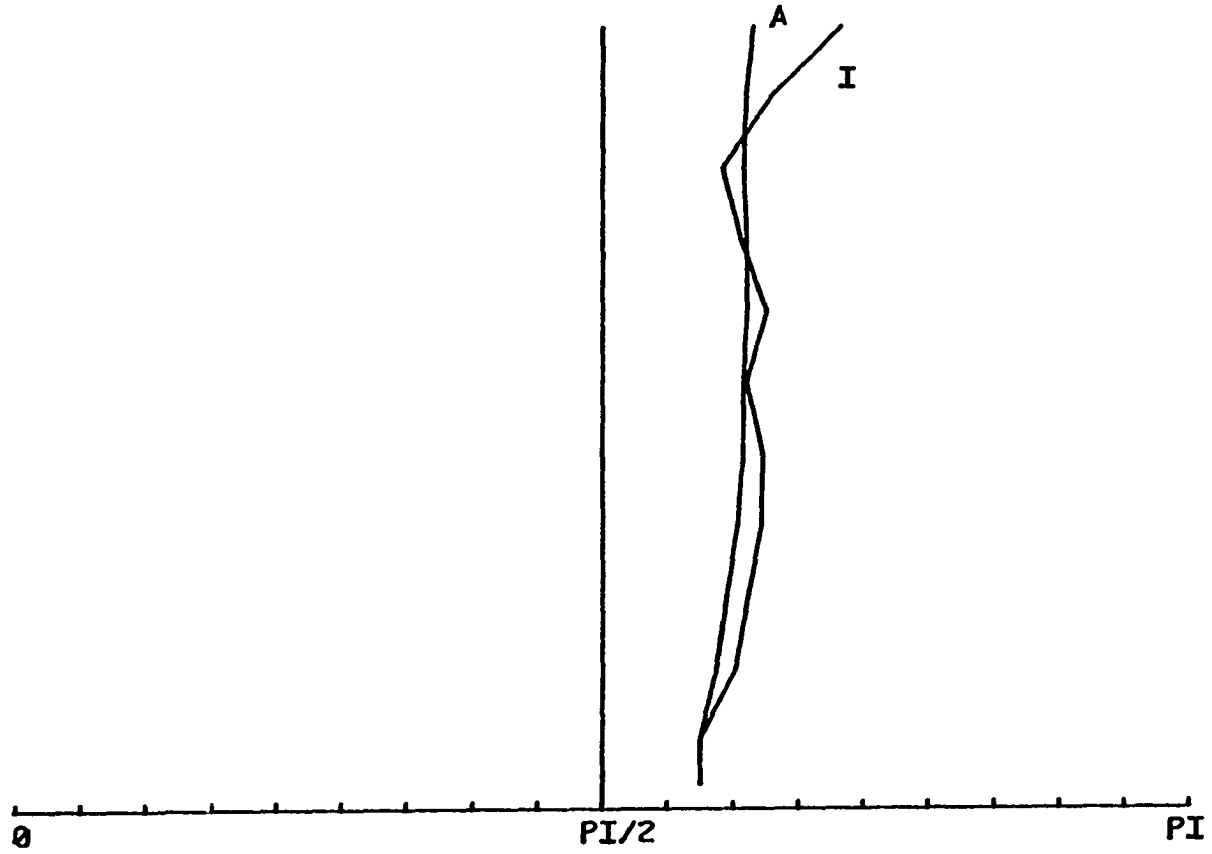
MILLIB



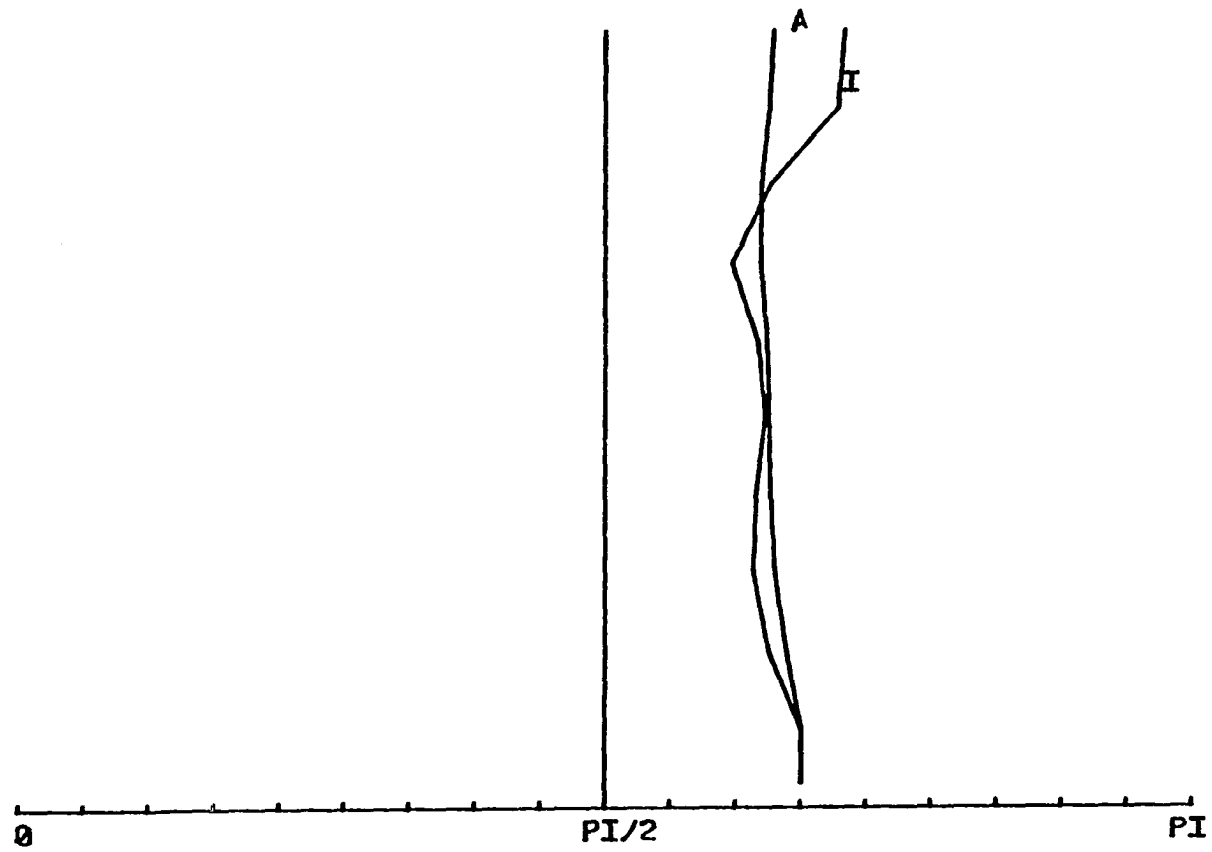
MILL2B



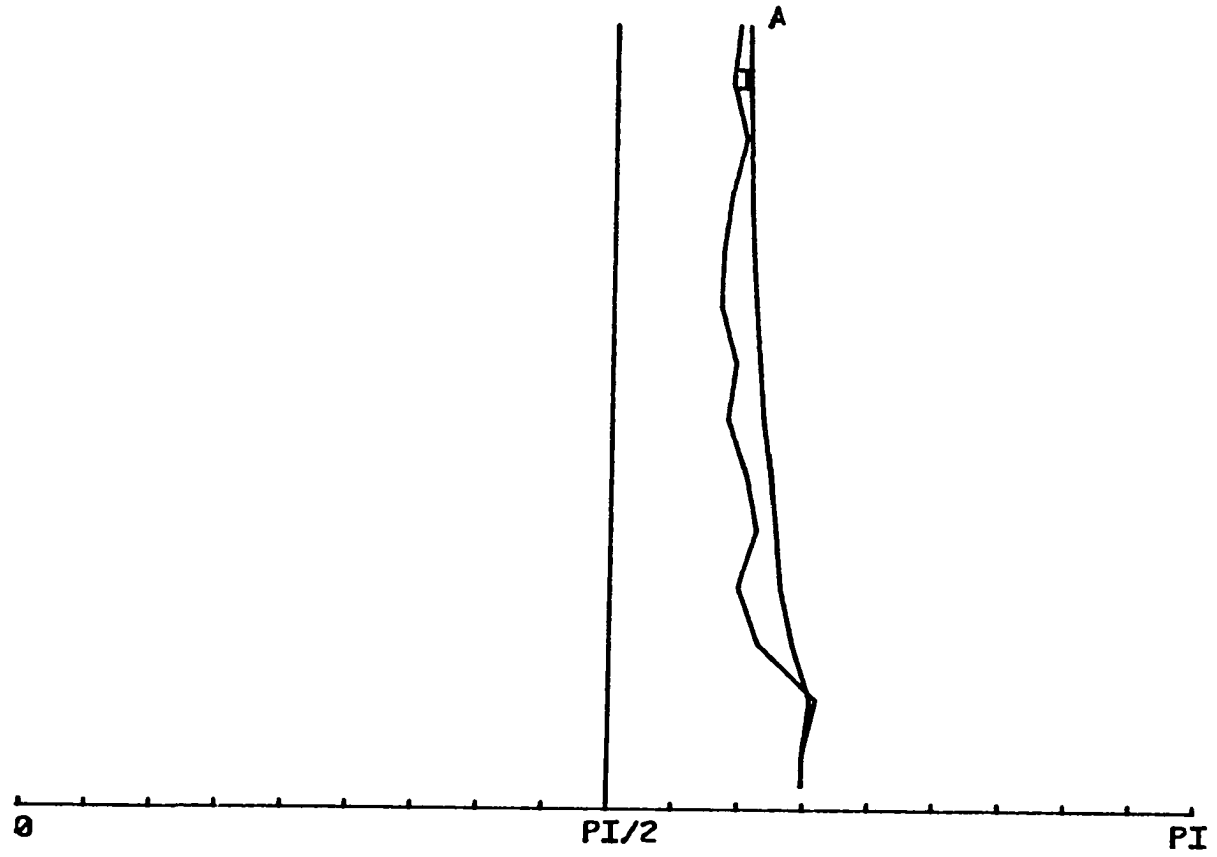
MILL3B



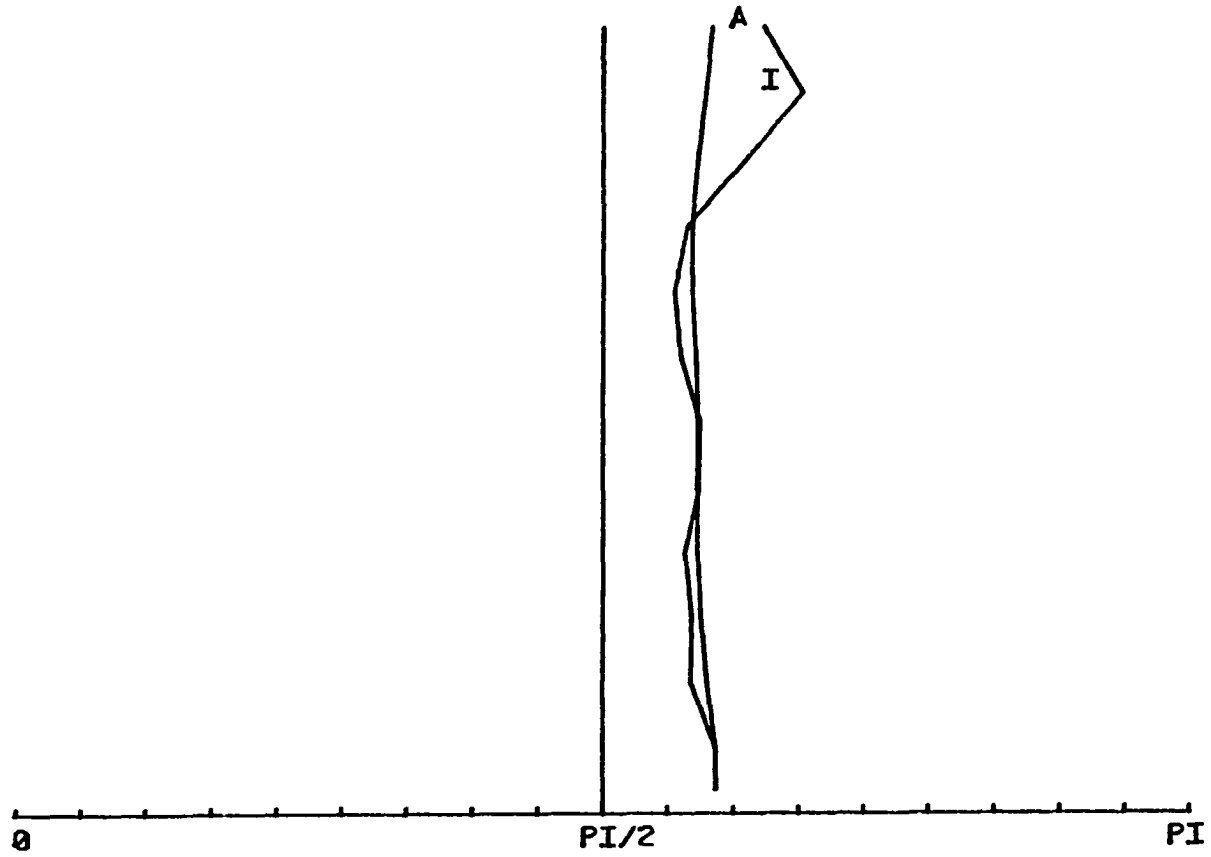
MILL 4B



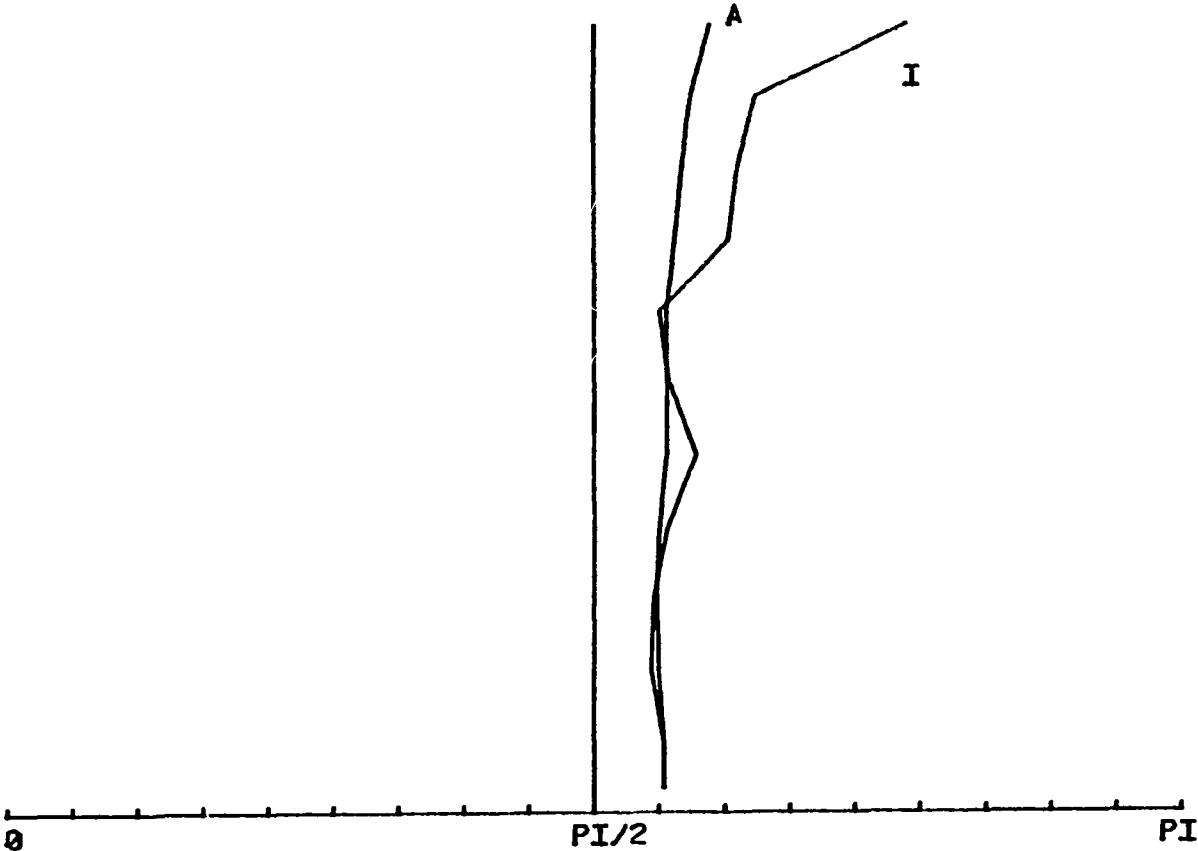
MILLSB



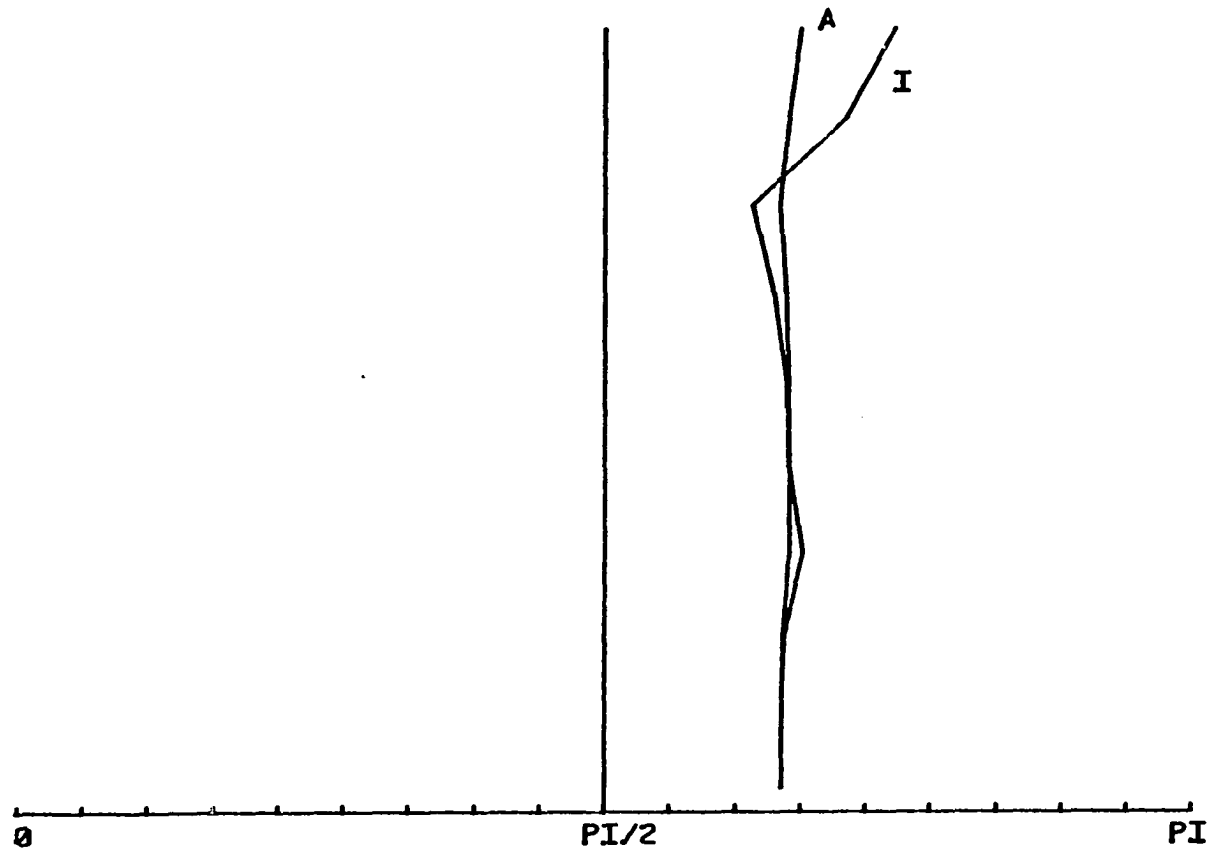
MILL6B



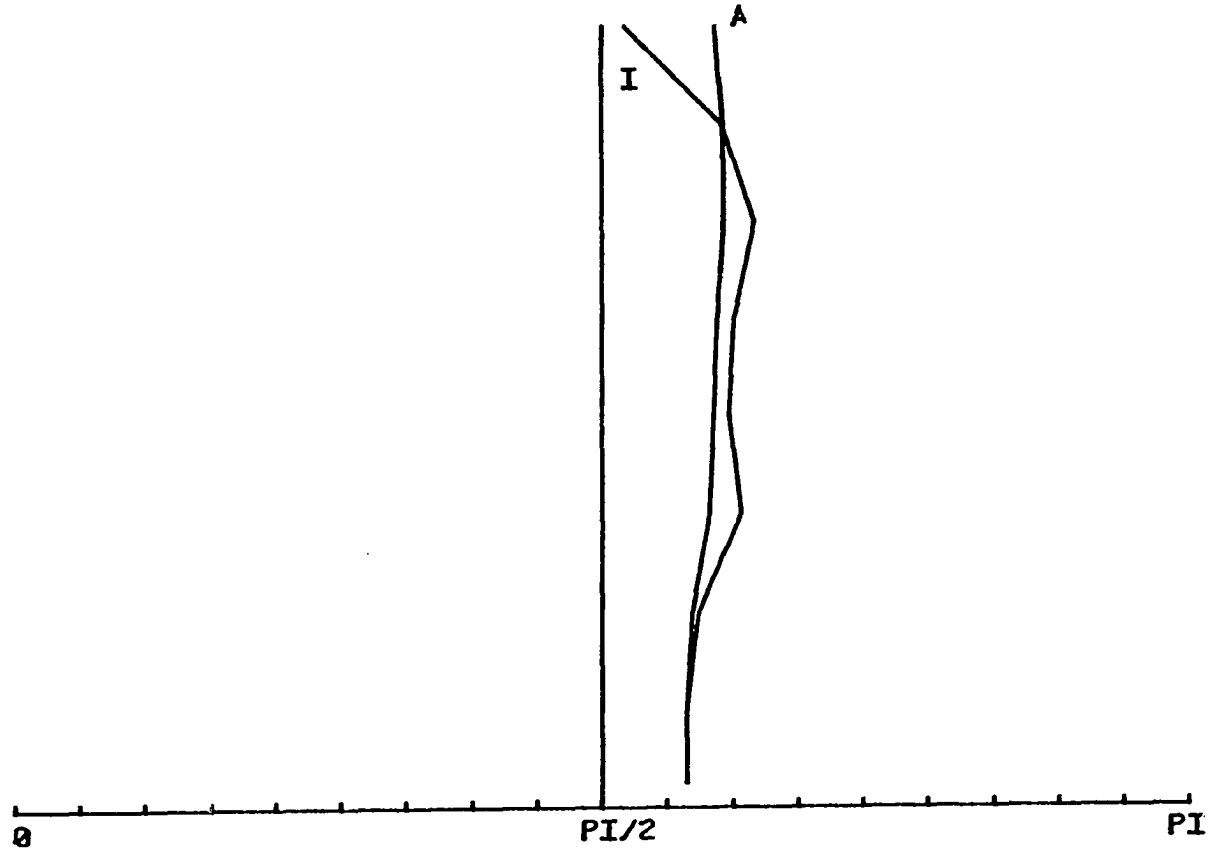
MILL7B



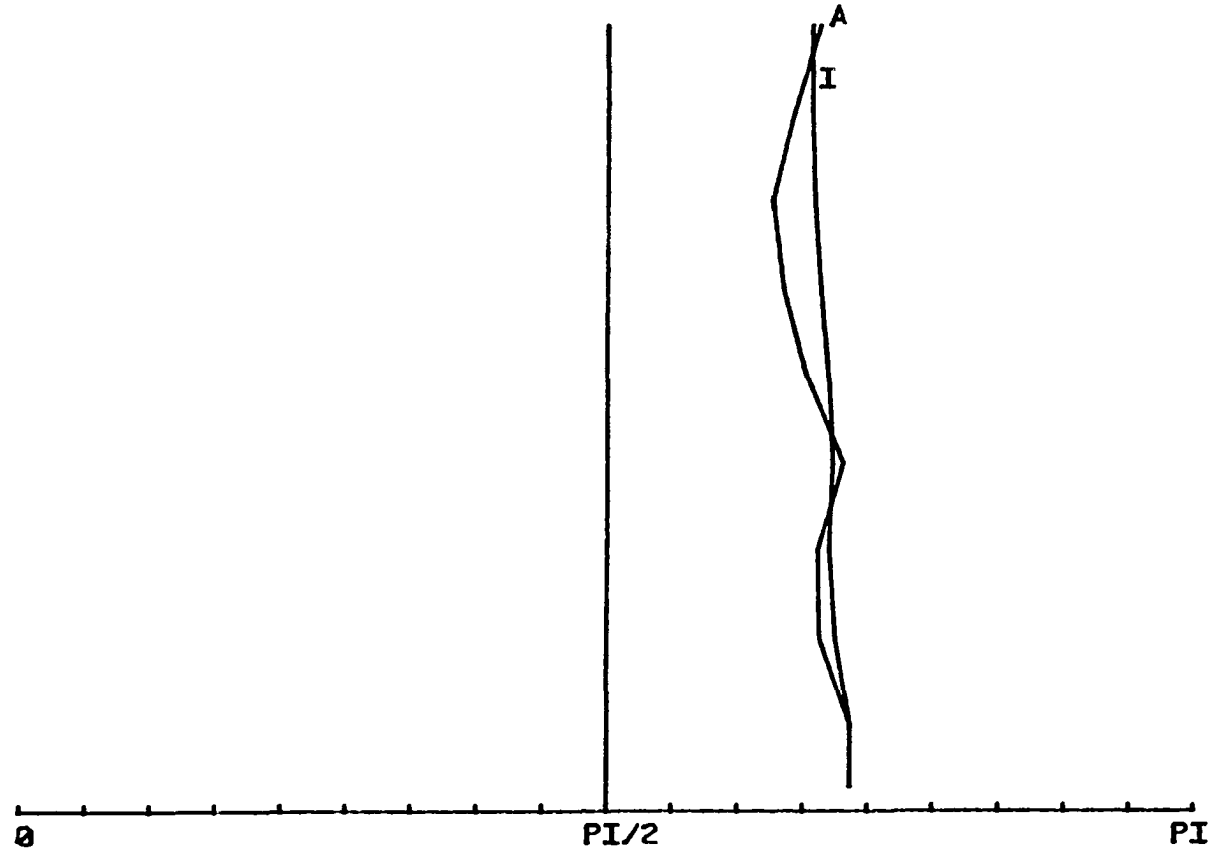
MILL8B



MILL9B

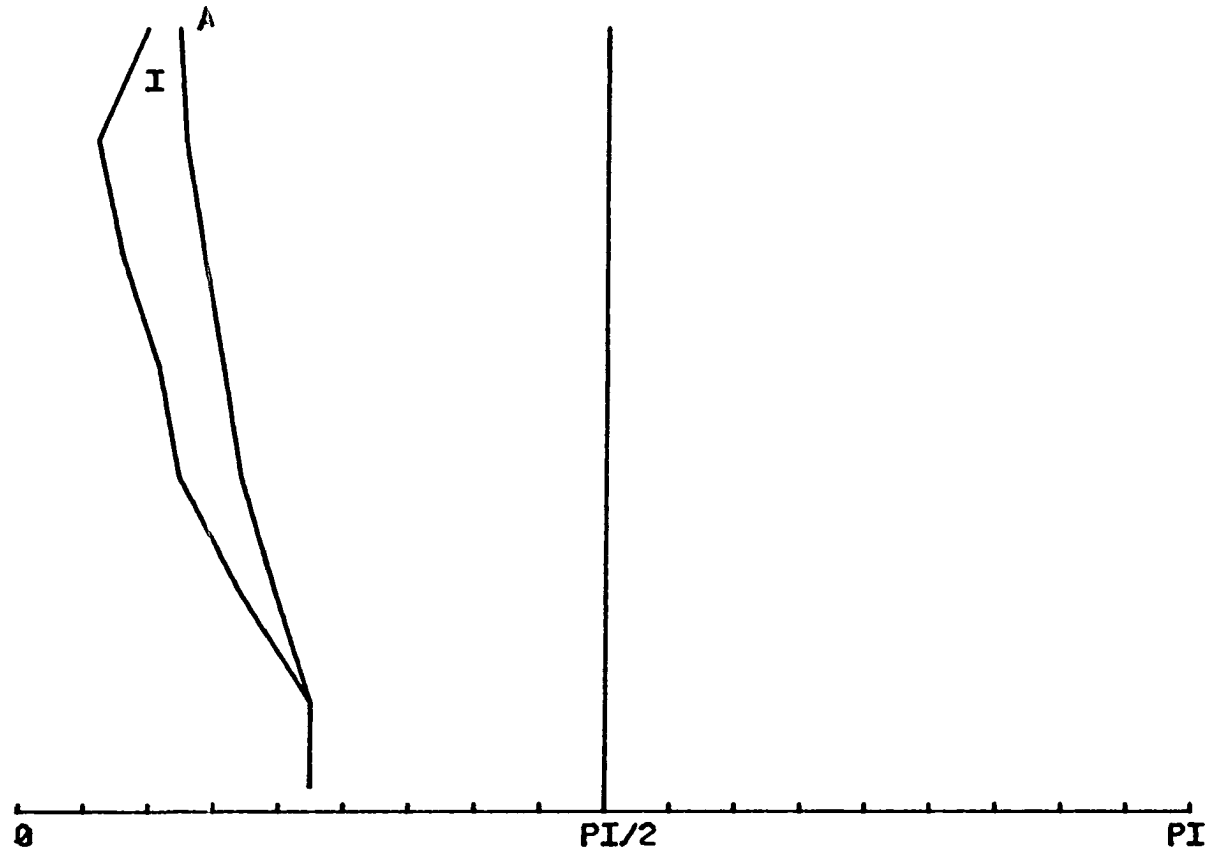


MILL 10B

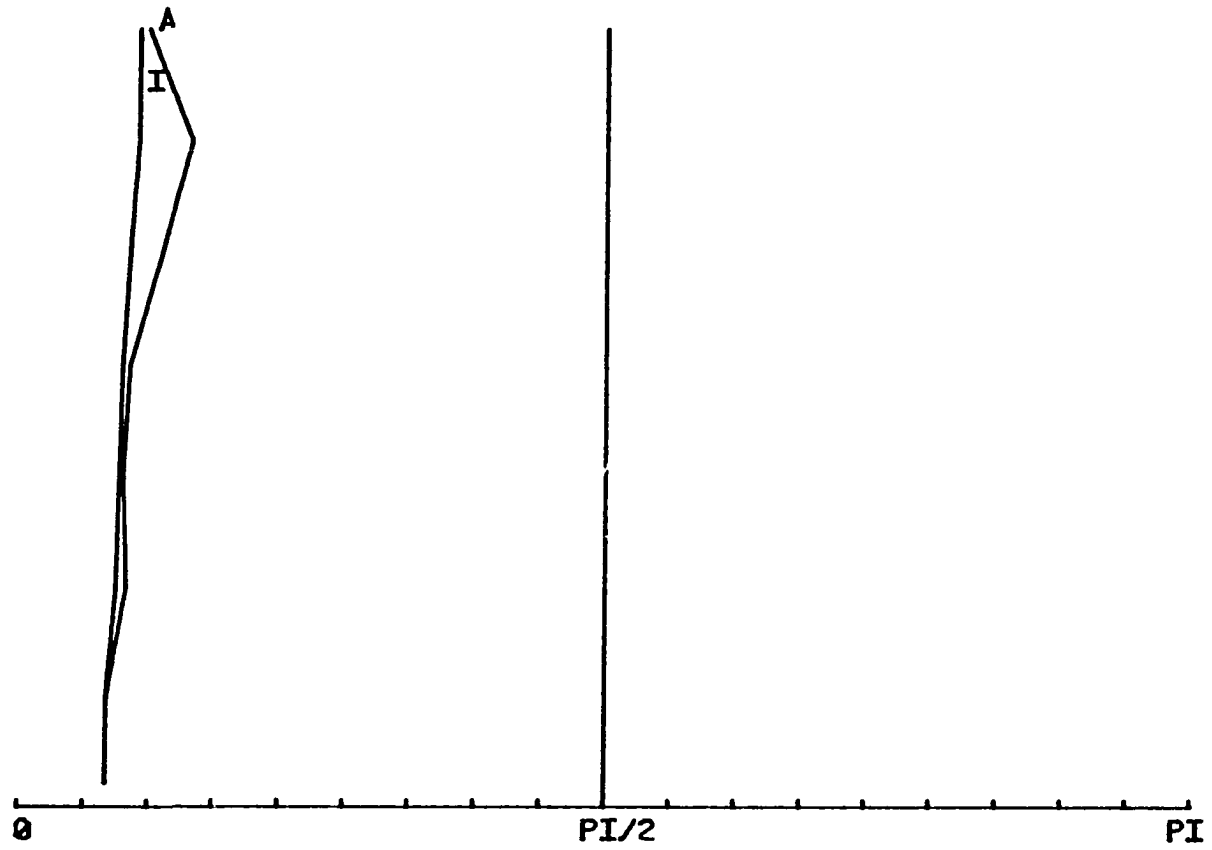


SAMPLE 939

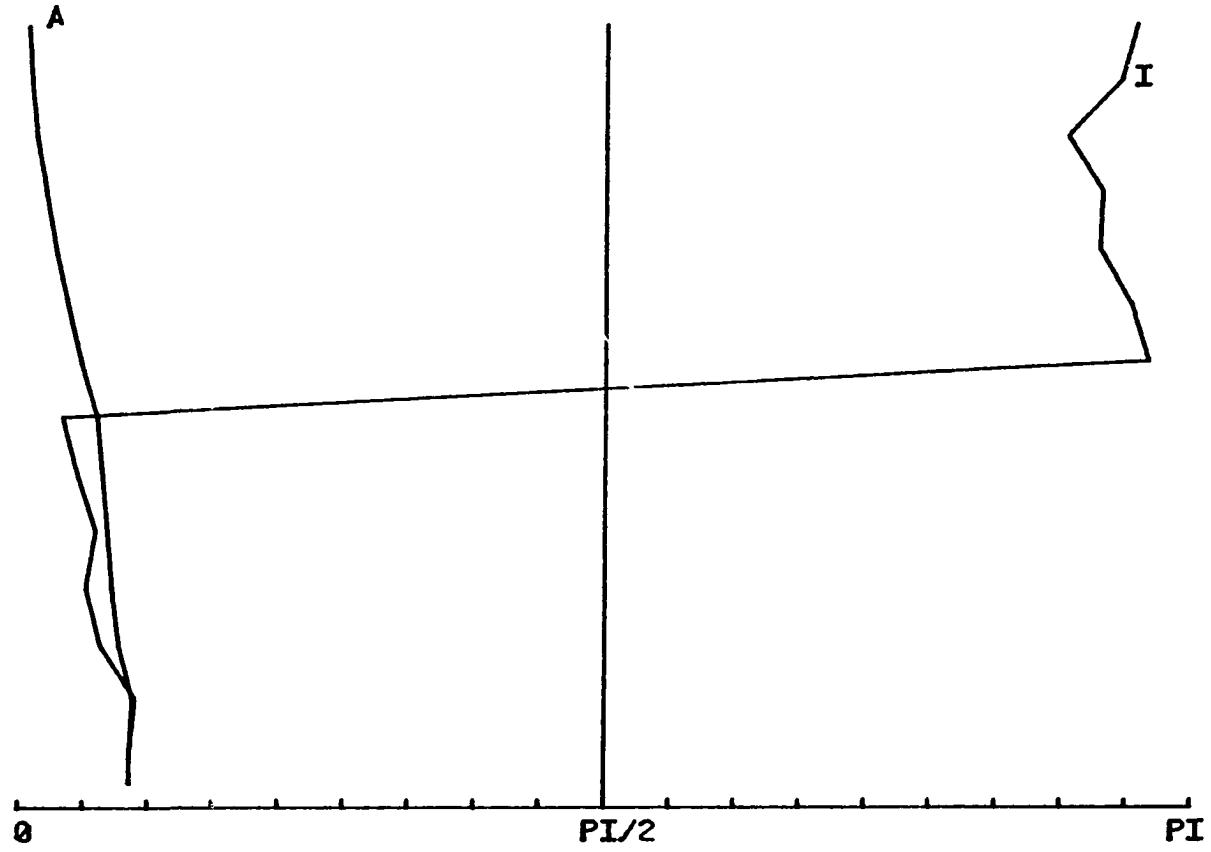
CRAIG24B



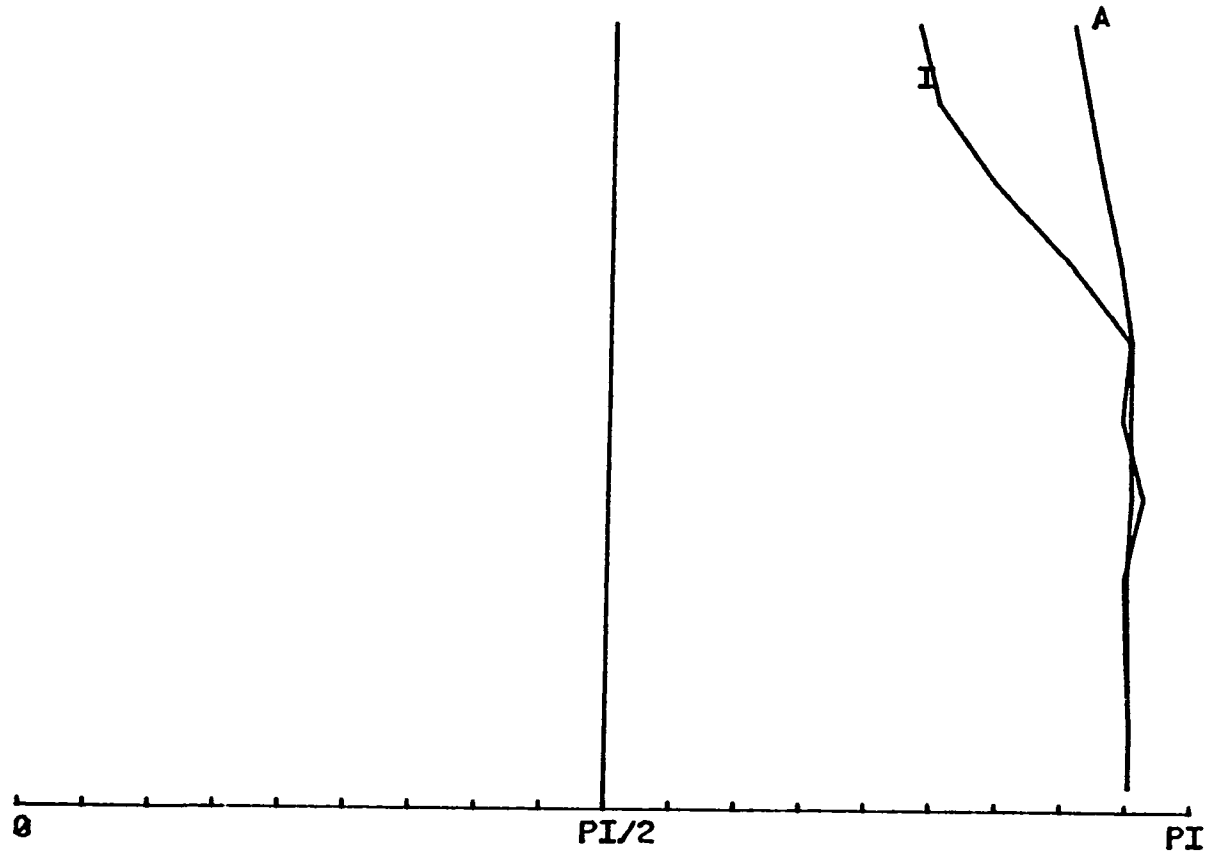
CRAIG25B



CRAIG29B

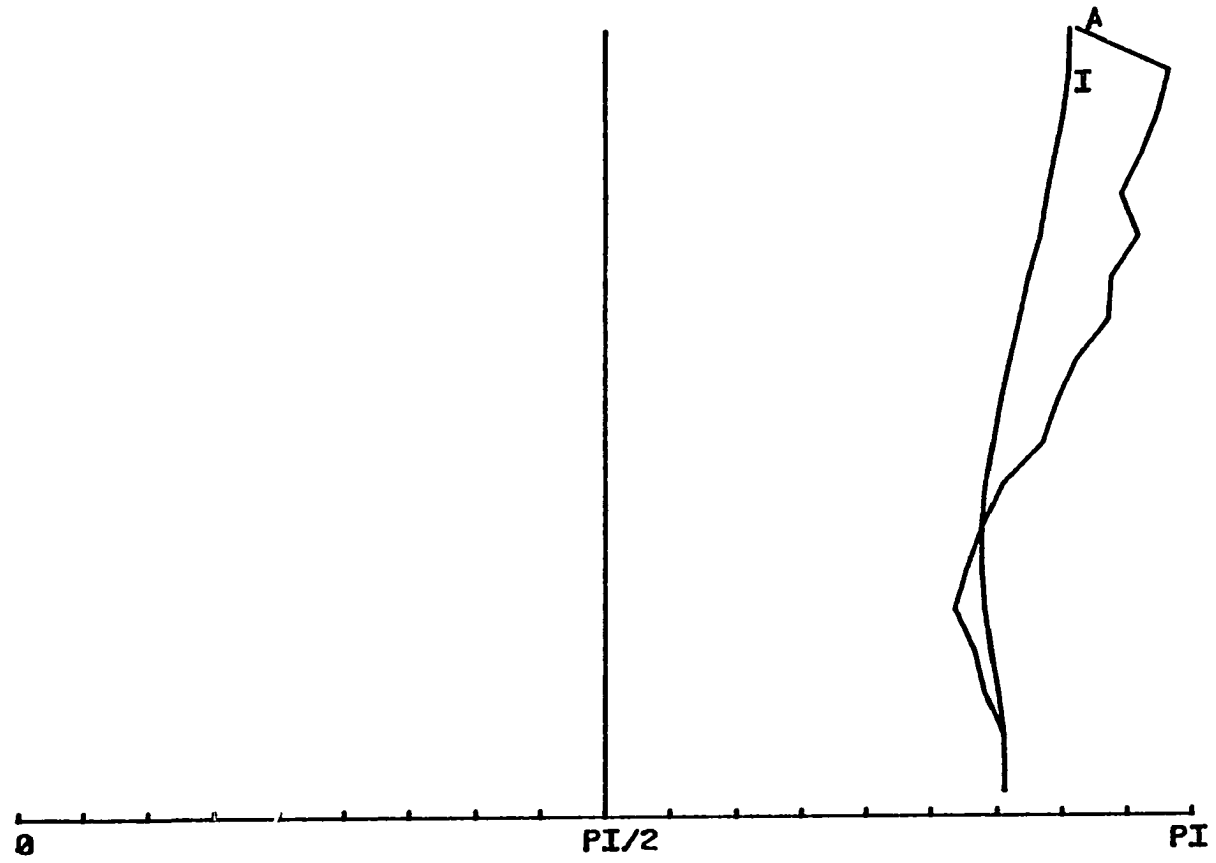


CRAIG33B

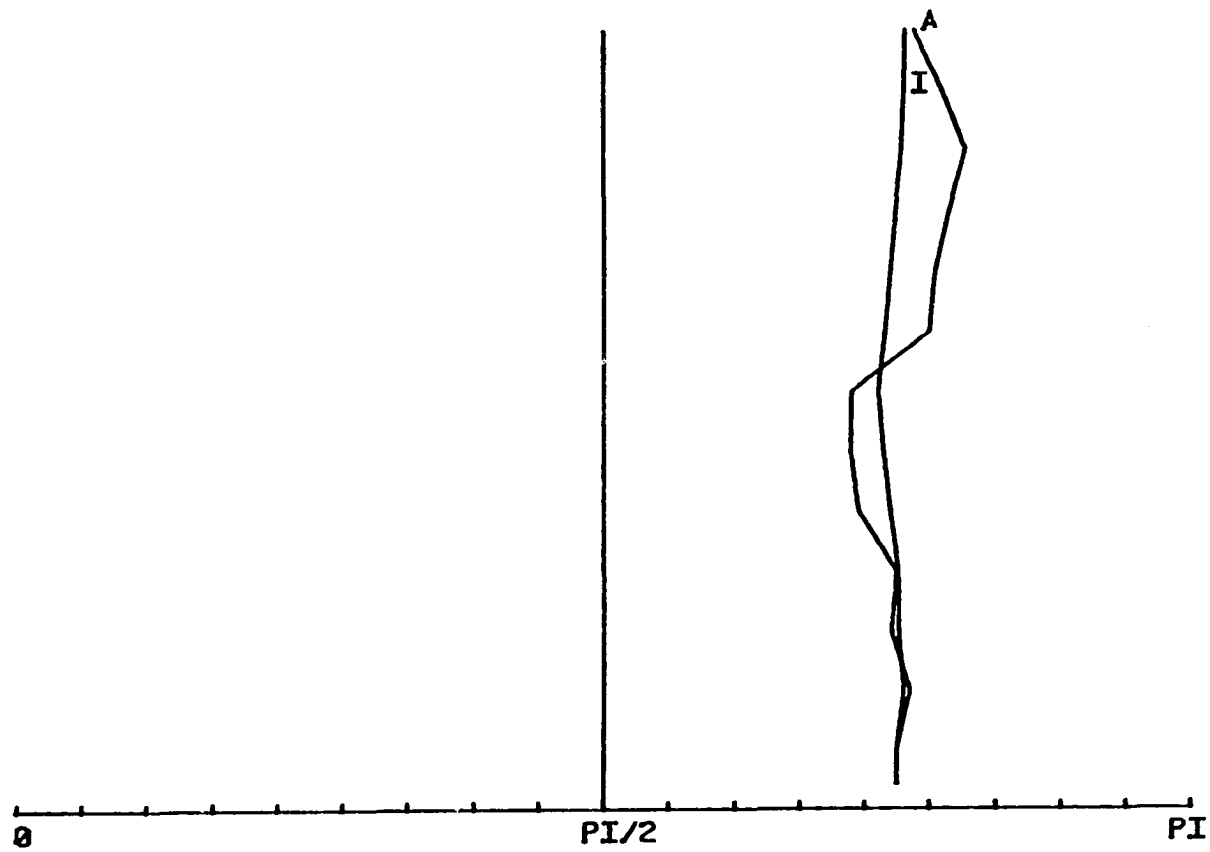


SAMPLE 942

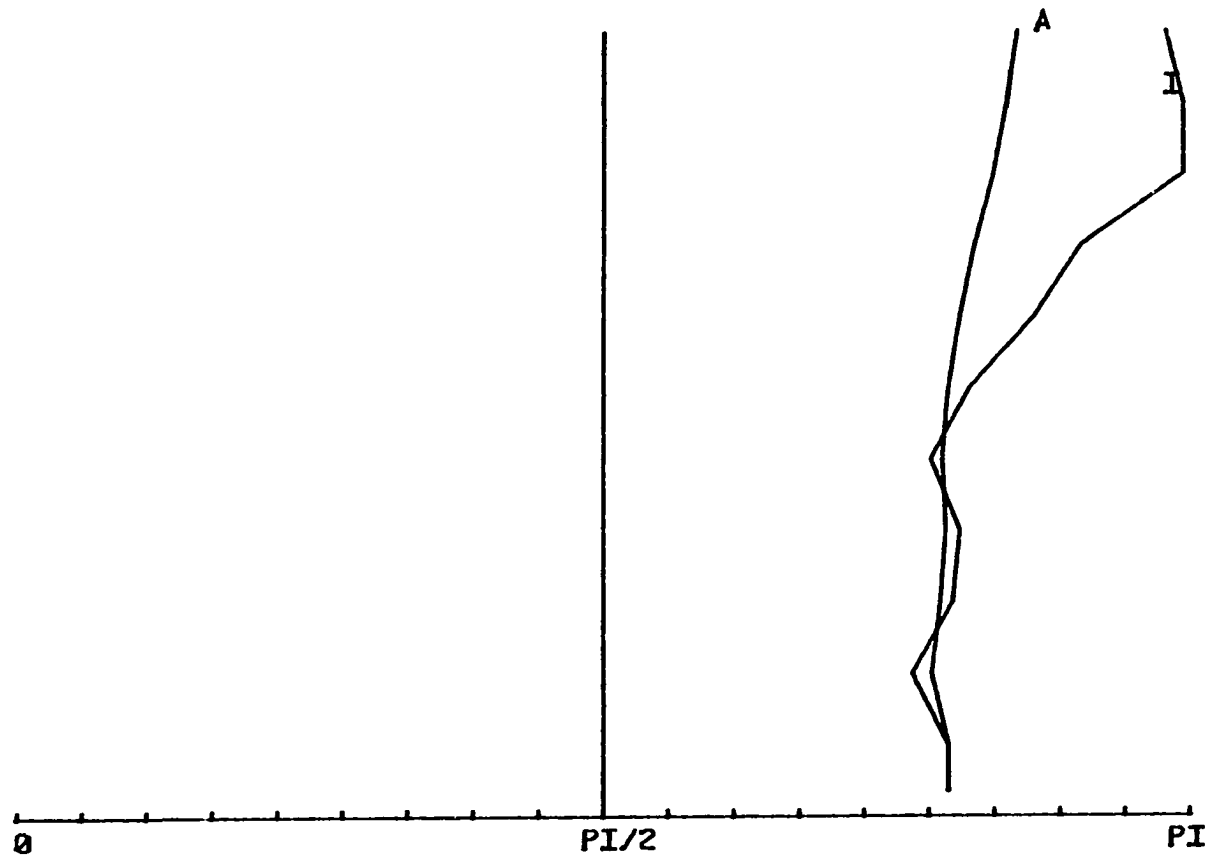
BULL 1B



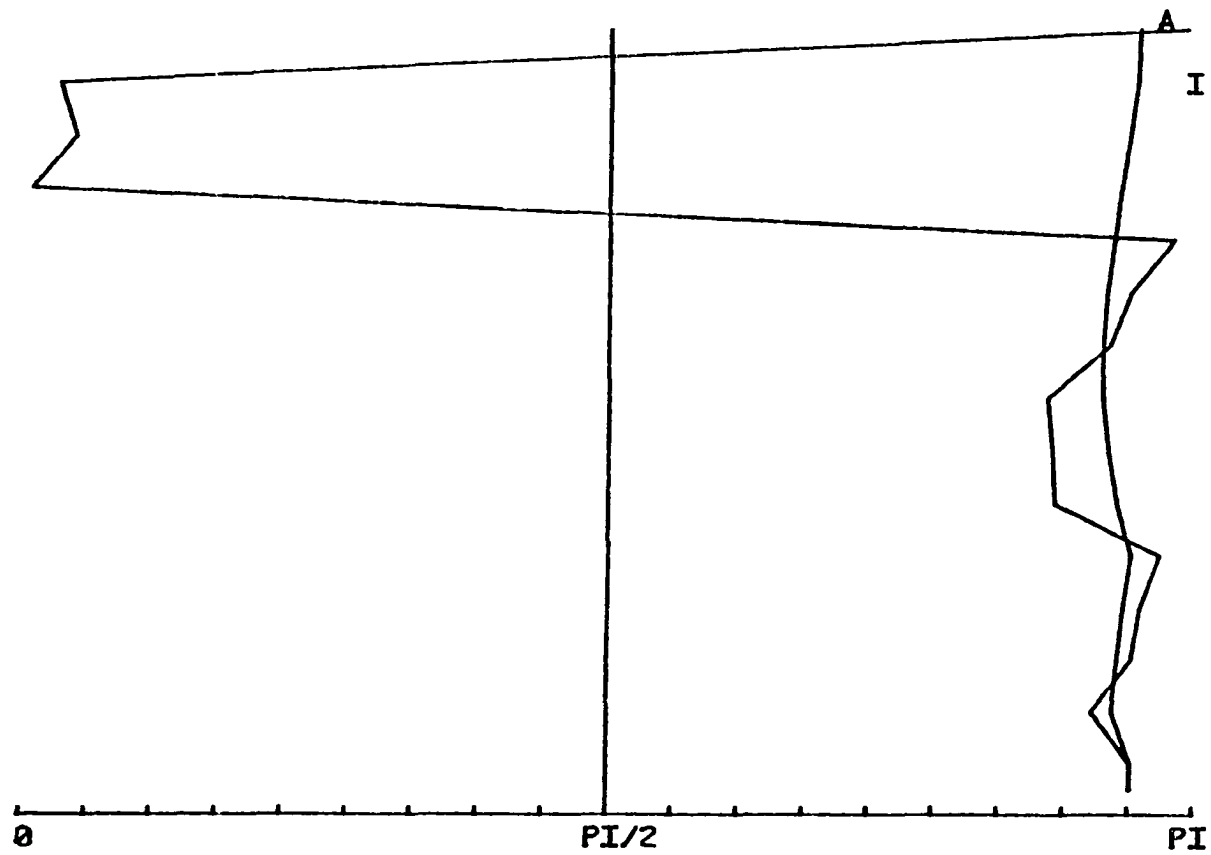
BULL2B



BULL3B

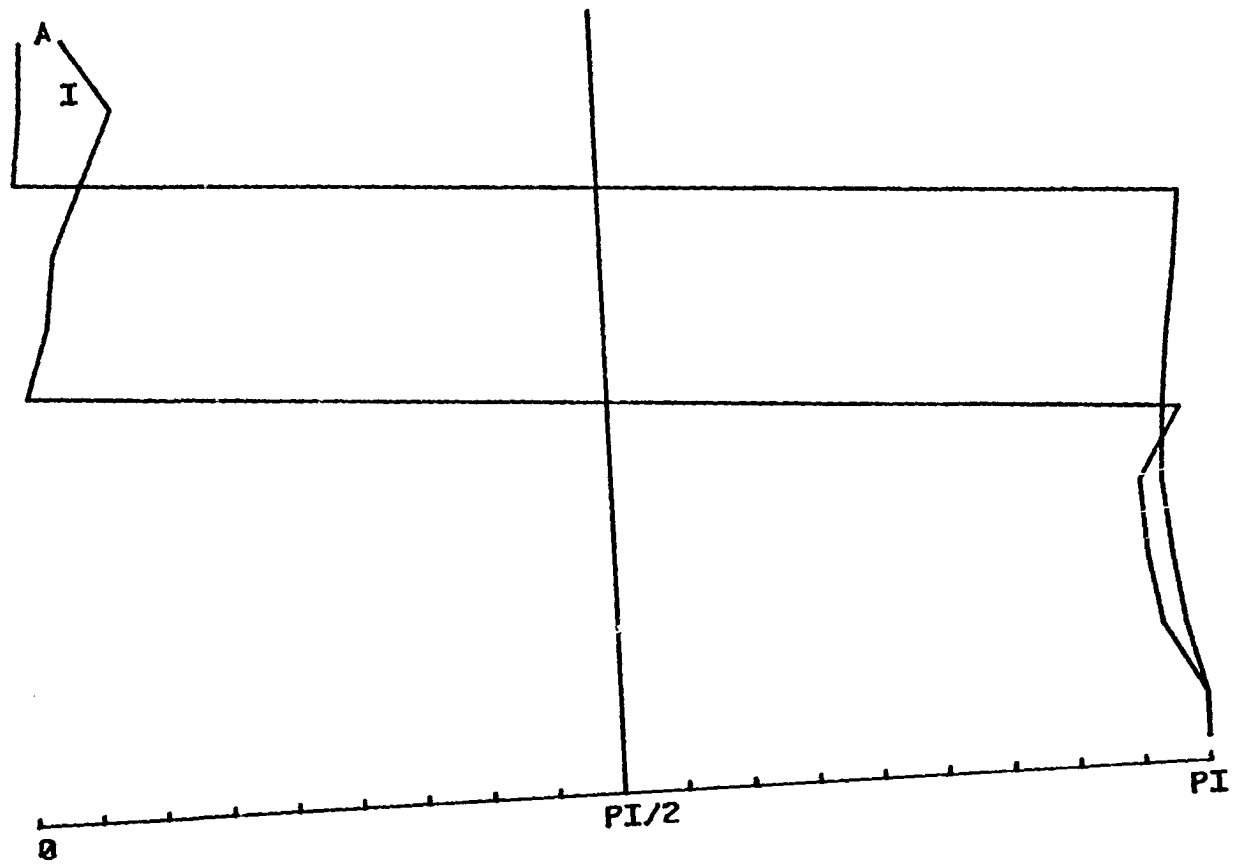


BULL4B

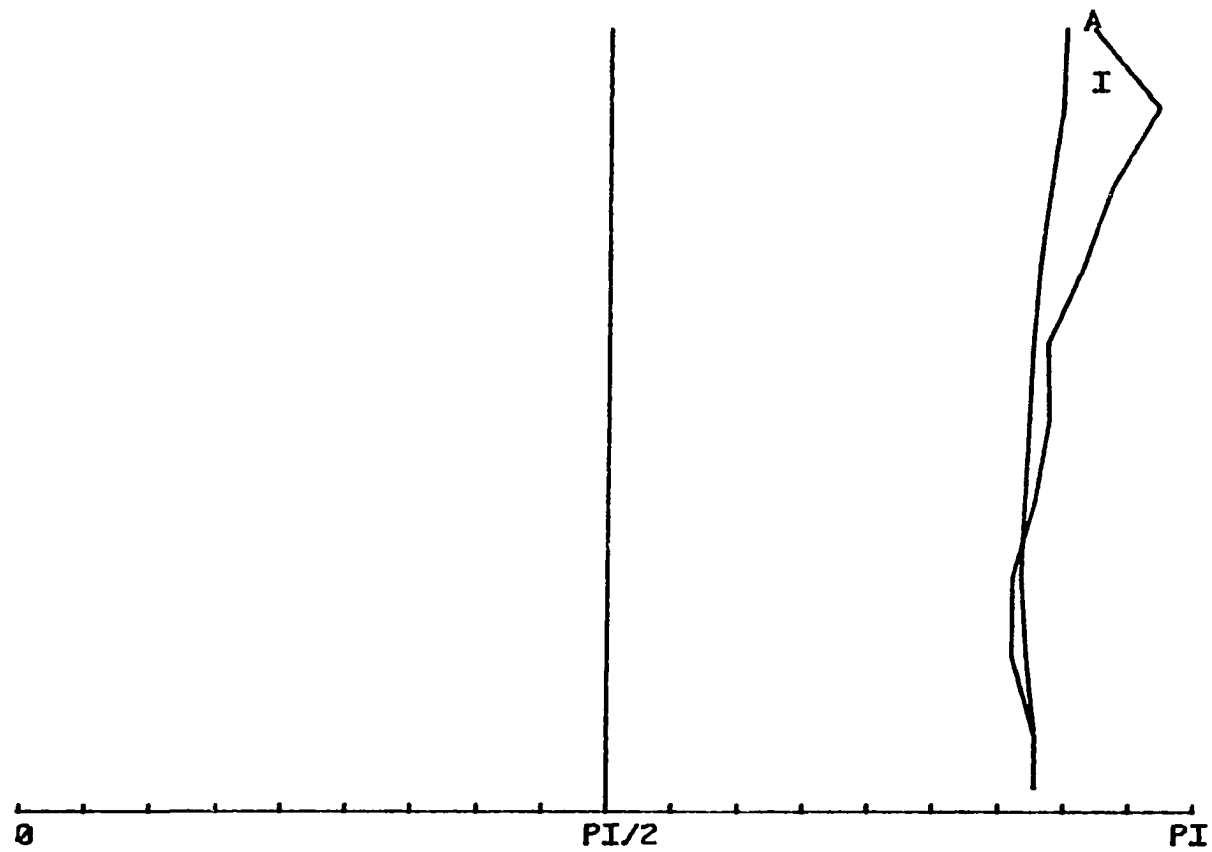


SAMPLE 943

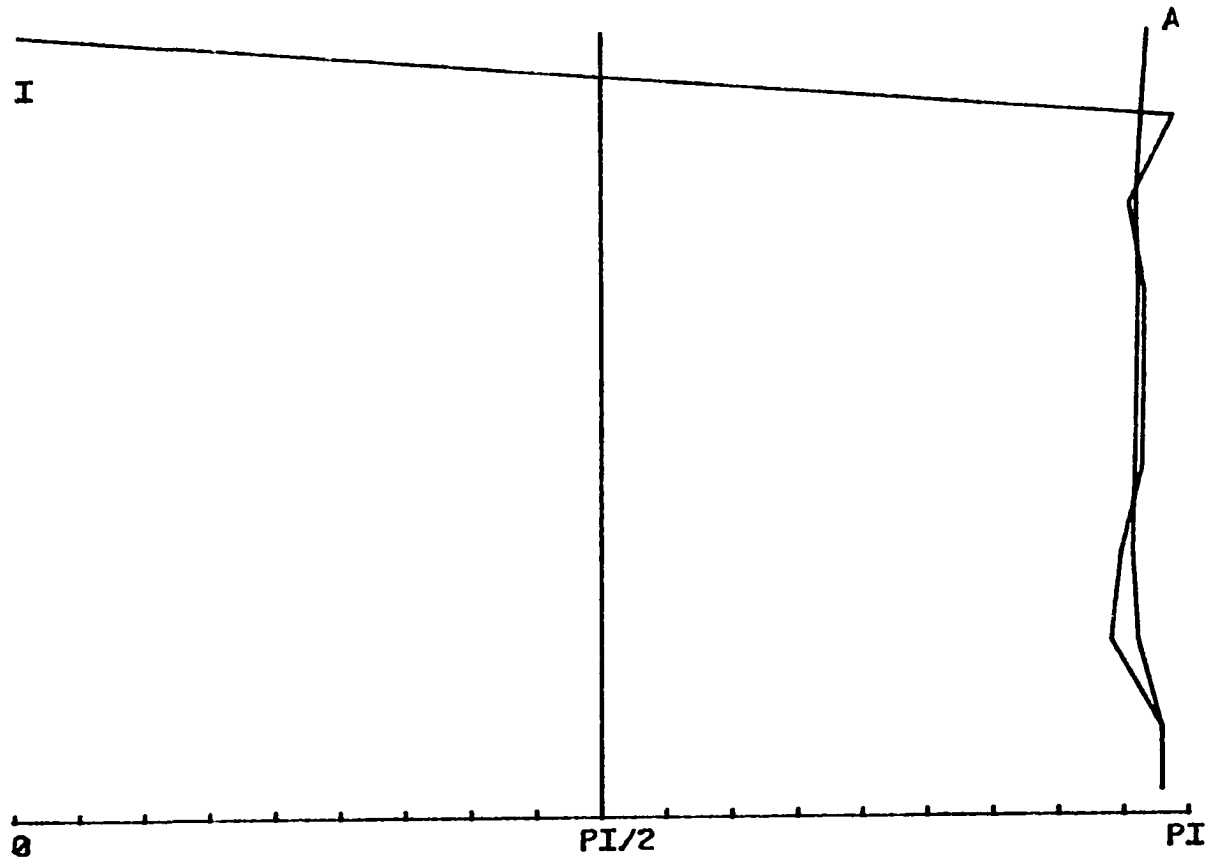
BULL5B



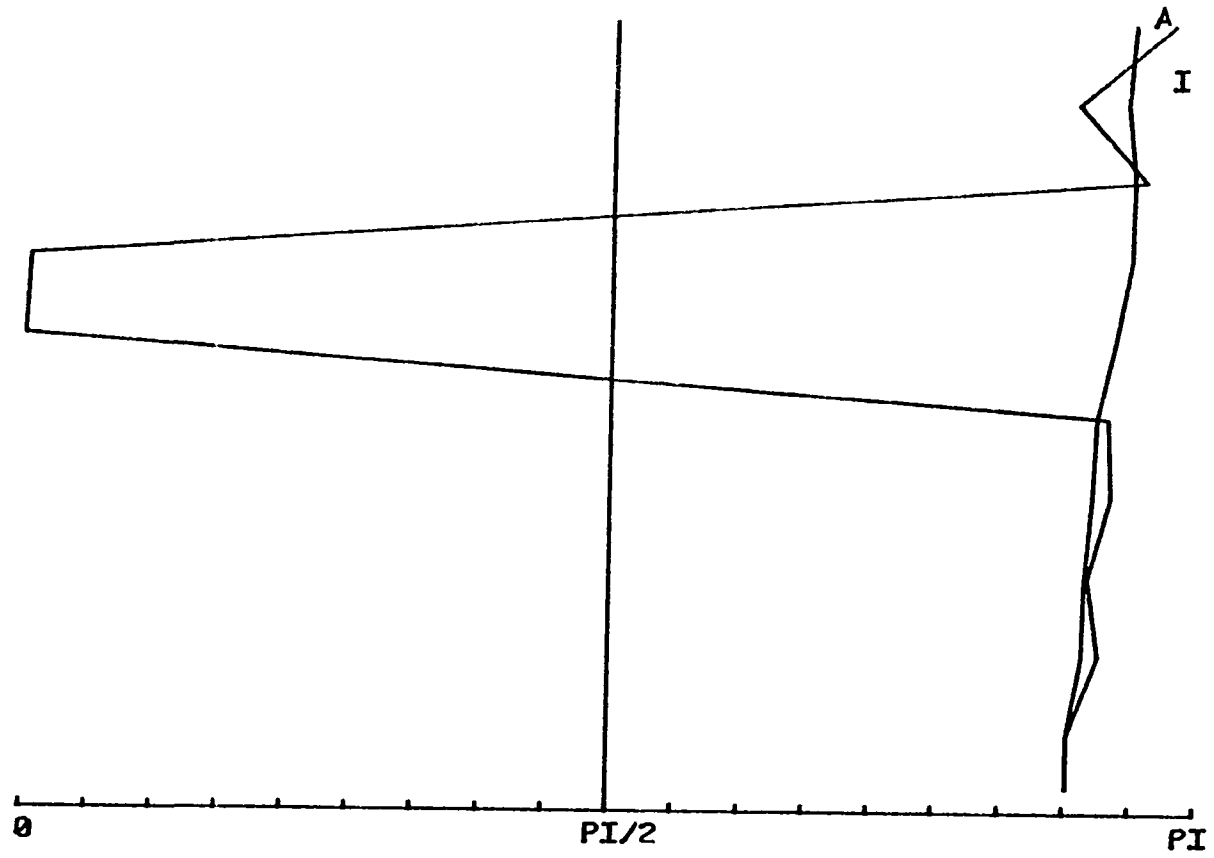
BULL6B



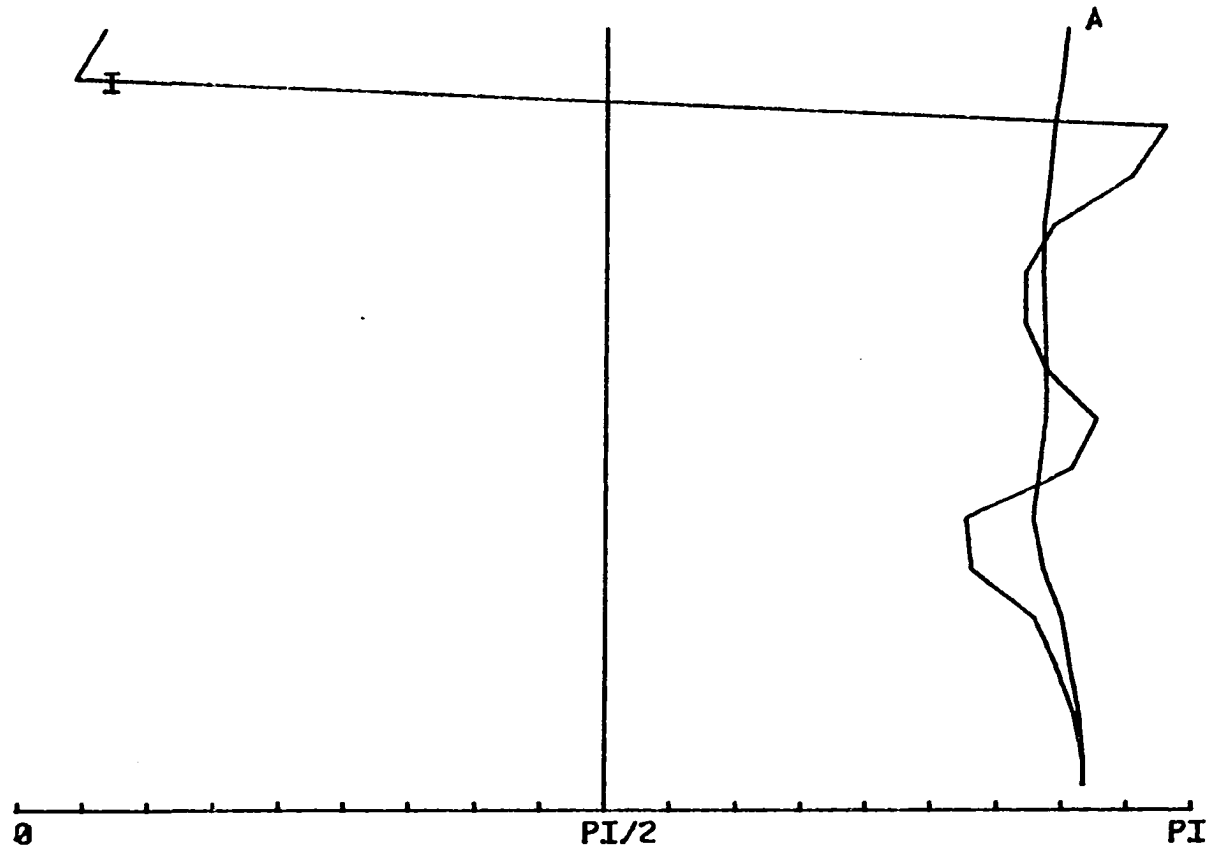
BULL7B



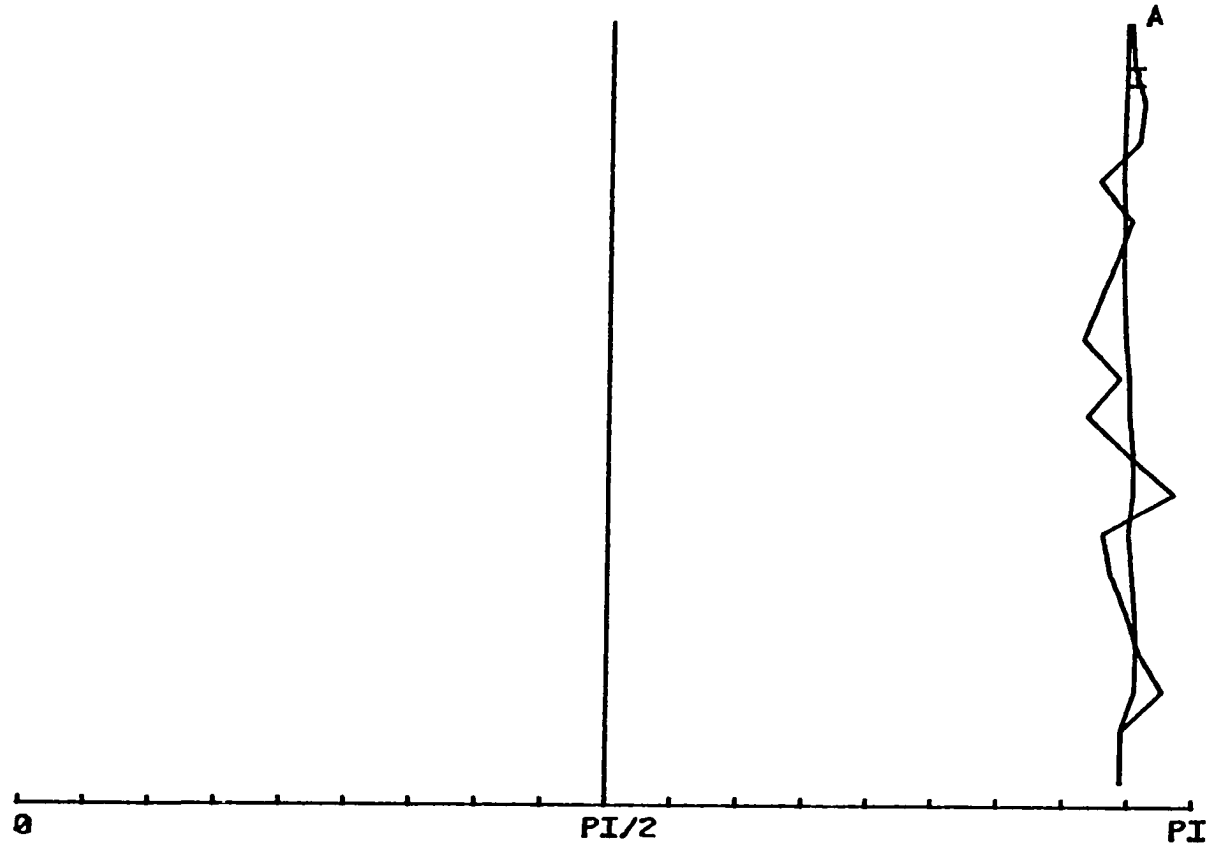
BULL8B



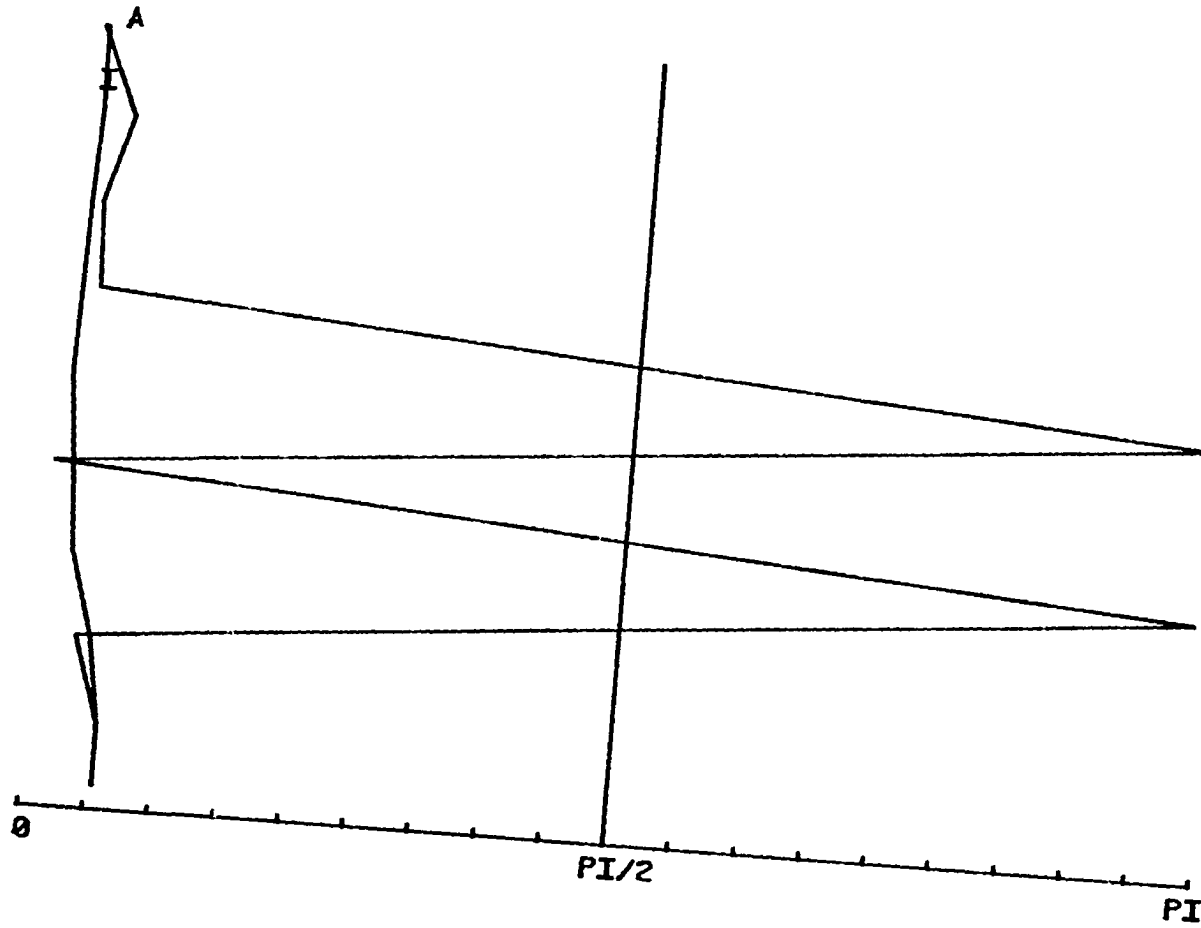
BULL9B



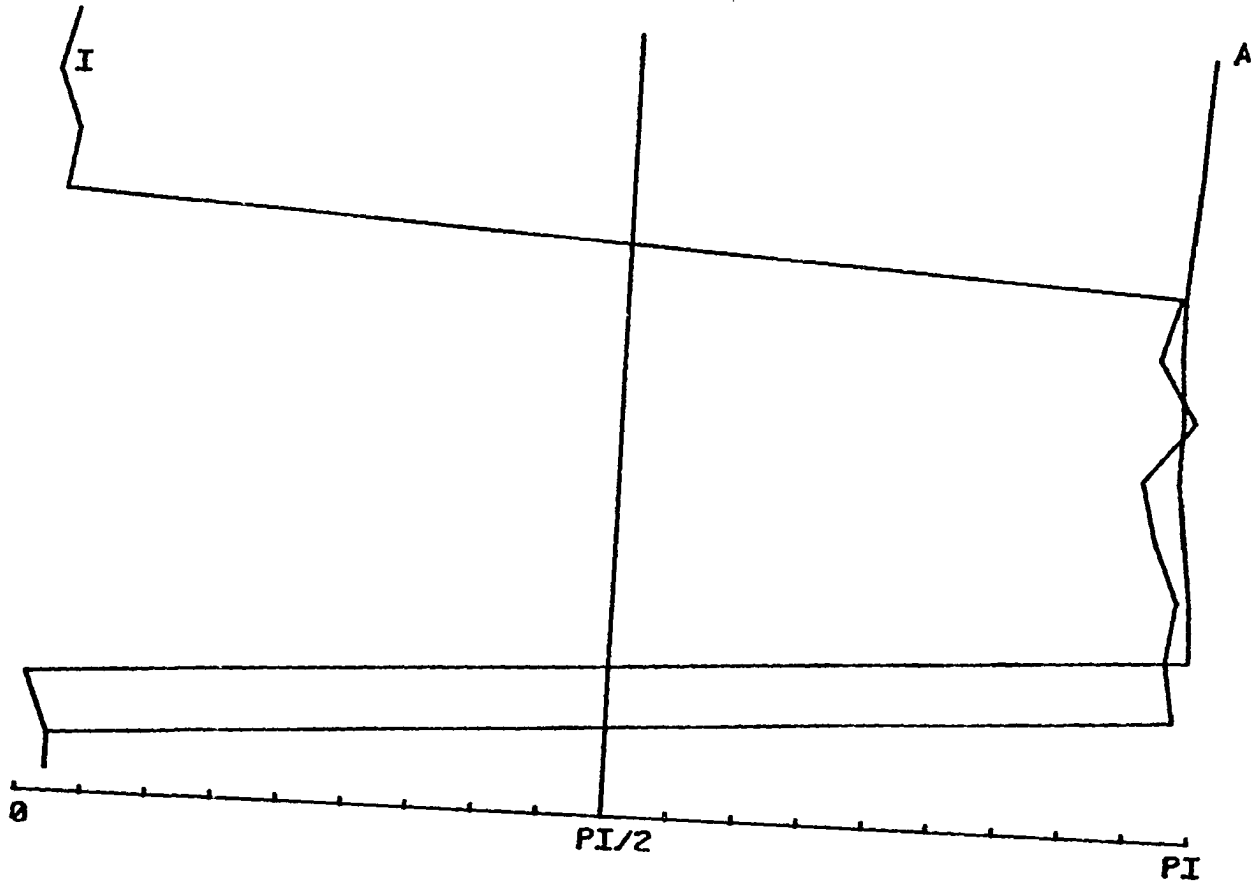
BULL 10B



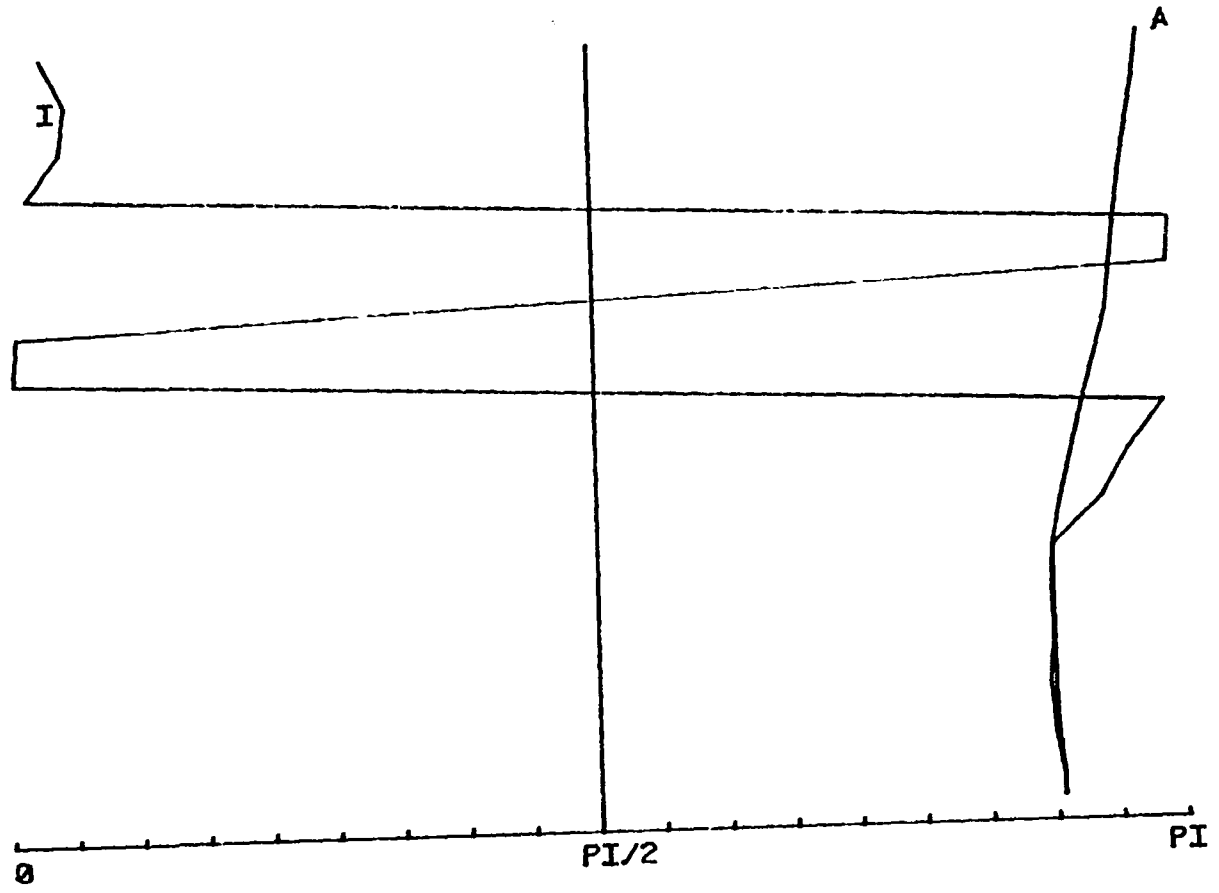
BULL 11B



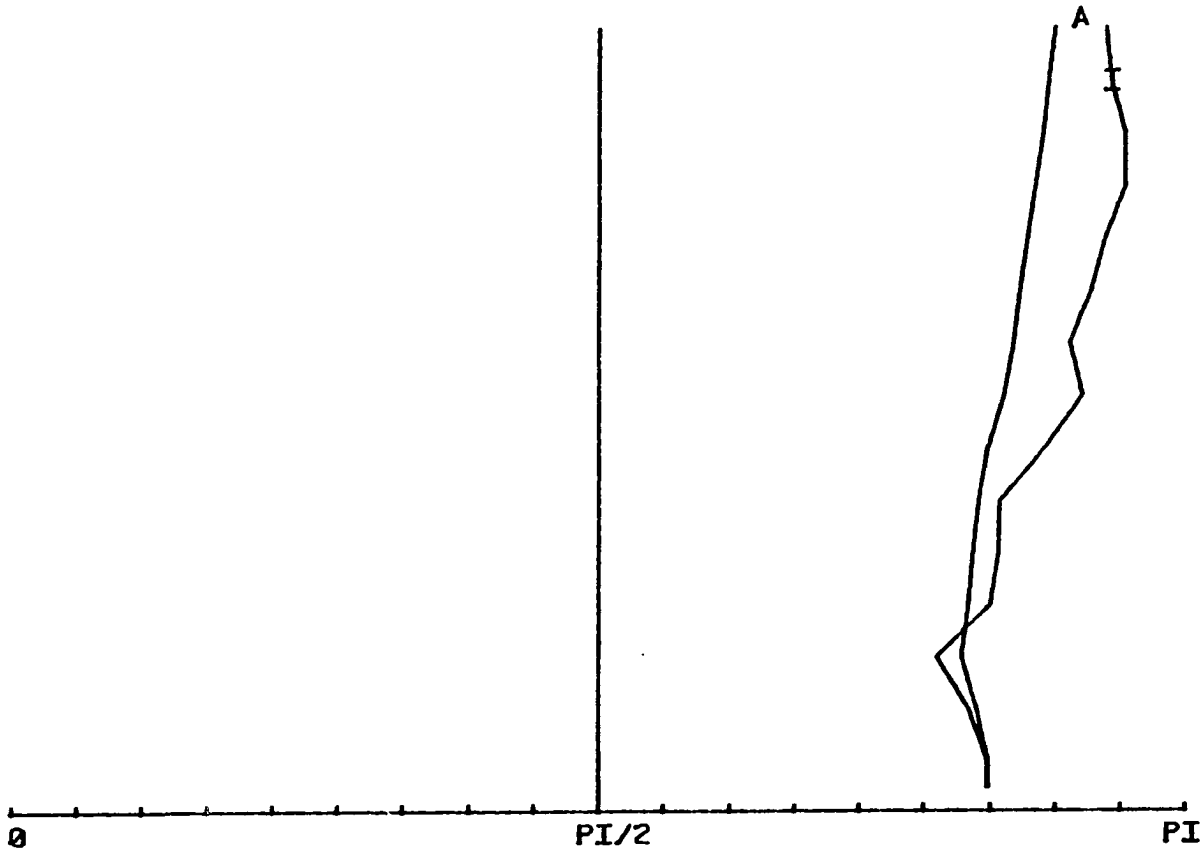
BULL12B



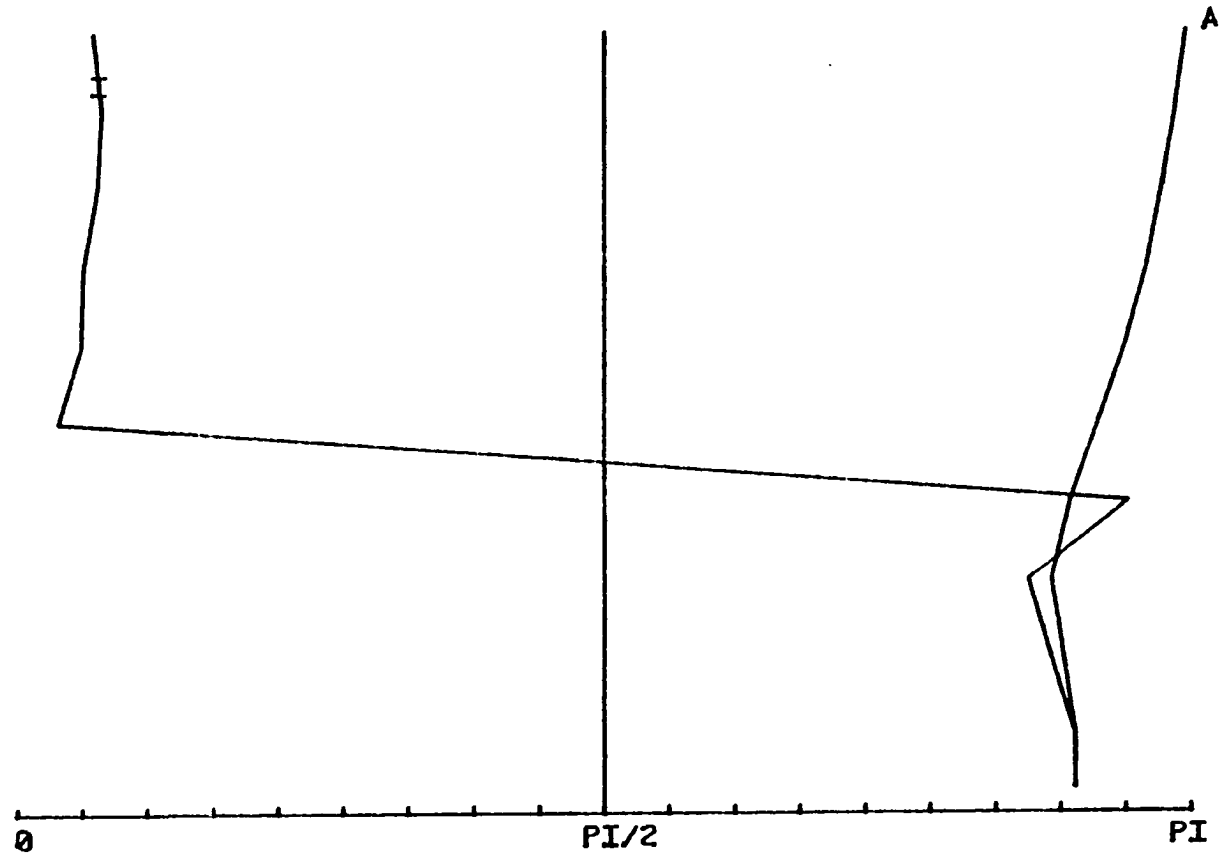
BULL13B



BULL 14B

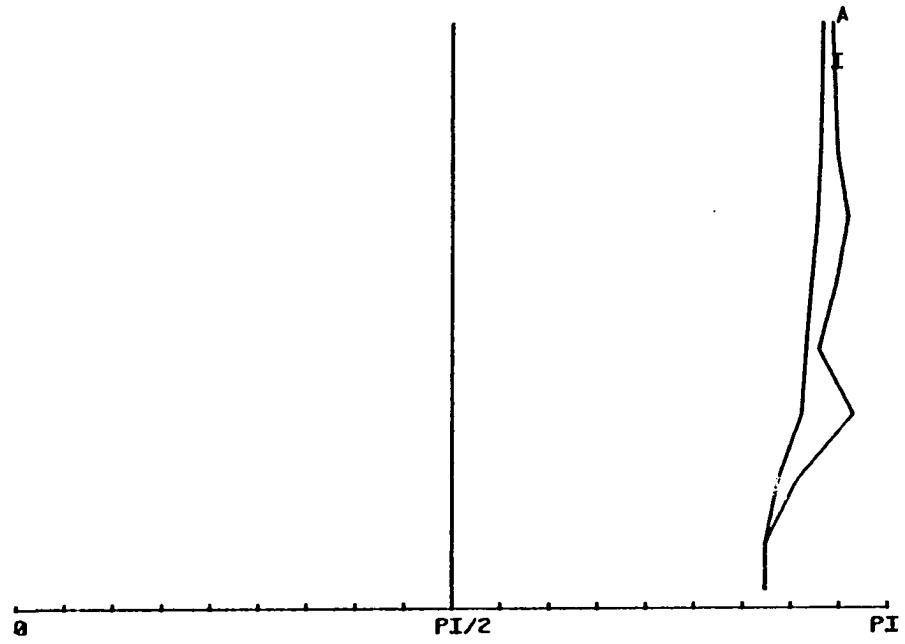


BULL 15B

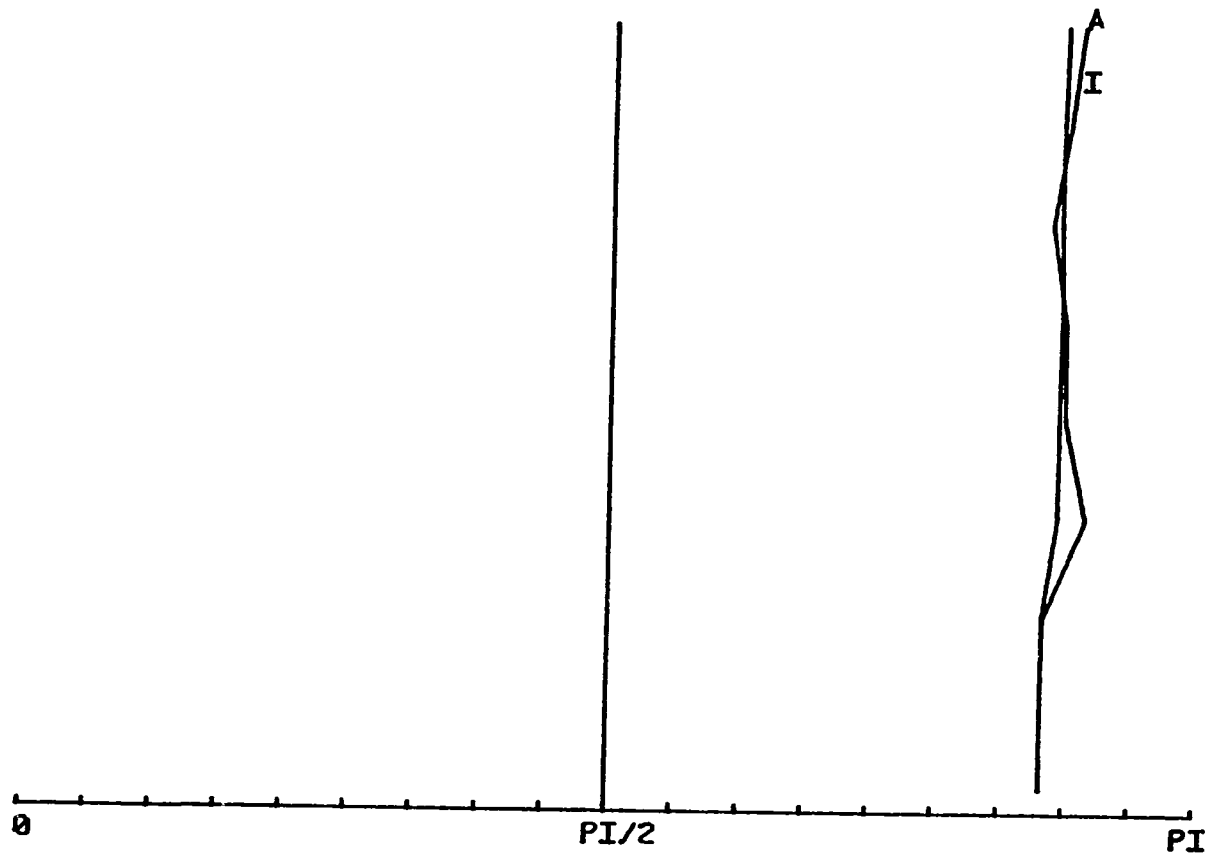


SAMPLE 944

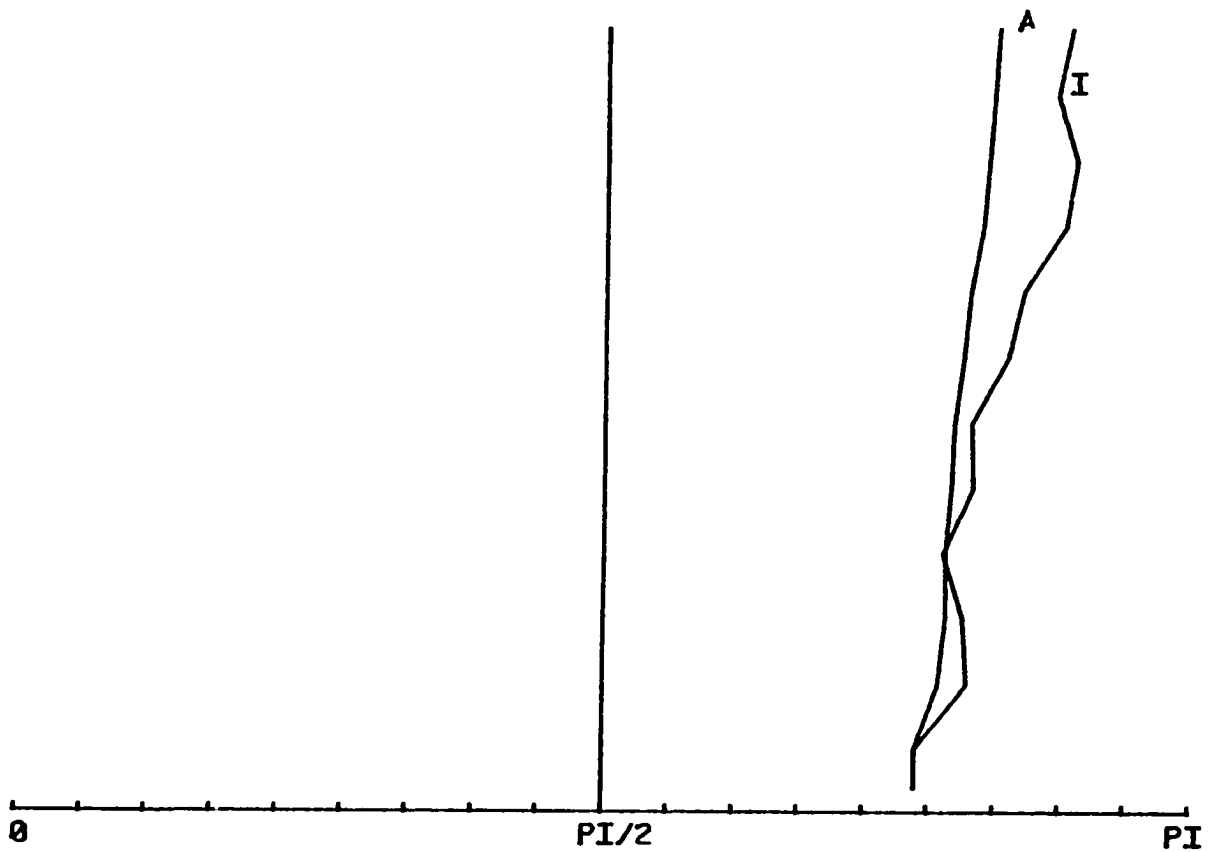
BULL17B



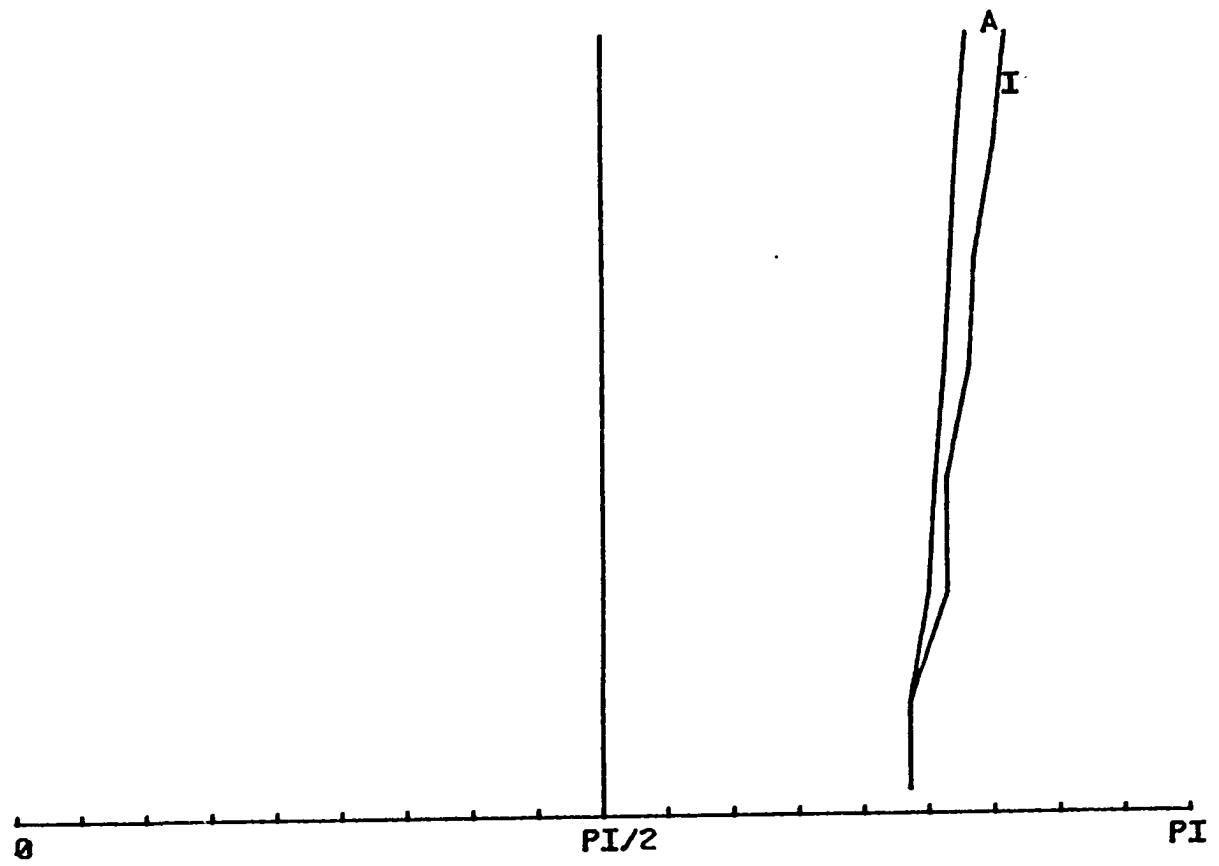
BULL16B



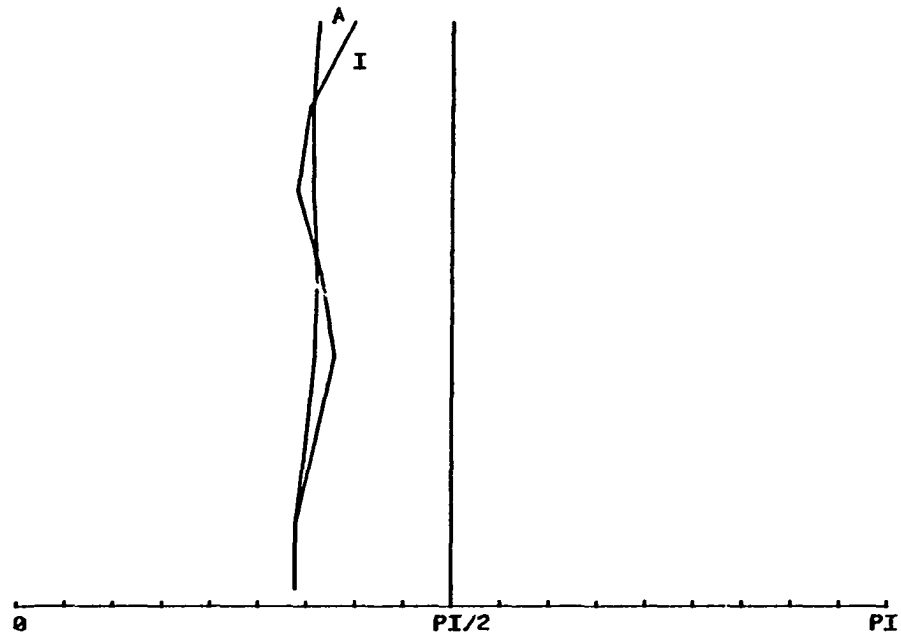
BULL 19B



BULL20B

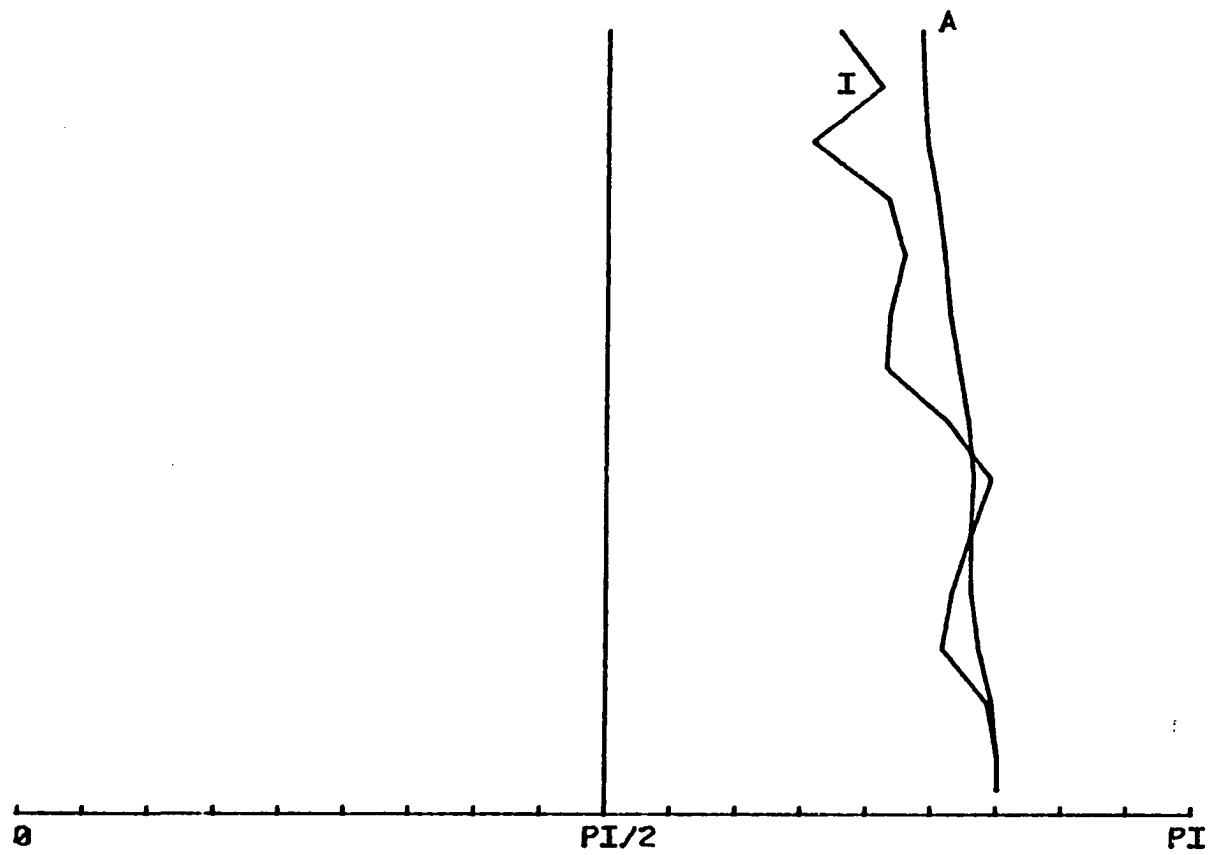


BULL21B

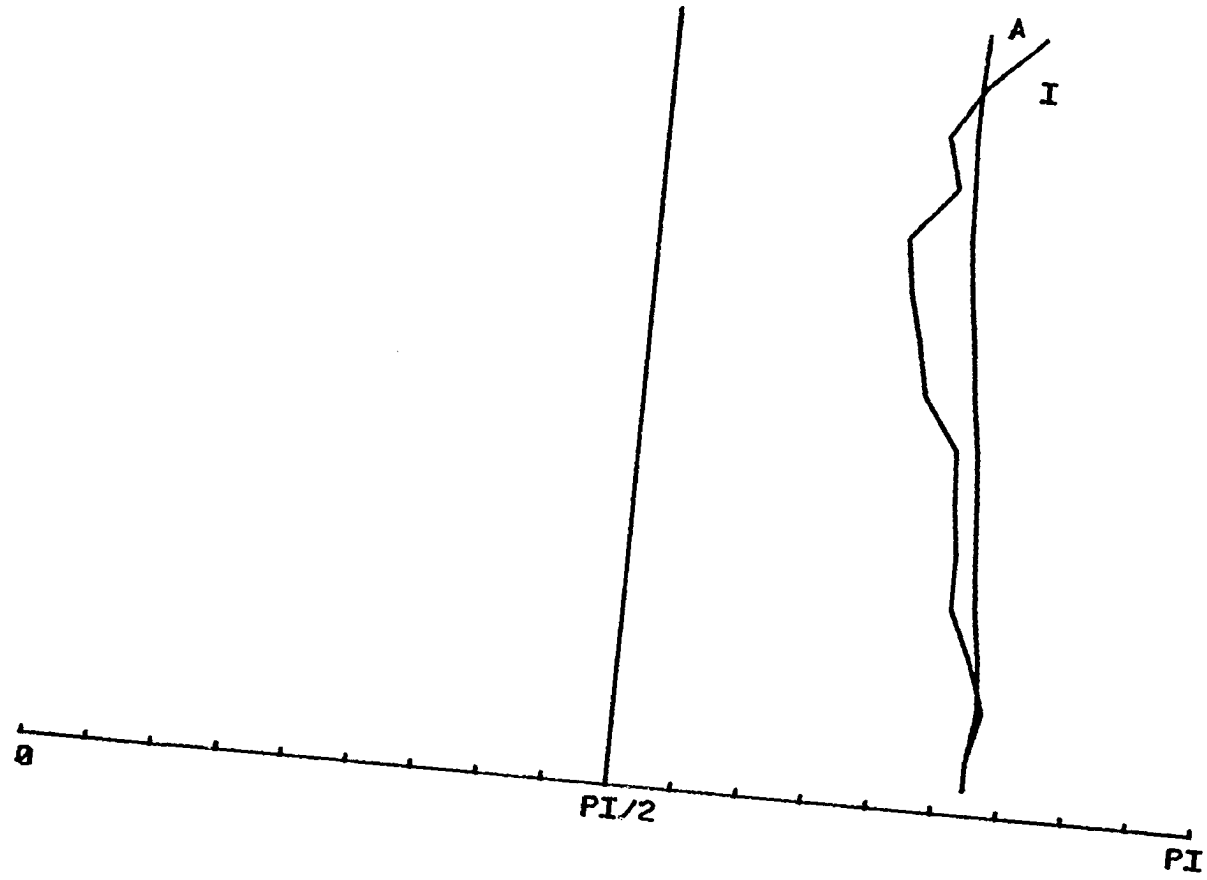


SAMPLE 946

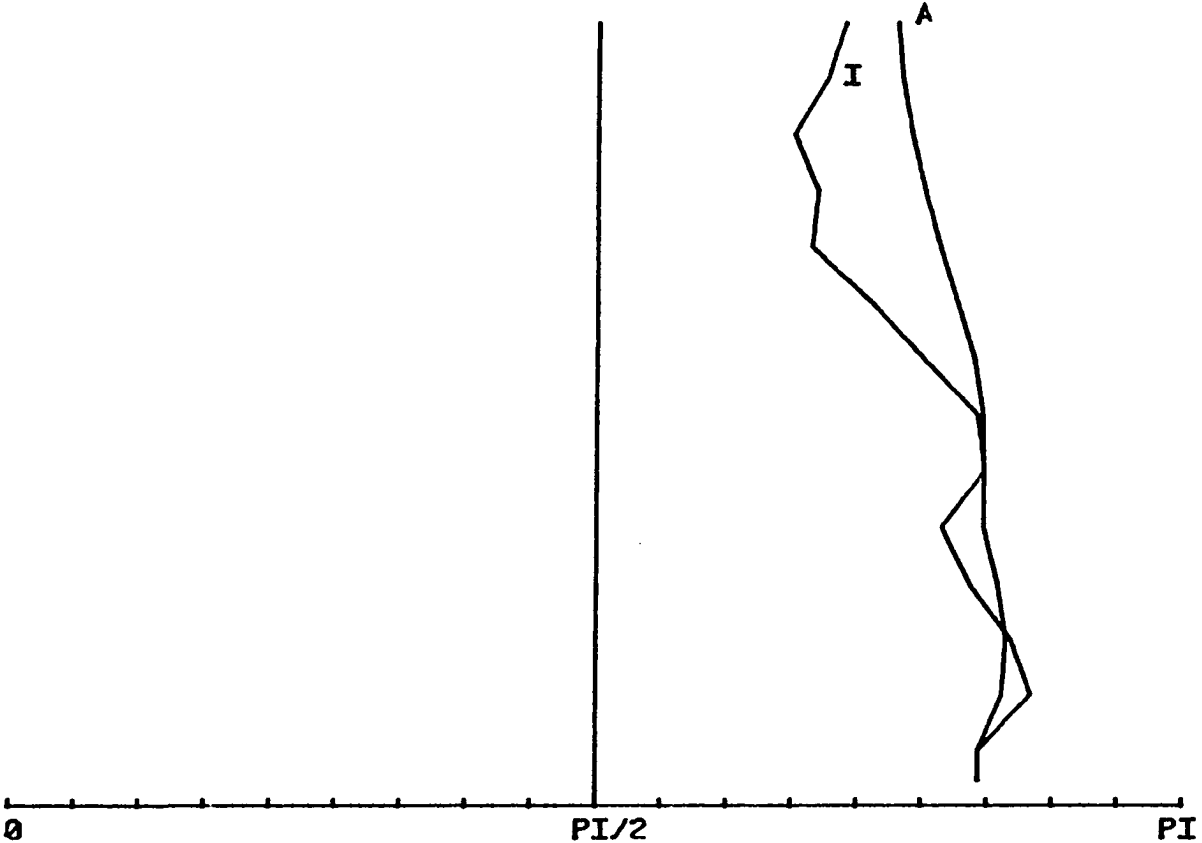
BULL23B



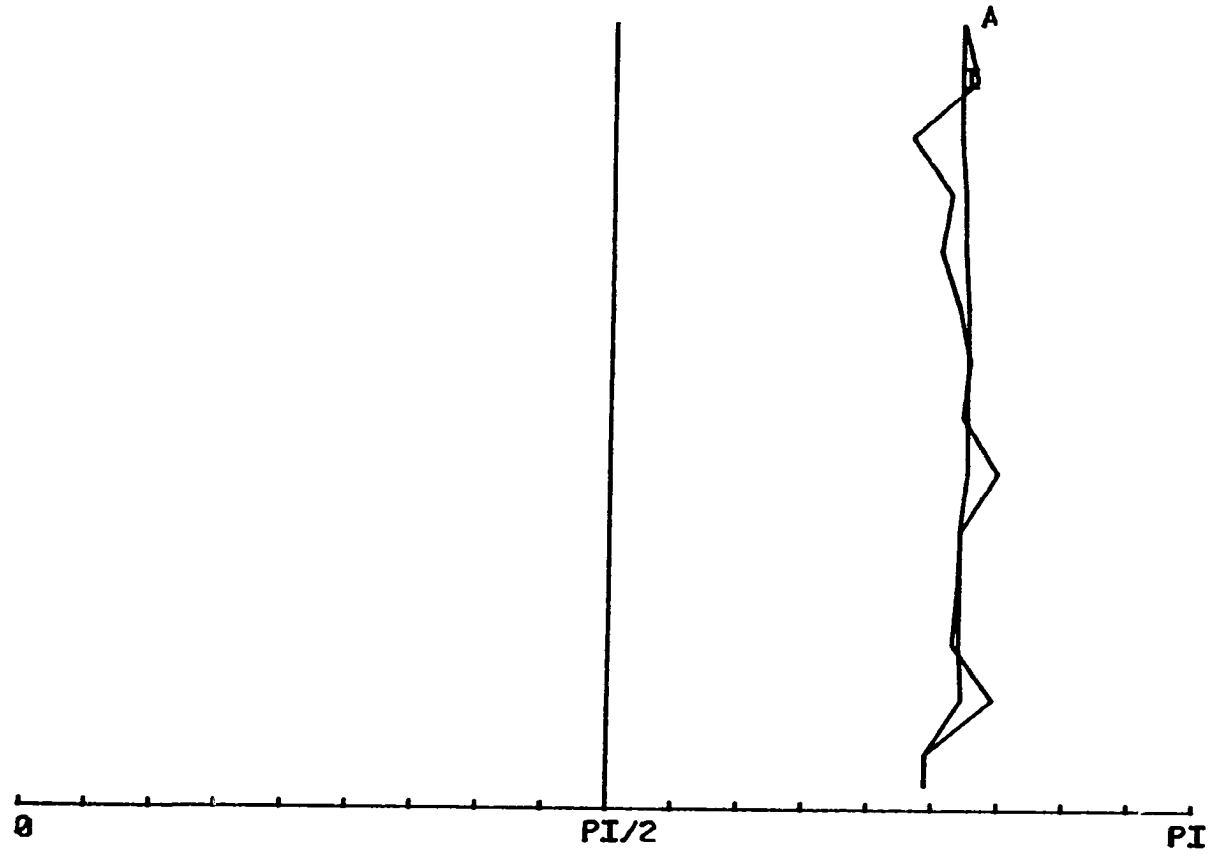
BULL24B



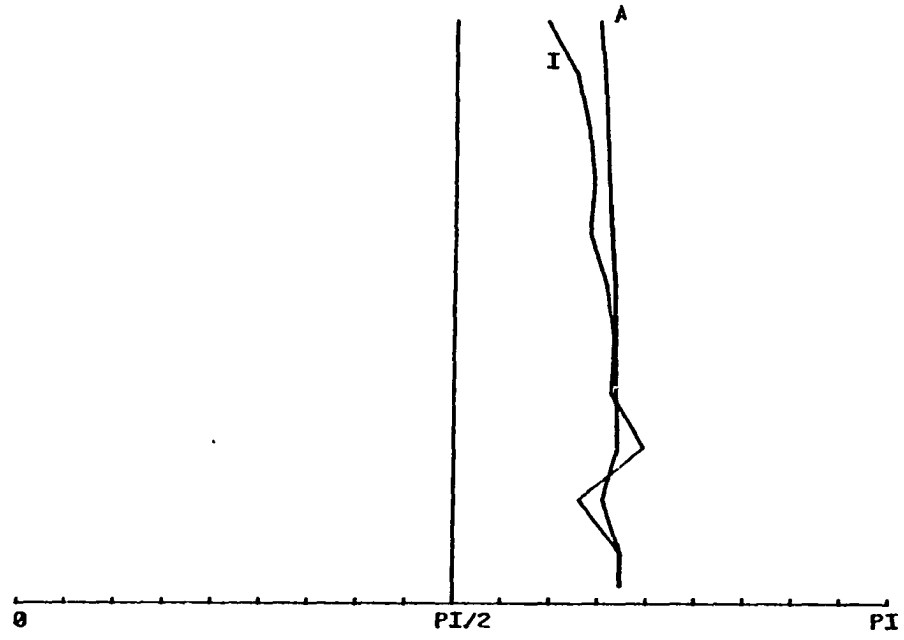
BULL25B



BULL26B



BULL27B



┌



Plat

Sample of

Scale 1:50,000

0

Berkeley Co.
Jefferson Co.

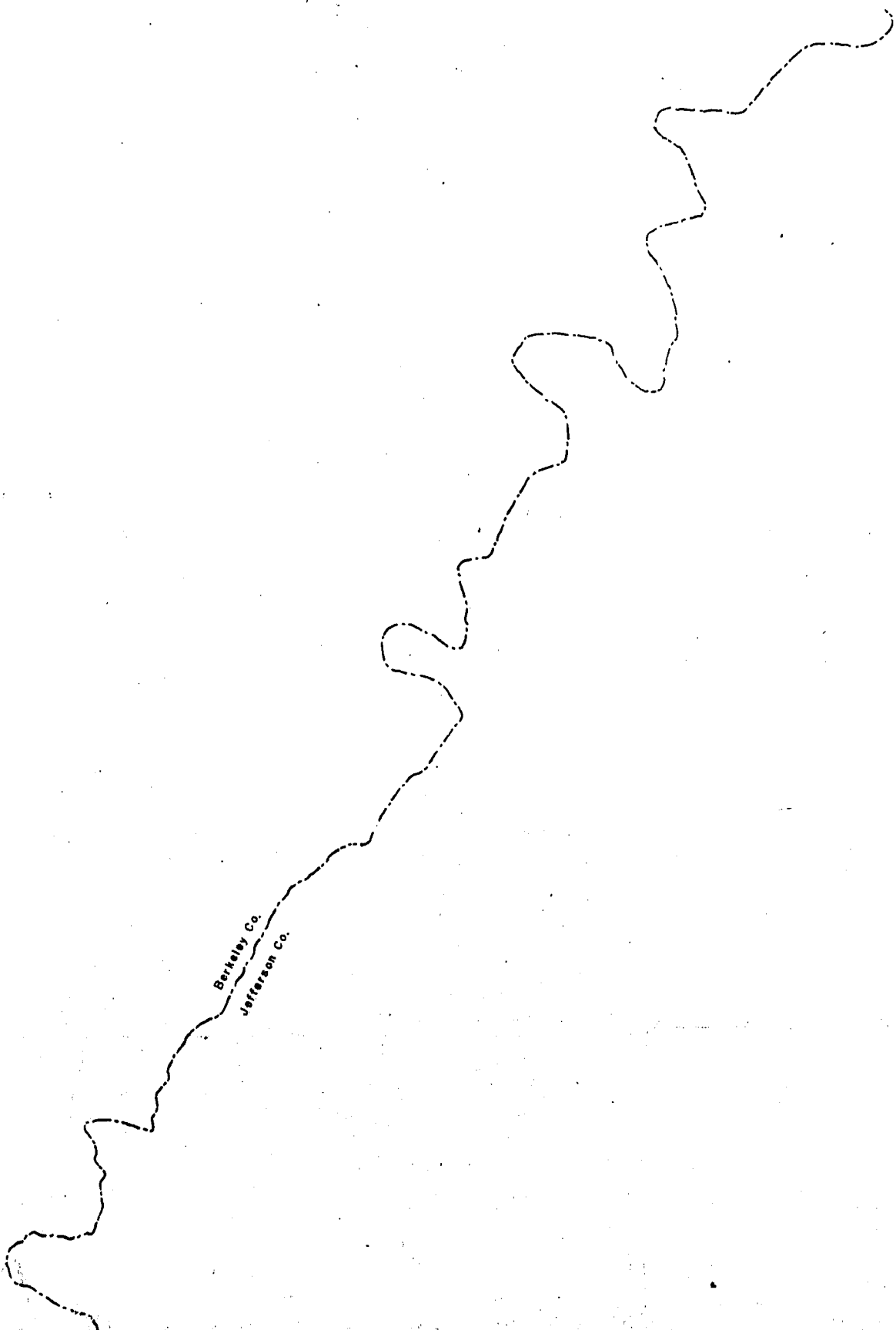
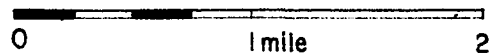


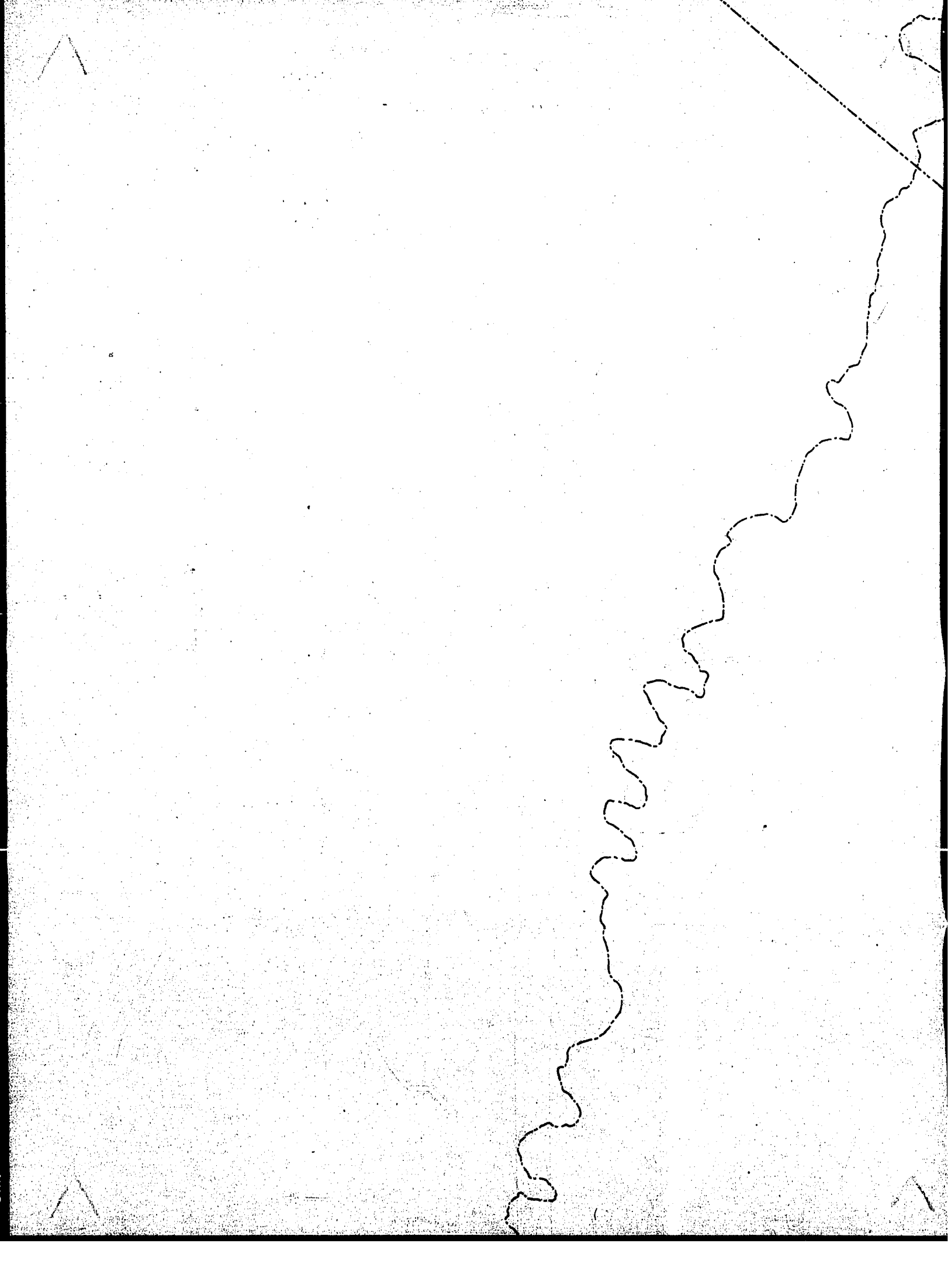
Plate I

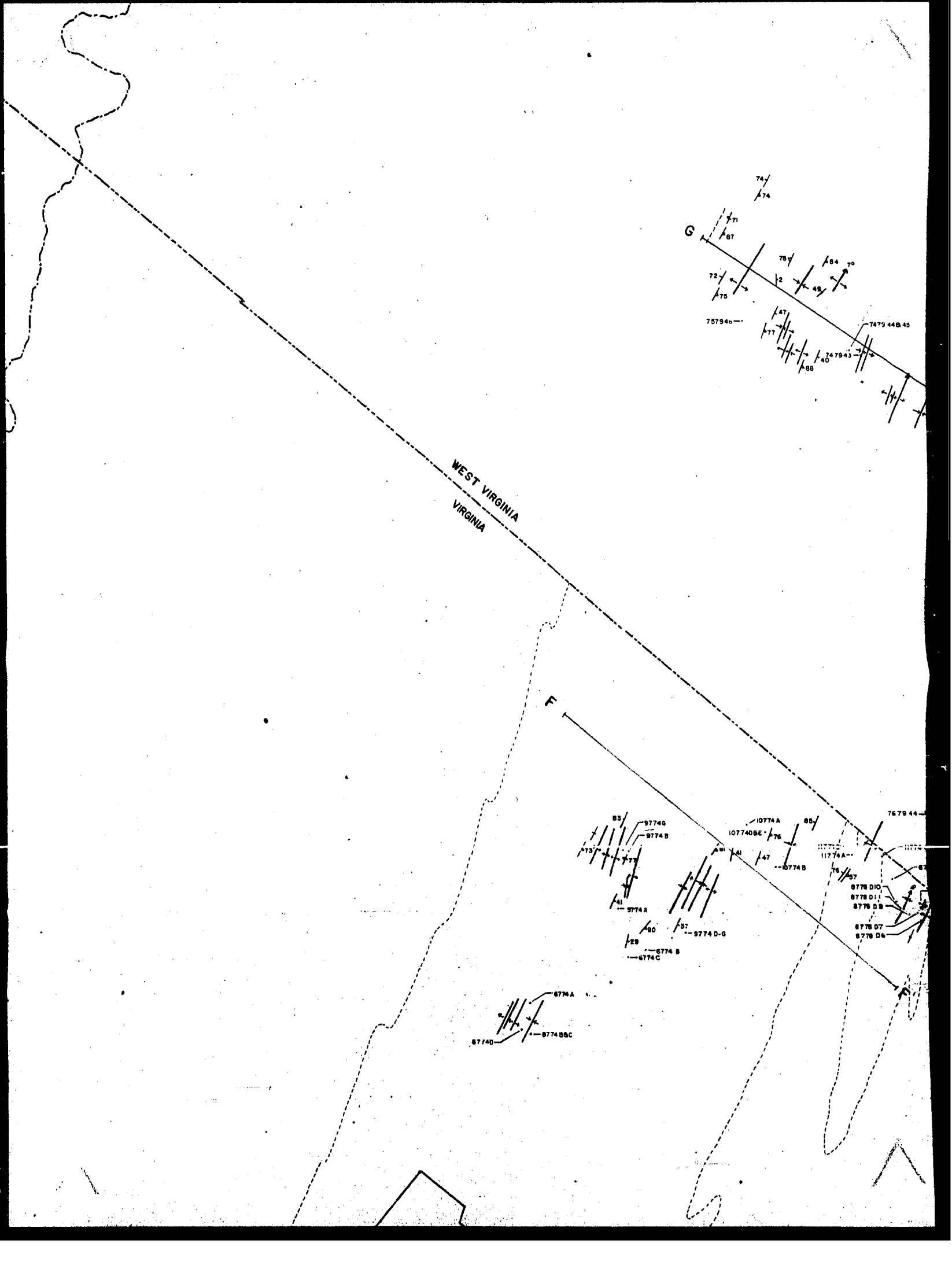
Sample and cross-section location.



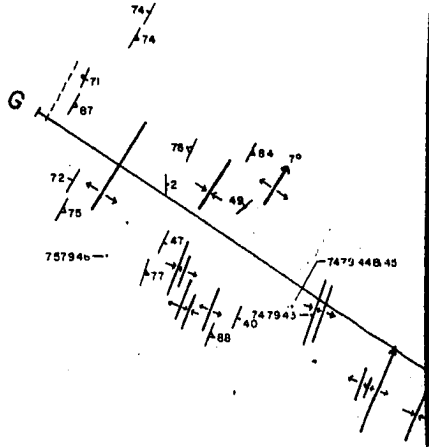
Scale 1:48000



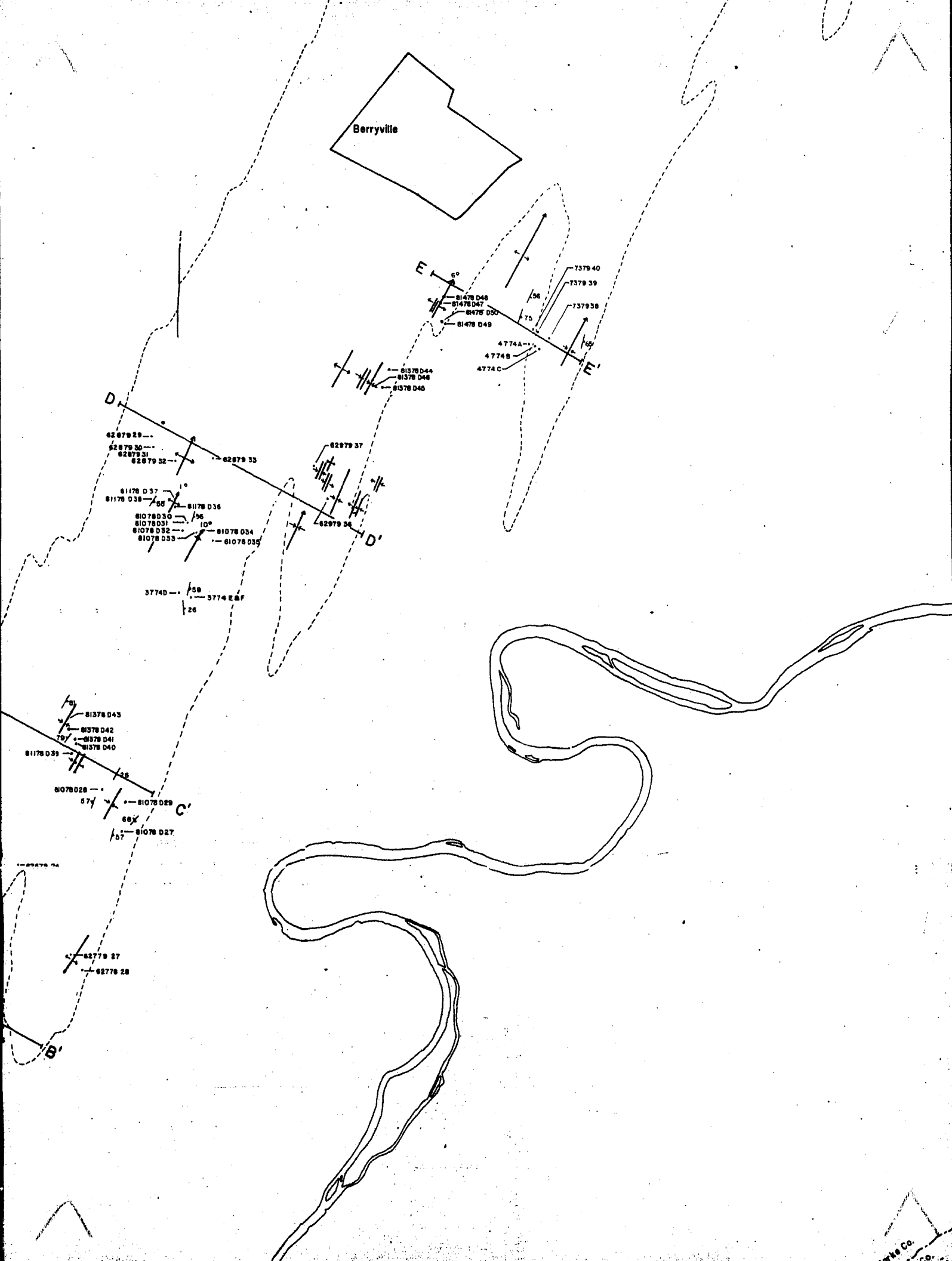




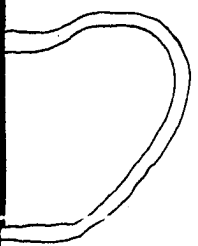
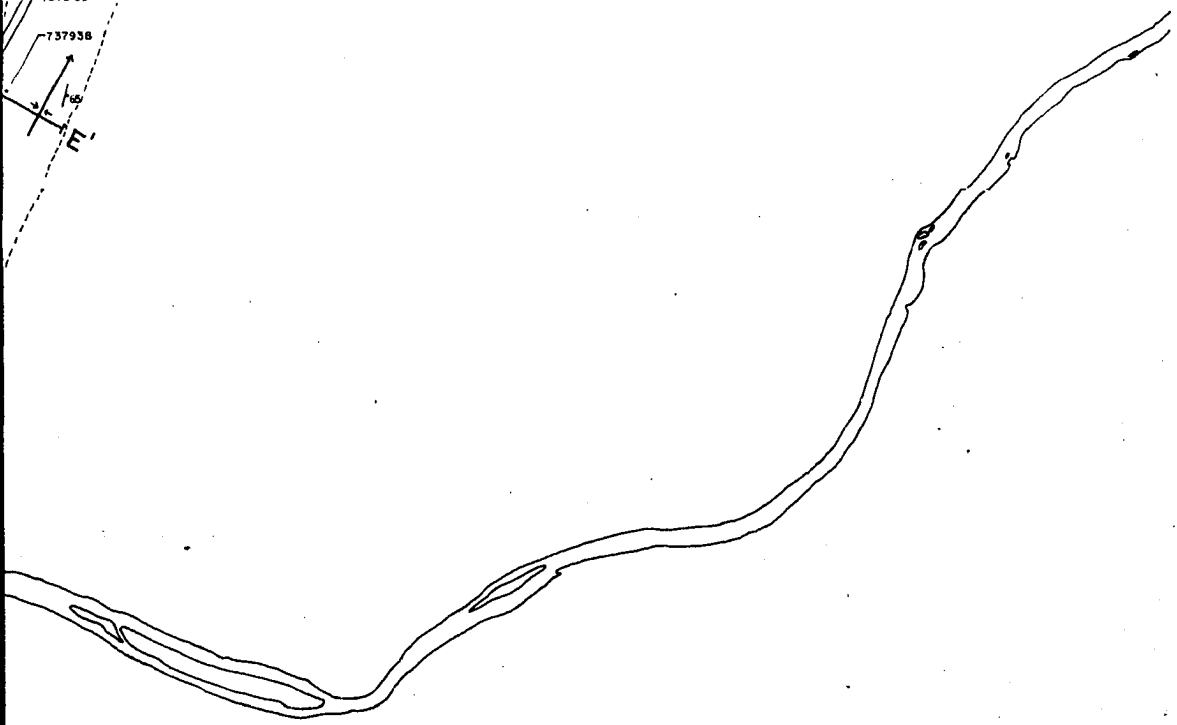
WEST VIRGINIA
VIRGINIA



Berryville



7379 40
7379 39
7379 38
E



Co.

81578 D43
81578 D42
81578 D41
81578 D40
81178 D39

81078 D26
57
81078 D25
66
81078 D27
57

82679 24
82779 27
82779 28

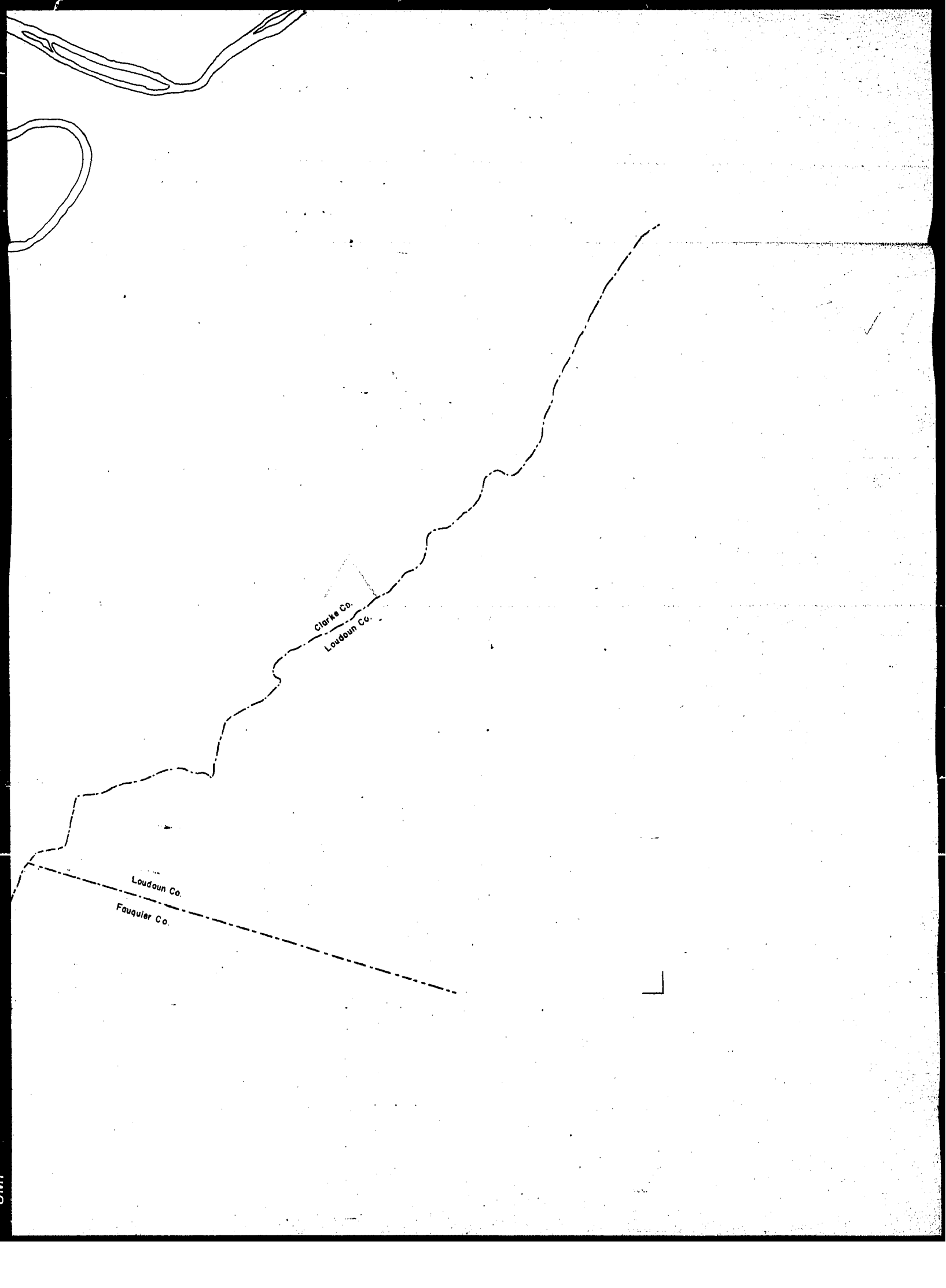
B

C

Clarke Co.
Loudoun Co.

Loudoun Co.
Fauquier Co.





Clarke Co.

Loudoun Co.

Loudoun Co.

Fauquier Co.

